Summary of the Bulletin of the International Seismological Centre

2010

January – June

Volume 47 Issue 1-6

www.isc.ac.uk

isc-mirror.iris.washington.edu

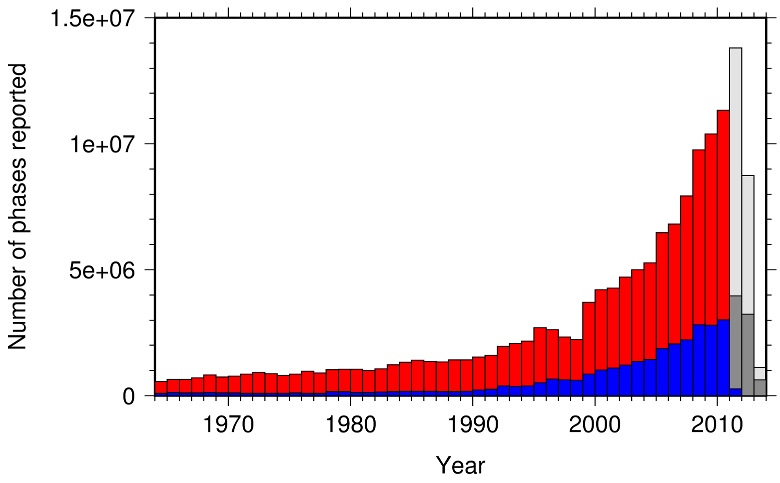

The number of phases (red) and number of amplitudes (blue) collected by the ISC for events each year since 1964. The data in grey covers the current period where data are still being collected before the ISC review takes place and are accurate at the time of publication. See Section 9.3.

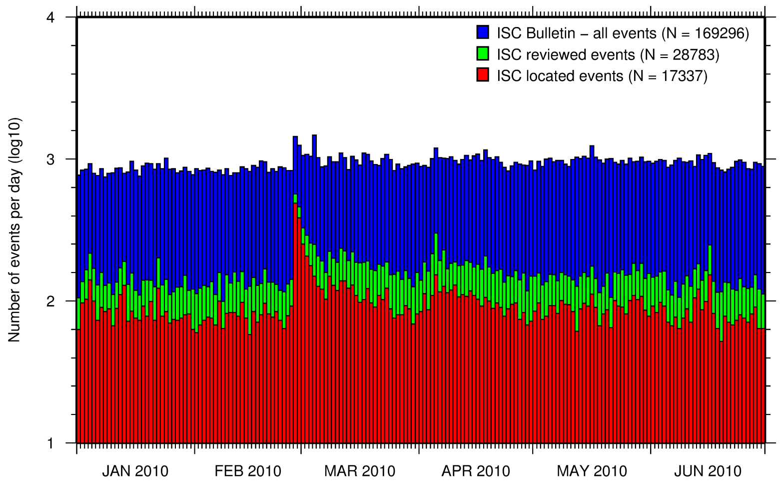

The number of events within the Bulletin for the current summary period. See Section 10.1.

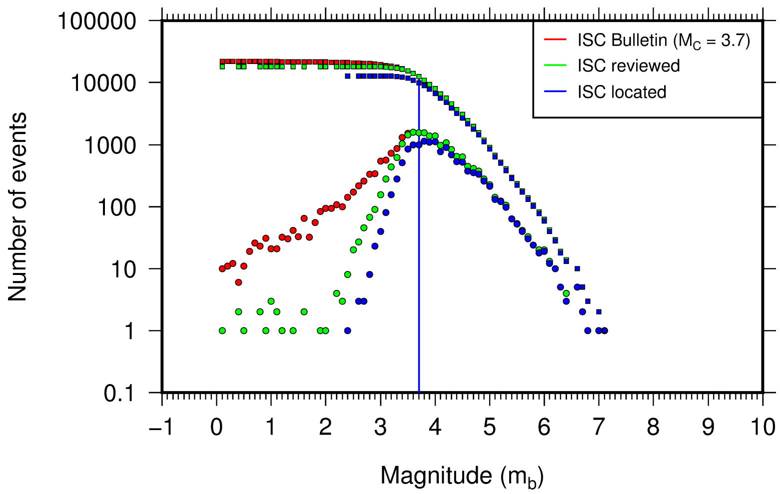

Frequency and cumulative frequency magnitude distribution for all events in the ISC Bulletin, ISC reviewed events and events located by the ISC. The magnitude of completeness (M_C) is shown for the ISC Bulletin. Note: only events with values of m_b are represented in the figure. See Section 10.4.

Contents

1

Preface

Dear Colleague,

I would like to offer you a new edition of the ISC printed product – the Summary of the ISC Bulletin.

From the 1960s the ISC published its earthquake bulletin data on paper since this was the only way for seismologists to receive earthquake information. Over the years, the volume of data substantially increased and made it impossible to print them all. At the same time the development of personal computers and the internet steadily made the red ISC Bulletin an ornamental placeholder on the shelves of many seismologists, who were now using the CD-ROMs and the website search engine to obtain the ISC data.

Following a recent decision of the ISC Executive Committee and the Governing Council, we stopped printing the ISC Bulletin. Instead, we set up this new publication that presents a summary of the ISC data available on the attached DVD-ROM. The summary greatly benefits from the extensive experience gained by the ISC analysts in presenting the annual ISC Bulletin analysis results at the numerous professional conferences worldwide.

This semi-annual Summary of the data in the ISC Bulletin is also accompanied by information on the ISC itself, its supporters and data providers, the history, staff and working statutes as well as important seismological standards and procedures used by the ISC in its operations. In addition, we will include small articles on notable seismic events that occurred during each half-year period, statistics of original data reports to the ISC and information on the institutions that provide most complete and versatile data to the ISC.

The contents of each issue will change but customarily we shall publish the analysis of contributed and published Bulletin data – the fundamental reason for the ISC continued operations.

We hope that you would find this new publication useful in your work. If your home-institution or company is unable, for one reason or another, to support the long-term international operations of the ISC in full by becoming a Member, then, please, consider subscribing to this publication by contacting us at admin@isc.ac.uk.

With great thanks to our Members, Sponsors, data contributors and users,

Dr Dmitry A. Storchak
Director
International Seismological Centre (ISC)

2

The International Seismological Centre

2.1 The ISC Mandate

The International Seismological Centre (ISC) was set up in 1964 with the assistance of UNESCO as a successor to the International Seismological Summary (ISS) to carry forward the pioneering work of earlier scientists in collecting, archiving and processing seismic station and network bulletins and preparing and distributing the definitive summary of world seismicity.

Under the umbrella of the International Association of Seismology and Physics of the Earth Interior (IASPEI/IUGG), the ISC has played an important role in setting international standards such as the International Seismic Bulletin Format (ISF), the IASPEI Standard Seismic Phase List (SSPL) and both the old and New IASPEI Manual of the Seismological Observatory Practice (NMSOP-2) (www.iaspei.org/projects/NMSOP.html).

The ISC has contributed to scientific research and prominent scientists such as John Hodgson, Eugine Herrin, Hal Thirlaway, Jack Oliver, Anton Hales, Ola Dahlman, Shigeji Suehiro, Nadia Kondorskaya, Vit Karnik, Stephan Müller, David Denham, Bob Engdahl, Adam Dziewonski, John Woodhouse and Guy Masters all considered it an important duty to serve on the ISC Executive Committee and the Governing Council.

The current mission of the ISC is to maintain:

- the ISC **Bulletin** – the longest continuous definitive summary of World seismicity (collaborating with 130 seismic networks and data centres around the world). (www.isc.ac.uk/iscbulletin/)
- the **International** Seismographic Station Registry (**IR**, jointly with the World Data Center for Seismology, Denver). (www.isc.ac.uk/registries/)
- the IASPEI Reference Event List (Ground Truth, **GT**, jointly with IASPEI). (www.isc.ac.uk/gtevents/)

These are fundamentally important tasks. Bulletin data produced, archived and distributed by the ISC for almost 50 years is the definitive source of such information and are used by thousands of seismologists worldwide for seismic hazard estimation, for tectonic studies and for regional and global imaging of the Earth's structure. Key information in global tomographic imaging is derived from the analysis of ISC data. The ISC Bulletin served as a major source of data for such well known products as the ak135 global 1-D velocity model and the EHB (*Engdahl et al.*, 1998) and Centennial (*Engdahl and Villaseñor*, 2002) catalogues. It presents an important quality-control benchmark for the Comprehensive Test Ban Treaty Organization (CTBTO). Hypocentre parameters from the ISC Bulletin are used by the Data Management Center of the Incorporated Research Institutions for Seismology (IRIS DMC) to serve event oriented user requests for waveform data. The ISC-GEM Bulletin is a cornerstone of the ISC-GEM Global Instrumental Reference Earthquake Catalogue for Global Earthquake risk Model (GEM).

The ISC relational database currently holds approximately 90 Gb of unique data. The ISC Bulletin contains over 5 million seismic events: earthquakes, chemical and nuclear explosions, mine blasts and mining induced events. As many as 1.5 million of them are regional and teleseismically recorded events that have been reviewed by the ISC analysts. The ISC Bulletin contains approximately 150 million individual seismic station readings of arrival times, amplitudes, periods, SNR, slowness and azimuth, reported by approximately 17,000 seismic stations currently registered in the IR. As many as 6,000 stations have contributed to the ISC Bulletin in recent years. This number includes the numerous sites of the USArray. The IASPEI GT List currently contains 7802 events for which latitude, longitude and depth of origin are known with high confidence (to 5 km or better) and seismic signals were recorded at regional and/or teleseismic distances.

2.2 Brief History of the ISC

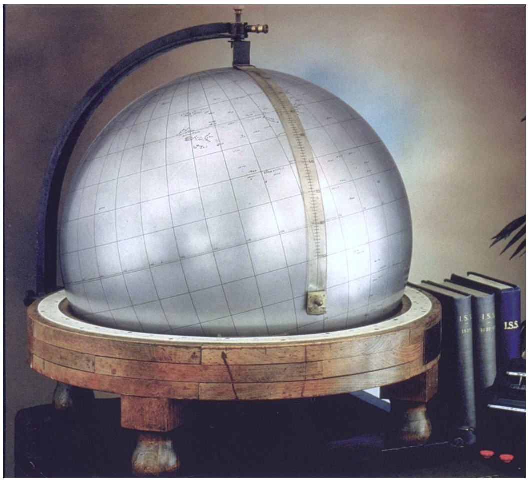

Figure 2.1: *The steel globe bearing positions of early seismic stations was used for locating positions of earthquakes for the International Seismological Summaries.*

Earthquake effects have been noted and documented from the earliest times, but it is only since the development of earthquake recording instruments in the latter half of the 19th century that a proper study of their occurrence has been possible. After the first teleseismic observation of an earthquake in 1889, the need for international exchange of readings was recognised in 1895 by Prof. John Milne and by Ernst von Rebeur Paschwitz together with Georg Gerland, resulting in the publication of the first international seismic bulletins. Milne's "Shide Circulars" were issued under the auspices of the Seismological Committee of the British Association for the Advancement of Science (BAAS), while co-workers of Gerland at the Central Bureau of the International Association of Seismology worked independently in Strasbourg (BCIS).

Following Milne's death in 1913, Seismological Bulletins of the BAAS were continued under Prof. H.H. Turner, later based at Oxford University. Upon formal post-war dissolution of the International Association of Seismology in 1922 the newly founded Seismological Section of the International Union of Geodesy and Geophysics (IUGG) set up the International Seismological Summary (ISS) to continue at Oxford under Turner, to produce the definitive global catalogues from the 1918 data-year onwards, under the auspices of IUGG and with the support of the BAAS.

ISS production, led by several professors at Oxford University, and Sir Harold Jeffreys at Cambridge University, continued until it was superseded by the ISC Bulletin, after the ISC was formed in Edinburgh in 1964 with Dr P.L. Willmore as its first director.

During the period 1964 to 1970, with the help of UNESCO and other international scientific bodies, the ISC was reconstituted as an international non-governmental body, funded by interested institutions from various countries. Initially there were supporting members from seven countries, now there are over 60, and member institutions include national academies, research foundations, government departments and research institutes, national observatories and universities. Each member, contributing a minimum unit of subscription or more, appoints a representative to the ISC's Governing Council, which meets every two years to decide the ISC's policy and operational programme. Representatives from the International Association of Seismology and Physics of the Earth's Interior also attend these meetings. The Governing Council appoints the Director and a small Executive Committee to oversee the ISC's operations.

Figure 2.2: *ISC building in Thatcham, Berkshire, UK.*

In 1975, the ISC moved to Newbury in southern England to make use of better computing facilities there. The ISC subsequently acquired its own computer and in 1986 moved to its own building at Pipers Lane, Thatcham, near Newbury. The internal layout of the new premises was designed for the ISC and includes not only office space but provision for the storage of extensive stocks of ISS and ISC publications and a library of seismological observatory bulletins, journals and books collected over many tens of years.

In 1997 the first set of the ISC Bulletin CD-ROMs was produced (not counting an earlier effort at USGS). The first ISC website appeared in 1998 and the first ISC database was put in day-to-day operations from 2001.

Throughout 2009-2011 a major internal reconstruction of the ISC building was undertaken to allow for more members of staff working in mainstream ISC operations as well as major development projects such as the CTBTO Link, ISC-GEM Catalogue and the ISC Bulletin Rebuild.

2.3 Former Directors of the ISC and its U.K. Predecessors

John Milne
Publisher of the Shide Circular Reports on Earthquakes
1899-1913

Herbert Hall Turner
Seismological Bulletins of the BAAS
1913-1922
Director of the ISS
1922-1930

Harry Hemley Plaskett
Director of the ISS
1931-1946

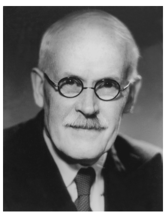

Harold Jeffreys
Director of the ISS
1946-1957

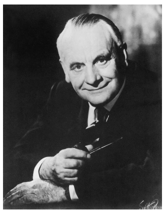

Robert Stoneley
Director of the ISS
1957-1963

P.L. (Pat) Willmore
Director of the ISS
1963-1970
Director of the ISC
1964-1970

Edouard P. Arnold
Director of the ISC
1970-1977

Anthony A. Hughes
Director of the ISC
1977-1997

Raymond J. Willemann
Director of the ISC
1998-2003

Avi Shapira
Director of the ISC
2004-2007

2.4 Evolution of the Printed ISC Bulletin

This new edition of the printed ISC Bulletin is entitled the 'Summary of the ISC Bulletin'. It began with the data of January 2010. The essence of the change is in the title – the ISC no longer publishes parameters of seismic events, leaving it to users to extract those either from an attached DVD-ROM or from the ISC website. Instead of the data themselves, we print a summary of data for each time period, along with essential documents on the ISC, its procedures as well as IASPEI standards that are used in the ISC operations.

This article traces the evolution of the ISC printed publication since 1964, during which time there was a constant improvement in computing facilities available to seismologists as well as a year-by-year increase in the number of registered seismic networks/agencies (Figure 2.3), registered stations around the world (Figure 2.4), the number of events detected around the world (Figure 2.5) and the number of event readings reported to the ISC (Figure 2.6). A reading here is a set of seismic arrivals reported by the same agency from a specific station for a specific event.

The ISC Bulletin has been printed for almost 50 years. During this time the purpose and use of this publication has changed dramatically. In the 1960s and 1970s the printed ISC Bulletin was the only form that was available to researchers. With the advent of personal computers and CD-ROMs in the 1980s and 1990s, the printed ISC Bulletin gradually became a secondary source of information, only useful for providing a quick reference on specific seismic events. The introduction of the ISC website in the late 1990s and consequent availability of ISC Bulletin via primitive web search engines and ftp further diminished the role of the printed ISC Bulletin so that by the 2000s it became merely a placeholder on many office shelves around the world, acting as a visual image of hard work that the ISC continues to

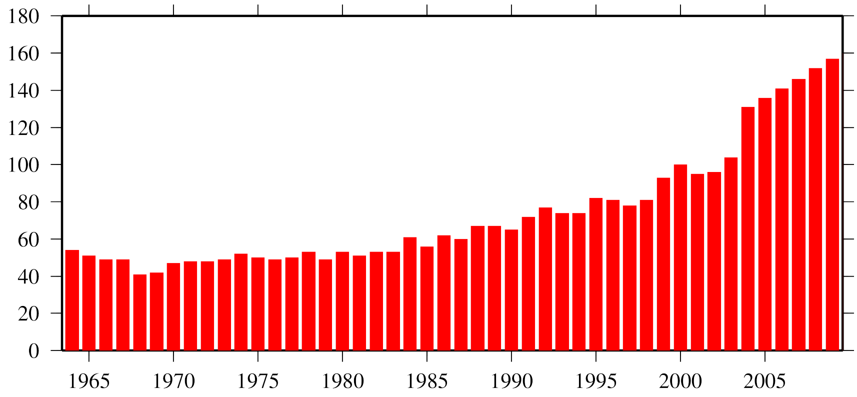

Figure 2.3: *The number of seismological agencies that reported hypocentre parameter data to the ISC in each calendar year since 1964.*

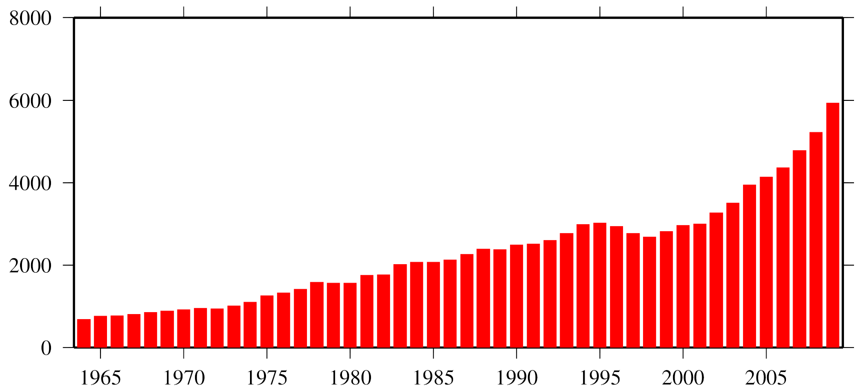

Figure 2.4: *The number of seismological stations that reported seismic phase arrival data to the ISC in each calendar year.*

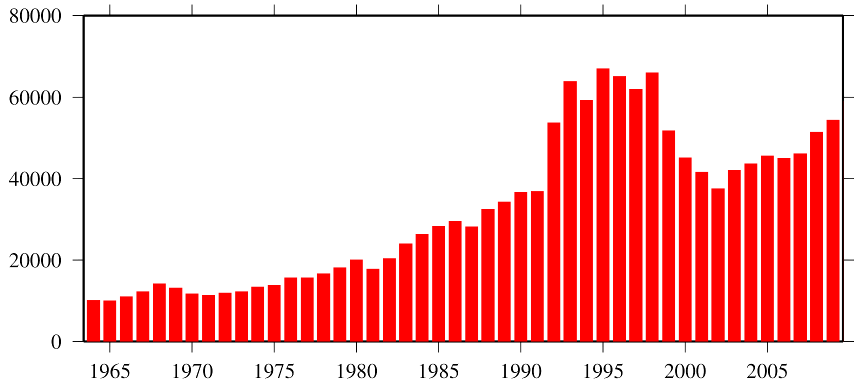

Figure 2.5: *The number of seismic events reviewed and printed by the ISC in each calendar year. A change in review procedures starting with year 1999 resulted in the noticeable although temporary dip in event numbers.*

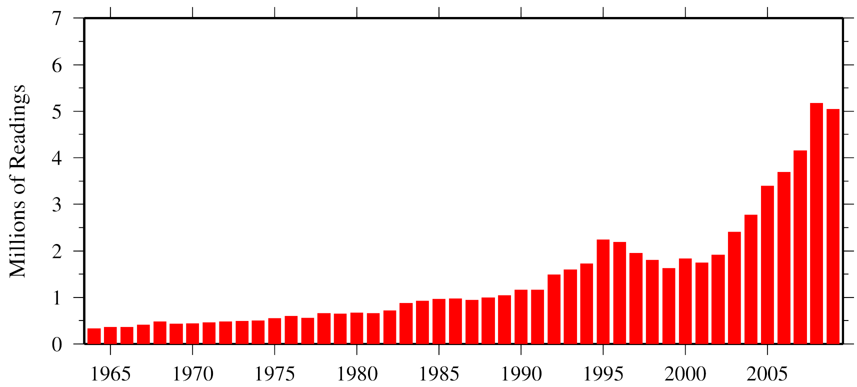

Figure 2.6: *The number of seismic event readings reviewed and printed by the ISC in each calendar year.*

perform for the geophysical community.

The first attempt to produce the ISC Bulletin was made under the supervision of the first ISC Director, Dr P.L. Willmore. This bulletin was found to have serious problems with its parameters of seismic events and was subsequently destroyed.

Hence, the ISC Executive Committee gave the job of producing the ISC Bulletin to Dr Edouard Arnold, who, with assistance from Slawomir J. Gibowicz put together the first ISC Bulletins in their final version. These bulletins (Figure 2.8, approximately A5 format) covering the data period 1964-1967 were typeset by Computaprint of London and printed by a jobbing printer, Smith & Ritchie, in Edinburgh, where the ISC resided at the time.

The annual ISC Bulletin at that time contained hypocentre parameters of approximately 10,000 seismic events reported by over 50 different agencies based on 220,000 readings reported by 700-800 seismic stations around the world.

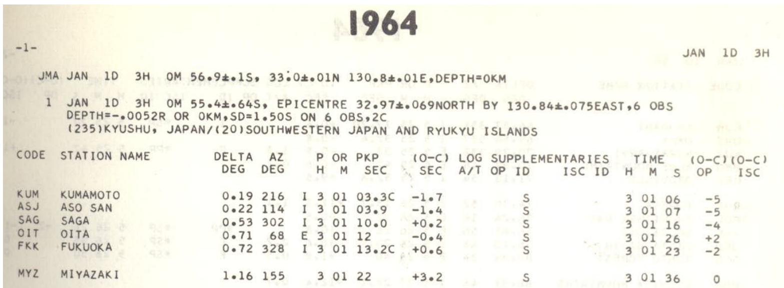
1964

-1-

JAN 1D 3H

JMA JAN 1D 3H OM 56.9±.1S, 33.0±.01N 130.8±.01E,DEPTH=OKM

1 JAN 1D 3H OM 55.4±.64S, EPICENTRE 32.97±.069NORTH BY 130.84±.075EAST,6 OBS
DEPTH=-.0052R OR OKM,SD=1.50S ON 6 OBS,2C
(235)KYUSHU, JAPAN/(20)SOUTHWESTERN JAPAN AND RYUKYU ISLANDS

CODE	STATION NAME	DELTA DEG	AZ DEG	P OR PKP H M SEC	(O-C) SEC	LOG A/T	SUPPLEMENTARIES OP ID	ISC ID	TIME H M S	(O-C) OP	(O-C) ISC
KUM	KUMAMOTO	0.19	216	I 3 01 03.3C	-1.7		S		3 01 06	-5	
ASJ	ASO SAN	0.22	114	I 3 01 03.9	-1.4		S		3 01 07	-5	
SAG	SAGA	0.53	302	I 3 01 10.0	+0.2		S		3 01 16	-4	
OIT	OITA	0.71	68	E 3 01 12	-0.4		S		3 01 26	+2	
FKK	FUKUOKA	0.72	328	I 3 01 13.2C	+0.6		S		3 01 23	-2	
MYZ	MIYAZAKI	1.16	155	3 01 22	+3.2		S		3 01 36	0	

Figure 2.7: *In the best traditions of Prof. John Milne, the first earthquake published by the ISC was a small event in Kyushu Island, Japan, with two hypocentre solutions authored by the Japan Meteorological Agency and the ISC.*

The ISC Bulletin contained a preface and introduction in English, a table of contributing agencies, a list of acceptable seismic phases and registered seismological observatories. Hypocentre parameters included depth computed as a fraction of the Earth radii. Magnitude estimates were infrequent and each station's information was contained on just one line. Notably, the first event published by the ISC was in Japan (Figure 2.7).

The need for keeping the costs down encouraged further development where the ISC Bulletin for 1968-1970 was typeset on a computer and printed by Kynoch Press in Birmingham (Figure 2.9).

The annual ISC Bulletin at that time contained hypocentre parameters of approximately 13,000 seismic events reported by 40-50 different agencies based on approximately 330,000 readings reported by 800-900 seismic stations around the world.

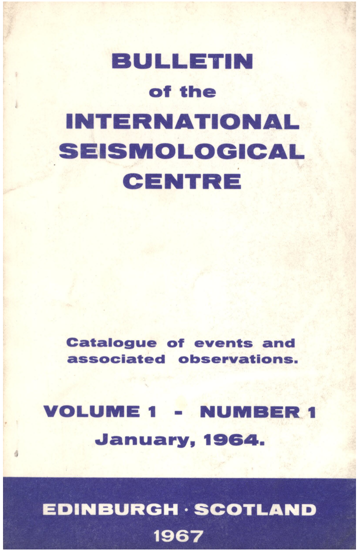

Figure 2.8: *Printed ISC Bulletin with the data of January 1964.*

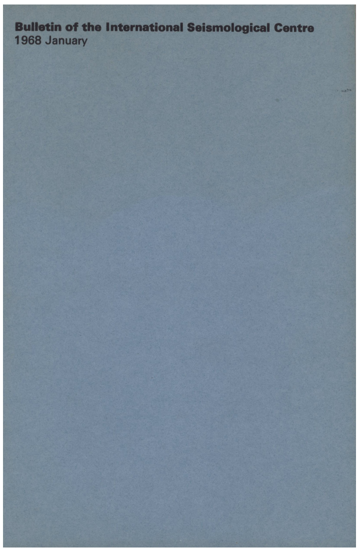

Figure 2.9: *Printed ISC Bulletin with the data of January 1968.*

From data year 1971 the ISC Bulletin gained its traditional ISC colours (red and white, Figure 2.10) and was printed in A4 format by Kynoch Press in Birmingham.

The format of the ISC Bulletin was changed considerably to better reflect parameters of hypocentres, particularly depth being measured in km. Secondary seismic arrivals were given further prominence. The ISC Bulletin had an introduction explaining the ISC operational procedures in three languages, English, French and Russian and acknowledgement of support from 26 Member Institutions as well as the list of seismic phases.

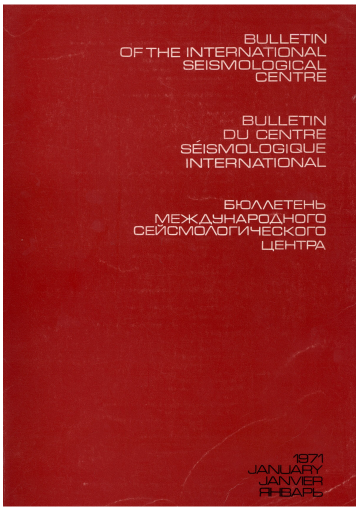

Figure 2.10: *Printed ISC Bulletin with the data of January 1971.*

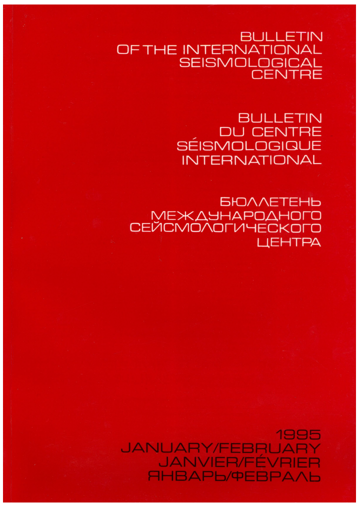

Figure 2.11: *Printed ISC Bulletin with the data of January/February 1995.*

Notably, it was then considered worthy to report, as part of an addendum, that a single station in France (SSB) has begun reporting observations to the ISC (currently there is an annual growth of 500 stations a year).

With the number of seismic stations and hence the number of reported events and station observations constantly growing, it was essential to keep the cost of printing under control. Hence, from data year 1972 the ISC Bulletin was printed by Thai Watana Panich Press Co Ltd in Bangkok, Thailand on thin bible paper.

Until October 1979 the typesetting of the ISC Bulletin was done by Kynoch Press, and thereafter by the ISC, using programs developed in-house to create Postscript and later PDF formats. Until the end of data year 1994, each issue contained one month's worth of seismic data.

Further changes to the ISC Bulletin were driven by the phenomenal growth in the number of seismic networks and reported data as well as by the constant desire to save on printing and distribution costs.

From data year 1993 seismic station observations were printed only for events of magnitude 5 and higher. This coincided with production of the first set of ISC-produced CD-ROMs containing all earthquakes with all station reports. Notably, the first CD-ROM containing ISC data (1964-August 1987) was produced by Gerald Dunphy at National Earthquake Information Center (NEIC/USGS) along with the user's guide explaining the structure of the Fixed Format Bulletin (FFB) files in great detail.

Figure 2.12: *Printed ISC Bulletin with the data of January through April 2002.*

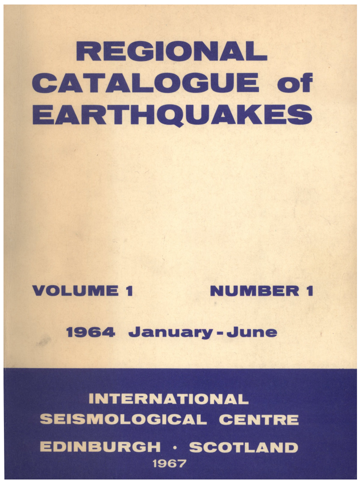

Figure 2.13: *Regional Catalogue of Earthquakes (1964-1970).*

From 1995, the ISC Bulletins became bi-monthly (Figure 2.11). At this point the annual ISC Bulletin contained hypocentre parameters of approximately 65,000 seismic events reported by ~80 different agencies based on the 1.5 million of seismic station readings reported by 3,000 seismic stations around the world.

From data year 1999, the ISC stopped the review of events with magnitude below ~3.5, allowing the attention of the ISC analysts to be given to earthquakes reported by several seismic networks. This explains the dip in the number of reviewed events on Figure 2.5. Thus the contents of the annual CD-ROM (all events) further deviated from the contents of the printed ISC Bulletin.

From 2002 printing of a four-monthly ISC Bulletin was done by Cambrian Printers in Aberwystwyth, Wales (Figure 2.12). The ISC Bulletin contained only hypocentre parameters and a CD-ROM with a full data set for four months attached to the back cover. Hence the ISC saved on printing over $1\frac{1}{4}$ million of seismic station readings per year, reported by over 3,200 seismic stations.

Printing of the hypocentre data continued in this way until the end of the data year 2009. By this time the annual ISC Bulletin contained hypocentre parameters of approximately 54,377 seismic events reported by 148 different agencies based on approximately 3.3 million of seismic station readings reported by 5,939 seismic stations around the world.

In parallel with the ISC Bulletin, two other complimentary publications were printed, the Regional Catalogue (Figure 2.13, data years 1964-1970 and Figure 2.14, data years 1971-2000) and Felt and Damaging Earthquakes (Figure 2.15, data years 1976-1990). These publicatons were useful at the time when a selection of the data for a region of interest or by event consequences was problematic due to the rarity of computers and databases. In addition, the Regional Catalogue was also a useful printed source of information on all seismic stations registered with the International Seismographic Station Registry (IR), jointly run by the ISC and the World Data Center for Seismology (Denver, USA).

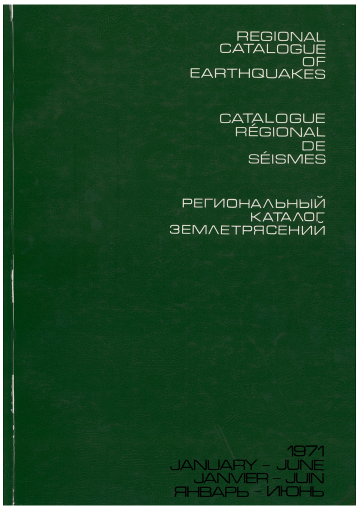

Figure 2.14: Regional Catalogue of Earthquakes (1971-2000).

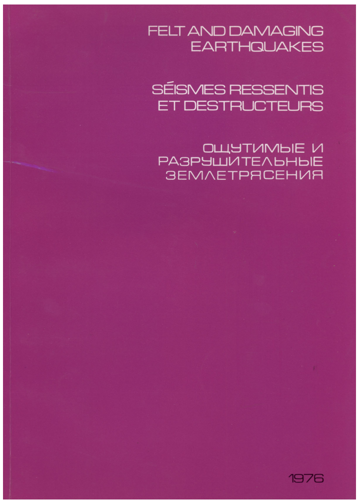

Figure 2.15: Felt and Damaging Earthquakes (1976-1990).

2.5 Member Institutions of the ISC

Article IV(a-b) of the ISC Working Statutes stipulates that any national academy, agency, scientific institution or other non-profit organisation may become a Member of the ISC on payment to the ISC of a sum equal to at least one unit of subscription and the nomination of a voting representative to serve on the ISC's governing body. Membership shall be effective for one year from the date of receipt at the ISC of the annual contribution of the Member and is thereafter renewable for periods of one year.

The ISC is currently supported with funding from its 58 Member Institutions and a four-year Grant Award EAR-0949072 from the US National Science Foundation.

Figures 2.16 and 2.17 show major sectors to which the ISC Member Institutions belong and proportional financial contributions that each of these sectors make towards the ISC's annual budget.

There follows a list of all current Member Institutions with a category (1 through 9) assigned according to the ISC Working Statutes. Each category relates to the number of membership units contributed.

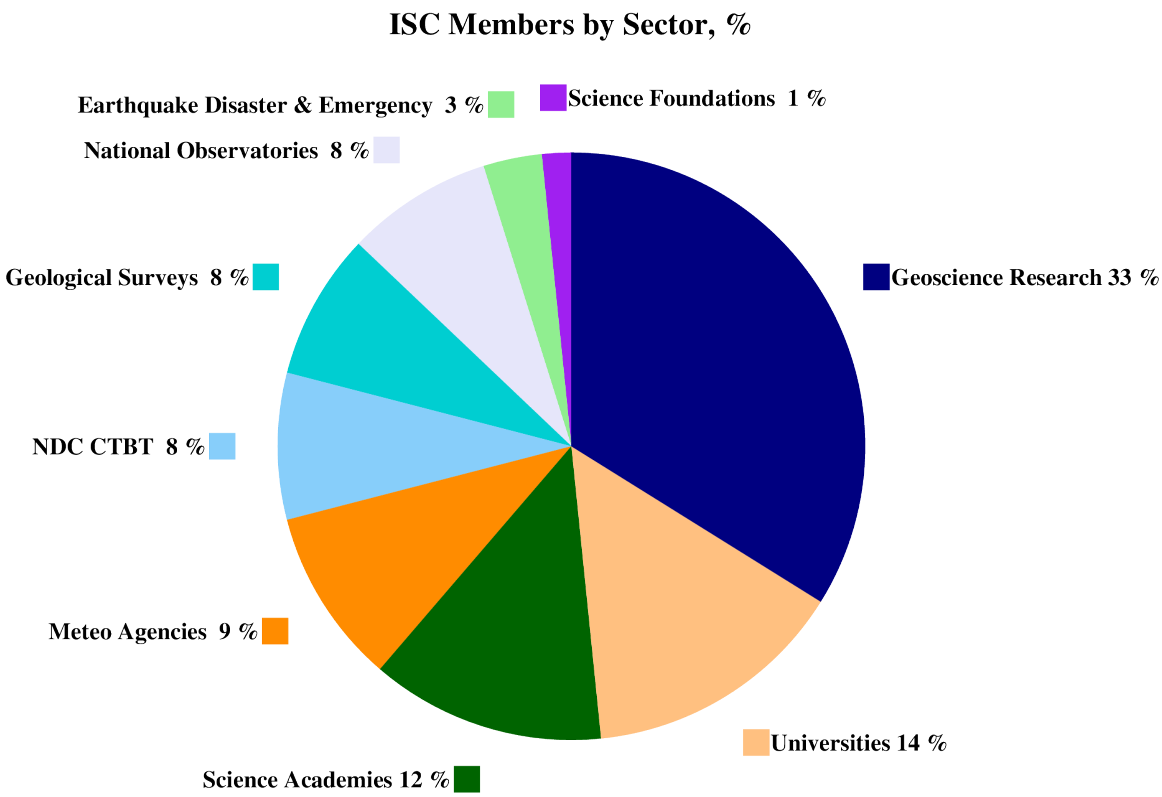

Figure 2.16: *Distribution of the ISC Member Institutions by sector in year 2012 as a percentage of total number of Members.*

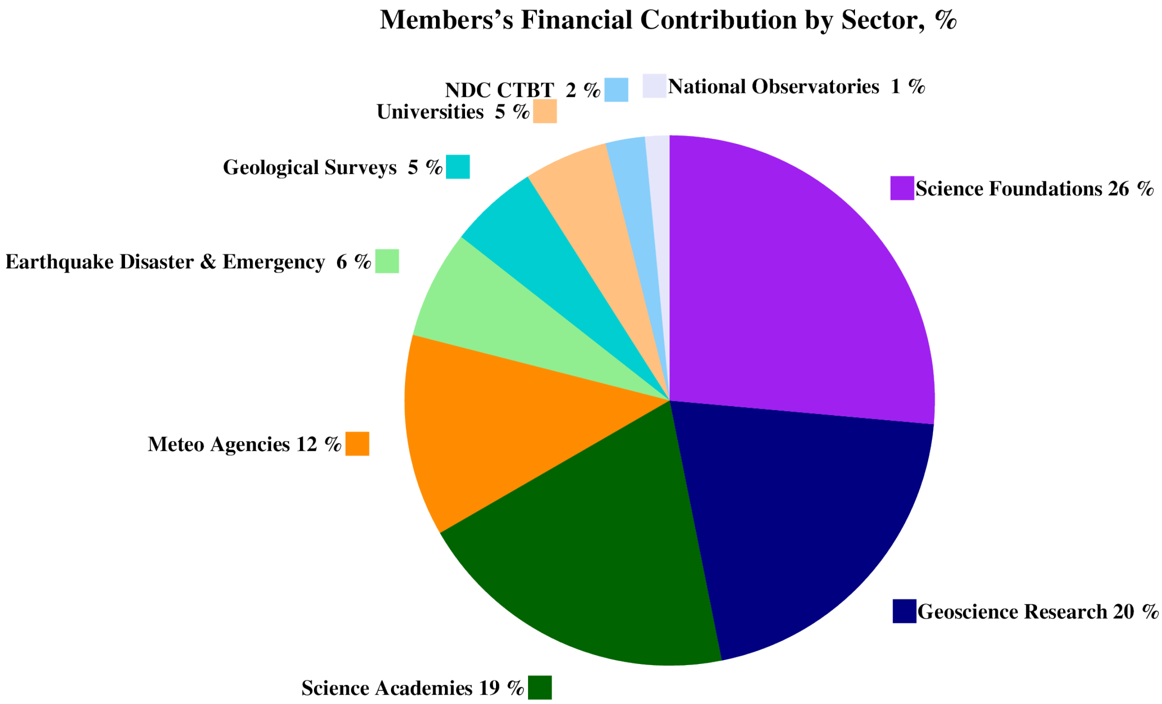

Figure 2.17: *Distribution of Member's financial contributions to the ISC by sector in year 2012 as a percentage of total annual Member contributions.*

Centre de Recherche en Astronomie, Astrophysique et Géophysique (CRAAG)
Algeria
www.craag.dz
Category: 1

Instituto Nacional de Prevención Sísmica (INPRES)
Argentina
www.inpres.gov.ar
Category: 1

Seismology Research Centre
Australia
www.seis.com.au
Category: 1

The University of Melbourne
Australia
www.unimelb.edu.au
Category: 1

Geoscience Australia
Australia
www.ga.gov.au
Category: 3

Bundesministerium für Wissenschaft und Forschung
Austria
www.bmbwk.gv.at
Category: 2

Centre of Geophysical Monitoring (CGM) of the National Academy of Sciences of Belarus
Belarus
www.cgm.org.by
Category: 1

Observatoire Royal de Belgique
Belgium
www.astro.oma.be
Category: 1

The Geological Survey of Canada
Canada
gsc.nrcan.gc.ca
Category: 4

China Earthquake Administration
China
www.gov.cn
Category: 5

Institute of Earth Sciences, Academia Sinica
Chinese Taipei
www.earth.sinica.edu.tw
Category: 1

Geological Survey Department
Cyprus
www.moa.gov.cy
Category: 1

Academy of Sciences of the Czech Republic
Czech Republic
www.cas.cz
Category: 2

Geological Survey of Denmark and Greenland - GEUS
Denmark
www.geus.dk
Category: 2

National Research Institute for Astronomy and Geophysics (NRIAG), Cairo
Egypt
www.nriag.sci.eg
Category: 1

The University of Helsinki
Finland
www.helsinki.fi
Category: 2

Laboratoire de Détection et de Géophysique / CEA
France
www-dase.cea.fr
Category: 2

Institut National des Sciences de l'Univers
France
www.insu.cnrs.fr
Category: 4

GeoForschungsZentrum Potsdam
Germany
www.gfz-potsdam.de
Category: 2

Bundesanstalt für Geowissenschaften und Rohstoffe
Germany
www.bgr.bund.de
Category: 4

The Seismological Institute, National Observatory of Athens
Greece
www.noa.gr
Category: 1

The Hungarian Academy of Sciences
Hungary
www.mta.hu
Category: 1

The Icelandic Meteorological Office
Iceland
www.vedur.is
Category: 1

India Meteorological Department
India
www.imd.ernet.in
Category: 4

Iraqi Seismic Network
Iraq
www.imos-tm.com
Category: 1

Dublin Institute for Advanced Studies
Ireland
www.dias.ie
Category: 1

Soreq Nuclear Research Centre (SNRC)
Israel
www.soreq.gov.il
Category: 1

The Geophysical Institute of Israel
Israel
www.gii.co.il
Category: 1

Istituto Nazionale di Geofisica e Vulcanologia
Italy
www.ingv.it
Category: 3

Istituto Nazionale di Oceanografia e di Geofisica Sperimentale
Italy
www.ogs.trieste.it
Category: 1

University of the West Indies
Jamaica
www.mona.uwi.edu
Category: 1

The Japan Meteorological Agency (JMA)
Japan
www.jma.go.jp
Category: 5

Japan Agency for Marine-Earth Science and Technology (JAMSTEC)
Japan
www.jamstec.go.jp
Category: 3

Earthquake Research Institute, University of Tokyo
Japan
www.eri.u-tokyo.ac.jp
Category: 3

Natural Resources Authority, Amman
Jordan
www.nra.gov.jo
Category: 1

Institute of Geophysics, National University of Mexico
Mexico
www.igeofcu.unam.mx
Category: 1

The Royal Netherlands Meteorological Institute
Netherlands
www.knmi.nl
Category: 2

Institute of Geological and Nuclear Sciences
New Zealand
www.gns.cri.nz
Category: 3

The University of Bergen
Norway
www.uib.no
Category: 2

Stiftelsen NORSAR
Norway
www.norsar.no
Category: 2

Institute of Geophysics, Polish Academy of Sciences
Poland
www.igf.edu.pl
Category: 1

The Institute for Meteorology
Portugal
www.meteo.pt
Category: 2

Red Sísmica de Puerto Rico
Puerto Rico
redsismica.uprm.edu
Category: 1

Korean Meterological Administration
Republic of Korea
www.kma.go.kr
Category: 1

National Institute for Earth Physics
Romania
www.infp.ro
Category: 1

Russian Academy of Sciences
Russia
www.ras.ru
Category: 5

Environmental Agency of Slovenia
Slovenia
www.arso.gov.si
Category: 1

Council for Geoscience
South Africa
www.geoscience.org.za
Category: 1

Instituto Geográfico Nacional
Spain
www.ign.es
Category: 3

National Defence Research Establishment
Sweden
www.foi.se
Category: 1

Uppsala Universitet
Sweden
www.uu.se
Category: 2

The Swiss Academy of Sciences
Switzerland
www.scnat.ch
Category: 2

University of the West Indies
Trinidad and Tobago
sta.uwi.edu
Category: 1

Kandilli Observatory and Earthquake Research Institute
Turkey
www.koeri.boun.edu.tr
Category: 1

Disaster and Emergency Management Presidency
Turkey
www.deprem.gov.tr
Category: 2

British Geological Survey
United Kingdom
www.bgs.ac.uk
Category: 2

AWE Blacknest
United Kingdom
www.blacknest.gov.uk
Category: 1

The Royal Society of London
United Kingdom
www.royalsociety.org
Category: 6

Incorporated Research Institutions for Seismology
U.S.A.
www.iris.edu
Category: 1

The National Science Foundation of the United States. (Grant No. EAR-0949072)
U.S.A.
www.nsf.gov
Category: 9

University of Texas at Austin
U.S.A.
www.utexas.edu
Category: 1

National Earthquake Information Center, U.S. Geological Survey
U.S.A.
www.neic.usgs.gov
Category: 2

In addition the ISC is currently in receipt of grants from the International Data Centre (IDC) of the Preparatory Commission of the Comprehensive Test Ban Treaty Organization (CTBTO), the Global Earthquake risk Model Foundation (GEM) and the International Union of Geodesy and Geophysics (IUGG).

2.6 Sponsoring Organisations

Article IV(c) of the ISC Working Statutes stipulates any commercial organisation with an interest in the objectives and/or output of the ISC may become an Associate Member of the ISC on payment of an Associate membership fee, but without entitlement to representation with a vote on the ISC's governing body.

www.reftek.com

REF TEK designs and manufactures application specific, high-performance, battery-operated, field-portable geophysical data acquisition devices for the global market. With over 35 years of experience, REF TEK provides customers with complete turnkey solutions that include high resolution recorders, broadband sensors, state-of-the-art communications (V-SAT, GPRS, etc), installation, training, and continued customer support. Over 7,000 REF TEK instruments are currently being used globally for multiple applications. From portable earthquake monitoring to telemetry earthquake monitoring, earthquake aftershock recording to structural monitoring and more, REF TEK equipment is suitable for a wide variety of application needs.

www.kinemetrics.com

Kinemetrics is a leader in earthquake instrumentation. For forty years, Kinemetrics has been creating products for monitoring earthquakes, volcanoes, tsunamis, and nuclear proliferation while helping society to understand these events on a global, regional and local scale. In addition the company has been creating products for monitoring civil structures, bridges, dams, and nuclear power plants as this monitoring provides important information about the structures' responses to natural or man-induced seismicity.

2.7 Data Contributing Agencies

In addition to its Members and Sponsors, the ISC owes its existence and successful long-term operations to its 126 seismic bulletin data contributors. These include government agencies responsible for national seismic networks, geoscience research institutions, geological surveys, meteorological agencies, universities, national data centres for monitoring the CTBT and individual observatories. There would be no ISC Bulletin available without the regular stream of data that are unselfishly and generously contributed to the ISC on a free basis.

The Institute of Seismology, Academy of Sciences of Albania
Albania
TIR

Centre de Recherche en Astronomie, Astrophysique et Géophysique
Algeria
CRAAG

Universidad Nacional de La Plata
Argentina
LPA

Instituto Nacional de Prevención Sísmica
Argentina
SJA

National Survey of Seismic Protection
Armenia
NSSP

Geoscience Australia
Australia
AUST

International Data Centre
Austria
IDC

Österreichischer Geophysikalischer Dienst
Austria
VIE

Republic Center of Seismic Survey
Azerbaijan
AZER

Centre of Geophysical Monitoring
Belarus
BELR

Royal Observatory of Belgium
Belgium
UCC

Instituto Astronomico e Geofísico
Brazil
VAO

Geophysical Institute, Bulgarian Academy of Sciences
Bulgaria
SOF

Canadian Hazards Information Service, Natural Resources Canada
Canada
OTT

Departamento de Geofísica, Universidad de Chile
Chile
GUC

China Earthquake Networks Center
China
BJI

Institute of Earth Sciences, Academia Sinica
Chinese Taipei
ASIES

Central American Seismic Center
Costa Rica
CASC

Seismological Survey of the Republic of Croatia
Croatia
ZAG

Servicio Sismológico Nacional Cubano
Cuba
SSNC

Cyprus Geological Survey Department
Cyprus
NIC

Geophysical Institute, Academy of Sciences of the Czech Republic
Czech Republic
PRU

West Bohemia Seismic Network
Czech Republic
WBNET

Geological Survey of Denmark and Greenland
Denmark
DNK

Observatoire Géophysique d'Arta
Djibouti
ARO

Servicio Nacional de Sismología y Vulcanología
Ecuador
IGQ

National Research Institute of Astronomy and Geophysics
Egypt
HLW

University of Addis Ababa
Ethiopia
AAE

Institute of Seismology, University of Helsinki
Finland
HEL

Centre Sismologique Euro-Méditerranéen
France
CSEM/EMSC

Institut de Physique du Globe
France
STR

Laboratoire de Détection et de Géophysique / CEA
France
LDG

Laboratoire de Géophysique / CEA
French Polynesia
PPT

Seismological Observatory Skopje
FYR Macedonia
SKO

Seismic Monitoring Centre of Georgia
Georgia
TIF

Geophysikalisches Observatorium Collm
Germany
CLL

Seismological Observatory Berggießhübel, TU Bergakademie Freiberg
Germany
BRG

Alfred Wegener Institute for Polar and Marine Research
Germany
AWI

Bundesanstalt für Geowissenschaften und Rohstoffe
Germany
BGR

Department of Geophysics, Aristotle University of Thessaloniki
Greece
THE

National Observatory of Athens
Greece
ATH

Hong Kong Observatory
Hong Kong
HKC

Geodetic and Geophysical Research Institute
Hungary
BUD

Icelandic Meteorological Office
Iceland
REY

National Geophysical Research Institute
India
HYB

India Meteorological Department
India
NDI

Badan Meteorologi, Klimatologi dan Geofisika
Indonesia
DJA

International Institute of Earthquake Engineering and Seismology (IIEES)
Iran
THR

Tehran University
Iran
TEH

Iraqi Meteorological and Seismology Organisation
Iraq
ISN

Dublin Institute for Advanced Studies
Ireland
DIAS

The Geophysical Institute of Israel
Israel
GII

Osservatorio Geofisico Sperimentale
Italy
TRI

Istituto Nazionale di Geofisica e Vulcanologia
Italy
ROM

Station Géophysique de Lamto
Ivory Coast
LIC

Jamaica Seismic Network
Jamaica
JSN

National Research Institute for Earth Science and Disaster Prevention
Japan
NIED

The Matsushiro Seismological Observatory
Japan
MAT

National Institute of Polar Research
Japan
SYO

Japan Meteorological Agency
Japan
JMA

Jordan Seismological Observatory
Jordan
JSO

National Nuclear Center
Kazakhstan
NNC

Kyrgyz Seismic Network
Kyrgyzstan
KNET

Institute of Seismology, Academy of Sciences of Kyrgyz Republic
Kyrgyzstan
KRNET

National Council for Scientific Research
Lebanon
GRAL

Geological Survey of Lithuania
Lithuania
LIT

Malaysian Meteorological Service
Malaysia
KLM

Instituto de Geofísica de la UNAM
Mexico
MEX

Red Sismica del Noroeste de Mexico (RESOM)
Mexico
ECX

Institute of Geophysics and Geology
Moldova
MOLD

Seismological Institute of Montenegro
Montenegro
PDG

Direccao Nacional de Geologia
Mozambique
MOZ

The Geological Survey of Namibia
Namibia
NAM

Department of Mines and Geology, Ministry of Industry of Nepal
Nepal
DMN

Koninklijk Nederlands Meteorologisch Instituut
Netherlands
DBN

IRD Centre de Nouméa
New Caledonia
NOU

Institute of Geological and Nuclear Sciences
New Zealand
WEL

University of Bergen
Norway
BER

Stiftelsen NORSAR
Norway
NAO

Sultan Qaboos University
Oman
OMAN

Micro Seismic Studies Programme, PINSTECH
Pakistan
MSSP

Philippine Institute of Volcanology and Seismology
Philippines
MAN

Manila Observatory
Philippines
QCP

Institute of Geophysics, Polish Academy of Sciences
Poland
WAR

Sistema de Vigilância Sismológica dos Açores
Portugal
SVSA

Instituto Geofisico do Infante Dom Luiz
Portugal
IGIL

Instituto Português do Mar e da Atmosfera, I.P.
Portugal
INMG

Korea Meteorological Administration
Republic of Korea
KMA

National Institute for Earth Physics
Romania
BUC

Yakutiya Regional Seismological Center, GS SB RAS
Russia
YARS

Kamchatkan Experimental and Methodical Seismological Department
Russia
KRSC

Baykal Regional Seismological Centre, GS SB RAS
Russia
BYKL

Sakhalin Experimental and Methodological Seismological Expedition, GS RAS
Russia
SKHL

Altai-Sayan Seismological Centre, GS SB RAS
Russia
ASRS

Kola Regional Seismic Centre, GS RAS
Russia
KOLA

Geophysical Survey of Russian Academy of Sciences
Russia
MOS

North Eastern Regional Seismological Centre, GS RAS
Russia
NERS

Saudi Geological Survey
Saudi Arabia
SGS

Seismological Survey of Serbia
Serbia
BEO

Geophysical Institute, Slovak Academy of Sciences
Slovakia
BRA

Environmental Agency of the Republic of Slovenia
Slovenia
LJU

Ministry of Mines, Energy and Rural Electrification
Solomon Islands
HNR

Council for Geoscience
South Africa
PRE

Instituto Geográfico Nacional
Spain
MDD

University of Uppsala
Sweden
UPP

Swiss Seismological Sevice (SED)
Switzerland
ZUR

National Syrian Seismological Center
Syria
NSSC

Thai Meteorological Department
Thailand
BKK

University of the West Indies
Trinidad and Tobago
TRN

Disaster and Emergency Management Presidency
Turkey
DDA

Kandilli Observatory and Research Institute
Turkey
ISK

Subbotin Institute of Geophysics, National Academy of Sciences
Ukraine
SIGU

Dubai Seismic Network
United Arab Emirates
DSN

British Geological Survey
United Kingdom
BGS

National Earthquake Information Center
U.S.A.
NEIC

Scripps Institution of Oceanography
U.S.A.
SIO

IRIS Data Management Center
U.S.A.
IRIS

The Global CMT Project
U.S.A.
GCMT

Pacific Northwest Seismic Network
U.S.A.
PNSN

Red Sísmica de Puerto Rico
U.S.A.
RSPR

United States Geological Survey
U.S.A.
USGS

Fundación Venezolana de Investigaciones Sismológicas
Venezuela
FUNV

National Center for Scientific Research
Vietnam
PLV

Yemen National Seismological Center
Yemen
DHMR

Goetz Observatory
Zimbabwe
BUL

CWB
Chinese Taipei
TAP

2.8 ISC Staff

Listed below are the staff (and their country of origin) who were employed at the ISC at the time of this ISC Bulletin Summary.

- Dmitry Storchak
- Director
- Russia/United Kingdom

- Maureen Aspinwall
- Administration Officer
- United Kingdom

- James Harris
- System and Database Administrator
- United Kingdom

- John Eve
- Data Collection Officer
- United Kingdom

- Emily Delahaye
- Seismologist/Lead Analyst
- Canada

- Elizabeth Robertson
- Seismologist/Analyst
- New Zealand

- Blessing Shumba
- Seismologist/Analyst
- Zimbabwe

- Rosemary Wylie
- Trainee Analyst
- United Kingdom

- István Bondár
- Senior Seismologist
- Hungary

- Wayne Richardson
- Senior Seismologist
- New Zealand

- Ben Dando
- Seismologist/Developer
- United Kingdom

- Domenico Di Giacomo
- Seismologist
- Italy

- Przemek Ozgo
- Junior System Administrator
- Poland

- Rebecca Verney
- Historical Data Entry Officer
- United Kingdom

- Natalia Safronova
- Historical Data Entry Officer
- Russia

3

ISC Operational Procedures

3.1 Introduction

The relational database at the ISC is the primary source for the ISC Bulletin. This database is also the source for the ISC web-based search, the ISC CD-ROMs and this printed Summary. The ISC database is also mirrored at several institutions such as the Data Management Center of the Incorporated Research Institutions for Seismology (IRIS DMC), Earthquake Research Institute (ERI) of the University of Tokyo and a few others.

The database holds information about ISC events, both natural and anthropogenic. Information on each event may include hypocentre estimates, moment tensors, event type, felt and damaging reports and associated station observations reported by different agencies and grouped together per physical event.

The majority of the ISC events (∼80%) are small and are not reviewed by the ISC analysts. Those that are reviewed (∼20%, usually magnitude greater than 3.5) may or may not include an ISC hypocentre solution and magnitude estimates. The decision depends on whether the wealth of combined information from several agencies as compared to the data of each single agency alone warrants the ISC location. The events are called ISC events regardless of whether they have been reviewed or located by the ISC or not.

All events located by the ISC are reviewed by the ISC analysts but not the other way round. Analyst review involves an examination of the integrity of all reported parametric information. It does not involve review of waveforms. Even if waveforms from all of the ∼6,000 stations included in a typical recent month of the ISC Bulletin were freely available, it would be an unmanageable task to inspect them all.

We shall now describe briefly current processes and procedures involved in producing the Bulletin of the International Seismological Centre. These have been developed from former practices described in the Introduction to earlier issues of the ISC Bulletin to account for modern methods and technologies of data collection and analysis.

3.2 Data Collection

Parametric data, mainly comprising seismic event hypocentre solutions, phase arrival observations and associated magnitude data, are now mostly emailed to the ISC (seismo@isc.ac.uk) by agencies around the world. Other macroseismic and source information associated with seismic events may also be incorporated in accordance with modern standards. The process of data collection at the ISC involves the automatic parsing of these data into the ISC relational database. The ISC now has over 200 individual parsers to account for legacy and current bulletin data formats used by data reporters.

Figure 3.1 shows the 304 agencies that have reported bulletin data to the ISC, directly or via regional data centres, during the entire period of the ISC existence: these agencies are also listed in Table 12.1 of the Appendix. In Figure 3.1, corresponding countries are shown shaded in red. Please note that the continent of Antarctica appears white on the map despite a steady stream of bulletin data from Antarctic stations: the agencies that run these stations are based elsewhere.

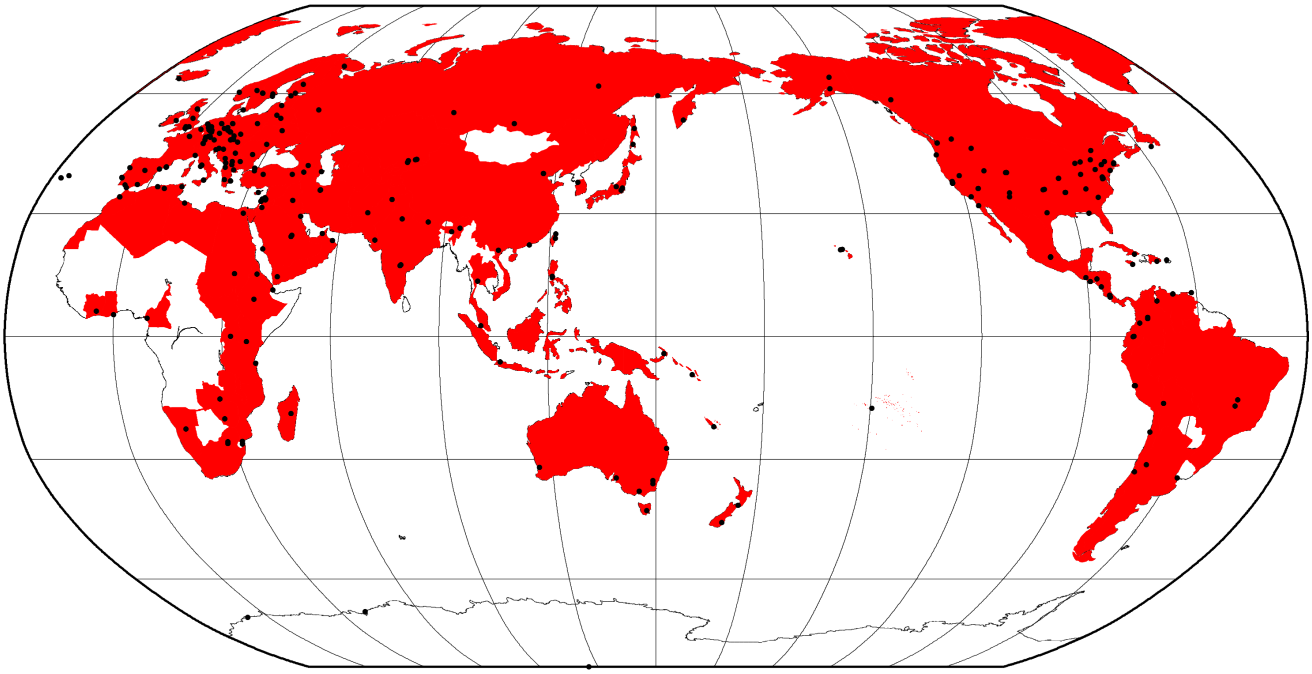

Figure 3.1: *Map of 304 agencies and corresponding countries that have reported seismic bulletin data to the ISC at least once during the entire period of the ISC operations, either directly or via regional data centres. Corresponding countries are shaded in red.*

3.3 ISC Automatic Procedures

3.3.1 Grouping

Grouping is the automatic process by which the many hypocentre solutions sent by the agencies reporting to the ISC for the same physical event are merged together into a single ISC event. This process possibly begins with an alert message and ends before a final review by ISC analysts. The process periodically runs through a set time interval of the input data stream, typically one day, looking for hypocentres in newly received data that are not yet grouped into an ISC event. Thus it considers only data more recent than the last data month reviewed by the ISC analysts. Immediately after grouping the seismic arrival associator is run on the same time interval, dealing with new phase arrival data not associated with any hypocentre.

The first stage of grouping gets a score where possible for each hypocentre to determine whether the reported hypocentre will be considered to be the primary estimate, or prime, for an ISC event. This score is based on the station arrival times reported in association with the hypocentre in four epicentral distance zones that characterise the networks of stations reporting:

1. Whole network
2. Local, 0 - 150 km
3. Near-regional, 3° - 10°
4. Teleseismic, 28° - 180°

For each distance zone, the azimuthal gap, the secondary azimuthal gap (the largest azimuthal gap filled by a single station), the minimum and maximum epicentral distance and number of stations are all used to calculate the value of dU, the normalised absolute deviation from best fitting uniformly distributed stations (*Bondár and McLaughlin*, 2009a). Clearly, this procedure can only use:

1. Bulletin data with hypocentres and sufficient associated seismic arrivals
2. Data for stations that are in the International Registry (IR)
3. Station data that are actually reported to ISC: CENC (China), for example, reports at most 24 stations, whilst many more may have been used to determine the hypocentre.

The hypocentres are then each considered in turn for grouping using one of two methods, the first by searching for a similar hypocentre, and the second by searching for the best fit of the reported phase arrival data that are associated with the candidate hypocentre. The method chosen for a reporter is based on feedback gained from ISC analysts.

For finding similar hypocentres, three sets of limits for origin-time difference and epicentral separation are used according to the type of bulletin data, be it alert, provisional or final: these limits are, respectively:

- ± 2 minutes and 10°
- ± 2 minutes and 4°
- ± 1 minutes and 2°

If there is no overlap with the hypocentre of an existing ISC event, a new event is formed. For each candidate hypocentre, a proximity score is otherwise calculated based on differences in time, t, and distance, s, between the candidate hypocentre and a hypocentre in an event with which it could potentially be grouped.

Proximity score $= 2 - (dt/dt_{max}) - (ds/ds_{max})$

where ds_{max} is the maximum distance between hypocentres and dt_{max} the maximum difference in origin time.

As long as there is no duplication of hypocentre (with the same author, origin time and location within tight limits) the candidate hypocentre together with the associated phase data is grouped with the prime hypocentre of the event and the initial dU score is used to reassess the prime hypocentre designation. Apparent duplicated hypocentre estimations, including preliminary solutions relayed by other agencies, need to be assessed to determine whether they should really be split between different events. Should there be two or more equally valid events, these can be assessed in turn and may eventually be merged together.

Grouping by fit of the associated phase arrival data is simpler. The residuals of the arrival data are calculated using ak135 travel times for all suitable prime hypocentres within the widest proximity limits given above for similar hypocentres. The hypocentre and associated phase arrival data is then grouped with the event with the best fitting prime hypocentre, which may similarly be re-designated according to the dU scores. Associations of phase arrival data are updated to be with the prime hypocentre estimate of each ISC event.

It follows that a hypocentre and associated phase arrival data submitted by a reporter will have the reported hypocentre set as the prime hypocentre in the ISC event if no other submitted hypocentre estimate is a closer match. It follows also that a hypocentre submitted without phase data can only be grouped with a similar hypocentre. Generally, early arriving data may be superseded by later arriving data: the data will still be in the ISC database but be deprecated, that is, marked as being no longer useful for further processes.

3.3.2 Association

Association is the automatic procedure, run routinely after grouping, that links reported phase arrivals at IR stations with the prime hypocentres of ISC events. As grouping took care of those phases associated with reported hypocentres, by associating the phases to the respective prime hypocentres of the ISC events without further checks, this procedure is only required for phase arrival observations that were sent without any association of event made for them by the reporter. Currently only 5% of arrival data is sent unassociated compared with 25% ten years ago.

If a phase arrival is found to be very similar to another already reported, it is placed in the same event, otherwise the procedure below is followed.

For associating a phase arrival, suitable events are sought with prime hypocentre origin-times in the window 40 minutes before and 100 s after the arrival time. For each phase arrival and prime hypocentre an ak135 travel-time residual is calculated for either the reported arrival phase name or an alternative from a default list if appropriate. Possible timing errors that are multiples of 60 s (a minute) are considered if the phase arrival is at a station not known to be digitally recording. A reporting likelihood is then determined based on the reported event magnitude: a magnitude default of 3.0 is used if no magnitude is given.

A final score is calculated from the residuals, from the likelihood of the phase observations for the magnitude of the event and from the S-P misfit. A phase arrival along with all other phase arrivals in that reading for the station is then associated with the prime hypocentre with the best score. If no suitable match is found, the reading remains unassociated but may be used at some later stage.

3.3.3 Thresholding

Thresholding is the process determining which events are to be reviewed by the ISC analysts. In former times, before email transmission of data was convenient, all events were reviewed, with magnitudes nearly always 3.5 or above. Nowadays, data contributors are encouraged to send all their data, which are stored in the ISC database. The overwhelming amount of data, including that for many more smaller events and from many more seismograph stations, led to the advent of ISC Comprehensive Bulletin, for all events, and the ISC Reviewed Bulletin, for selected events reviewed by ISC analysts. Thresholding has been under constant review since the start of the 1999 data year.

Several criteria are considered to decide which events merit review. Once a decision is made, whether or not an event is to be reviewed, further criteria are not considered.

In this section, M is the maximum magnitude reported by any agency for the event. The sequence of tests in the automatic decision process for reviewing events is currently:

- All events reported by the International Data Centre (IDC) of the Comprehensive Test Ban Treaty Organization (CTBTO) are reviewed.
- If M is greater than or equal to 3.5, the event is reviewed.
- If M is less than 2.5, the event is not reviewed.
- If M is unknown, the number of data sources of hypocentres and phase arrivals is used. Care is taken here to avoid counting indirect reports arriving via agencies such as NEIC, CSEM and CASC, which compile regional and global data:
  - If the number of hypocentre authors is greater than two and the maximum epicentral distance of arrival data is greater than 10°, the event is reviewed.
  - If the number of arrival authors is greater than two and the maximum epicentral distance of arrival data is greater than 10°, the event is reviewed.
  - Otherwise the event is not reviewed.
- If M is between 2.5 and 3.5:
  - If the number of hypocentre and seismic arrival authors is less than two, the event is not reviewed.
  - If any bulletin contributing to the event has at least ten stations within 3° and the secondary azimuthal gap (the largest azimuthal gap filled by a single station) is less than 135°, the event is not reviewed.

3.3.4 Location by the ISC

The automatic processes group and associate incoming data into ISC events as indicated above. These data are available to users before review by the ISC analysts but there will be no ISC hypocentre solutions for any of the events. The candidate events due for review by the ISC analysts are determined by the thresholding process, which is why many smaller events remain without an ISC hypocentre solution even after the analyst review.

Several further checks of the data are made in preparation for the analyst review, and initial trial estimates for ISC hypocentres are then generated using the accumulated data. If sufficiently robust, the ISC hypocentre estimation will be retained and be made the prime solution for the event, but this, of course, will itself be subject to the analyst review.

It is important to note that not all reviewed events will have an ISC hypocentre. For the reviewed events certain criteria must be met for an initial ISC location of an event to be made. These criteria are shown below:

- All events with an IDC hypocentre, unless IDC is the only hypocentre author and there are less than six associated phases.
- Two or more reporters of data
- Phase data at epicentral distance $\geq 20°$

The ISC locator also needs an intial seed location; in all events except those with eight or more reporters of data where the existing prime is used, this is calculated using a Neighbourhood Algorithm (NA) (*Sambridge*, 1999; *Sambridge and Kennett*, 2001). More information about the ISC location algorithm and initial seed is given in the next section.

3.4 ISC Location Algorithm

The new ISC location algorithm is described in detail in *Bondár and Storchak* (2011) (doi: 10.1111/j.1365-246X.2011.05107.x, Manual www.isc.ac.uk/iscbulletin/iscloc/); here we give a short summary of the major features. Ever since the ISC came into existence in 1964, it has been committed to providing a homogeneous bulletin that benefits scientific research. Hence the location algorithm used by the ISC, except for some minor modifications, has remained largely unchanged for the past 40 years (*Adams et al.*, 1982; *Bolt*, 1960). While the ISC location procedures have served the scientific community well in the past, they can certainly be improved.

Linearised location algorithms are very sensitive to the initial starting point for the location. The old procedures made the assumption that a good initial hypocentre is available among the reported hypocentres. However, there is no guarantee that any of the reported hypocentres are close to the global minimum in the search space. Furthermore, attempting to find a free-depth solution was futile when the data had no resolving power for depth (e.g. when the first arrival is not within the inflection point of the P travel-time curve). When there was no depth resolution, the algorithm would simply pick a point on the origin time – depth trade-off curve. The old ISC locator assumed that the observational errors are independent. The recent years have seen a phenomenal growth both in the number of reported events and phases, owing to the ever-increasing number of stations worldwide. Similar ray paths will produce correlated travel-time prediction errors due to unmodelled heterogeneities in the Earth, resulting in underestimated location uncertainties and for unfavourable network geometries, location bias. Hence, accounting for correlated travel-time prediction errors becomes imperative if we want to improve (or simply maintain) location accuracy as station networks become progressively denser. Finally, publishing network magnitudes that may have been derived from a single station measurement was rather prone to producing erroneous event magnitude estimates.

To meet the challenge imposed by the ever-increasing data volume from heavily unbalanced networks we introduced a new ISC location algorithm to ensure the efficient handling of data and to further improve the location accuracy of events reviewed by the ISC. The new ISC location algorithm

- Uses all ak135 (*Kennett et al.*, 1995) predicted phases (including depth phases) in the location;
- Obtains the initial hypocentre guess via the Neighbourhood Algorithm (NA) (*Sambridge*, 1999; *Sambridge and Kennett*, 2001);
- Performs iterative linearised inversion using an *a priori* estimate of the full data covariance matrix to account for correlated model errors (*Bondár and McLaughlin*, 2009b);
- Attempts a free-depth solution if and only if there is depth resolution, otherwise it fixes the depth to a region-dependent default depth;
- Scales uncertainties to 90% confidence level and calculates location quality metrics for various distance ranges;
- Obtains a depth-phase depth estimate based on reported surface reflections via depth-phase stacking (*Murphy and Barker*, 2006);
- Provides robust network magnitude estimates with uncertainties.

3.4.1 Seismic Phases

One of the major advantages of using the ak135 travel-time predictions (*Kennett et al.*, 1995) is that they do not suffer from the baseline difference between P, S and PKP phases compared with the Jeffreys-Bullen tables (*Jeffreys and Bullen*, 1940). Furthermore, ak135 offers an abundance of phases from the IASPEI Standard Seismic List (*Storchak et al.*, 2003; 2011) that can be used in the location, most notably the PKP branches and depth-sensitive phases. Elevation and ellipticity corrections (*Dziewonski and Gilbert*, 1976; *Engdahl et al.*, 1998; *Kennett et al.*, 1996), using the WG84 ellipsoid parameters, are added to the ak135 predictions. For depth phases, bounce point (elevation correction at the surface reflection point) and water depth (for pwP) corrections are calculated using the algorithm of *Engdahl et al.* (1998). We use the ETOPO1 global relief model (*Amante and Eakins*, 2009) to obtain the elevation or the water depth at the bounce point.

Phase picking errors are described by *a priori* measurement error estimates derived from the inspection of the distribution of ground truth residuals (residuals calculated with respect to the ground truth location) from the IASPEI Reference Event List (*Bondár and McLaughlin*, 2009a). For phases that do not have a sufficient number of observations in the ground truth database we establish *a priori* measurement errors so that the consistency of the relative weighting schema is maintained. First-arriving P-type phases (P, Pn, Pb, Pg) are picked more accurately than later phases, so their measurement error estimates are the smallest, 0.8 s. The measurement error for first-arriving S-phases (S, Sn, Sb, Sg) is set to 1.5 s. Phases traversing through or reflecting from the inner/outer core of the Earth have somewhat larger (1.3 s for PKP, PKS, PKKP, PKKS and P'P' branches as well as PKiKP, PcP and PcS, and 1.8 s for SKP, SKS, SKKP, SKKS and S'S' branches as well as SKiKP, ScP and ScS) measurement error estimates to account for possible identification errors among the various branches. Free-surface reflections and conversions (PnPn, PbPb, PgPg, PS, PnS, PgS and SnSn, SbSb, SgSg, SP, SPn, SPg) are observed less frequently and with larger uncertainty, and therefore suffer from large, 2.5 s, measurement errors. Similarly, a measurement error of 2.8 s is assigned to the longer period and typically emergent diffracted phases (Pdif, Sdif, PKPdif). The *a priori* measurement error for the commonly observed depth phases (pP, sP, pS, sS and pwP) is set to 1.3 s, while the remaining depth phases (pPKP, sPKP, pSKS, sSKS branches and pPb, sPb, sSb, pPn, sPn, sSn) have the measurement error estimate set to 1.8 s. We set the measurement error estimate to 2.5 s for the less reliable depth phases (pPg, sPg, sSg, pPdif, pSdif, sPdif and sSdif). Note that we also allow for distance-dependent measurement errors. For instance, to account for possible phase identification errors at far-regional distances the *a priori* measurement error for Pn and P is increased from 0.8 s to 1.2 s and for Sn and S from 1.5 s to 1.8 s between 15° and 28°. The measurement errors between 40° and 180° are set to 1.3 s and 1.8 s for the prominent PP and SS arrivals respectively, but they are increased to 1.8 s and 2.5 s between 25° and 40°.

The relative weighting scheme (Figure 3.2) described above ensures that arrivals picked less reliably or prone to phase identification errors are down-weighted in the location algorithm. Since the ISC works with reported parametric data with wildly varying quality, we opted for a rather conservative set of *a priori* measurement error estimates.

3.4.2 Correlated travel-time prediction error structure

Most location algorithms, either linearised or non-linear, assume that all observational errors are independent. This assumption is violated when the separation between stations is less than the scale length of local velocity heterogeneities. When correlated travel-time prediction errors are present, the data covariance matrix is no longer diagonal, and the redundancy in the observations reduces the effective number of degrees of freedom. Thus, ignoring the correlated error structure inevitably results in underestimated location uncertainty estimates. For events located by an unbalanced seismic network this may also lead to a biased location estimate. *Chang et al.* (1983) demonstrated that accounting for correlated error structure in a linearised location algorithm is relatively straightforward once an estimate of the non-diagonal data covariance matrix is available. To determine the data covariance matrix we follow the approach described by *Bondár and McLaughlin* (2009b). They assume that the similarity between ray paths is well approximated by the station separation. This simplifying assumption allows for the estimation of covariances between station pairs from a generic P variogram model derived from ground truth residuals. Because the overwhelming number of phases in the ISC Bulletin is teleseismic P, we expect that the generic variogram model will perform reasonably well anywhere on the globe.

Since in this representation the covariances depend only on station separations, the covariance matrix (and its inverse) needs to be calculated only once. We assume that different phases owing to the different ray paths they travel along as well as station pairs with a separation larger than 1000 km are uncorrelated. Hence, the data covariance matrix is a sparse, block-diagonal matrix. Furthermore, if the stations in

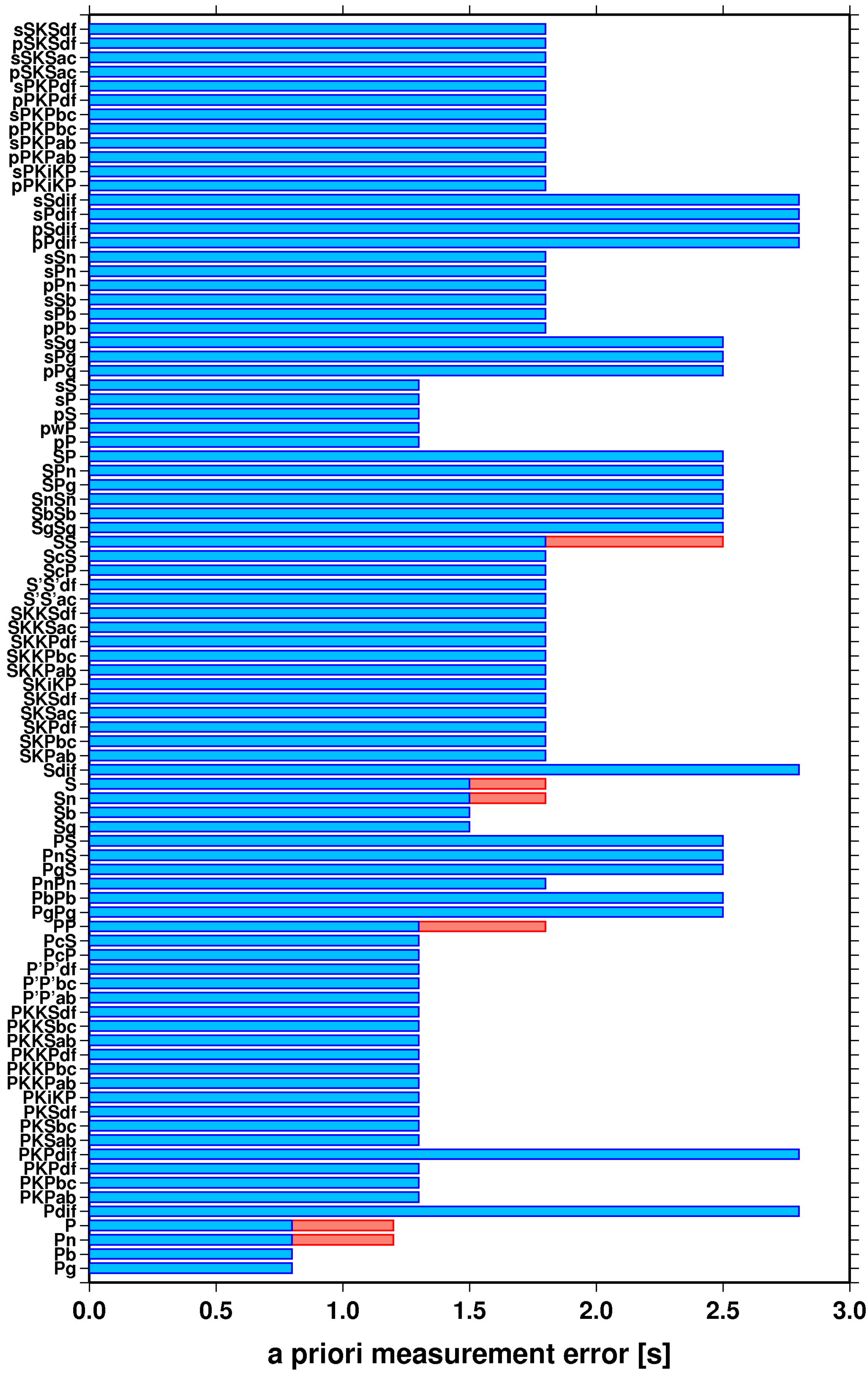

Figure 3.2: A priori *measurement error estimates for phases used in the location algorithm. The red coloured errors are distance-dependent, which are applied for distances when phase identification errors may occur (see text).*

each phase block are ordered by their nearest neighbour distance, the phase blocks themselves become block-diagonal. To reduce the computational time of inverting large matrices we exploit the inherent block-diagonal structure by inverting the covariance matrix block-by-block. The *a priori* measurement error variances are added to the diagonal of the data covariance matrix.

3.4.3 Depth resolution

In principle, depth can be resolved if there is a mixture of upgoing and downgoing waves emanating from the source, that is, if there are stations covering the distance range where the vertical partial derivative of the travel-time of the first-arriving phase changes sign (local networks), or if there are phases with vertical slowness of opposite sign (depth phases). Core reflections, such as PcP, and to a lesser extent, secondary phases (S in particular) could also help in resolving the depth.

We developed a number of criteria to test whether the reported data for an event have sufficient depth resolution:

- local network: one or more stations within 0.2° with time-defining phases
- depth phases: five or more time-defining depth phases reported by at least two agencies (to reduce a chance of misinterpretation by a single inexperienced analyst)
- core reflections: five or more time-defining core reflections (PcP, ScS) reported by at least two agencies
- local/near regional S: five or more time-defining S and P pairs within 3°

We attempt a free-depth solution if any of the above criteria are satisfied; otherwise we fix the depth to a default depth dependent on the epicentre location. The default depth grid was derived from the EHB (*Engdahl et al.*, 1998) free-depth solutions, including the fixed-depth EHB earthquakes that were flagged as having reliable depth estimate (personal communication with Bob Engdahl), as well as from free-depth solutions obtained by the new locator when locating the entire ISC Bulletin data-set. As Figure 3.3 indicates, the default depth grid provides a reasonable depth estimate where seismicity is well established. Note that the depths of known anthropogenic events and landslides are fixed to the surface.

3.4.4 Depth-phase stack

While we use depth phases directly in the location, the depth-phase stacking method (*Murphy and Barker*, 2006) provides an independent means to obtain robust depth estimates. Because the depth obtained from the depth-phase stacking method implicitly depends on the epicentre itself, we perform the depth-phase stack only twice: first, with respect to the initial location in order to obtain a reasonable starting point for the depth in the grid search described in the following section; second, with respect to the final location to obtain the final estimate for the depth-phase constrained depth.

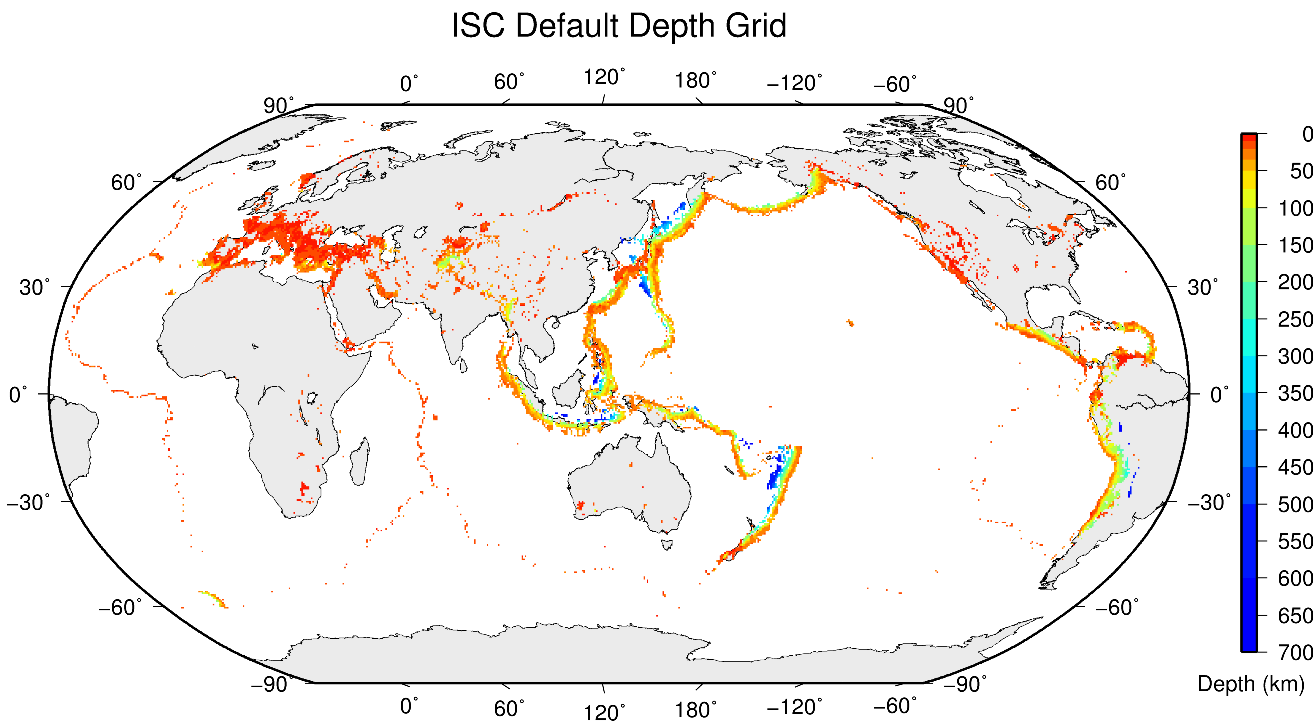

Figure 3.3: *Default depths on a 0.5×0.5 degree grid derived from EHB free-depth solutions and EHB events flagged as reliable depth, as well as free-depth solutions from the entire ISC Bulletin located with the new locator.*

3.4.5 Initial hypocentre

For poorly recorded events the reported hypocentres may exhibit a large scatter and they could suffer from large location errors, especially if they are only recorded teleseismically. In order to obtain a good initial hypocentre guess for the linearised location algorithm we employ the Neighbourhood Algorithm (NA) (*Sambridge*, 1999; *Sambridge and Kennett*, 2001). NA is a nonlinear grid search method capable of exploring a large search space and rapidly closing in on the global optimum. *Kennett* (2006) discusses in detail the NA algorithm and its use for locating earthquakes.

We perform a search around the median of reported hypocentre parameters with a generously defined search region – within a 2° radius circle around the median epicentre, 10 s around the median origin time and 150 km around the median reported depth. These default search parameters were obtained by trial-and-error runs to achieve a compromise between execution time and allowance for gross errors in the median reported hypocentre parameters. Note that if our test for depth resolution fails, we fix the depth to the region-dependent default depth. The initial hypocentre estimate will be the one with the smallest L1-norm misfit among the NA trial hypocentres. Once close to the global optimum, we proceed with the linearised location algorithm to obtain the final solution and corresponding formal uncertainties.

3.4.6 Iterative linearised location algorithm

We adopt the location algorithm described in detail in *Bondár and McLaughlin* (2009b). Recall that in the presence of correlated travel-time prediction errors the data covariance matrix is no longer diagonal.

Using the singular value decomposition of the data covariance matrix we construct a projection matrix that orthogonalises the data set and projects redundant observations into the null space. In other words, we solve the inversion problem in the eigen coordinate system in which the transformed observations are independent.

The model covariance matrix yields the four-dimensional error ellipsoid whose projections provide the two-dimensional error ellipse and one-dimensional errors for depth and origin time. These uncertainties are scaled to the 90% confidence level. Note that since we projected the system of equations into the eigen coordinate system, the number of independent observations is less than the total number of observations. Hence, the estimated location error ellipses necessarily become larger, providing a more realistic representation of the location uncertainties. The major advantage of this approach is that the projection matrix is calculated only once for each event location.

3.4.7 Validation tests

To demonstrate improvements due to the new location procedures, we located some 7,200 GT0-5 events in the IASPEI Reference Event List (*Bondár and McLaughlin*, 2009a) both with the old ISC locator (which constitutes the baseline) and with the new location algorithm. We also located the entire (1960-2010) ISC Bulletin, including four years of the International Seismological Summary (ISS, the predecessor of the ISC) catalogue (*Villaseñor and Engdahl*, 2005; 2007).

The location of GT events demonstrated that the new ISC location algorithm provides small but consistent location improvements, considerable improvements in depth determination and significantly more accurate formal uncertainty estimates. Even using a 1-D model and a variogram model that fits teleseismic observations we could achieve realistic uncertainty estimates, as the 90% confidence error ellipses cover the true locations 80-85% of the time. The default depth grid provides reasonable depth estimates where there is seismicity. We have shown that the location and depth accuracy obtained by the new algorithm matches or surpasses the EHB accuracy.

We noted above that the location improvements for the ground truth events are consistent, but minor. This is not surprising as most of the events in the IASPEI Reference Event List are very well-recorded with a small azimuthal gap and dominated by P-type phases. In these circumstances we could expect significant location improvements only for heavily unbalanced networks where large numbers of correlated ray paths conspire to introduce location bias. On the other hand, the ISC Bulletin represents a plethora of station configurations ranging from reasonable to the most unfavourable network geometries. Hence, we could expect more dramatic location improvements when locating the entire ISC Bulletin. Although in this case we cannot measure the improvement in location accuracy due to the lack of ground truth information, we show that with the new locator we obtain significantly better clustering of event locations (Figure 3.4), thus providing an improved view of the seismicity of the Earth.

3.4.8 Magnitude calculation

Currently the ISC locator calculates body and surface wave magnitudes. MS is calculated for shallow events (depth $<$ 60 km) only. At least three station magnitudes are required for a network (mb or

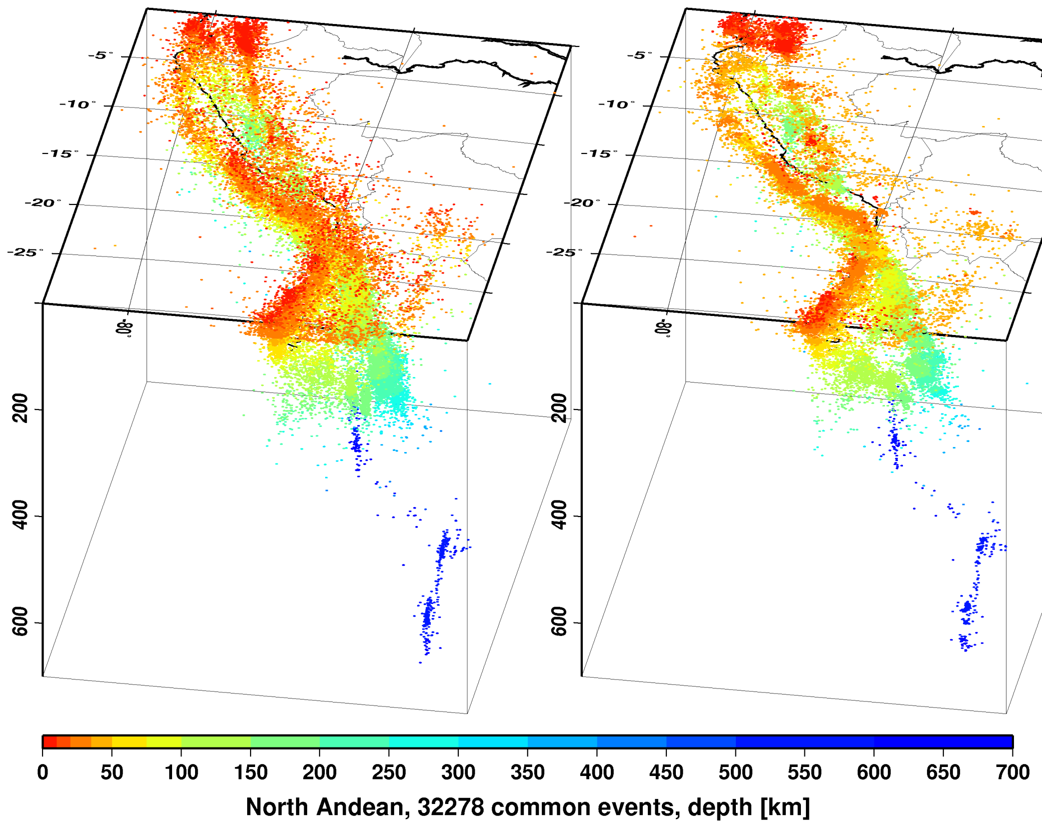

(a)

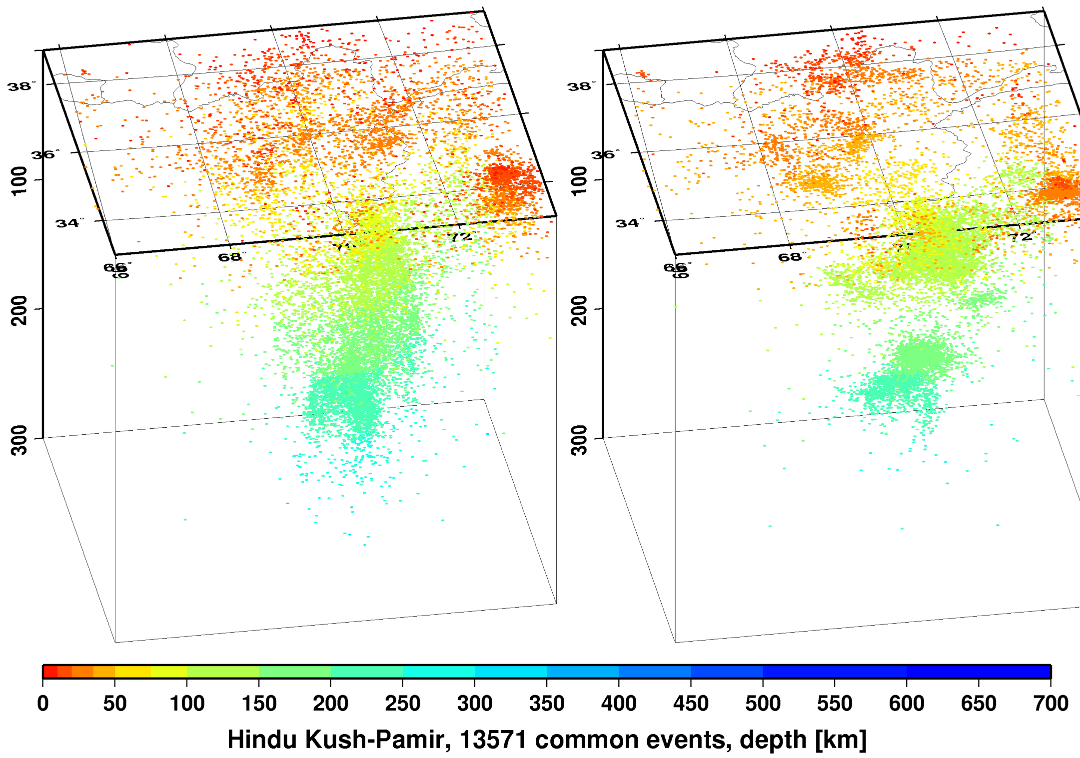

(b)

Figure 3.4: *Comparison of seismicity maps for common events in the reviewed ISC Bulletin (old locator, left) and the located ISC Bulletin (new locator, right) for the North Andean (a) and Hindu Kush - Pamir regions (b). The events are better clustered when located with the new locator.*

MS) magnitude. The network magnitude is defined as the median of the station magnitudes, and its uncertainty is defined as the standard median absolute deviation (SMAD) of the alpha-trimmed (*alpha* = 20%) station magnitudes.

The station magnitude is defined as the median of reading magnitudes for a station. The reading magnitude is defined as the magnitude computed from the maximal log(A/T) in a reading. Amplitude magnitudes are calculated for each reported amplitude-period pair.

3.4.9 Body-wave magnitudes

Body-wave magnitudes are calculated for each reported amplitude-period pair, provided that the phase is in the list of phases that can contribute to mb (P, pP, sP, AMB, IAmb, pmax), the station is between the epicentral distances 21 – 100° and the period is less than 3 s.

A reading contains all parametric data reported by a single agency for an event at a station, and it may have several reported amplitude and periods. The amplitudes are measured as zero-to-peak values in nanometres. For each pair an amplitude mb is calculated.

$$mb_{amp} = log(A/T) + Q(\Delta, h) - 3 \tag{3.1}$$

If no amplitude-period pairs are reported for a reading, the body-wave magnitude is calculated using the reported logat values for $log(A/T)$.

$$mb_{amp} = logat + Q(\Delta, h) - 3 \tag{3.2}$$

where the magnitude attenuation $Q(\Delta, h)$ value is calculated using the Gutenberg-Richter tables (*Gutenberg and Richter*, 1956).

For each reading the ISC locator finds the reported amplitude-period pair for which A/T is maximal:

$$mb_{rd} = log(max(A/T)) + Q(\Delta, h) - 3 \tag{3.3}$$

Or, if no amplitude-period pairs were reported for the reading:

$$mb_{rd} = max(logat) + Q(\Delta, h) - 3 \tag{3.4}$$

Several agencies may report data from the same station. The station magnitude is defined as the median of the reading magnitudes for a station.

$$mb_{sta} = median(mb_{rd}) \tag{3.5}$$

Once all station mb values are determined, the station magnitudes are sorted and the lower and upper alpha percentiles are made non-defining. The network mb and its uncertainty are then calculated as the median and the standard median absolute deviation (SMAD) of the alpha-trimmed station magnitudes, respectively.

3.4.10 Surface-wave magnitudes

Surface-wave magnitudes are calculated for each reported amplitude-period pair, provided that the phase is in the list of phases that can contribute to MS (*AMS, IAMs_20, LR, MLR, M, L*), the station is between the epicentral distances $20 - 160°$ and the period is between $10 - 60$ s.

For each reported amplitude-period pair MS is calculated using the Prague formula (*Vaněk et al.*, 1962). Amplitude MS is calculated for each component (Z, E, N) separately.

$$MS_{amp} = log(A/T) + 1.66 * log(\Delta) + 0.3 \tag{3.6}$$

To calculate the reading MS, the ISC locator first finds the reported amplitude-period pair for which A/T is maximal on the vertical component.

$$MS_Z = log(max(A_Z/T_Z)) + 1.66 * log(\Delta) + 0.3 \tag{3.7}$$

Then it finds the max(A/T) for the E and N components for which the period measured on the horizontal components is within ±5s from the period measured on the vertical component.

$$MS_E = log(max(A_E/T_E)) + 1.66 * log(\Delta) + 0.3 \tag{3.8}$$

$$MS_N = log(max(A_N/T_N)) + 1.66 * log(\Delta) + 0.3 \tag{3.9}$$

The horizontal MS is calculated as

$$max(A/T)h = \begin{cases} \sqrt{2(max(A_E/T_E))^2} & \text{if } MS_N \text{ does not exist} \\ \sqrt{(max(A_E/T_E))^2 + (max(A_N/T_N))^2} & \text{if } MS_E \text{ and } MS_N \text{ exist} \\ \sqrt{2(max(A_N/T_N))^2} & \text{if } MS_E \text{ does not exist} \end{cases} \tag{3.10}$$

$$MS_H = log(max(A/T)_H) + 1.66 * log(\Delta) + 0.3 \tag{3.11}$$

The reading MS is defined as

$$MS = \begin{cases} (MS_Z + MS_H)/2 & \text{if } MS_Z \text{ and } MS_H \text{ exist} \\ MS_H & \text{if } MS_Z \text{ does not exist} \\ MS_Z & \text{if } MS_H \text{ does not exist} \end{cases} \tag{3.12}$$

Several agencies may report data from the same station. The station magnitude is defined as the median of the reading magnitudes for a station.

$$MS_{sta} = median(MS_{rd}) \tag{3.13}$$

Once all station MS values are determined, the station magnitudes are sorted and the lower and upper alpha percentiles are made non-defining. The network MS and its uncertainty are calculated as the median and the standard median absolute deviation (SMAD) of the alpha-trimmed station magnitudes, respectively.

3.5 Review Process

Typically, for each month, the ISC analysts now review approximately 20% of the events in the ISC database, currently 3,500-5,000 per data month. This review is done about 24 months behind real time to allow for the comprehensive collection of data from networks and data centres worldwide.

Users of the ISC Bulletin can be assured that all ISC Bulletin events with an ISC hypocentre solution have been reviewed by the ISC analysts. Not all reviewed events will end up having an ISC hypocentre solution, but events that have not been reviewed are flagged accordingly.

An automatic process creates a monthly listing of the events for the analysts to review. The analysis is performed in batches: thus, events are generally not finalised one at a time, and a completed month of events is published after all the analysis is finished.

The first batch of editing involves careful examination of all events selected for review for the month. The entire month is then reprocessed incorporating the editing changes deemed necessary by the analysts. The analysts next review the same events again in a second pass through the data, checking for each event where there is a change that the result was as could be expected by comparing the revised solution against the initial solution. When the analysts are satisfied with an event, it is no longer revised in a subsequent pass but analysis continues in several passes until all events are considered satisfactory.

The analysts initially print the entire monthly listing, which is split into sections each with about 150 events. Each event, uniquely identified in the monthly printout, shows the reported hypocentres, magnitudes and phase arrivals grouped and associated for the event, as well as an ISC solution of hypocentre, if there is one, along with quality metrics, error estimates, redetermined magnitudes and phase arrival-time residuals. Ancillary information including the geographic region and reported macroseismic observations is also present in the listing for each pass.

The analysts have the capability to execute a variety of commands that can be used to merge or split events, to move phase arrivals or hypocentres from one event to another or to modify the reported phase names. Each of these changes initiates a new revision of the relevant events and ISC hypocentre solutions. There are also several commands to change the starting depth or location in the location algorithm.

The main tasks in reviewing the ISC Bulletin are to:

1. Check that the grouping of hypocentres and association of phase arrivals is appropriate.
2. Check that the depth and location is appropriate for the region and reported phase arrivals.

3. Check that no data are missing for an event, given the region and magnitude, and that included data are appropriate.

4. Examine the phase arrival-time residuals to check that the ISC hypocentre solution is appropriate.

5. Look for outliers in the observations and for misassociated phases.

As well as examining each event closely, it is also important to scan the hypocentres and phase arrivals of adjacent events, close in time and space, to ensure that there is uniformity in the composition of the events. In some cases, two events should be merged into one event, as apparent in some other case. In other cases, one apparent event needs to be split into two events, when the automatic grouping has erroneously created one event with more than one reported hypocentre out of the observations for two real events that are distinct but closely occurring.

Misassociated phase arrivals are returned to the unassociated data stream, if not immediately placed by the analyst in another event where they belong, These unassociated phases are then available to be associated with some other event if the time and location is appropriate. The analysts also check that no phase is associated to more than one event.

Towards the end of the monthly analysis, the ISC 'Search' procedure runs, attempting to build events from the remaining set of unassociated phase arrivals. The algorithm is based on the methodology of *Engdahl and Gunst* (1966). Candidate events are validated or rejected by attempting to find ISC hypocentres for them using the ISC locator. The surviving events are then reviewed. Those events with phase arrival observations reported by stations from at least two networks are added to the ISC Bulletin if the solutions meet the standards set by the ISC analysts. These events have only an ISC determination of hypocentre.

At the end of analysis for a data month, a set of final checks is run for quality control, with the results reviewed by an analyst and the defects rectified. These are checks for inconsistencies and errors to ensure the general integrity of the ISC Bulletin.

3.6 History of Operational Changes

- From data-month January 2001 onwards, both P and S groups of arrival times are used in location.

- From data-month September 2002 onwards, the printed ISC Bulletins have been generated directly from the ISC Relational Database.

- From data-month October 2002, a new location program ISCloc has been used in operations. Also, the IASPEI standard phase list has now been adopted by the ISC. Please see Section 6.1 for details.

- From data-month January 2003 onwards, an updated regionalisation scheme has been adopted (*Young et al.*, 1996).

- From data-month January 2006 the ISC hypocentres are computed using the *ak135* earth velocity model (*Kennett et al.*, 1995) and then reviewed by ISC seismologists. The ISC still produces the hypocentre solutions based on Jeffreys-Bullen travel time tables (agency code ISCJB), yet these solutions are no longer reviewed.

The ISC is planning to re-compute the entire ISC dataset using *ak135* once new procedures for the rebuild are designed, tested, discussed and approved by the ISC Governing Council. Until that time the automatic ISCJB locations will continue to be produced alongside the *ak135* solutions to maintain the long-time continuity of the ISC Bulletin.

- From data-month January 2009, a new location program (*Bondár and Storchak*, 2011) has been used in operations. The new program uses all predicted *ak135* phases and accounts for correlated model errors. An overview of the location algorithm is provided in this volume (Section 3.4).

4

Availability of the ISC Bulletin

The ISC Bulletin is available from the following sources:

- Web searches
  The entire ISC Bulletin is available directly from the ISC website via a number of searches.
  (www.isc.ac.uk/iscbulletin/search)
  (isc-mirror.iris.washington.edu/iscbulletin/search)

  - Bulletin search - provides the most verbose output of the ISC Bulletin in ISF or QuakeML.
  - Event catalogue - only outputs the prime hypocentre for each event, producing a simple list of events, locations and magnitudes.
  - Arrivals - search for arrivals in the ISC Bulletin. Users can search for specific phases for selected stations and events.

- CD-ROMs/DVD-ROMs

  CDs/DVDs can be ordered from the ISC for any published volume (one per year), or for all back issues of the Bulletin (not including the latest volume). The data discs contain the Bulletin as a PDF, in IASPEI Seismic Format (ISF), and in Fixed Format Bulletin (FFB) format. An event catalogue is also included, together with the International Registry of seismic station codes.

- FTP site

  The ISC Bulletin is also available to download from the ISC ftp site, which contains the Bulletin in PDF, ISF and FFB formats. (ftp://www.isc.ac.uk)
  (ftp://isc-mirror.iris.washington.edu)

Mirror service

A mirror of the ISC database, website and ftp site is available at IRIS DMC (isc-mirror.iris.washington.edu), which benefits from their high-speed internet connection, providing an alternative method of accessing the ISC Bulletin.

5

Citing the International Seismological Centre

Data from the ISC should always be cited. This includes use by academic or commercial organisations, as well as individuals. A citation should show how the data were retrieved and may be in one of these suggested forms:

Data retrieved from the ISC web site:

- International Seismological Centre, On-line Bulletin, http://www.isc.ac.uk, Internatl. Seis. Cent., Thatcham, United Kingdom, 2010.

Data transcribed from the IASPEI reference event bulletin:

- International Seismological Centre, Reference Event Bulletin, http://www.isc.ac.uk, Internatl. Seis. Cent., Thatcham, United Kingdom, 2010.

Data transcribed from the EHB bulletin:

- International Seismological Centre, EHB Bulletin, http://www.isc.ac.uk, Internatl. Seis. Cent., Thatcham, United Kingdom, 2010.

Data copied from ISC CD-ROMs/DVD-ROMs:

- International Seismological Centre, Bulletin Disks, Internatl. Seis. Cent., Thatcham, United Kingdom, 2010.

Data transcribed from the printed Bulletin:

- International Seismological Centre, Bull. Internatl. Seis. Cent., 36(1), Thatcham, United Kingdom, 2010.

The ISC is named as a valid data centre for citations within American Geophysical Union (AGU) publications. As such, please follow the AGU guidelines when referencing ISC data in one of their journals. The ISC may be cited as both the institutional author of the Bulletin and the source from which the data were retrieved.

BibTex entry example:

@manual{ISCcitation2010,
author = "International Seismological Centre",

title = "On-line Bulletin",
organization = "Int. Seis. Cent.",
note = "http://www.isc.ac.uk",
address = "Thatcham, United Kingdom",
year = "2010"
}

6

IASPEI Standards

6.1 Standard Nomenclature of Seismic Phases

The following list of seismic phases was approved by the IASPEI Commission on Seismological Observation and Interpretation (CoSOI) and adopted by IASPEI on 9th July 2003. More details can be found in *Storchak et al.* (2003) and *Storchak et al.* (2011). Ray paths for some of these phases are shown in Figures 6.1–6.6.

Crustal Phases	
Pg	At short distances, either an upgoing P wave from a source in the upper crust or a P wave bottoming in the upper crust. At larger distances also arrivals caused by multiple P-wave reverberations inside the whole crust with a group velocity around 5.8 km/s.
Pb	Either an upgoing P wave from a source in the lower crust or a P wave bottoming in the lower crust (alt: P*)
Pn	Any P wave bottoming in the uppermost mantle or an upgoing P wave from a source in the uppermost mantle
PnPn	Pn free-surface reflection
PgPg	Pg free-surface reflection
PmP	P reflection from the outer side of the Moho
PmP*N*	PmP multiple free surface reflection; *N* is a positive integer. For example, PmP2 is PmPPmP.
PmS	P to S reflection from the outer side of the Moho
Sg	At short distances, either an upgoing S wave from a source in the upper crust or an S wave bottoming in the upper crust. At larger distances also arrivals caused by superposition of multiple S-wave reverberations and SV to P and/or P to SV conversions inside the whole crust.
Sb	Either an upgoing S wave from a source in the lower crust or an S wave bottoming in the lower crust (alt: S*)
Sn	Any S wave bottoming in the uppermost mantle or an upgoing S wave from a source in the uppermost mantle
SnSn	Sn free-surface reflection
SgSg	Sg free-surface reflection
SmS	S reflection from the outer side of the Moho
SmS*N*	SmS multiple free-surface reflection; *N* is a positive integer. For example, SmS2 is SmSSmS.
SmP	S to P reflection from the outer side of the Moho
Lg	A wave group observed at larger regional distances and caused by superposition of multiple S-wave reverberations and SV to P and/or P to SV conversions inside the whole crust. The maximum energy travels with a group velocity around 3.5 km/s.
Rg	Short-period crustal Rayleigh wave

Mantle Phases

P	A longitudinal wave, bottoming below the uppermost mantle; also an upgoing longitudinal wave from a source below the uppermost mantle
PP	Free-surface reflection of P wave leaving a source downward
PS	P, leaving a source downward, reflected as an S at the free surface. At shorter distances the first leg is represented by a crustal P wave.
PPP	Analogous to PP
PPS	PP to S converted reflection at the free surface; travel time matches that of PSP
PSS	PS reflected at the free surface
PcP	P reflection from the core-mantle boundary (CMB)
PcS	P to S converted reflection from the CMB
PcPN	PcP multiple free-surface reflection; N is a positive integer. For example, PcP2 is PcPPcP.
Pz+P	P reflection from outer side of a discontinuity at depth z; z may be a positive numerical value in km. For example, P660+P is a P reflection from the top of the 660 km discontinuity. (alt: PzP)
Pz-P	P reflection from inner side of discontinuity at depth z. For example, P660-P is a P reflection from below the 660 km discontinuity, which means it is precursory to PP.
Pz+S	P to S converted reflection from outer side of discontinuity at depth z (alt: PzS)
Pz-S	P to S converted reflection from inner side of discontinuity at depth z
PScS	P (leaving a source downward) to ScS reflection at the free surface
Pdif	P diffracted along the CMB in the mantle (old: Pdiff)
S	Shear wave, bottoming below the uppermost mantle; also an upgoing shear wave from a source below the uppermost mantle
SS	Free-surface reflection of an S wave leaving a source downward
SP	S, leaving source downward, reflected as P at the free surface. At shorter distances the second leg is represented by a crustal P wave.
SSS	Analogous to SS
SSP	SS to P converted reflection at the free surface; travel time matches that of SPS
SPP	SP reflected at the free surface
ScS	S reflection from the CMB
ScP	S to P converted reflection from the CMB
ScSN	ScS multiple free-surface reflection; N is a positive integer. For example, ScS2 is ScSScS.
Sz+S	S reflection from outer side of a discontinuity at depth z; z may be a positive numerical value in km. For example, S660+S is an S reflection from the top of the 660 km discontinuity. (alt: SzS)
Sz-S	S reflection from inner side of discontinuity at depth z. For example, S660-S is an S reflection from below the 660 km discontinuity, which means it is precursory to SS.
Sz+P	S to P converted reflection from outer side of discontinuity at depth z (alt: SzP)
Sz-P	S to P converted reflection from inner side of discontinuity at depth z
ScSP	ScS to P reflection at the free surface
Sdif	S diffracted along the CMB in the mantle (old: Sdiff)

Core Phases

PKP	Unspecified P wave bottoming in the core (alt: P’)
PKPab	P wave bottoming in the upper outer core; ab indicates the retrograde branch of the PKP caustic (old: PKP2)
PKPbc	P wave bottoming in the lower outer core; bc indicates the prograde branch of the PKP caustic (old: PKP1)
PKPdf	P wave bottoming in the inner core (alt: PKIKP)

PKPpre	A precursor to PKPdf due to scattering near or at the CMB (old: PKhKP)
PKPdif	P wave diffracted at the inner core boundary (ICB) in the outer core
PKS	Unspecified P wave bottoming in the core and converting to S at the CMB
PKSab	PKS bottoming in the upper outer core
PKSbc	PKS bottoming in the lower outer core
PKSdf	PKS bottoming in the inner core
P'P'	Free-surface reflection of PKP (alt: PKPPKP)
P'*N*	PKP reflected at the free surface *N* - 1 times; *N* is a positive integer. For example, P'3 is P'P'P'. (alt: PKP*N*)
P'*z*-P'	PKP reflected from inner side of a discontinuity at depth *z* outside the core, which means it is precursory to P'P'; *z* may be a positive numerical value in km
P'S'	PKP to SKS converted reflection at the free surface; other examples are P'PKS, P'SKP (alt: PKPSKS)
PS'	P (leaving a source downward) to SKS reflection at the free surface (alt: PSKS)
PKKP	Unspecified P wave reflected once from the inner side of the CMB
PKKPab	PKKP bottoming in the upper outer core
PKKPbc	PKKP bottoming in the lower outer core
PKKPdf	PKKP bottoming in the inner core
P*N*KP	P wave reflected *N* - 1 times from inner side of the CMB; *N* is a positive integer
PKKPpre	A precursor to PKKP due to scattering near the CMB
PKiKP	P wave reflected from the inner core boundary (ICB)
PK*N*IKP	P wave reflected *N* - 1 times from the inner side of the ICB
PKJKP	P wave traversing the outer core as P and the inner core as S
PKKS	P wave reflected once from inner side of the CMB and converted to S at the CMB
PKKSab	PKKS bottoming in the upper outer core
PKKSbc	PKKS bottoming in the lower outer core
PKKSdf	PKKS bottoming in the inner core
PcPP'	PcP to PKP reflection at the free surface; other examples are PcPS', PcSP', PcSS', PcPSKP, PcSSKP (alt: PcPPKP)
SKS	unspecified S wave traversing the core as P (alt: S')
SKSac	SKS bottoming in the outer core
SKSdf	SKS bottoming in the inner core (alt: SKIKS)
SPdifKS	SKS wave with a segment of mantleside Pdif at the source and/or the receiver side of the ray path (alt: SKPdifS)
SKP	Unspecified S wave traversing the core and then the mantle as P
SKPab	SKP bottoming in the upper outer core
SKPbc	SKP bottoming in the lower outer core
SKPdf	SKP bottoming in the inner core
S'S'	Free-surface reflection of SKS (alt: SKSSKS)
S'*N*	SKS reflected at the free surface *N* - 1 times; *N* is a positive integer
S'*z*-S'	SKS reflected from inner side of discontinuity at depth *z* outside the core, which means it is precursory to S'S'; *z* may be a positive numerical value in km
S'P'	SKS to PKP converted reflection at the free surface; other examples are S'SKP, S'PKS (alt: SKSPKP)
S'P	SKS to P reflection at the free surface (alt: SKSP)
SKKS	Unspecified S wave reflected once from inner side of the CMB
SKKSac	SKKS bottoming in the outer core
SKKSdf	SKKS bottoming in the inner core
S*N*KS	S wave reflected *N* - 1 times from inner side of the CMB; *N* is a positive integer
SKiKS	S wave traversing the outer core as P and reflected from the ICB
SKJKS	S wave traversing the outer core as P and the inner core as S
SKKP	S wave traversing the core as P with one reflection from the inner side of the CMB and then continuing as P in the mantle
SKKPab	SKKP bottoming in the upper outer core

SKKPbc	SKKP bottoming in the lower outer core
SKKPdf	SKKP bottoming in the inner core
ScSS'	ScS to SKS reflection at the free surface; other examples are ScPS', ScSP', ScPP', ScSSKP, ScPSKP (alt: ScSSKS)

Near-source Surface reflections (Depth Phases)

pP*y*	All P-type onsets (P*y*), as defined above, which resulted from reflection of an upgoing P wave at the free surface or an ocean bottom. WARNING: The character *y* is only a wild card for any seismic phase, which could be generated at the free surface. Examples are pP, pPKP, pPP, pPcP, etc.
sP*y*	All Py resulting from reflection of an upgoing S wave at the free surface or an ocean bottom; for example, sP, sPKP, sPP, sPcP, etc
pS*y*	All S-type onsets (S*y*), as defined above, which resulted from reflection of an upgoing P wave at the free surface or an ocean bottom; for example, pS, pSKS, pSS, pScP, etc
sS*y*	All Sy resulting from reflection of an upgoing S wave at the free surface or an ocean bottom; for example, sSn, sSS, sScS, sSdif, etc
pwP*y*	All Py resulting from reflection of an upgoing P wave at the ocean's free surface
pmP*y*	All Py resulting from reflection of an upgoing P wave from the inner side of the Moho

Surface Waves

L	Unspecified long-period surface wave
LQ	Love wave
LR	Rayleigh wave
G	Mantle wave of Love type
G*N*	Mantle wave of Love type; *N* is integer and indicates wave packets travelling along the minor arcs (odd numbers) or major arc (even numbers) of the great circle
R	Mantle wave of Rayleigh type
R*N*	Mantle wave of Rayleigh type; *N* is integer and indicates wave packets travelling along the minor arcs (odd numbers) or major arc (even numbers) of the great circle
PL	Fundamental leaking mode following P onsets generated by coupling of P energy into the waveguide formed by the crust and upper mantle SPL S wave coupling into the PL waveguide; other examples are SSPL, SSSPL

Acoustic Phases

H	A hydroacoustic wave from a source in the water, which couples in the ground
HPg	H phase converted to Pg at the receiver side
HSg	H phase converted to Sg at the receiver side
HRg	H phase converted to Rg at the receiver side
I	An atmospheric sound arrival which couples in the ground
IPg	I phase converted to Pg at the receiver side
ISg	I phase converted to Sg at the receiver side
IRg	I phase converted to Rg at the receiver side
T	A tertiary wave. This is an acoustic wave from a source in the solid earth, usually trapped in a low-velocity oceanic water layer called the SOFAR channel (SOund Fixing And Ranging).
TPg	T phase converted to Pg at the receiver side
TSg	T phase converted to Sg at the receiver side
TRg	T phase converted to Rg at the receiver side

Amplitude Measurement Phases

A	Unspecified amplitude measurement
AML	Amplitude measurement for local magnitude
AMB	Amplitude measurement for body-wave magnitude

AMS	Amplitude measurement for surface-wave magnitude
END	Time of visible end of record for duration magnitude

Unidentified Arrivals

x	unidentified arrival (old: i, e, NULL)
rx	unidentified regional arrival (old: i, e, NULL)
tx	unidentified teleseismic arrival (old: i, e, NULL)
Px	unidentified arrival of P type (old: i, e, NULL, (P), P?)
Sx	unidentified arrival of S type (old: i, e, NULL, (S), S?)

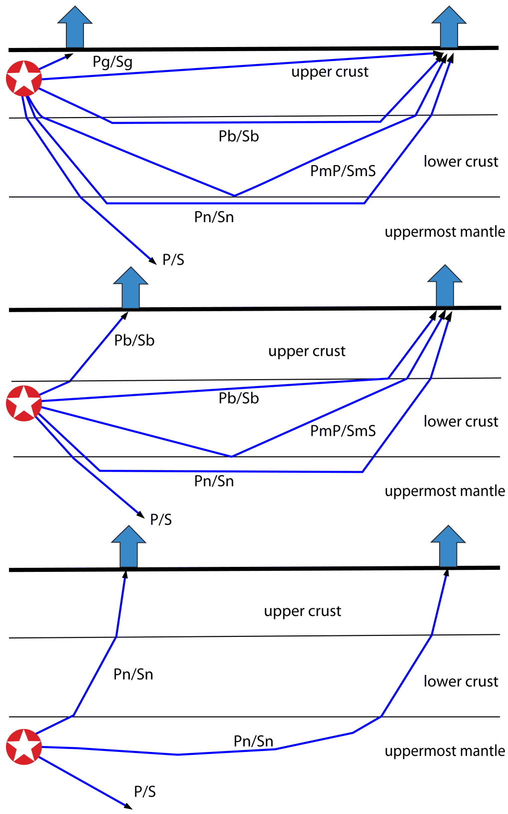

Figure 6.1: *Seismic 'crustal phases' observed in the case of a two-layer crust in local and regional distance ranges (0°<D< about 20°) from the seismic source in the: upper crust (top); lower crust (middle); and uppermost mantle (bottom).*

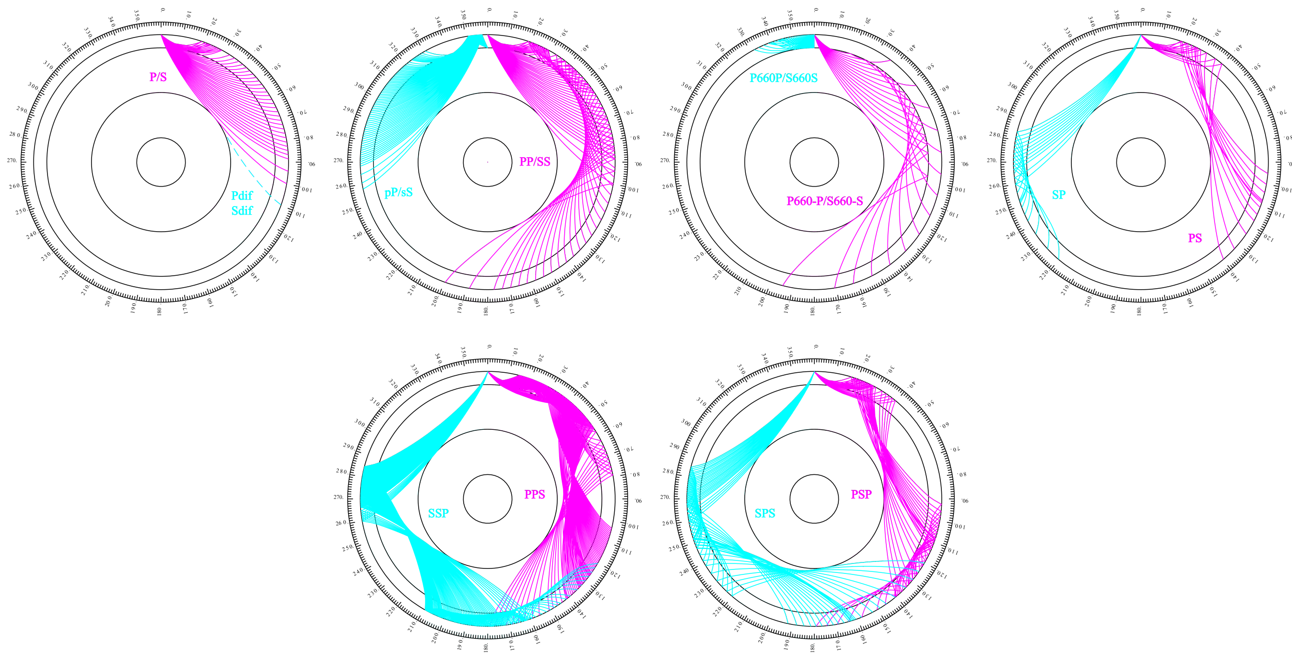

Figure 6.2: *Mantle phases observed at the teleseismic distance range D > about 20°.*

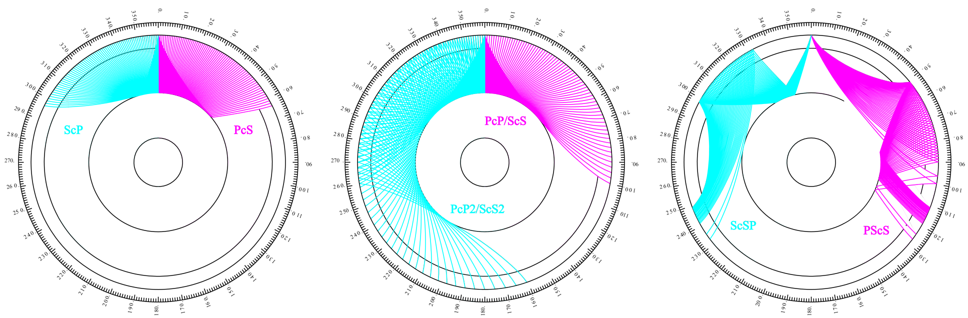

Figure 6.3: *Reflections from the Earth's core.*

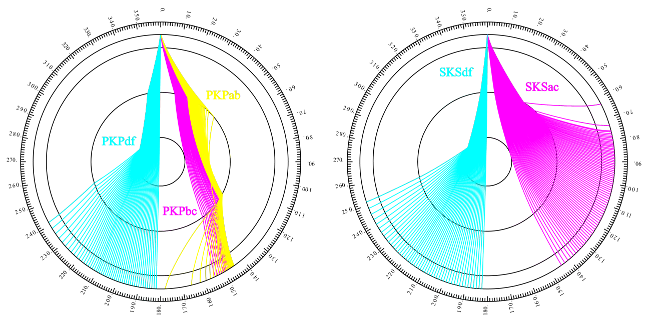

Figure 6.4: *Seismic rays of direct core phases.*

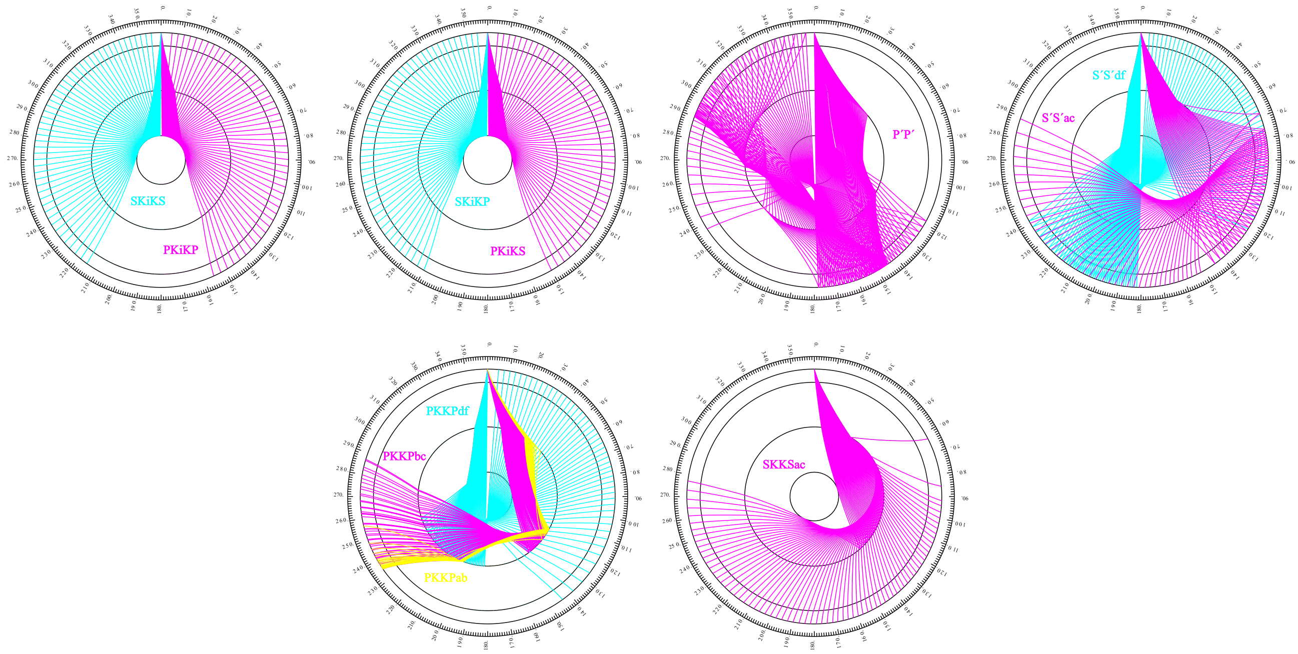

Figure 6.5: *Seismic rays of single-reflected core phases.*

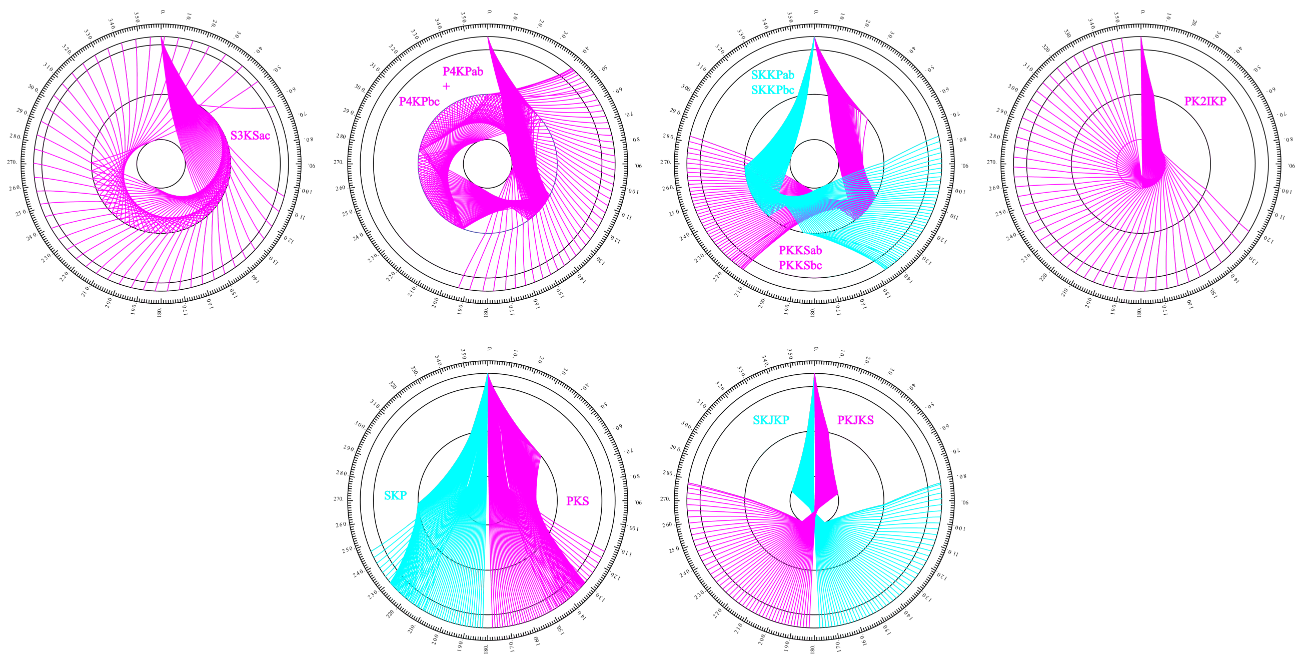

Figure 6.6: *Seismic rays of multiple-reflected and converted core phases.*

6.2 Flinn-Engdahl Regions

The Flinn-Engdahl regions were first proposed by *Flinn and Engdahl* (1965), with the standard defined by *Flinn et al.* (1974). The latest version of the schema, published by *Young et al.* (1996), divides the Earth into 50 seismic regions (Figure 6.7), which are further subdivided producing a total of 754 geographical regions (listed below). The geographic regions are numbered 1 to 757 with regions 172, 299 and 550 no longer in use. The boundaries of these regions are defined at one-degree intervals.

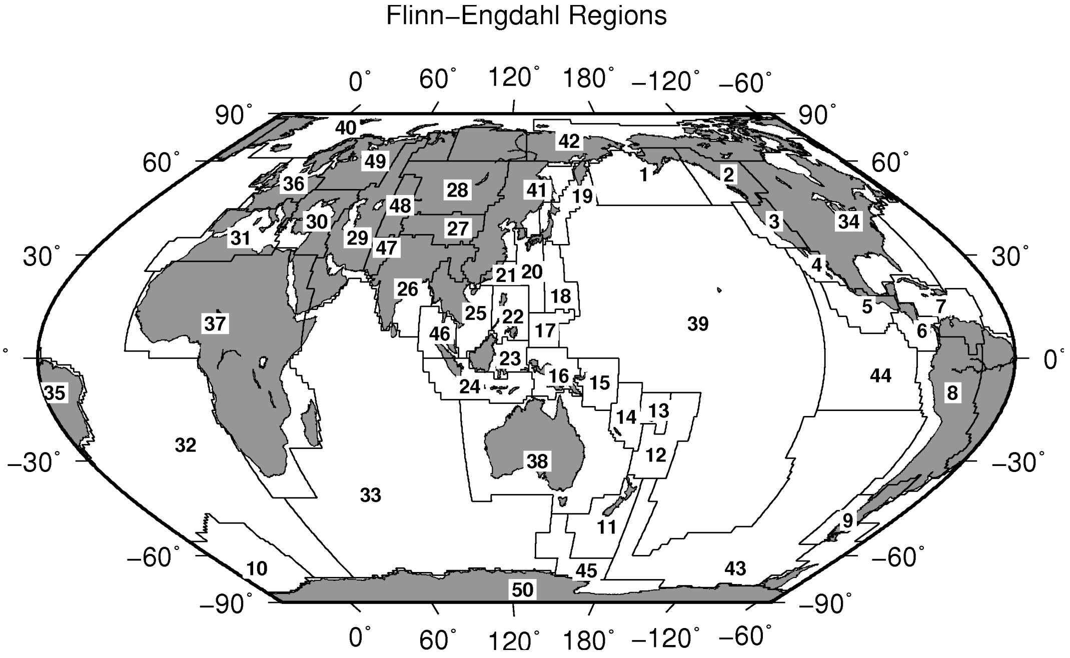

Figure 6.7: *Map of all Flinn-Engdahl seismic regions.*

Seismic Region 1
Alaska-Aleutian Arc
1. Central Alaska
2. Southern Alaska
3. Bering Sea
4. Komandorsky Islands region
5. Near Islands
6. Rat Islands
7. Andreanof Islands
8. Pribilof Islands
9. Fox Islands
10. Unimak Island region
11. Bristol Bay
12. Alaska Peninsula
13. Kodiak Island region
14. Kenai Peninsula
15. Gulf of Alaska
16. South of Aleutian Islands
17. South of Alaska

Seismic Region 2
Eastern Alaska to Vancouver Island
18. Southern Yukon Territory
19. Southeastern Alaska
20. Off coast of southeastern Alaska
21. West of Vancouver Island
22. Queen Charlotte Islands region
23. British Columbia
24. Alberta
25. Vancouver Island region
26. Off coast of Washington
27. Near coast of Washington
28. Washington-Oregon border region
29. Washington

Seismic Region 3
California-Nevada Region
30. Off coast of Oregon
31. Near coast of Oregon
32. Oregon
33. Western Idaho
34. Off coast of northern California
35. Near coast of northern California
36. Northern California
37. Nevada
38. Off coast of California
39. Central California
40. California-Nevada border region
41. Southern Nevada
42. Western Arizona
43. Southern California
44. California-Arizona border region
45. California-Baja California border region
46. Western Arizona-Sonora border region

Seismic Region 4
Lower California and Gulf of California
47. Off west coast of Baja California
48. Baja California
49. Gulf of California
50. Sonora
51. Off coast of central Mexico
52. Near coast of central Mexico

Seismic Region 5
Mexico-Guatemala Area

53. Revilla Gigedo Islands region
54. Off coast of Jalisco
55. Near coast of Jalisco
56. Near coast of Michoacan
57. Michoacan
58. Near coast of Guerrero
59. Guerrero
60. Oaxaca
61. Chiapas
62. Mexico-Guatemala border region
63. Off coast of Mexico
64. Off coast of Michoacan
65. Off coast of Guerrero
66. Near coast of Oaxaca
67. Off coast of Oaxaca
68. Off coast of Chiapas
69. Near coast of Chiapas
70. Guatemala
71. Near coast of Guatemala
730. Northern East Pacific Rise

Seismic Region 6
Central America

72. Honduras
73. El Salvador
74. Near coast of Nicaragua
75. Nicaragua
76. Off coast of central America
77. Off coast of Costa Rica
78. Costa Rica
79. North of Panama
80. Panama-Costa Rica border region
81. Panama
82. Panama-Colombia border region
83. South of Panama

Seismic Region 7
Caribbean Loop

84. Yucatan Peninsula
85. Cuba region
86. Jamaica region
87. Haiti region
88. Dominican Republic region
89. Mona Passage
90. Puerto Rico region
91. Virgin Islands
92. Leeward Islands
93. Belize
94. Caribbean Sea
95. Windward Islands
96. Near north coast of Colombia
97. Near coast of Venezuela
98. Trinidad
99. Northern Colombia
100. Lake Maracaibo
101. Venezuela
731. North of Honduras

Seismic Region 8
Andean South America

102. Near west coast of Colombia
103. Colombia
104. Off coast of Ecuador
105. Near coast of Ecuador
106. Colombia-Ecuador border region
107. Ecuador
108. Off coast of northern Peru
109. Near coast of northern Peru
110. Peru-Ecuador border region
111. Northern Peru
112. Peru-Brazil border region
113. Western Brazil
114. Off coast of Peru
115. Near coast of Peru
116. Central Peru
117. Southern Peru
118. Peru-Bolivia border region
119. Northern Bolivia
120. Central Bolivia
121. Off coast of northern Chile
122. Near coast of northern Chile
123. Northern Chile
124. Chile-Bolivia border region
125. Southern Bolivia
126. Paraguay
127. Chile-Argentina border region
128. Jujuy Province
129. Salta Province
130. Catamarca Province
131. Tucuman Province
132. Santiago del Estero Province
133. Northeastern Argentina
134. Off coast of central Chile
135. Near coast of central Chile
136. Central Chile
137. San Juan Province
138. La Rioja Province
139. Mendoza Province
140. San Luis Province
141. Cordoba Province
142. Uruguay

Seismic Region 9
Extreme South America

143. Off coast of southern Chile
144. Southern Chile
145. Southern Chile-Argentina border region
146. Southern Argentina

Seismic Region 10
Southern Antilles

147. Tierra del Fuego
148. Falkland Islands region
149. Drake Passage
150. Scotia Sea
151. South Georgia Island region
152. South Georgia Rise
153. South Sandwich Islands region
154. South Shetland Islands
155. Antarctic Peninsula
156. Southwestern Atlantic Ocean
157. Weddell Sea
732. East of South Sandwich Islands

Seismic Region 11
New Zealand Region

158. Off west coast of North Island
159. North Island
160. Off east coast of North Island
161. Off west coast of South Island
162. South Island
163. Cook Strait
164. Off east coast of South Island
165. North of Macquarie Island
166. Auckland Islands region
167. Macquarie Island region
168. South of New Zealand

Seismic Region 12
Kermadec-Tonga-Samoa Area

169. Samoa Islands region
170. Samoa Islands
171. South of Fiji Islands
172. West of Tonga Islands (REGION NOT IN USE)
173. Tonga Islands
174. Tonga Islands region
175. South of Tonga Islands
176. North of New Zealand
177. Kermadec Islands region
178. Kermadec Islands
179. South of Kermadec Islands

Seismic Region 13
Fiji Area

180. North of Fiji Islands
181. Fiji Islands region
182. Fiji Islands

Seismic Region 14
Vanuatu (New Hebrides)

183. Santa Cruz Islands region
184. Santa Cruz Islands
185. Vanuatu Islands region
186. Vanuatu Islands
187. New Caledonia
188. Loyalty Islands

189. Southeast of Loyalty Islands

Seismic Region 15
Bismarck and Solomon Islands
190. New Ireland region
191. North of Solomon Islands
192. New Britain region
193. Bougainville-Solomon Islands region
194. D'Entrecasteaux Islands region
195. South of Solomon Islands

Seismic Region 16
New Guinea
196. Irian Jaya region
197. Near north coast of Irian Jaya
198. Ninigo Islands region
199. Admiralty Islands region
200. Near north coast of New Guinea
201. Irian Jaya
202. New Guinea
203. Bismarck Sea
204. Aru Islands region
205. Near south coast of Irian Jaya
206. Near south coast of New Guinea
207. Eastern New Guinea region
208. Arafura Sea

Seismic Region 17
Caroline Islands to Guam
209. Western Caroline Islands
210. South of Mariana Islands

Seismic Region 18
Guam to Japan
211. Southeast of Honshu
212. Bonin Islands region
213. Volcano Islands region
214. West of Mariana Islands
215. Mariana Islands region
216. Mariana Islands

Seismic Region 19
Japan-Kurils-Kamchatka
217. Kamchatka Peninsula
218. Near east coast of Kamchatka Peninsula
219. Off east coast of Kamchatka Peninsula
220. Northwest of Kuril Islands
221. Kuril Islands
222. East of Kuril Islands
223. Eastern Sea of Japan
224. Hokkaido region
225. Off southeast coast of Hokkaido
226. Near west coast of eastern Honshu
227. Eastern Honshu
228. Near east coast of eastern Honshu
229. Off east coast of Honshu
230. Near south coast of eastern Honshu

Seismic Region 20
Southwestern Japan and Ryukyu Islands
231. South Korea
232. Western Honshu
233. Near south coast of western Honshu
234. Northwest of Ryukyu Islands
235. Kyushu
236. Shikoku
237. Southeast of Shikoku
238. Ryukyu Islands
239. Southeast of Ryukyu Islands
240. West of Bonin Islands
241. Philippine Sea

Seismic Region 21
Taiwan
242. Near coast of southeastern China
243. Taiwan region
244. Taiwan
245. Northeast of Taiwan
246. Southwestern Ryukyu Islands
247. Southeast of Taiwan

Seismic Region 22
Philippines
248. Philippine Islands region
249. Luzon
250. Mindoro
251. Samar
252. Palawan
253. Sulu Sea
254. Panay
255. Cebu
256. Leyte
257. Negros
258. Sulu Archipelago
259. Mindanao
260. East of Philippine Islands

Seismic Region 23
Borneo-Sulawesi
261. Borneo
262. Celebes Sea
263. Talaud Islands
264. North of Halmahera
265. Minahassa Peninsula, Sulawesi
266. Northern Molucca Sea
267. Halmahera
268. Sulawesi
269. Southern Molucca Sea
270. Ceram Sea
271. Buru
272. Seram

Seismic Region 24
Sunda Arc
273. Southwest of Sumatera
274. Southern Sumatera
275. Java Sea
276. Sunda Strait
277. Jawa
278. Bali Sea
279. Flores Sea
280. Banda Sea
281. Tanimbar Islands region
282. South of Jawa
283. Bali region
284. South of Bali
285. Sumbawa region
286. Flores region
287. Sumba region
288. Savu Sea
289. Timor region
290. Timor Sea
291. South of Sumbawa
292. South of Sumba
293. South of Timor

Seismic Region 25
Myanmar and Southeast Asia
294. Myanmar-India border region
295. Myanmar-Bangladesh border region
296. Myanmar
297. Myanmar-China border region
298. Near south coast of Myanmar
299. Southeast Asia (REGION NOT IN USE)
300. Hainan Island
301. South China Sea
733. Thailand
734. Laos
735. Kampuchea
736. Vietnam
737. Gulf of Tongking

Seismic Region 26
India-Xizang-Szechwan-Yunnan
302. Eastern Kashmir
303. Kashmir-India border region
304. Kashmir-Xizang border region

305. Western Xizang-India border region
306. Xizang
307. Sichuan
308. Northern India
309. Nepal-India border region
310. Nepal
311. Sikkim
312. Bhutan
313. Eastern Xizang-India border region
314. Southern India
315. India-Bangladesh border region
316. Bangladesh
317. Northeastern India
318. Yunnan
319. Bay of Bengal

Seismic Region 27
Southern Xinjiang to Gansu

320. Kyrgyzstan-Xinjiang border region
321. Southern Xinjiang
322. Gansu
323. Western Nei Mongol
324. Kashmir-Xinjiang border region
325. Qinghai

Seismic Region 28
Alma-Ata to Lake Baikal

326. Southwestern Siberia
327. Lake Baykal region
328. East of Lake Baykal
329. Eastern Kazakhstan
330. Lake Issyk-Kul region
331. Kazakhstan-Xinjiang border region
332. Northern Xinjiang
333. Tuva-Buryatia-Mongolia border region
334. Mongolia

Seismic Region 29
Western Asia

335. Ural Mountains region
336. Western Kazakhstan
337. Eastern Caucasus
338. Caspian Sea
339. Northwestern Uzbekistan
340. Turkmenistan
341. Iran-Turkmenistan border region
342. Turkmenistan-Afghanistan border region
343. Turkey-Iran border region
344. Iran-Armenia-Azerbaijan border region
345. Northwestern Iran
346. Iran-Iraq border region
347. Western Iran
348. Northern and central Iran
349. Northwestern Afghanistan
350. Southwestern Afghanistan
351. Eastern Arabian Peninsula
352. Persian Gulf
353. Southern Iran
354. Southwestern Pakistan
355. Gulf of Oman
356. Off coast of Pakistan

Seismic Region 30
Middle East-Crimea-Eastern Balkans

357. Ukraine-Moldova-Southwestern Russia region
358. Romania
359. Bulgaria
360. Black Sea
361. Crimea region
362. Western Caucasus
363. Greece-Bulgaria border region
364. Greece
365. Aegean Sea
366. Turkey
367. Turkey-Georgia-Armenia border region
368. Southern Greece
369. Dodecanese Islands
370. Crete
371. Eastern Mediterranean Sea
372. Cyprus region
373. Dead Sea region
374. Jordan-Syria region
375. Iraq

Seismic Region 31
Western Mediterranean Area

376. Portugal
377. Spain
378. Pyrenees
379. Near south coast of France
380. Corsica
381. Central Italy
382. Adriatic Sea
383. Northwestern Balkan Peninsula
384. West of Gibraltar
385. Strait of Gibraltar
386. Balearic Islands
387. Western Mediterranean Sea
388. Sardinia
389. Tyrrhenian Sea
390. Southern Italy
391. Albania
392. Greece-Albania border region
393. Madeira Islands region
394. Canary Islands region
395. Morocco
396. Northern Algeria
397. Tunisia
398. Sicily
399. Ionian Sea
400. Central Mediterranean Sea
401. Near coast of Libya

Seismic Region 32
Atlantic Ocean

402. North Atlantic Ocean
403. Northern Mid-Atlantic Ridge
404. Azores Islands region
405. Azores Islands
406. Central Mid-Atlantic Ridge
407. North of Ascension Island
408. Ascension Island region
409. South Atlantic Ocean
410. Southern Mid-Atlantic Ridge
411. Tristan da Cunha region
412. Bouvet Island region
413. Southwest of Africa
414. Southeastern Atlantic Ocean
738. Reykjanes Ridge
739. Azores-Cape St. Vincent Ridge

Seismic Region 33
Indian Ocean

415. Eastern Gulf of Aden
416. Socotra region
417. Arabian Sea
418. Lakshadweep region
419. Northeastern Somalia
420. North Indian Ocean
421. Carlsberg Ridge
422. Maldive Islands region
423. Laccadive Sea
424. Sri Lanka
425. South Indian Ocean
426. Chagos Archipelago region
427. Mauritius-Reunion region
428. Southwest Indian Ridge
429. Mid-Indian Ridge
430. South of Africa
431. Prince Edward Islands region
432. Crozet Islands region
433. Kerguelen Islands region
434. Broken Ridge
435. Southeast Indian Ridge
436. Southern Kerguelen Plateau
437. South of Australia
740. Owen Fracture Zone region
741. Indian Ocean Triple Junction
742. Western Indian-Antarctic

Ridge

Seismic Region 34
Eastern North America
438. Saskatchewan
439. Manitoba
440. Hudson Bay
441. Ontario
442. Hudson Strait region
443. Northern Quebec
444. Davis Strait
445. Labrador
446. Labrador Sea
447. Southern Quebec
448. Gaspe Peninsula
449. Eastern Quebec
450. Anticosti Island
451. New Brunswick
452. Nova Scotia
453. Prince Edward Island
454. Gulf of St. Lawrence
455. Newfoundland
456. Montana
457. Eastern Idaho
458. Hebgen Lake region, Montana
459. Yellowstone region
460. Wyoming
461. North Dakota
462. South Dakota
463. Nebraska
464. Minnesota
465. Iowa
466. Wisconsin
467. Illinois
468. Michigan
469. Indiana
470. Southern Ontario
471. Ohio
472. New York
473. Pennsylvania
474. Vermont-New Hampshire region
475. Maine
476. Southern New England
477. Gulf of Maine
478. Utah
479. Colorado
480. Kansas
481. Iowa-Missouri border region
482. Missouri-Kansas border region
483. Missouri
484. Missouri-Arkansas border region
485. Missouri-Illinois border region
486. New Madrid region, Missouri
487. Cape Girardeau region, Missouri
488. Southern Illinois
489. Southern Indiana
490. Kentucky
491. West Virginia
492. Virginia
493. Chesapeake Bay region
494. New Jersey
495. Eastern Arizona
496. New Mexico
497. Northwestern Texas-Oklahoma border region
498. Western Texas
499. Oklahoma
500. Central Texas
501. Arkansas-Oklahoma border region
502. Arkansas
503. Louisiana-Texas border region
504. Louisiana
505. Mississippi
506. Tennessee
507. Alabama
508. Western Florida
509. Georgia
510. Florida-Georgia border region
511. South Carolina
512. North Carolina
513. Off east coast of United States
514. Florida Peninsula
515. Bahama Islands
516. Eastern Arizona-Sonora border region
517. New Mexico-Chihuahua border region
518. Texas-Mexico border region
519. Southern Texas
520. Near coast of Texas
521. Chihuahua
522. Northern Mexico
523. Central Mexico
524. Jalisco
525. Veracruz
526. Gulf of Mexico
527. Bay of Campeche

Seismic Region 35
Eastern South America
528. Brazil
529. Guyana
530. Suriname
531. French Guiana

Seismic Region 36
Northwestern Europe
532. Eire
533. United Kingdom
534. North Sea
535. Southern Norway
536. Sweden
537. Baltic Sea
538. France
539. Bay of Biscay
540. The Netherlands
541. Belgium
542. Denmark
543. Germany
544. Switzerland
545. Northern Italy
546. Austria
547. Czech and Slovak Republics
548. Poland
549. Hungary

Seismic Region 37
Africa
550. Northwest Africa (REGION NOT IN USE)
551. Southern Algeria
552. Libya
553. Egypt
554. Red Sea
555. Western Arabian Peninsula
556. Chad region
557. Sudan
558. Ethiopia
559. Western Gulf of Aden
560. Northwestern Somalia
561. Off south coast of northwest Africa
562. Cameroon
563. Equatorial Guinea
564. Central African Republic
565. Gabon
566. Congo
567. Zaire
568. Uganda
569. Lake Victoria region
570. Kenya
571. Southern Somalia
572. Lake Tanganyika region
573. Tanzania
574. Northwest of Madagascar
575. Angola
576. Zambia
577. Malawi
578. Namibia
579. Botswana
580. Zimbabwe
581. Mozambique
582. Mozambique Channel
583. Madagascar
584. South Africa
585. Lesotho
586. Swaziland
587. Off coast of South Africa
743. Western Sahara

744. Mauritania
745. Mali
746. Senegal-Gambia region
747. Guinea region
748. Sierra Leone
749. Liberia region
750. Cote d'Ivoire
751. Burkina Faso
752. Ghana
753. Benin-Togo region
754. Niger
755. Nigeria

Seismic Region 38
Australia

588. Northwest of Australia
589. West of Australia
590. Western Australia
591. Northern Territory
592. South Australia
593. Gulf of Carpentaria
594. Queensland
595. Coral Sea
596. Northwest of New Caledonia
597. New Caledonia region
598. Southwest of Australia
599. Off south coast of Australia
600. Near coast of South Australia
601. New South Wales
602. Victoria
603. Near southeast coast of Australia
604. Near east coast of Australia
605. East of Australia
606. Norfolk Island region
607. Northwest of New Zealand
608. Bass Strait
609. Tasmania region
610. Southeast of Australia

Seismic Region 39
Pacific Basin

611. North Pacific Ocean
612. Hawaiian Islands region
613. Hawaiian Islands
614. Eastern Caroline Islands region
615. Marshall Islands region
616. Enewetak Atoll region
617. Bikini Atoll region
618. Gilbert Islands region
619. Johnston Island region
620. Line Islands region
621. Palmyra Island region
622. Kiritimati region
623. Tuvalu region
624. Phoenix Islands region
625. Tokelau Islands region
626. Northern Cook Islands
627. Cook Islands region
628. Society Islands region
629. Tubuai Islands region
630. Marquesas Islands region
631. Tuamotu Archipelago region
632. South Pacific Ocean

Seismic Region 40
Arctic Zone

633. Lomonosov Ridge
634. Arctic Ocean
635. Near north coast of Kalaallit Nunaat
636. Eastern Kalaallit Nunaat
637. Iceland region
638. Iceland
639. Jan Mayen Island region
640. Greenland Sea
641. North of Svalbard
642. Norwegian Sea
643. Svalbard region
644. North of Franz Josef Land
645. Franz Josef Land
646. Northern Norway
647. Barents Sea
648. Novaya Zemlya
649. Kara Sea
650. Near coast of northwestern Siberia
651. North of Severnaya Zemlya
652. Severnaya Zemlya
653. Near coast of northern Siberia
654. East of Severnaya Zemlya
655. Laptev Sea

Seismic Region 41
Eastern Asia

656. Southeastern Siberia
657. Priamurye-Northeastern China border region
658. Northeastern China
659. North Korea
660. Sea of Japan
661. Primorye
662. Sakhalin Island
663. Sea of Okhotsk
664. Southeastern China
665. Yellow Sea
666. Off east coast of southeastern China

Seismic Region 42
Northeastern Asia, Northern Alaska to Greenland

667. North of New Siberian Islands
668. New Siberian Islands
669. Eastern Siberian Sea
670. Near north coast of eastern Siberia
671. Eastern Siberia
672. Chukchi Sea
673. Bering Strait
674. St. Lawrence Island region
675. Beaufort Sea
676. Northern Alaska
677. Northern Yukon Territory
678. Queen Elizabeth Islands
679. Northwest Territories
680. Western Kalaallit Nunaat
681. Baffin Bay
682. Baffin Island region

Seismic Region 43
Southeastern and Antarctic Pacific Ocean

683. Southeastcentral Pacific Ocean
684. Southern East Pacific Rise
685. Easter Island region
686. West Chile Rise
687. Juan Fernandez Islands region
688. East of North Island
689. Chatham Islands region
690. South of Chatham Islands
691. Pacific-Antarctic Ridge
692. Southern Pacific Ocean
756. Southeast of Easter Island

Seismic Region 44
Galapagos Area

693. Eastcentral Pacific Ocean
694. Central East Pacific Rise
695. West of Galapagos Islands
696. Galapagos Islands region
697. Galapagos Islands
698. Southwest of Galapagos Islands
699. Southeast of Galapagos Islands
757. Galapagos Triple Junction region

Seismic Region 45
Macquarie Loop

700. South of Tasmania
701. West of Macquarie Island
702. Balleny Islands region

Seismic Region 46
Andaman Islands to Sumatera

703. Andaman Islands region
704. Nicobar Islands region
705. Off west coast of northern Sumatera
706. Northern Sumatera

707. Malay Peninsula
708. Gulf of Thailand

Seismic Region 47
Baluchistan
709. Southeastern Afghanistan
710. Pakistan
711. Southwestern Kashmir
712. India-Pakistan border region

Seismic Region 48
Hindu Kush and Pamir
713. Central Kazakhstan
714. Southeastern Uzbekistan
715. Tajikistan
716. Kyrgyzstan
717. Afghanistan-Tajikistan border region
718. Hindu Kush region
719. Tajikistan-Xinjiang border region
720. Northwestern Kashmir

Seismic Region 49
Northern Eurasia
721. Finland
722. Norway-Murmansk border region
723. Finland-Karelia border region
724. Baltic States-Belarus-Northwestern Russia
725. Northwestern Siberia
726. Northern and central Siberia

Seismic Region 50
Antarctica
727. Victoria Land
728. Ross Sea
729. Antarctica

6.3 IASPEI Magnitudes

The ISC publishes a diversity of magnitude data. Although trying to be as complete and specific as possible, preference is now given to magnitudes determined according to standard procedures recommended by the Working Group on Magnitude Measurements of the IASPEI Commission on Seismological Observation and Interpretation (CoSOI). So far, such standards have been agreed upon for the local magnitude ML, the local-regional mb_Lg, and for two types each of body-wave (mb and mB_BB) and surface-wave magnitudes (Ms_20 and Ms_BB). With the exception of ML, all other standard magnitudes are measured on vertical-component records only. BB stands for direct measurement on unfiltered velocity broadband records in a wide range of periods, provided that their passband covers at least the period range within which mB_BB and Ms_BB are supposed to be measured. Otherwise, a deconvolution has to be applied prior to the amplitude and period measurement so as to assure that this specification is met. In contrast, mb_Lg, mb and Ms_20 are based on narrowband amplitude measurements around periods of 1 s and 20 s, respectively.

ML is consistent with the original definition of the local magnitude by *Richter* (1935) and mB_BB in close agreement with the original definition of medium-period body-wave magnitude mB measured in a wide range of periods between some 2 to 20 s and calibrated with the *Gutenberg and Richter* (1956) Q-function for vertical-component P waves. Similarly, Ms_BB is best tuned to the unbiased use of the IASPEI (1967) recommended standard magnitude formula for surface-wave amplitudes in a wide range of periods and distances, as proposed by its authors *Vaněk et al.* (1962). In contrast, mb and Ms_20 are chiefly based on measurement standards defined by US agencies in the 1960s in conjunction with the global deployment of the World-Wide Standard Seismograph Network (WWSSN), which did not include medium-period or broadband recordings. Some modifications were made in the 1970s to account for IASPEI recommendations on extended measurement time windows for mb. Although not optimal for calibrating narrow-band spectral amplitudes measured around 1 s and 20 s only, mb and Ms_20 use the same original calibrations functions as mB_BB and Ms_BB. But mb and Ms_20 data constitute by far the largest available magnitude data sets. Therefore they continue to be used, with appreciation for their advantages (e.g., mb is by far the most frequently measured teleseismic magnitude and often the only available and reasonably good magnitude estimator for small earthquakes) and their shortcomings (see section 3.2.5.2 of Chapter 3 in NMSOP-2).

Abbreviated descriptions of the standard procedures for ML, mb_Lg, mb, mB_BB and Ms_BB are summarised below. For more details, including also the transfer functions of the simulation filters to be used, see www.iaspei.org/commissions/CSOI/Summary_WG-Recommendations_20130327.pdf.

All amplitudes used in the magnitude formulas below are in most circumstances to be measured as one-half the maximum deflection of the seismogram trace, peak-to-adjacent-trough or trough-to-adjacent-peak, where the peak and trough are separated by one crossing of the zero-line: this measurement is sometimes described as "one-half peak-to-peak amplitude." The periods are to be measured as twice the time-intervals separating the peak and adjacent-trough from which the amplitudes are measured. The amplitude-phase arrival-times are to be measured and reported too as the time of the zero-crossing between the peak and adjacent-trough from which the amplitudes are measured. The issue of amplitude and period measuring procedures, and circumstances under which alternative procedures are acceptable or preferable, is discussed further in Section 5 of IS 3.3 and in section 3.2.3.3 of Chapter 3 of NMSOP-2.

Amplitudes measured according to recommended IASPEI standard procedures should be reported with the following ISF amplitude "phase names": IAML, IAmb_Lg, IAmb, IAMs_20, IVmB_BB and IVMs_BB. "I" stands for "International" or "IASPEI", "A" for displacement amplitude, measured in nm, and "V" for velocity amplitude, measured in nm/s. Although the ISC will calculate standard surface-wave magnitudes only for earthquakes shallower than 60 km, contributing agencies or stations are encouraged to report standard amplitude measurements of IAMs_20 and IVMs_BB for deeper earthquakes as well.

Note that the commonly known classical calibration relationships have been modified in the following to be consistent with displacements measured in nm, and velocities in nm/s, which is now common with high-resolution digital data and analysis tools. With these general definitions of the measurement parameters, where R is hypocentral distance in km (typically less than 1000 km), Δ is epicentral distance in degrees and h is hypocentre depth in km, the standard formulas and procedures read as follows:

ML:

$$ML = \log_{10}(A) + 1.11 \log_{10} R + 0.00189R - 2.09 \tag{6.1}$$

for crustal earthquakes in regions with attenuative properties similar to those of southern California, and with A being the maximum trace amplitude in nm that is measured on output from a horizontal-component instrument that is filtered so that the response of the seismograph/filter system replicates that of a Wood-Anderson standard seismograph (but with a static magnification of 1). For the normalised simulated response curve and related poles and zeros see Figure 1 and Table 1 in IS 3.3 of NMSOP-2.

Equation (6.1) is an expansion of that of *Hutton and Boore* (1987). The constant term in equation (6.1), -2.09, is based on an experimentally determined static magnification of the Wood-Anderson of 2080 (see *Uhrhammer and Collins* (1990)), rather than the theoretical magnification of 2800 that was specified by the seismograph's manufacturer. The formulation of equation (6.1) assures that reported ML amplitude data are not affected by uncertainty in the static magnification of the Wood-Anderson seismograph.

For seismographic stations containing two horizontal components, amplitudes are measured independently from each horizontal component and each amplitude is treated as a single datum. There is no effort to measure the two observations at the same time, and there is no attempt to compute a vector average. For crustal earthquakes in regions with attenuative properties that are different from those of coastal California and for measuring magnitudes with vertical-component seismographs the constants in the above equation have to be re-determined to adjust for the different regional attenuation and travel paths as well as for systematic differences between amplitudes measured on horizontal and vertical seismographs.

mb_Lg:

$$mb\_Lg = \log_{10}(A) + 0.833 \log_{10} R + 0.434\gamma(R - 10) - 0.87 \tag{6.2}$$

where A = "sustained ground-motion amplitude" in nm, defined as the third largest amplitude in the time window corresponding to group velocities of 3.6 to 3.2 km/s, in the period (T) range 0.7 s to 1.3 s; R = epicentral distance in km, γ = coefficient of attenuation in km^{-1}. γ is related to the quality factor Q through the equation $\gamma = \pi/(QUT)$, where U is group velocity and T is the wave period of the L_g wave. γ is a strong function of crustal structure and should be determined specifically for the region in which the mb_Lg is to be used. A and T are measured on output from a vertical-component instrument that is filtered so that the frequency response of the seismograph/filter system replicates that of a WWSSN short-period seismograph (see Figure 1 and Table 1 in IS 3.3 of NMSOP-2). Arrival times with respect to the origin of the seismic disturbance are used, along with epicentral distance, to compute group velocity U.

mb:

$$mb = \log_{10}(A/T) + Q(\Delta, h) - 3.0 \tag{6.3}$$

where A = vertical component P-wave ground amplitude in nm measured at distances $20° \leq \Delta \leq 100°$ and calculated from the maximum trace-amplitude with $T < 3$ s in the entire P-phase train (time spanned by P, pP, sP, and possibly PcP and their codas, and ending preferably before PP). A and T are measured on output from an instrument that is filtered so that the frequency response of the seismograph/filter system replicates that of a WWSSN short-period seismograph (see Figure 1 and Table 1 in IS 3.3 of NMSOP-2). A is determined by dividing the maximum trace amplitude by the magnification of the simulated WWSSN-SP response at period T.

$Q(\Delta, h)$ = attenuation function for PZ (P-waves recorded on vertical component seismographs) established by *Gutenberg and Richter* (1956) in the tabulated or algorithmic form as used by the U.S. Geological Survey/National Earthquake Information Center (USGS/NEIC) (see Table 2 in IS 3.3 and program description PD 3.1 in NMSOP-2);

mB_BB:

$$mB\_BB = \log_{10}(Vmax/2\pi) + Q(\Delta, h) - 3.0 \tag{6.4}$$

where $Vmax$ = vertical component ground velocity in nm/s at periods between $0.2\text{ s} < T < 30\text{ s}$, measured in the range $20° \leq \Delta \leq 100°$. $Vmax$ is calculated from the maximum trace-amplitude in the entire P-phase train (see mb), as recorded on a seismogram that is proportional to velocity at least in the period range of measurements. $Q(\Delta, h)$ = attenuation function for PZ established by *Gutenberg and Richter* (1956). Equation (6.3) differs from the equation for mB of *Gutenberg and Richter* (1956) by virtue of the $log_{10}(Vmax/2\pi)$ term, which replaces the classical $\log_{10}(A/T)_{max}$ term. Contributors should continue to send observations of A and T to ISC.

Ms_20:

$$Ms\_20 = \log_{10}(A/T) + 1.66\log_{10}\Delta + 0.3 \tag{6.5}$$

where A = vertical-component ground displacement in nm at $20° \leq \Delta \leq 160°$ epicentral distance measured from the maximum trace amplitude of a surface-wave phase having a period T between 18 s and 22 s on a waveform that has been filtered so that the frequency response of the seismograph/filter replicates that of a WWSSN long-period seismograph (see Figure 1 and Table 1 in IS 3.3 of NMSOP-2). A is determined by dividing the maximum trace amplitude by the magnification of the simulated WWSSN-LP response at period T. Equation (6.5) is formally equivalent to the Ms equation proposed by *Vaněk et al.* (1962) but is here applied to vertical motion measurements in a narrow range of periods.

Ms_BB:

$$Ms\_BB = \log_{10}(Vmax/2\pi) + 1.66\log_{10}\Delta + 0.3 \tag{6.6}$$

where $Vmax$ = vertical-component ground velocity in nm/s associated with the maximum trace-amplitude in the surface-wave train at periods between 3 s $< T <$ 60 s as recorded at distances $2^\circ \leq \Delta \leq 160^\circ$ on a seismogram that is proportional to velocity in that range of considered periods. Equation (6.6) is based on the Ms equation proposed by *Vaněk et al.* (1962), but is here applied to vertical motion measurements and is used with the $\log_{10}(Vmax/2\pi)$ term replacing the $\log_{10}(A/T)_{max}$ term of the original. As for mB_BB, observations of A and T should be reported to ISC.

Mw:

$$Mw = (\log_{10} M_0 - 9.1)/1.5 \tag{6.7}$$

Moment magnitude Mw is calculated from data of the scalar seismic moment M_0 (when given in Nm), or

$$Mw = (\log_{10} M_0 - 16.1)/1.5 \tag{6.8}$$

its CGS equivalent when M_0 is in dyne·cm.

Please note that the magnitude nomenclature used in this section uses the IASPEI standards as the reference. However, the magnitude type is typically written in plain text in most typical data reports and so it is in this document. Moreover, writing magnitude types in plain text allows us to reproduce the magnitude type as stored in the database and provides a more direct identification of the magnitude type reported by different agencies. A short description of the common magnitude types available in this Summary is reported in Table 9.6.

6.4 The IASPEI Seismic Format (ISF)

The ISF is the IASPEI approved standard format for the exchange of parametric seismological data (hypocentres, magnitudes, phase arrivals, moment tensors, etc) and is one of the formats used by the ISC. It was adopted as standard in August 2001 and is an extension of the International Monitoring System 1.0 (IMS1.0) standard, which was developed for exchanging data used to monitor the Comprehensive Test Ban Treaty. An example of the ISF is shown in Listing 6.1.

Bulletins which use the ISF are comprised of origin and arrival information, provided in a series of data blocks. These include: a bulletin title block; an event title block; an origin block; a magnitude sub-block; an effect block; a reference block; and a phase block.

Within these blocks an important extension of the IMS1.0 standard is the ability to add additional comments and thus provide further parametric information. The ISF comments are distinguishable within the open parentheses required for IMS1.0 comments by beginning with a hash mark (#) followed by a keyword identifying the type of formatted comment. Each additional line required in the ISF comment begins with the hash (within the comment parentheses) followed by blank spaces at least as long as the keyword. Optional lines within the comment are signified with a plus sign (+) instead of a hash mark. The keywords include `PRIME` (to designate a prime origin of a hypocentre); `CENTROID` (to indicate the centroid origin); `MOMTENS` (moment tensor solution); `FAULT_PLANE` (fault plane solution); `PRINAX` (principal axes); `PARAM` (an origin parameter, e.g. hypocentre depth given by a depth phase).

The full documentation for the ISF is maintained at the ISC and can be downloaded from:
www.isc.ac.uk/doc/code/isf/isf.pdf

The documentation for the IMS1.0 standard can be downloaded from:
www.isc.ac.uk/doc/code/isf/ims1_0.pdf

Listing 6.1: *Example of an ISF formatted event*

```
Event 15146084 Near east coast of eastern Honshu
   Date       Time        Err   RMS Latitude Longitude  Smaj  Smin  Az Depth   Err Ndef Nsta Gap  mdist  Mdist Qual   Author      OrigID
2010/09/01 07:32:00                37.9000  141.9000f                  44.0                                              NIED      17047453
 (#MOMTENS sc    M0 fCLVD    MRR    MTT    MPP    MRT    MTP    MPR NST1 NST2 Author   )
 (#             eM0 eCLVD    eRR    eTT    ePP    eRT    eTP    ePR NCO1 NCO2 Duration )
 (#       16 5.760                                                    NIED      )
 (#                                                                             )
 (#FAULT_PLANE Typ Strike   Dip    Rake  NP  NS Plane Author    )
 (#            BDC 199.00 19.00   86.00               NIED      )
 (+                23.00 71.00   91.00                          )
 (Epicenter information from JMA Focal Mechanism Solution Determined Manually Variance reduction = 96.98%)
2010/09/01 07:32:47.50        1.470  37.8300  142.2400                 37.0          71       281  11.00  51.10     uk BJI       15275482
2010/09/01 07:32:52.20   0.92        38.0320  141.8090   6.7   4.5 110  44.0         114                                 MOS       16741494
2010/09/01 07:32:52.53   0.35 0.889  37.9202  141.8229 4.090 2.740 145  49.7  2.76  490  478 122   0.65  92.01 m i fe ISCJB     01631732
 (#PARAM pP_DEPTH=41.11021)
2010/09/01 07:32:52.60   0.10        37.9100  141.8700   1.1   0.9  -1  43.0   1.0                                    fe JMA       16271222
 (Felt I=III-III J1)
2010/09/01 07:32:53.66   0.42 0.770  37.9250  141.7880   5.1   3.4 140  44.4   3.9  102       127   3.17 127.67     fe NEIC      01134459
 (#MOMTENS sc    M0 fCLVD    MRR    MTT    MPP    MRT    MTP    MPR NST1 NST2 Author   )
 (#             eM0 eCLVD    eRR    eTT    ePP    eRT    eTP    ePR NCO1 NCO2 Duration )
 (#       16 5.800         3.600 -0.550 -3.040  1.850 -1.140  4.150           NIED      )
 (#                                                                             )
 (#FAULT_PLANE Typ Strike   Dip    Rake  NP  NS Plane Author    )
 (#            BDC 199.00 19.00   86.00               NIED      )
 (+                23.00 71.00   91.00                          )
 (Recorded [3 JMA] in Miyagi; [2 JMA] in Fukushima and Iwate; [1 JMA] in Akita, Aomori, Ibaraki, Tochigi and Yamagata.)
2010/09/01 07:32:53.70   0.20        37.9300  142.0600 2.224 1.112  -1  50.3   1.0  262   89                             GCMT      00124877
 (#CENTROID)
 (#MOMTENS sc    M0 fCLVD    MRR    MTT    MPP    MRT    MTP    MPR NST1 NST2 Author   )
 (#             eM0 eCLVD    eRR    eTT    ePP    eRT    eTP    ePR NCO1 NCO2 Duration )
 (#       16 6.891         5.430 -0.440 -4.990  1.500 -2.070  3.710   64   89 GCMT      )
 (#                        0.173  0.118  0.120  0.100  0.094  0.110  102  160      0.90 )
 (#FAULT_PLANE Typ Strike   Dip    Rake  NP  NS Plane Author    )
 (#            BDC  22.00 63.00   91.00               GCMT      )
 (+               201.00 27.00   89.00                          )
 (#PRINAX sc  T_val T_azim  T_pl  B_val B_azim  B_pl  P_val P_azim  P_pl Author    )
 (#       16  6.711 293.00 72.00  0.360 201.00  0.00 -7.072 111.00 18.00 GCMT      )
 (nsta1 refers to body waves, cutoff=40s. nsta2 refers to surface waves, cutoff=50s.)
2010/09/01 07:32:55.05   1.77 1.070  37.8692  141.9450  12.9  10.4 100  63.6  16.8   36       127   3.24 117.04     uk IDC       16680924
2010/09/01 07:32:52.23   0.30 1.333  37.8836  141.9148 5.558 4.001 142  38.9  2.33  542  478  61   0.72 141.68 m i se ISC       01237353
 (#PRIME)
 (#PARAM pP_DEPTH=39.00000)

Magnitude  Err Nsta Author      OrigID
Mw      5.1          NIED      17047453
Ms      4.8       61 BJI       15275482
Ms7     4.6       58 BJI       15275482
mB      5.1       48 BJI       15275482
mb      5.0       63 BJI       15275482
MS      4.7       19 MOS       16741494
mb      5.2       49 MOS       16741494
MS      4.6       43 ISCJB     01631732
mb      4.9      138 ISCJB     01631732
        5.0          JMA       16271222
mb      5.0       55 NEIC      01134459
MW      5.1          NIED      01134459
MW      5.2       89 GCMT      00124877
MS      4.4 0.1   28 IDC       16680924
Ms1     4.4 0.1   28 IDC       16680924
mb      4.4 0.1   27 IDC       16680924
mb1     4.5 0.0   33 IDC       16680924
mb1mx   4.4 0.0   37 IDC       16680924
mbtmp   4.7 0.1   33 IDC       16680924
ms1mx   4.3 0.1   31 IDC       16680924
MS      4.7 0.2   43 ISC       01237353
mb      4.9 0.2  145 ISC       01237353

Sta     Dist  EvAz Phase        Time      TRes  Azim AzRes   Slow   SRes Def   SNR       Amp   Per Qual Magnitude    ArrID
JIO     0.72 322.1 Pn       07:33:05.9   -0.06                            T__                      d_               49540510
JIO     0.72 322.1 Sn       07:33:15.0   -0.82                            T__                      __               49540511
JMM     0.89 269.2 Pn       07:33:08.4     0.2                            T__                      d_               49540512
JMM     0.89 269.2 Sn       07:33:19.2   -0.68                            T__                      __               49540513
JFK     0.97 238.3 Pn       07:33:09.5     0.1                            T__                      d_               49540514
JFK     0.97 238.3 Sn       07:33:21.5   -0.54                            T__                      __               49540515
JOU     1.10 296.4 Pn       07:33:11.5     0.4                            T__                      d_               49540516
JOU     1.10 296.4 Sn       07:33:25.4     0.3                            T__                      _e               49540517
ONAJ    1.18 229.0 Pn       07:33:12.4     0.1                            T__                      d_               49540530
JMK     1.20 333.1 Pn       07:33:12.5     0.0                            T__                      d_               49540518
JMK     1.20 333.1 Sn       07:33:27.1   -0.39                            T__                      _e               49540519
OFUJ    1.21 350.9 Pn       07:33:12.3   -0.34                            T__                      d_               49540531
.
.
.
532A   91.05  49.8 P        07:45:52.799 -0.00  90.9                      T__                      __               05504129
334A   91.18  47.9 P        07:45:54.012   0.7  91.0                      T__                      __               05504128
H06N1  91.36  64.9 T        09:27:33.559                                  ___   6.0                __               58438458
MIAR   91.43  42.9 P        07:45:54.85    0.5  91.2                      T__                      __               05504179
Y39A   91.60  43.6 P        07:45:55.543   0.4  91.4                      T__                      __               05504214
534A   91.98  49.0 P        07:45:57.308   0.2  91.8                      T__                      __               05504130
KEST   94.59 323.1 LR       08:33:52.432       320.5         38.70        ___             466.5 18.65  __               58438480
ESDC   96.70 334.2 LR       08:34:40.011       345.0         38.30        ___             375.8 20.18  __               58438449
TORD  117.01 315.6 PKPdf    07:51:32.55  -0.82  17.7          2.30        T__   5.1         0.4  0.70  __               58438504
TORD  117.01 315.6 PP       07:52:39.3   -2.90  31.2          6.30        T__   6.5         1.3  0.68  __               58438505
QSPA  127.62 180.0 PKPdf    07:51:52.02  -0.16                            T__                      _e               23535420
SNAA  141.68 197.1 PKPdf    07:52:13.751 -4.52                            T__                      __               20375340
VNA2  143.24 196.3 PKPbc    07:52:18.562   0.4 122.0          2.31        ___                      __               20375338
VNA1  143.64 196.2 PKPbc    07:52:19.77    0.6                            ___                      __               20375339
```

6.5 Ground Truth (GT) Events

Accurate locations are crucial in testing Earth models derived from body and surface wave tomography as well as in location calibration studies. 'Ground Truth' (GT) events are well-established source locations and origin times. A database of IASPEI reference events (GT earthquakes and explosions) is hosted at the ISC (www.isc.ac.uk). A full description of GT selection criteria can be found in *Bondár and McLaughlin* (2009a).

The events are coded by category GT0, GT1, GT2 or GT5, where the epicentre of a GTX event is known to within X km to a 95% confidence level. A map of all IASPEI reference events is shown in Figure 6.8 and the types of event are categorised in Figure 6.9. GT0 are explosions with announced locations and origin times. GT1 and GT2 are typically explosions, mine blasts or rock bursts either associated to explosion phenomenology located upon overhead imagery with seismically determined origin times, or precisely located by in-mine seismic networks. GT1-2 events are assumed to be shallow, but depth is unknown.

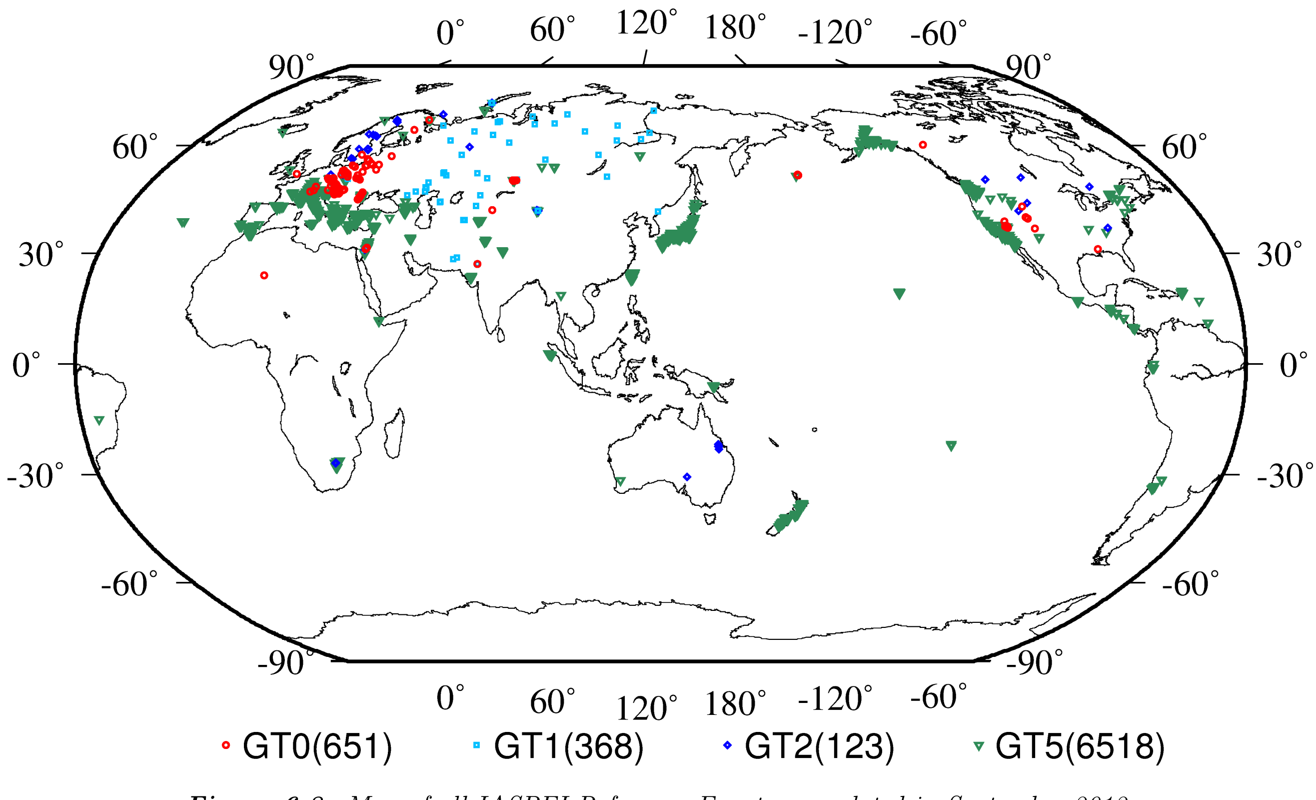

Figure 6.8: *Map of all IASPEI Reference Events as updated in September 2012.*

The database consists of nuclear explosions of GT0–5 quality, adopted from the Nuclear Explosion Database (*Bennett et al.*, 2010); GT0–5 chemical explosions, rock bursts, mine-induced events, as well as a few earthquakes, inherited from the reference event set by *Bondár et al.* (2004); GT5 events (typically earthquakes with crustal depths) that have been identified using either the method of *Bondár et al.* (2008) (2,275 events) or *Bondár and McLaughlin* (2009a) (updated regularly from the EHB catalogue (*Engdahl et al.*, 1998)), which uses the following criteria:

- 10 or more stations within 150 km from the epicentre

- one or more stations within 10 km
- $\Delta U \leq 0.35$
- a secondary azimuthal gap $\leq 160°$

where ΔU is the network quality metric defined as the mean absolute deviation between the best-fitting uniformly distributed network of stations and the actual network:

$$\Delta U = \frac{4 \sum |esaz_i - (unif_i + b)|}{360N}, 0 \leq \Delta U \leq 1 \tag{6.9}$$

where N is the number of stations, $esaz_i$ is the ith event-to-station azimuth, $unif_i = 360i/N$ for $i = 0$, ..., $N - 1$, and $b = avg\,(esaz_i) - avg\,(unif_i)$. ΔU is normalised so that it is 0 when the stations are uniformly distributed in azimuth and 1 when all the stations are at the same azimuth.

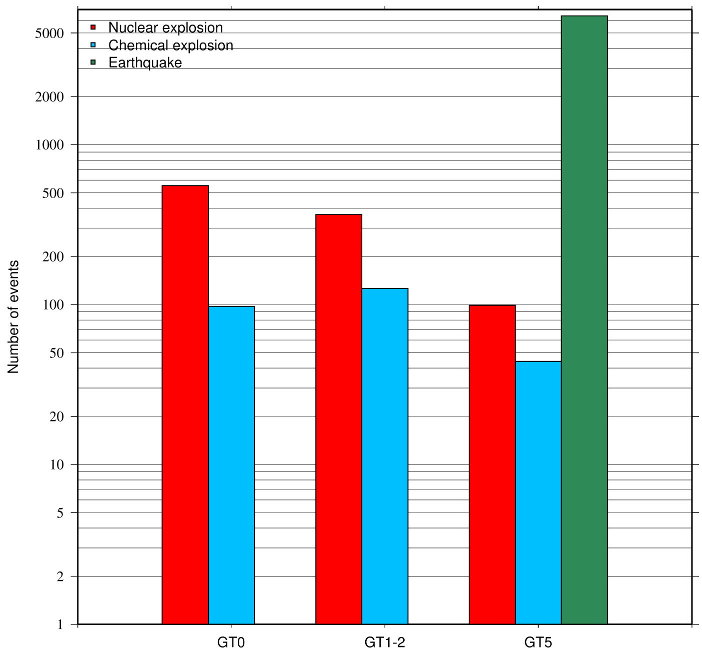

Figure 6.9: *Histogram showing the event types within the IASPEI Reference Event List as updated in September 2012.*

The seismological community is invited to participate in this project by nominating seismic events for the reference event database. Submitters may be contacted for further confirmation and for arrival time data. The IASPEI Reference Event List will be periodically published both in written and electronic form with proper acknowledgement of all submitters.

6.6 Nomenclature of Event Types

The nomenclature of event types currently used in the ISC Bulletin takes its origin from the IASPEI International Seismic Format (ISF).

Event type codes are composed of a leading character that generally indicates the confidence with which the type of the event is asserted and a trailing character that generally gives the type of the event. The leading and trailing characters may be used in any combination.

The **leading** characters are:

- s = suspected
- k = known
- f = felt (implies known)
- d = damaging (implies felt and known)

The **trailing** characters are:

- c = meteoritic event
- e = earthquake
- h = chemical explosion
- i = induced event
- l = landslide
- m = mining explosion
- n = nuclear explosion
- r = rock burst
- x = experimental explosion

A chemical explosion might be for mining or experimental purposes, and it is conceivable that other types of event might be assigned two or more different event type codes. This is deliberate, and matches the ambiguous identification of events in existing databases.

In addition, the code `uk` is used for events of unknown type and `ls` is used for known landslides.

The frequency of the different event types designated in the ISC Bulletin since 1964 is indicated in Figure 6.10.

There are currently plans to revise this nomenclature as part of the coordination process between the National Earthquake Information Center (NEIC/USGS), Centre Sismologique Euro-Méditerranéen (CSEM/EMSC) and the ISC.

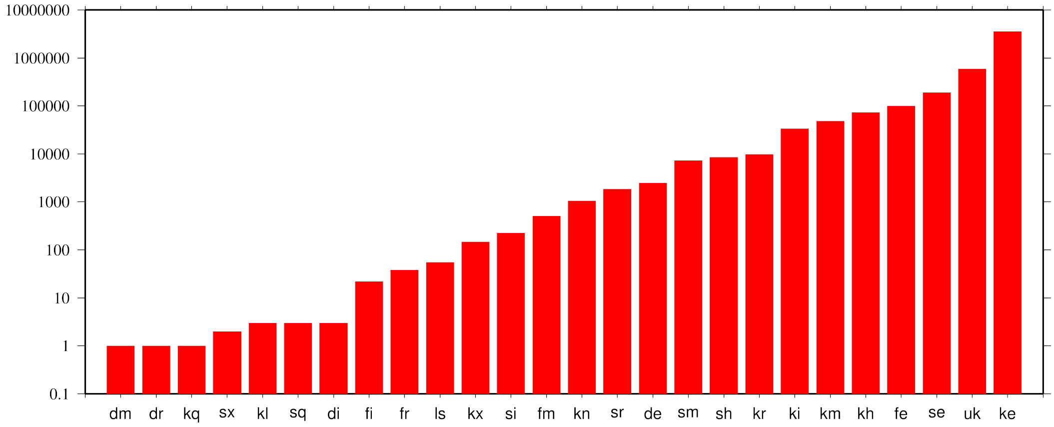

Figure 6.10: *Counts of event types in the ISC Bulletin*

7

Summary of Seismicity, January - June 2010

The first half of 2010 has seen one of the deadliest earthquakes in recorded history. The 2010 January Mw 7.0 Haiti earthquake probably claimed over 100,000 lives, with one official estimate indicating 316,000 lives lost. The 2010 February Mw 8.8 Maule, Chile, earthquake was at that time the fifth largest recorded earthquake since 1900, claiming at least 523 lives. Elazig, Turkey, was struck in March by an Mw 6.1 earthquake with a death toll of at least 42 people. In April, Qinghai province, China, was hit by an Mw 6.9 earthquake killing at least 2,698 people. An Mw 7.2 earthquake struck the Mexicali Valley in Baja California, Mexico, in April, killing two and injuring many more. In June, Papua, Indonesia, was hit by an Mw 7.0 earthquake, killing at least 17 people. The death toll for earthquakes in the first half of 2010 is clearly dominated by that from the Haiti earthquake.

The ISC analysts worked through a large amount of data following the Haiti and Chile earthquakes. The earthquake in Haiti resulted in several hundred aftershocks reported to the ISC in the months of January and February. However, following the Chilean earthquake, over 3000 aftershocks were reported to ISC in the months of February, March, April and May. The Baja California earthquake in April also produced over 700 aftershocks in the months of April, May and June. These three earthquakes all occurred relatively close to North America and therefore all moderately sized aftershocks were well recorded by the US Array, Earthscope stations. The US Array data contribution to the ISC for the mainshocks and aftershocks of these three events was substantial.

The number of events in this Bulletin Summary categorised by type are given in Table 7.1.

Table 7.1: *Summary of events by type between 2010 January and June.*

damaging earthquake	31
felt earthquake	2296
suspected earthquake	7715
known earthquake	145823
suspected mine explosion	762
known mine explosion	8359
suspected chemical explosion	63
known chemical explosion	3363
felt induced event	1
suspected induced event	1
known induced event	3247
felt rockburst	1
known rockburst	45
suspected rockburst	334
suspected experimental explosion	1
total	172042

Figure 7.1 shows the number of moderate and large earthquakes in the first half of 2010. The distribution of the number of earthquakes should follow the Gutenberg-Richter law.

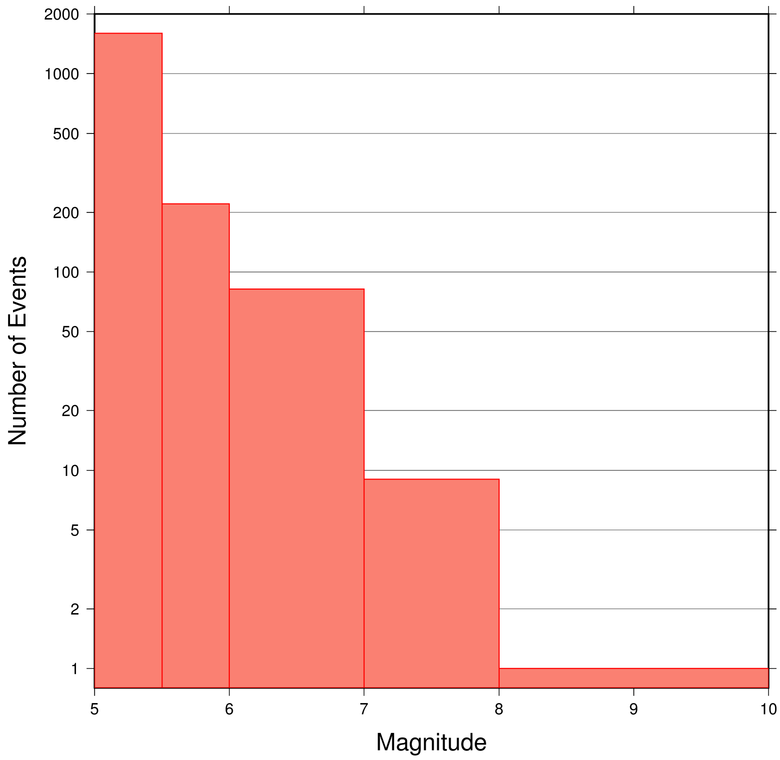

Figure 7.1: *Number of moderate and large earthquakes between 2010 January and June. The non-uniform magnitude bins here correspond with the magnitude intervals used in Figures 7.2 to 7.6.*

The period January-June 2010 produced 10 earthquakes with Mw $\geq$ 7; these are listed in Table 7.2.

Table 7.2: *Summary of the earthquakes of magnitude Mw $\geq$ 7 between 2010 January and June.*

Date	lat °	lon °	depth km	Mw	Flinn-Engdahl Region
2010-02-27 06:34:13	-36.15	-72.93	28	8.8	Near coast of central Chile
2010-04-06 22:15:02	2.36	97.11	33	7.8	Northern Sumatera
2010-06-12 19:26:50	7.85	91.95	31	7.5	Nicobar Islands region
2010-02-27 08:01:23	-37.84	-75.21	35	7.3	Off coast of central Chile
2010-05-09 05:59:42	3.73	96.03	42	7.3	Northern Sumatera
2010-04-04 22:40:43	32.28	-115.26	5	7.2	California - Baja California border region
2010-05-27 17:14:46	-13.67	166.67	35	7.2	Vanuatu Islands
2010-01-03 22:36:29	-8.88	157.42	30	7.1	Bougainville - Solomon Islands region
2010-01-12 21:53:10	18.38	-72.59	15	7.0	Haiti region
2010-06-16 03:16:29	-2.20	136.59	22	7.0	Irian Jaya region

Figures 7.2 to 7.6 show the geographical distribution of moderate and large earthquakes in various magnitude ranges.

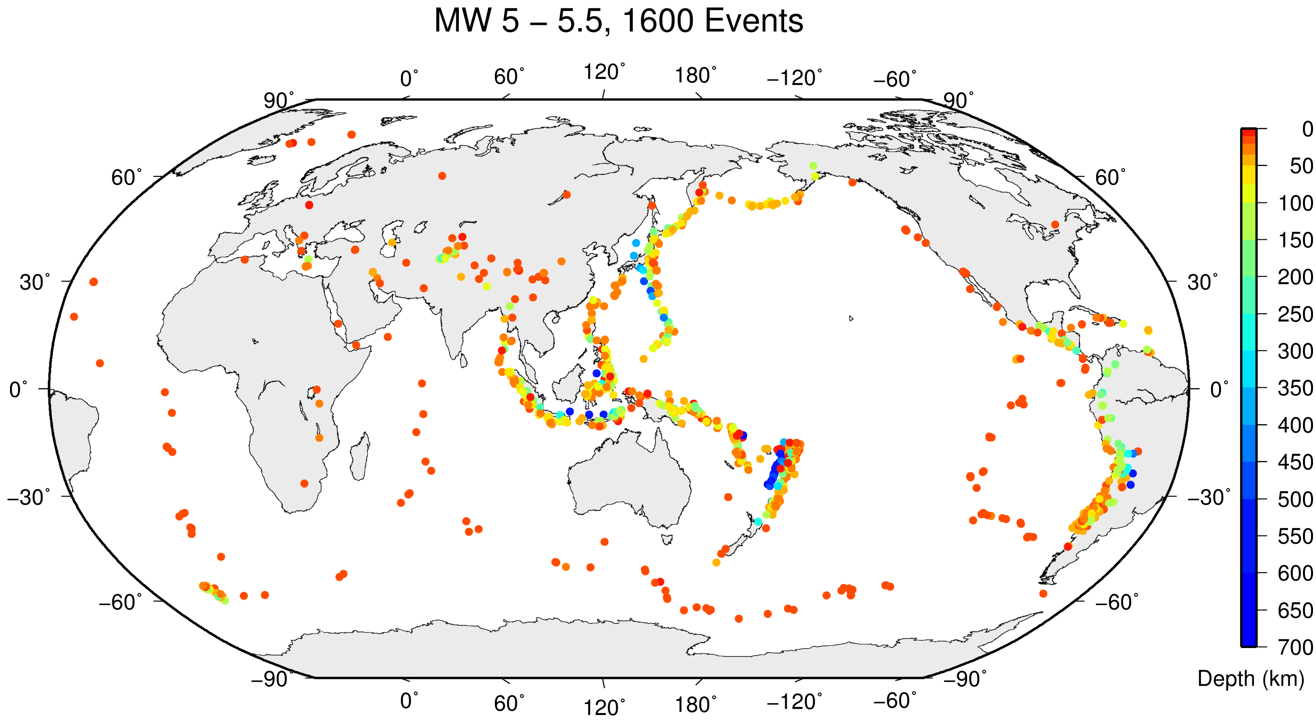

Figure 7.2: *Geographic distribution of magnitude 5-5.5 earthquakes between 2010 January and June.*

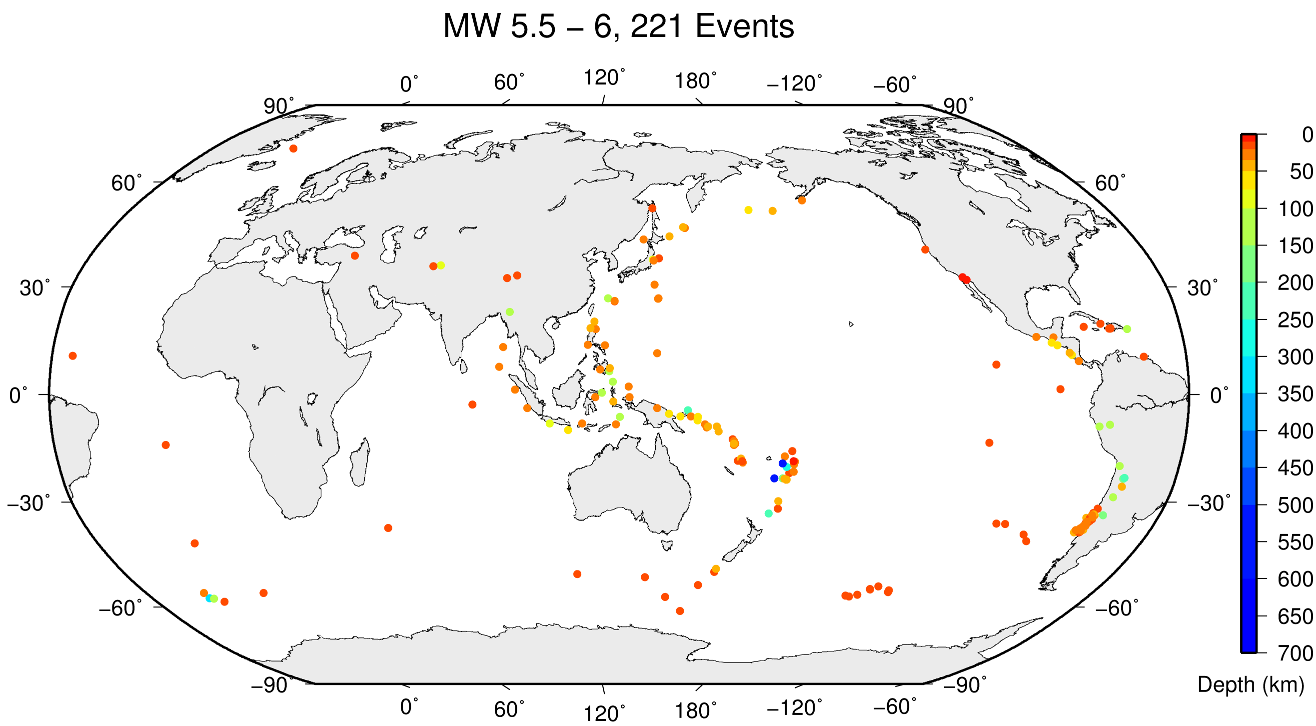

Figure 7.3: *Geographic distribution of magnitude 5.5-6 earthquakes between 2010 January and June.*

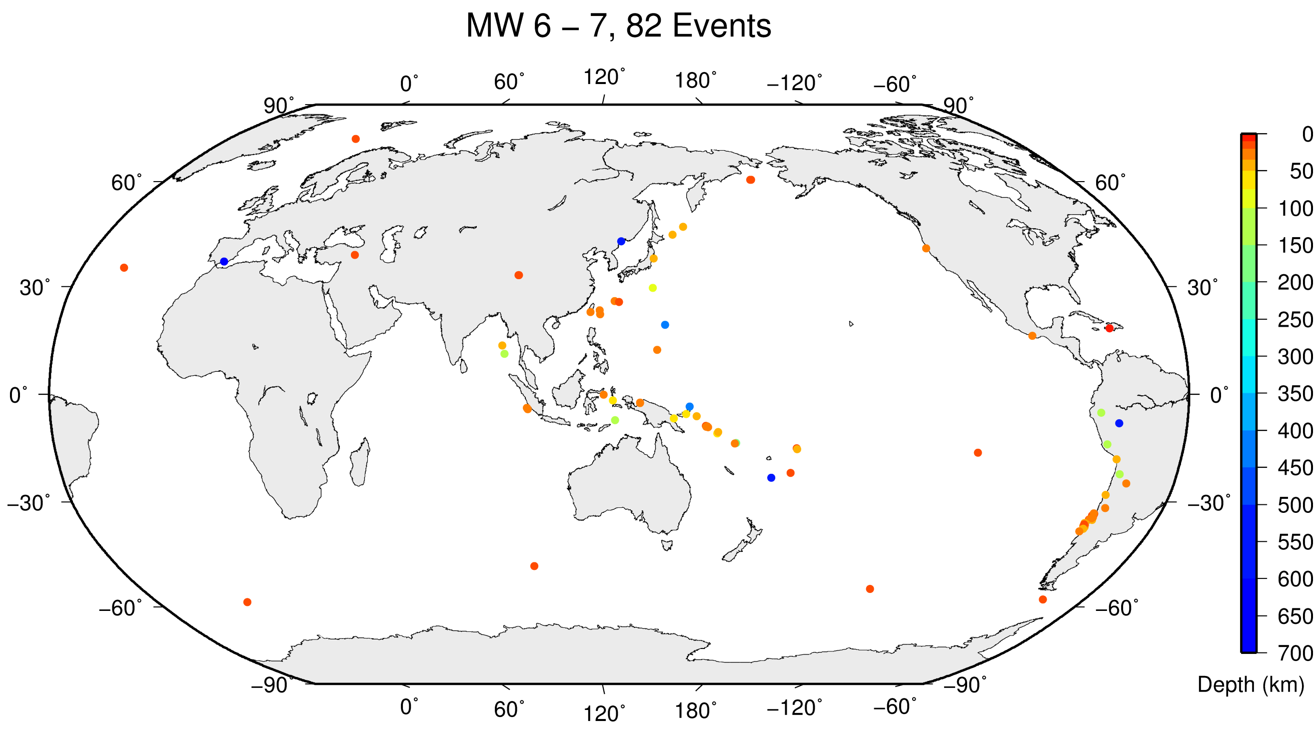

Figure 7.4: *Geographic distribution of magnitude 6-7 earthquakes between 2010 January and June.*

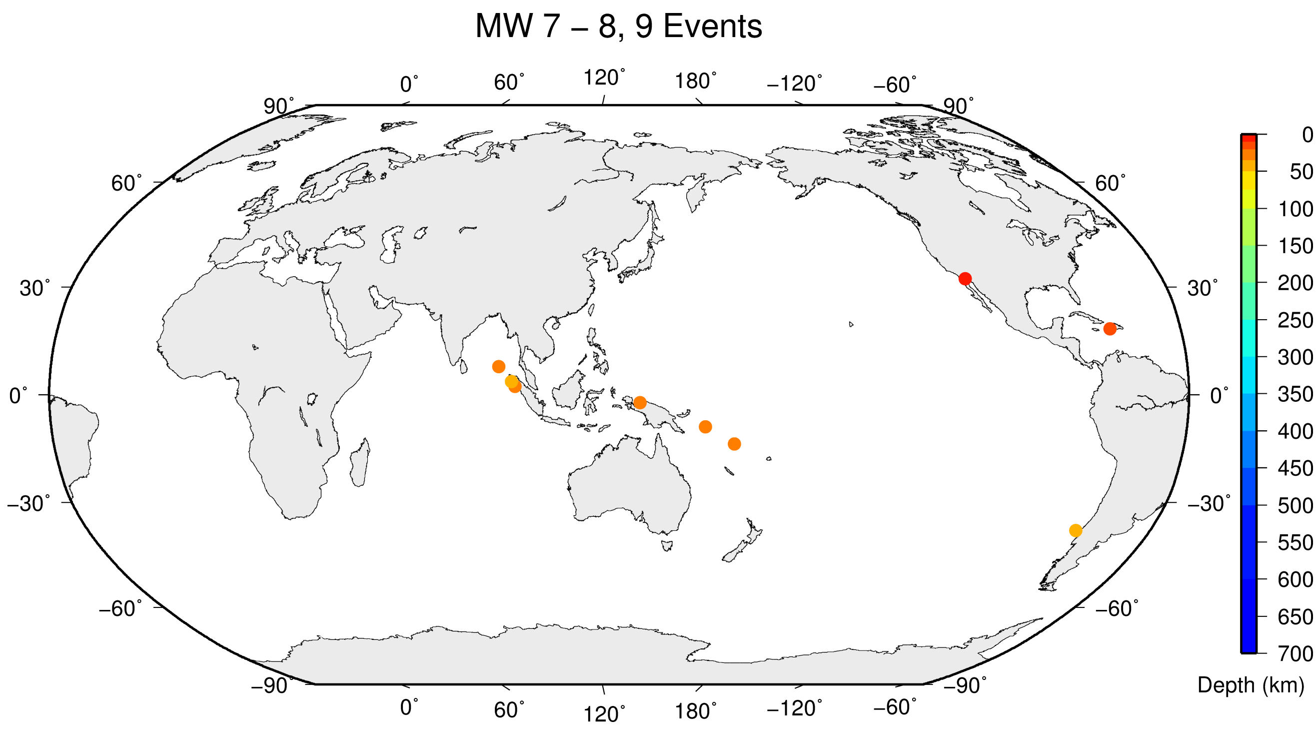

Figure 7.5: *Geographic distribution of magnitude 7-8 earthquakes between 2010 January and June.*

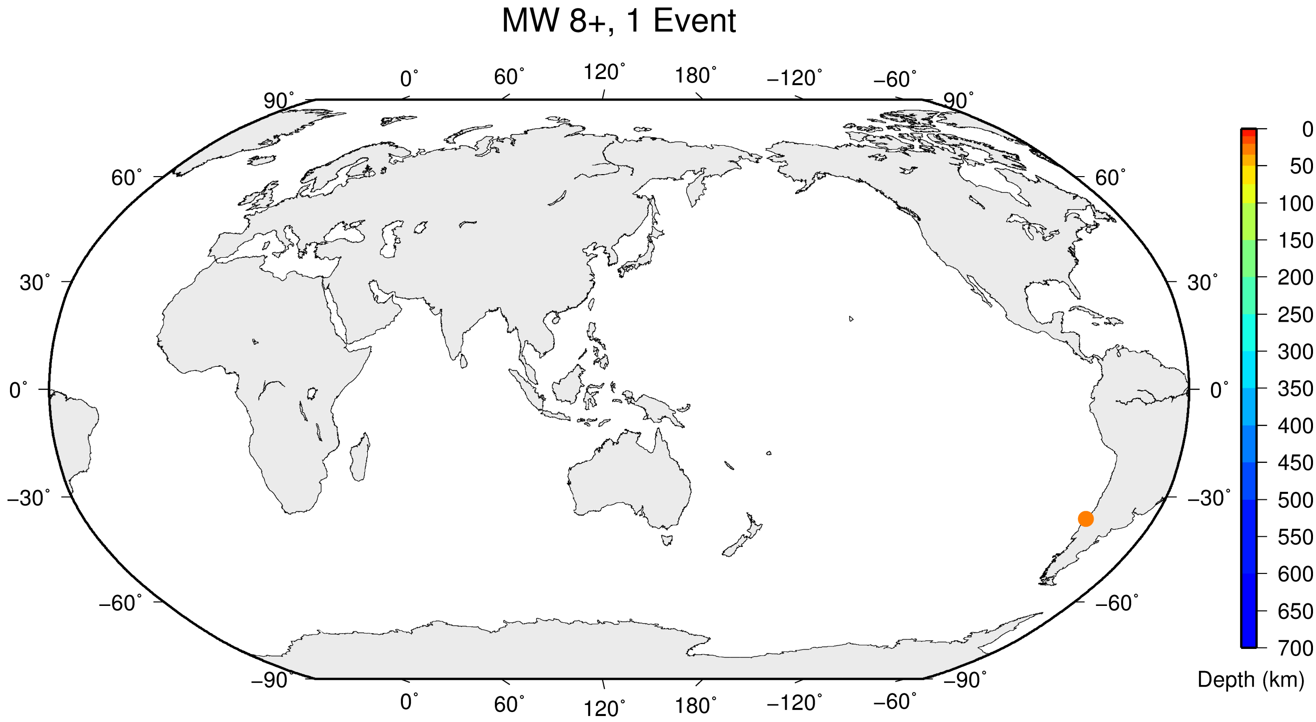

Figure 7.6: *Geographic distribution of magnitude 8+ earthquakes between 2010 January and June.*

8

Notable Events

8.1 The 12^{th} January 2010 M_W 7.0 Haiti Earthquake

Allison Bent
Geological Survey of Canada

8.1.1 Introduction

The magnitude (Mw) 7.0 Haiti earthquake of 12 January 2010 is likely the most devastating earthquake to have occurred in the western hemisphere both in terms of the number of fatalities and the impact on a nation as a whole. Estimates of the death toll range from less than 50 000 to over 300 000 with the most likely value being in the range of 137 000 (Daniell and Vervaek, 2012). Another 300 000 were injured and 1.3 million left homeless. Two years after the earthquake many people are still living in temporary shelters.

The earthquake occurred at 16:53 local time (21:53 UT) approximately 25 km WSW of the capital city of Port-au-Prince (18.443°N, 72.571°W, USGS, 2012), The mainshock was followed by a vigorous aftershock sequence including a magnitude (Mw) 6.0 event that occurred about 7 minutes after the mainshock and an Mw 5.9 earthquake on 20 January.

The location and style of faulting (strike-slip) of the mainshock initially suggested that it occurred on the Enriquillo-Plaintain Garden Fault (EPGF), a fault known to be capable of generating large earthquakes and which may have ruptured during several comparable sized earthquakes in the past (1751, 1770) but which had been relatively inactive for the past 200 years leading to a lack of earthquake awareness among the general population. Figures 8.1 and 8.2 contrast the seismicity of the 50 years preceding the magnitude 7.0 earthquake to that of the two years following it. More discussion of historical earthquakes in Haiti may be found in Bakun *et al* (2012) and the references therein.

Despite the magnitude and relatively shallow depth (10-15 km) of the earthquake, reconnaissance teams found no evidence for surface rupture on the EPGF (Eberhard *et al*, 2010) perhaps providing the first clue that the situation was more complicated than it first appeared. Subsequent research discussed later in this paper suggests that the earthquake sequence may not have occurred on the EPGF or that it was not the sole fault to rupture during the earthquake sequence.

Prior to the 2010 earthquake, seismic monitoring in Haiti had been extremely poor. While global

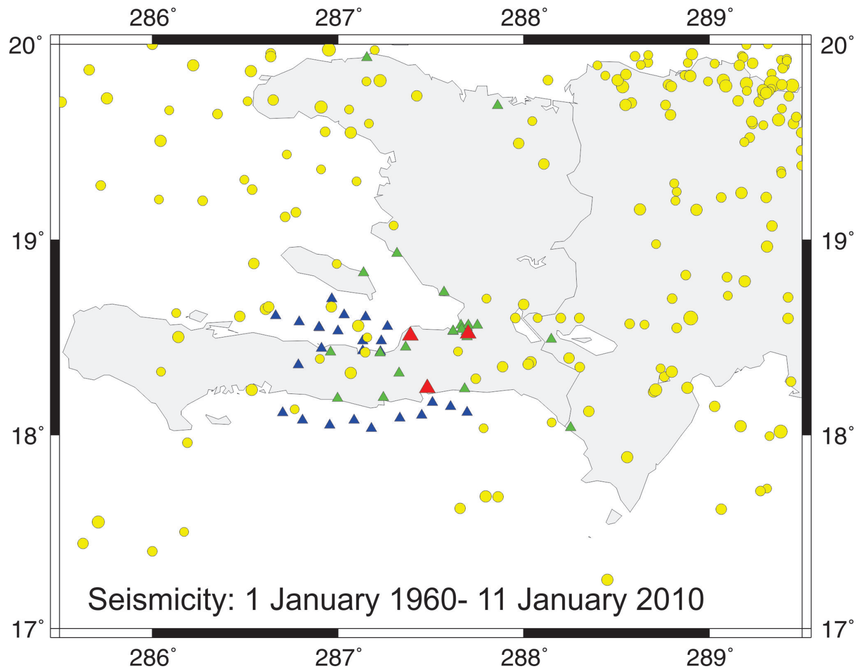

Figure 8.1: *Seismicity of Haiti and surrounding regions from 1960 until the day prior to the 2010 Mw 7.0 earthquake. Earthquakes of magnitude (any type) 3.5 and greater are plotted. Epicenters and magnitudes from the ISC catalog (ISC, 2012). Symbol size is scaled to magnitude. The triangles show the stations installed after the 2010 earthquake: Canadian real-time (red), French (blue) and American (green). The school station HAIF would plot very close to the stations at Port-au-Prince (upper right of the three red and in the cluster of green triangles).*

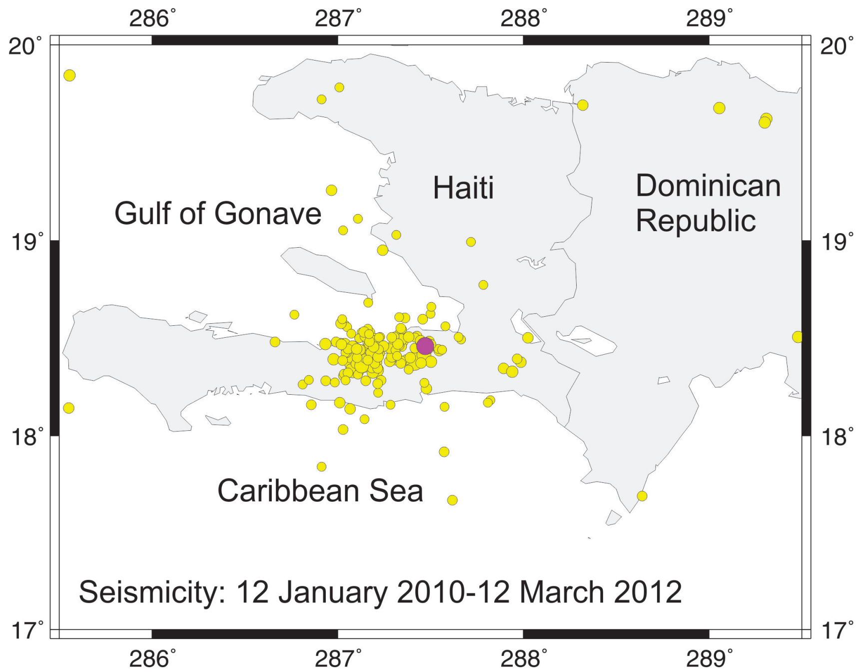

Figure 8.2: *Seismicity of Haiti and surrounding regions since 12 January 2012. The mainshock is shown in red. Magnitudes (3.5 and greater) and epicenters from the ISC (2012). Symbol size is scaled to magnitude.*

and Caribbean stations would have captured any moderate to large earthquakes, smaller ones would have for the most part gone undetected. At the time of the 12 January 2010 earthquake, the only seismograph station operating in Haiti was one at the Lycée français Alexandre Dumas in Port-au-Prince that formed part of a French-based school network (www.edusismo.org/index.asp). This station provided the closest recording of the mainshock (https://geoazur.oca.eu/spip.php?article672). Since that time several international organizations installed temporary or permanent stations in Haiti and the monitoring situation has somewhat improved (see subsequent section on New Stations and Figure 8.1).

The intent of this paper is to summarize the earthquake and work that has been done since January 2010 to better understand the earthquake sequence and seismic hazard in Haiti. The focus is on the seismological data and research but it should be noted that much has been learned through other data sets including, but not limited to, GPS and INSAR.

8.1.2 New Stations

Historically very few seismograph stations have operated in Haiti. At the time of the earthquake, the only known station in Haiti was a school seismograph in Port-au-Prince discussed in the previous section. Recent improvements to networks elsewhere in the Caribbean ensure that the moderate and larger earthquakes in Haiti are recorded but these stations do not catch all of the smaller earthquakes needed to establish relative recurrence rates and to build a reliable earthquake catalog for that country. Following the 2011 earthquake, many temporary and some long-term seismograph stations were deployed in and around Haiti by several organizations, in particular the Geological Survey of Canada, the United States Geological Survey and Géoazur (Figure 8.1).

In late January 2010, the United States Geological Survey sent a reconnaissance team to Haiti. Among other tasks, they installed four seismometers to monitor aftershocks (Eberhard *et al*, 2010; Hough *et al*, 2010). Data from these stations have been archived and are available from the Incorporated Research Institutes for Seismology (IRIS) data management center. Additional stations were installed over the next few months and included eight RefTek instruments, nine strong-motion (K2) accelerometers and three broadband stations all of which were installed primarily in the epicentral region (Altidor *et al*, 2010). Several of these temporary stations have since been replaced with permanent strong-motion NetQuakes instruments. Data from many of the K2 instruments and a list of station coordinates may be found at http://pasadena.wr.usgs.gov/office/hough/DATA.

In early February 2010 a team of French scientists primarily associated with Géoazur deployed twenty-one ocean bottom seismometers (OBS) in the nearshore regions surrounding the southern peninsula of Haiti. All were four component (3 seismograph and 1 hydrophone) stations. Fifteen short-period instruments operated until early March 2010. The remaining six broadband instruments remained in operation until mid-May 2010. Additionally, four broadband seismometers were installed on land in the eastern part of the rupture zone where the bathymetry was not suitable for OBS deployment. A more detailed account of the deployment including the station coordinates may be found at https://geoazur.oca.eu/spip.php?article670.

In February 2010 the Geological Survey of Canada installed three real-time, satellite-linked seismograph stations consisting of three-component broadband seismometers and three component strong motion instruments in Port-au-Prince, Jacmel and Leogâne (Figure 8.3). Aftershocks were located by GSC seismologists and the phase data and solutions were forwarded to the International Seismological Centre and other international organizations on a daily basis during the months immediately following the earthquake. The data are forwarded in real time to IRIS and the Caribbean Tsunami Warning Centre. The stations continue to operate but their reliability has somewhat decreased with time primarily due to problems with the power supply and security. Further information about the Canadian deployment may be found at http://www.earthquakescanada.nrcan.gc.ca/haiti/index-eng.php.

Figure 8.3: *The station installed in Léogâne by the Geological Survey of Canada. Photo by C. Andrews, GSC.*

8.1.3 Focal Mechanisms and Other Fault Parameters

While the initial focal mechanism for the mainshock (for example see GCMT, 2012, or USGS 2012) was primarily strike-slip consistent with rupture on the EPGF, subsequent analysis of aftershocks and non-seismological data implies that the rupture sequence was much more complex and raises significant doubts as to whether the events occurred on the EPGF. Analysis the mainshock and aftershocks using several different methods and data sets all find that the majority of the aftershocks are thrust events, incompatible with the strike-slip nature of the EPGF.

Hayes *et al* (2010) focused on modeling the mainshock in detail using a combination of seismological, geologic and geodetic data. Their model suggests a complex primarily unilateral rupture (toward the west) with small amounts of rupture occurring on subsidiary faults. The integrated data set suggests that little, if any, of the rupture occurred on the EPGF and raises the possibility of a future large earthquake on the EPGF. Mercier de Lépinay *et al* (2011) and Vallée (https://geoazur.oca.eu/spip.php?article614) also modeled the mainshock in detail and reached similar conclusions- a westward propagating but complex rupture unlikely to have occurred on the EPGF.

Many studies were undertaken to determine the focal mechanisms of the numerous aftershocks that followed the Mw 7.0 earthquake. A variety of methods and data sets were employed but all reached similar conclusions and raised the same questions about rupture on the EPGF as the in-depth mainshock models. Most of the aftershocks, including the largest, were found to have thrust mechanisms. Those that had strike-slip mechanisms generally occurred at the eastern end of the aftershock zone close to the epicenter of the mainshock. These studies include those of Nettles *et al* (2010) based on teleseismic moment tensor inversions, Bent (2011) from regional moment tensor analysis for the larger events and composite first motion mechanisms for the smaller ones, and Mercier de Lépinay *et al* (2011) from broadband modeling of regional data. A wide range of depths were obtained for the aftershocks through these studies but all were crustal and the largest number occurred at depths near 10 km.

8.1.4 Aftershock Locations

While existing global networks were used to monitor and locate the largest of the aftershocks, the newly deployed stations significantly lowered the magnitude location threshold. The earliest aftershock locations using the stations discussed in the previous section were generally undertaken by the organizations that deployed them using their own stations, primarily because much of the data were not available in real time. The data sets were in some cases supplemented by data from pre-existing regional stations, including Guantanamo Bay, Grand Turk and several stations in the Dominican Republic. Aftershock locations from the American, French and Canadian data sets all showed an aftershock zone extending roughly east-west and parallel to the EPGF. However, there were systematic differences in the locations with the American (USGS) locations being on or just north of the EPGF (USGS, 2012), the French (Géoazur) being north of those locations but generally onshore except at the western end of the aftershock zone (Mercier de Lépimay *et al*, 2011) and the Canadian (GSC) epicenters being mostly just offshore in the Gulf of Gonâve. While some of the differences may be due to differences in which events were being located, the fact that they are systematic suggests that they are more likely related to some combination of the choice of velocity model and to the network geometry.

Douilly *et al* (2011, 2012) are in the process of relocating the aftershocks using the data from all available stations, which should increase the accuracy of the locations. Their results suggest that the events are occurring not on the EPGF but on the Léogâne Fault, which is a previously unmapped fault just north of the EPGF described as 60° north dipping oblique thrust fault. They note that there is also some evidence that some of the activity at the western end of the rupture zone may be occurring on the offshore Trois Baies fault. The Léogâne Fault was also proposed for the mainshock rupture by Calais *et al* (2010) using GPS and INSAR data.

8.1.5 Summary/Conclusions

The 2010 Mw 7.0 earthquake that devastated much of southern Haiti occurred in a gap in the global earthquake monitoring system. Several international seismological agencies helped fill that gap in subsequent weeks and months through the deployment of temporary and permanent seismograph stations. Because much of the recorded data were not available in real time and therefore not immediately accessible to the international seismological community, valuable coordination was provided through data repositories such as the ISC for phase and other derived data and IRIS for waveform archiving.

The 2010 earthquake sequence has been and continues to be studied as the recovery continues. What initially appeared to be a simple rupture on a previously known fault (EPGF) has turned out to be a complex rupture sequence predominantly on the nearby and newly-identified Léogâne fault, raising concerns that the EPGF may be "due" for a larger earthquake. Although not explicitly discussed in this text, the data recorded by the Haitian stations are also being used to produce improved velocity and attenuation models for Haiti and to evaluate the site conditions beneath the stations. While seismic monitoring in Haiti continues to be poor it has considerably improved since the time of the earthquake and seismic awareness, at least for the moment, has increased.

8.1.6 Additional Information

By necessity this report is brief and failure to mention any particular paper on the 2010 Haiti earthquake is not intended as a slight or a criticism by this author. Following the earthquake many papers have been and continue to be published on the earthquake and related issues. These include a large collection of Haiti related articles in Nature Geoscience (November 2010) and Earthquake Spectra (October 2011), the latter of which focuses primarily on the engineering aspects of the earthquake but which includes new earthquake hazard maps for Haiti (Frankel *et al*, 2011). The Earthquake Engineering Research Institute established an online clearing house for information on the earthquake that is still available (www.eqclearinghouse.org/20100112-haiti/). The Group on Earth Observations also has a website containing a wide variety of information on the earthquake (supersites.earthobservation.org/Haiti.php). Several conferences, including the 2010 Seismological Society of America annual meeting, the 2010 European Seismological Commission general assembly, the 2010 fall meeting of the American Geophysical Union and the 2011 meeting of the International Union of Geodesy and Geophysics included special sessions on this earthquake. The abstract volumes for these conferences outline much of the early work on the earthquake, some of which has been subsequently followed up and published in more detail.

8.1.7 Acknowledgements

I thank Sue Hough and Bill Ellsworth for providing me with an update on the work of the USGS and Bernard Mercier de Lépinay for an update on the activities of Géoazur. John Adams provided constructive comments on an earlier version of the manuscript. The photo of the station at Léogâne appears courtesy of Calvin Andrews.

8.1.8 References

Altidor, J. R., D. Anglade, W. Ellsworth, D. Given, S. E. Hough, M. G. Janvier, J. Z. Maharrey, M. Meremonte, B. Saint-Louis Midor, C. Prepetit and A. Yong (2010). Seismic Monitoring and Post-Seismic Investigations following the 12 January 2010 Mw 7.0 Haiti Earthquake, (abstract) Fall Meeting of the American Geophysical Union.

Bakun, W. H., C. H. Flores and U. S. ten Brink (2012). Significant Earthquakes on the Enriquillo Fault System, Hispaniola, 1500-2010: Implications for Seismic Hazard, Bulletin of the Seismological Society of America, 102, 18-30, doi:10.1785/012010077.

Bent, A. L. (2011). Focal Mechanisms and Depths of Aftershocks of the 2010 Haiti Earthquake, Geological Survey of Canada Open File 6713, 23 pp.

Calais, E., A. Freed, G. Mattioli, F. Amelung, S. Jónsson, P. Jansma, S.-H. Hong, T. Dixon, C. Prépetit and R. Momplaisir (2010). Transpressional rupture of an unmapped fault during the 2010 Haiti rupture, Nature Geoscience, 3, 794-799.

Daniell, J. and A. Vervaek (2012). Damaging Earthquakes Database 2011- The Year in Review, earthquake-report.com/2012/01/09/catdat-damaging-earthquakes-database-2011-annual-review/.

Douilly, R., S. J. Haase, W. L. Ellsworth, M. Bouin, E. Calais, J. G. Armbruster, B. F. Mercier de Lepinay, A. Deschamps, and S. E. Hough (2011). Improving the resolution of the fault geometry of the 2010 Haiti earthquake (abstract), 2011 Fall Meeting of the American Geophysical Union.

Douilly, R., S. J. Haase, W. L. Ellsworth, M. Bouin, E. Calais, J. G. Armbruster, B. F. Mercier de Lepinay, A. Deschamps and S. E. Hough (2012). Triggered activity on an adjacent fault deduced from relocated aftershocks of the 2010 Haiti earthquake, (abstract) to be presented at the 2012 meeting of the Seismological Society of America.

Eberhard, M. O., S. Baldridge, J. Marshall, W. Mooney and G. J. RIx (2010). The Mw 7.0 Haiti earthquake of January 12, 2010, USGS/EERI Advance Reconnaissance Team Report, U. S. Geological Survey Open-File Report 2010-1048, 58 pp.

Frankel, A., S. Harmsen, C. Mueller, E. Calais and J. Haase (2011). Seismic Hazard Maps for Haiti, Earthquake Spectra, 27, S23-S41.

Global Centroid Moment Tensor Project (2012). On line data base,
http://www.globalcmt.org/CMTsearch.html.

Hayes, G. P., R. W. Briggs, A. Sladen, E. J. Fielding, C. Prentice, K. Hudnut, P. Mann, F. W. Taylor, A. J. Crone, R. Gold, T. Ito and M. Simons (2010). Complex rupture during the 12 January 2010 Haiti earthquake, Nature Geoscience, 3, 800-805.

Hough, S. E., J. R. Altidor, D. Anglade, D. Given, M. G. Janvier, J. Z. Maharrey, M. Meremonte, B. Saint-Louis, Mildor, C. Prepetit and A. Young (2010). Localized damage caused by topographic amplification during the 2010 M 7.0 Haiti earthquake, Nature Geoscience, 3, 778-782.

International Seismological Centre (2012). On-line bulletin, http://www.isc.ac.uk, International Seismological Centre, Thatcham, UK.

Mercier de Lépinay, A. Deschamps, F. Klingelhoefer, Y. Mazabraud, B. Delouis, V. Clouard, Y. Hello, J. Crozon, B. Marcaillou, D. Gaindorge, M. Vallée, J. Perrot, M.-P. Bouin, J.-M. Saurel, P. Charvis and M. St-Louis (2011). The 2010 Haiti earthquake: A complex fault pattern constrained by seismologic and tectonic observations, Geophysical Research Letters, 38, L22305, doi:10.1029/2011GL049799.

Nettles, M. and V. Hjörleifsdóttir (2010). Earthquake source parameters for the 2010 January Haiti mainshock and aftershock sequence, Geophysical Journal International, 183, 375-380, doi:10.1111/j.1365-246X.2010.04732.x.

United States Geological Survey, (2012). On line data base,

earthquake.usgs.gov/earthquakes/eqinthenews/2010/us2010rja6.

8.2 An overview of the Feb 27, 2010 Mw 8.8 Maule, Chile earthquake sequence

Gavin P. Hayes
National Earthquake Information Center
United States Geological Survey
Golden, CO.
USA

8.2.1 Introduction

On February 27, 2010, at 06:34:14 UTC (03:34 at the epicenter), the Mw 8.8 Maule earthquake ruptured an approximately 400 km long section of the South American subduction zone in south-central Chile (epicentral location 36.12°S, 72.90°W, depth 22 km; USGS NEIC, http://on.doi.gov/yKhpUb). The earthquake occurred along the subduction interface separating the Nazca and South American plates, where oceanic lithosphere of the Nazca plate obliquely subducts beneath South America at a rate of approximately 7.4 cm/yr (DeMets *et al.*, 2010). This event caused extensive damage to nearby coastal cities and excited a large near- and far-field tsunami, the former of which caused localized run-up as high as 29 m near Constitución (Fritz *et al.*, 2011). Aftershocks of the earthquake covered an area approximately 700x300 km^2 in size, slightly overlapping the northern extent of the great 1960 Mw 9.5 Chile earthquake to the south, and the southern extent of the 1985 M 8.2 Central Chile earthquake to the north.

Before the Maule earthquake, the plate interface extending ~150 km south of the mainshock hypocenter, which had been referred to as the South Central Chile seismic gap (Ruegg *et al.*, 2009), had not slipped co-seismically in a large earthquake since a M 8.5 megathrust earthquake in 1835 (Figures 8.4 & 8.5). The region north of the hypocenter, on the other hand, had partially failed during large earthquakes in 1906 (M 8.4), 1928 (M 8.0) and in 1985 (M 8.2) (e.g., Beck *et al.*, 1998). Recent geodetic studies reveal that the plate interface between 38.0°S to 35.5°S was nearly fully locked during the six year period from 1996 to 2002 (Ruegg *et al.*, 2009; Moreno *et al.*, 2010).

The USGS W-phase (Kanamori and Rivera, 2008; Hayes *et al.*, 2009; Duputel *et al.*, 2011, Deputel *et al.*, 2012) centroid moment tensor (CMT) solution (http://on.doi.gov/z5LHcG) indicates the earthquake ruptured a shallow thrust fault that aligns well with the geometry of the slab up-dip of the hypocenter (Figure 8.4), with a best double-couple fault plane of strike $\varphi = 016°$, dip $\delta = 14°$, and rake $\lambda = 104°$. This solution has a seismic moment of $M_o = 2.00 \times 10^{29}$ dyne-cm. The CMT solution of the global Centroid Moment Tensor project (GCMT; http://www.globalcmt.org, Ekström *et al.*, 2012) has a seismic moment of $M_o = 1.86 \times 10^{29}$ dyne-cm, in close agreement with the W-phase moment, though with a slightly steeper dip ($\delta = 18°$). These solutions indicate that this earthquake, at the time, represented the fifth-largest event recorded during the modern era of instrumental seismology (eclipsed since by the March 11, 2011 Mw 9.0 Tohoku earthquake; Hayes, 2011; Hayes *et al.*, 2011; http://on.doi.gov/X4d1J1).

In this paper I present an overview of the source characteristics of this mega-earthquake and the tectonic framework of its aftershocks, inferred from studies involving this author (e.g., Hayes *et al.* 2012b, in review) and from other published investigations (e.g., Rietbrock *et al.*, 2012; Lange *et al.*, 2012; Ryder *et al.*, 2012; etc). This work is thus meant to provide a review of our current understanding of this earthquake sequence, and its implications for future events along this portion of the South America megathrust plate boundary.

8.2.2 Mainshock Source Characteristics

In the hours and days following the Maule earthquake, several different groups published finite fault models describing the slip distribution of this event based on seismic data (e.g., Hayes, 2010; Shao *et al.*, 2010; Sladen, 2010). Since then, many more models have been published with various combinations of seismic, GPS, geologic, tsunami and InSAR data (e.g., Lay *et al.*, 2010; Delouis *et al.*, 2010; Tong *et al.*, 2011; Lorito *et al.*, 2011; Pollitz *et al.*, 2011; Vigny *et al.*, 2011). Those models generally infer earthquake source characteristics at relatively low frequencies, when inverting seismic data, or directly infer fault displacement when using geodetics. The models can also be kinematic (again, if they are using seismic data), thereby providing information on the time-history of the rupture process, or are static only (when using geodetic offsets). Some authors (e.g., Lay *et al.*, 2010; Kiser & Ishii, 2011; Wang & Mori, 2011; Lay *et al.*, 2012) have also analyzed the source characteristics of the earthquake at higher frequencies using the back-projection of body waves, as discussed further below.

Vigny *et al.* (2011) compare how most of the finite fault models published at the time of their study fit a dense suite of GPS displacement vectors from the epicentral region of the earthquake, collected as both continuous and campaign data. While their model (constructed via an inversion of the GPS vectors) fits these data best, they show that the USGS model (Hayes, 2010) fit the data reasonably well, and better than the other seismic-only models. The majority of the misfit between the Hayes (2010) model and the GPS data comes from a lack of slip in the southern part of the rupture area, also a problem in the other seismic-only solutions.

Vigny *et al.* (2011) also note their favored low-frequency earthquake onset is shifted approximately 50 km southwest of the USGS-NEIC hypocenter. Rupture velocities for the earthquake were variably reported as 1.75-2.75 km/s (Hayes, 2010); 2.0-2.5 km/s (Lay *et al.*, 2010); averaging 2.6 km/s but as high as 3.2 km/s (Delouis *et al.*, 2010); and 3.1 km/s (Vigny *et al.*, 2011). Finally, most models used a single-plane geometry for their inversion (with the exception of Lorito *et al.*, 2011), though some did explore the affect of changing the assumed dip angle for both single (Lay *et al.*, 2010; Pollitz *et al.*, 2011) and multiple (Lay *et al.*, 2010) planes. Each models' geometry was based on approximate fits to the local subduction zone and/or the GCMT solution, using dips varying from 15°-18° (for single-planes).

Hayes *et al.* (2012b) conduct an in-depth reanalysis of their original teleseismic inversion, aimed at resolving some of these discrepancies between various published models by more fully exploring the parameter space of the inversion procedure. In particular, they examine the effects of better accounting for the variation in slab geometry over the rupture by dividing the model space into several individual planes. Their results show that, while single-, three-, and five-plane models can all fit teleseismic data reasonably well (explaining 88-90% of the inverted data), the same models produce significant differences in fits to regional GPS data. Conversely, this implies that improvements in fits to GPS data are made with stepwise improvements to the assumed fault geometry; in other words, careful consideration of slab

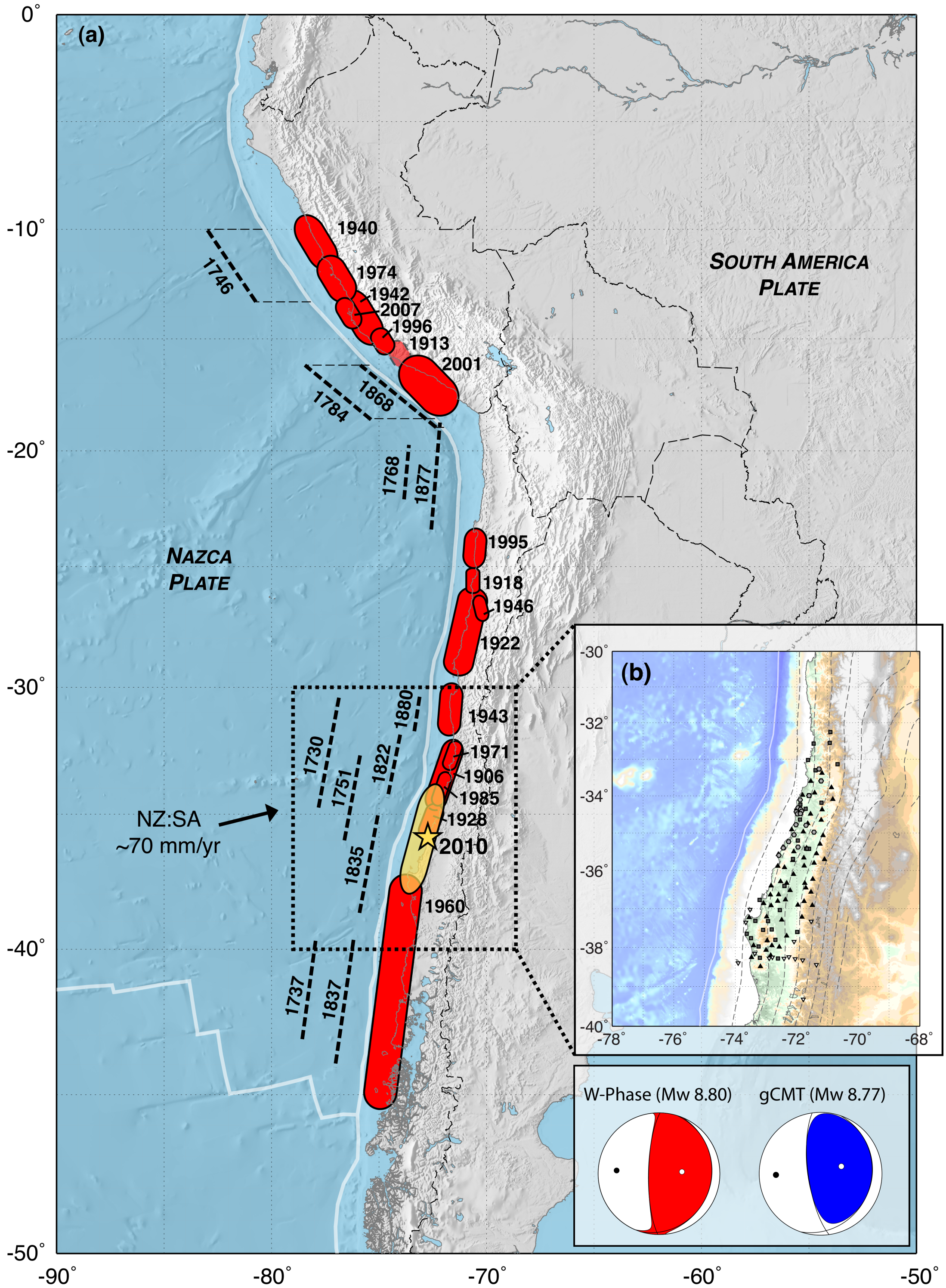

Figure 8.4: *Tectonic setting of the February 27, 2010 Mw 8.8 Maule earthquake. (a) shows the seismologic history of the South America subduction zone; Major 20th century ruptures are shown with red polygons representing their approximate rupture extent, following Beck et al., (1998). Approximate rupture lengths of major pre-20th century earthquakes are shown with black lines outboard of the subduction zone for clarity. The extent of the 2010 rupture is illustrated with a yellow polygon; the star represents the earthquake epicenter. CMT mechanisms for the mainshock are given in the inset. The black arrow represents Nazca:South America plate motion of 70 mm/yr. The dashed black box shows the extent of all subsequent figures, and of (b), which shows stations from the IMAD aftershock deployment. Different symbols represent the operating institution; black triangles are IRIS (US) stations, inverted white triangles UK, dark gray squares French, and hexagons German. Background bathymetric data, here and in subsequent figures, is taken from the GEBCO_08 grid, version 20100927, http://www.gebco.net).*

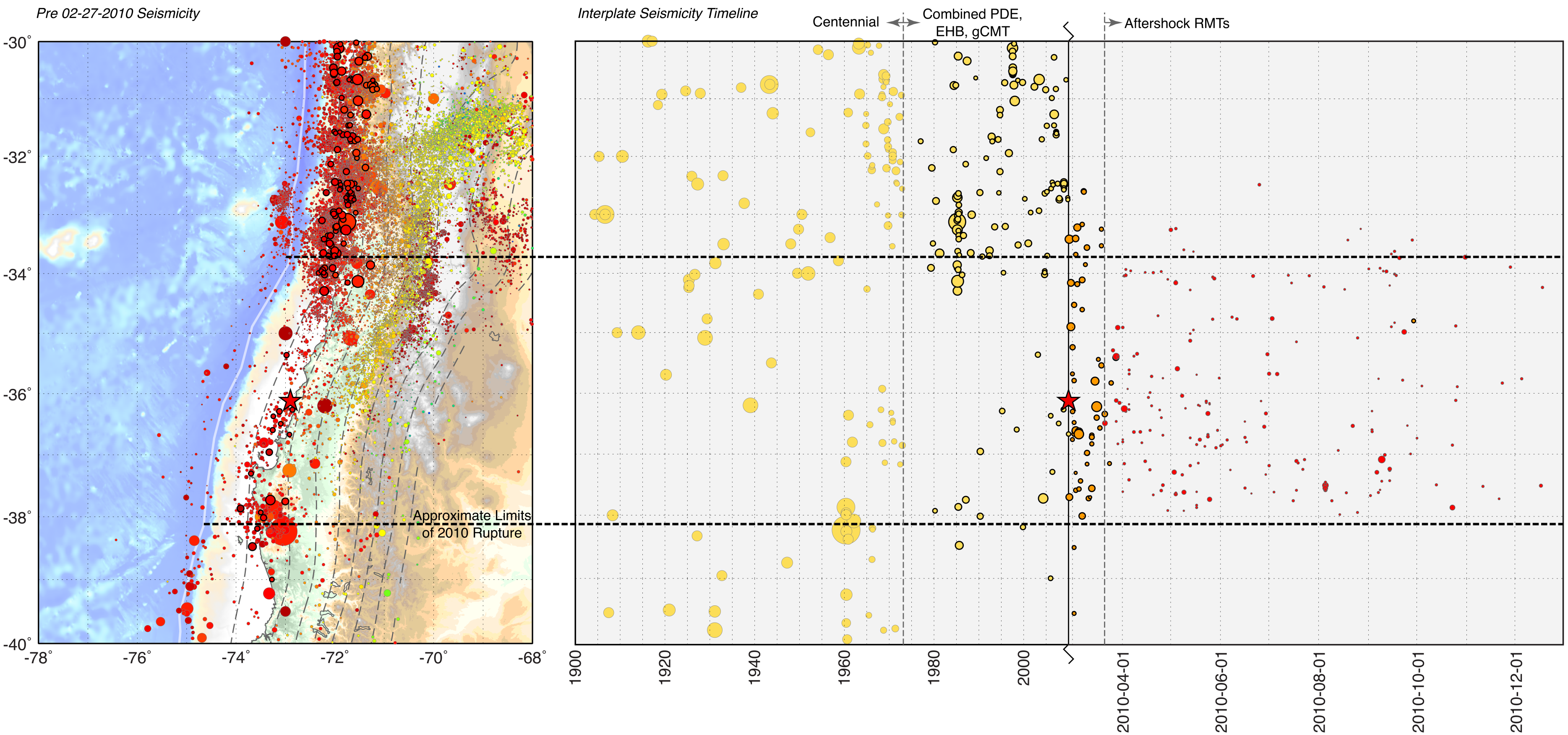

Figure 8.5: *(a) Pre- February 27, 2010 seismicity in the Centennial (Villeseñor and Engdahl, 2002; plotted 1900-1973), EHB (Engdahl et al., 1998; plotted 1973-present) and USGS PDE (plotted 1973-present, for those events without EHB locations) catalogs. Earthquake symbols are sized by magnitude and colored by depth. Those shown with thicker black outlines represent interplate earthquakes, discriminated via a comparison of their hypocenters and associated GCMT mechanisms to the Slab1.0 subduction zone model for the region (see text for details). Slab1.0 model contours are shown with dashed gray lines. The location of the February 27, 2010 epicenter is shown with a star. Approximate rupture limits are illustrated with dashed black lines. In (b), I show a timeline of Centennial catalog (pre-1976) and interplate seismicity (post-1976, the beginning of the GCMT catalog) in the source region of the Maule earthquake, showing the relative quiescence of the rupture area prior to the 2010 rupture. Yellow circles with light gray outlines are Centennial catalog events; yellow circles with thicker black outlines are EHB/PDE/GCMT catalog interface events. Orange circles represent post-mainshock events from the PDE catalog, while red circles represent aftershocks used in this study. Both of these later two data sets have also been filtered according to either their GCMT (for PDE/orange events) or RMT (for regional aftershocks/red events) mechanism to identify interplate earthquakes.*

geometry can improve seismic data inversions to levels comparable to many inversions based on the local and regional geodetic data, without the specific inclusion of those data in the inversion process.

The importance of geometrical control on resulting slip distributions is discussed further – and perhaps dealt with most satisfactorily – by Moreno *et al.* (2012), who use a three-dimensional fault geometry in a spherical-earth finite-element model to solve for a static slip distribution using regional GPS data. As discussed below, their resulting model is very similar to those of Hayes *et al.* (2012b) and Vigny *et al.* (2011). Moreno *et al.* (2012) goes on to compare co-seismic slip distributions for the 2010 earthquake to estimates of pre-event interface coupling, in a similar manner to Moreno *et al.* (2010), and Lorito *et al.* (2011), who reached opposing conclusions – the former implying a pre-event Constitución seismic gap had been filled, and the latter inferring it had not. This more detailed and updated Moreno *et al.* (2012) analysis confirms the earlier findings of Moreno *et al.* (2010) – that this gap was most likely closed by the Maule earthquake – and indeed that the 2010 slip may have been larger than that which had accumulated since the last megathrust earthquake in the region in 1835, implying either some local overshoot or inherited slip deficit in the region from strain accumulation before 1835.

Resulting favored slip distributions – in the Hayes *et al.* (2012b; Figure 8.6), Vigny *et al.* (2011), and Moreno *et al.* (2012) models – are similar, and indicate rupture dominated by two or three major asperities, in the northern shallow trench near 35°S, and in the south near 36°S-37°S (this slip patch is slightly further north in the Hayes model, and is separated into two smaller patches in the Moreno model). The Hayes model also shows a third asperity south of and along strike from the hypocenter just off the coast, down-dip from the second asperity, and covering a larger area than a similar feature in the Vigny model. In all models, peak slips reach approximately 15-20 m. These three models also imply a convergence of solutions showing offshore slip was dominant in this earthquake, in contrast to some other previous models favoring slip on the deeper portion of the megathrust (e.g., Lorito *et al.*, 2011), an inconsistency raised and discussed in more detail in Rietbrock *et al.* (2012).

Another interesting feature of the Hayes and Vigny models is a prominent slip minima very close to the hypocenter – up-dip and to the west-northwest in the Hayes model, and west-southwest in the Vigny model. In the latter model, this "anti-asperity" co-locates with after-slip derived in Vigny *et al.* (2011): in the former model, with the approximate rupture area of the M 8.0 1928 megathrust earthquake (Figure 8.4), though the precise slip distribution of that event is unclear. The small difference in the location of this low-slip region in each of these models may be related to the differences in hypocentral location, which is further south in Vigny *et al.* (2011). In the kinematic models of Hayes *et al.* (2012b), the hypocenter is used as the point of rupture initiation, thus influencing the resulting locations of slip on the modeled fault plane. Moreno *et al.* (2012) use a hypocenter closer to the Hayes model, derived from relocations of the mainshock and aftershock sequence as discussed in the following section.

As previously mentioned, several models of high-frequency rupture propagation have also been published via the use of the back-projection technique (Lay *et al.*, 2010; Kiser & Ishii, 2011; Wang & Mori, 2011; Lay *et al.*, 2012). In general, these studies favor rupture models dominated by northward rupture propagation, though both Kiser & Ishii (2011) and Wang & Mori (2011) also identify rupture south of the hypocenter, with dominant frequencies much lower than those related to rupture further north. Wang & Mori (2011) suggest these characteristics may be reflective of the coupling properties of the megathrust prior to the earthquake, such that areas of high coupling may cause greater heterogeneity in

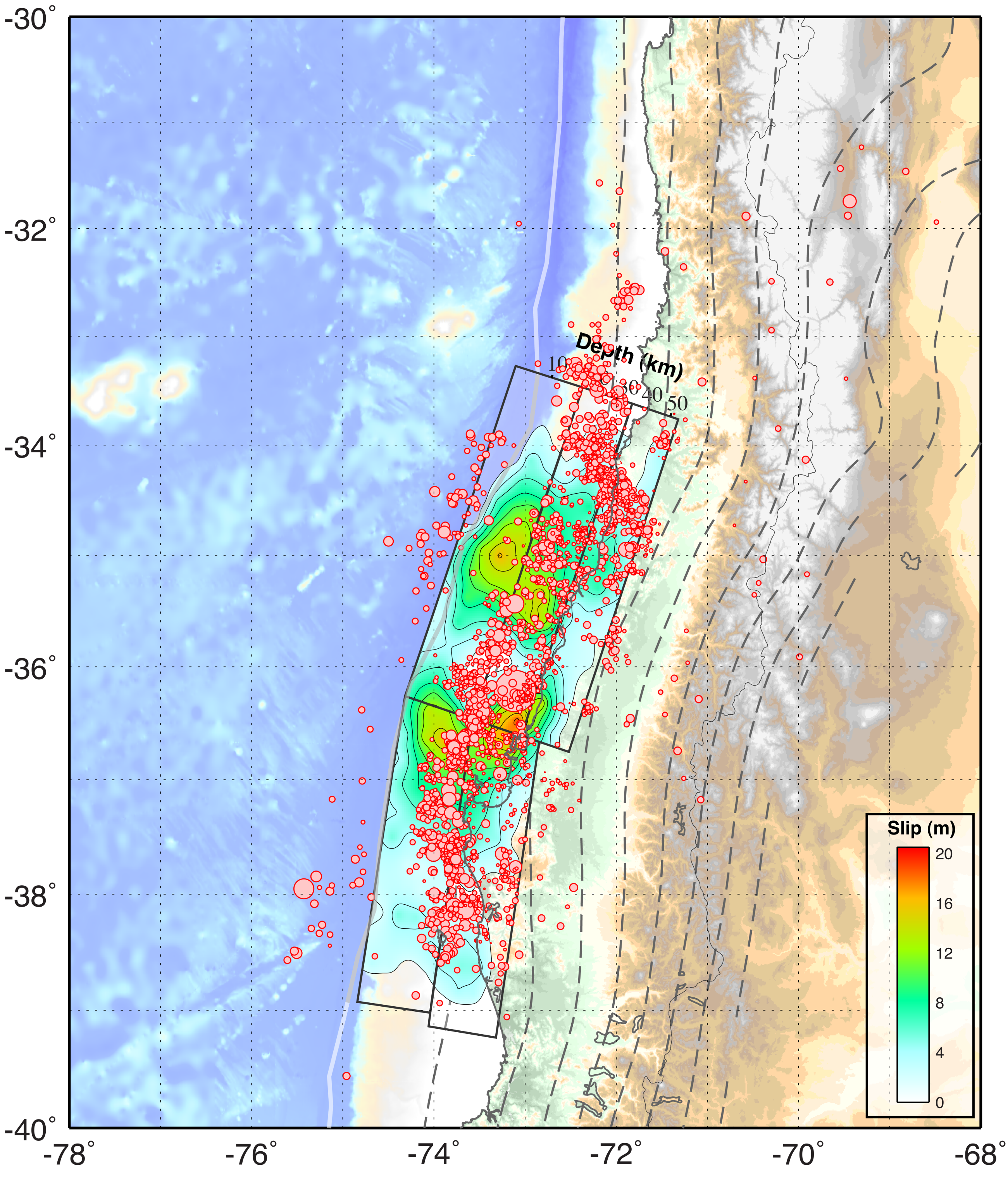

Figure 8.6: *Favored co-seismic slip model from Hayes et al. (2012b), from the inversion of teleseismic data over five planes (black rectangles encompassing slip distribution) approximating the subduction zone interface (gray dashed contours, from Slab1.0, Hayes et al., 2012a). Slip is contoured in 4m intervals. Overlain on this slip model is the relocated aftershock catalog of approximately 2,500 events from the same study, sized by magnitude. The thick transparent white line represents the inferred location of the Nazca:South America plate boundary.*

fault properties and have higher overall stress, resulting in more efficient high frequency energy radiation during subsequent earthquakes. Issues of frequency-dependent rupture properties of the megathrust have been explored in more detail by Lay *et al.* (2012), after the extremely interesting observation during the Mw 9.0 Tohoku, Japan earthquake that high-frequency energy radiation was predominantly located along deeper portions of the plate interface than was the low frequency radiation and dominant fault slip. They find similar patterns of depth variation in seismic wave radiation for the Maule earthquake, and for the 2004 Mw 9.1 Sumatra earthquake, implying such features may be characteristic of megathrust earthquakes, and highlighting the necessity for studies of earthquake rupture properties across a broad range of frequencies.

8.2.3 Studies of the Aftershock Sequence

In the weeks following the Maule earthquake, an unprecedented international collaboration involving teams and instruments from Chilean Universities, the Incorporated Research Institutions for Seismology (IRIS) in the US, the Institut National des Sciences de l'Univers of the Centre National de la Recherche Scientifique (INSU, CNRS) in France, Geo Forschungs Zentrum Posdam (GFZ) in Germany, and the University of Liverpool in the UK was established to deploy the International Maule Aftershock Deployment (IMAD) temporary network. Over 160 mostly broadband sensors were deployed over the on-land extent of the earthquake source region (Figure 8.6). Data from almost all of these stations were made available immediately following their collection through IRIS and GFZ, spanning March-December, 2010.

Several published studies have produced catalogs of this aftershock sequence, both from automatic picking of the datasets (e.g., Rietbrock *et al.*, 2012; Lange *et al.*, 2012) and from higher-resolution (and conversely lower event density) earthquake relocation analysis (Hayes *et al.*, 2012b). Analyses of aftershock source processes have also been published, using dominantly teleseismic (Aguerto *et al.*, 2012) and denser regional (Hayes *et al.*, 2012b) moment tensor data sets.

Through the automatic picking and processing of the first six months of IMAD data, Lange *et al.* (2012) located over 20,000 aftershocks in the source region of the Maule earthquake. They identify several distinct tectonic settings active during this period: 1) earthquakes in a region they call the outer rise, outboard of the subduction zone and adjacent to the mainshock rupture; 2) plate interface seismicity in or adjacent to the regions of highest co-seismic slip; 3) seismicity in a cluster at the deeper limit of interface seismogenesis below the mainshock rupture zone, and thus likely associated with after-slip; 4) earthquakes at intermediate (80-120 km) depths, within the subducting slab; and 5) earthquakes in the upper plate at the northern end of the rupture along crustal faults oblique to the subduction zone, associated with two major normal faulting aftershocks on March 11, 2010. These authors note that comparisons between aftershock locations and slip are dependent on the slip model used in the comparison – in other words, reliability of the source inversion procedure and thus of the resulting model is an important factor in studying such correlations. Comparisons of their aftershock catalog to the Vigny *et al.* (2011) model show aftershock activity predominantly down-dip of the regions of highest co-seismic slip.

The Rietbrock *et al.* (2012) study also uses automated picking and processing algorithms, and builds a catalog of over 30,000 earthquakes occurring over just the first two months of the IMAD deployment. This study also attempts to improve upon the accuracy of automated detection algorithms by incorporating S-wave arrivals, and by using a two dimensional velocity model. Resulting locations from the Rietbrock catalog agree well with those from Lange *et al.* (2012), identifying aftershock activity outboard of the subduction zone with the oceanic plate, in two distinct clusters along the subduction zone thrust, and within the upper plate surrounding the Pichilemu region, where the March 11, 2010 normal faulting aftershocks occurred. This study goes on to use aftershock distributions to discriminate between slip models of varying quality, based on the assumption that aftershocks should generally occur in areas of rapid transition between high and low slip, surrounding (but not co-located with) areas of high slip. Under such a premise, the slip model of Vigny *et al.* (2011) is preferred over those of (for example) Lorito *et al.* (2011) and Delouis *et al.* (2010), because aftershocks locate at the down-dip extent of shallow high-slip regions, rather than somewhat coincident with highest slip. Their findings support a model where aftershocks occur predominantly in the transitional regions between high and low slip, rather than preferentially in areas of lowest slip.

The Aguerto *et al.* (2012) study builds on the catalog produced by Rietbrock *et al.* (2012), analyzing the largest events to produce a catalog of approximately 125 regional moment tensor (RMT) solutions. They also relocate centroid moment tensor (CMT) solutions from the global CMT catalog (http://www.globalcmt.org), adding almost 150 further moment tensors to their dataset. Using this catalog, they infer that most large aftershocks (70%) occur on the subduction thrust interface. Like Rietbrock *et al.* (2012), Aguerto *et al.* (2012) conclude that such events occur predominantly away from the areas of highest co-seismic slip, based on comparisons to the slip model of Moreno *et al.* (2012). Interestingly, they also note that, in contrast to their findings for large events, small (M<4) aftershocks predominantly occur where co-seismic slip is highest, possibly as a result of processes occurring in the damage zone around the megathrust interface.

These studies highlight the importance of an accurate source inversion for comparisons of aftershock distributions to co-seismic slip. Also vital for such studies is confidence in the accuracy of aftershock locations. Hayes *et al.* (2012b) attempt to address both issues by relocating the largest aftershocks (producing a catalog of over 2000 well-located earthquakes, with horizontal uncertainties averaging +/- 2.8 km; Figure 8.6), and carefully analyzing modeling parameters in kinematic source inversions with teleseismic data, aided by the forward modeling of regional GPS signals, as discussed above. They derive a model (Figure 8.6) that fits both the teleseismic data and the available regional GPS data better than most other published source models (which predominantly use GPS and InSAR data when conducting joint inversions, thereby solving for the static and not the kinematic rupture history), and derive an aftershock catalog which, while smaller than those of Lange *et al.* (2012) and Reitbrock *et al.* (2012), provides precise locations that can be confidently used for the detailed analysis of aftershock distributions with respect to co-seismic slip.

In addition, Hayes *et al.* (2012b) derive RMTs for 475 of the largest aftershocks (Figure 8.7), directly tied in to the rest of the relocated aftershock sequence, and categorize those events by their occurrence in the upper and lower-plates or on the subduction thrust interface based on comparisons to the Slab1.0 subduction zone geometry model (Hayes *et al.*, 2012a). Their analyses show that, if one classifies thrust interface earthquakes in a similar manner to Asano *et al.* (2011) and filters moment tensors by depth difference from the slab (±10 km), mechanism type (thrust) and rotation angle from the interface geometry (within a Kagan angle of 35°; Kagan 1991), then just over 50% of the 475 aftershocks with RMTs can be classified as occurring on the plate boundary. Following the approach taken by Aguerto *et al.* (2012) and discriminating events on just mechanism type (thrust) and depth difference from the slab (±5 km), that number rises to 58%, in slight contrast to the figure of 70% found in Aguerto *et al.* (2012). Using the entire catalog rather than just the RMT dataset, 43% of events lie within ±5 km of the plate boundary. Like Aguerto *et al.* (2012), the Hayes *et al.* (2012b) study finds that the majority of the interplate after-slip occurs away from peaks in co-seismic slip, where slip is either low or relatively moderate with respect to co-seismic maxima. However, comparisons with co-seismic slip gradients show that aftershocks do not necessarily occur where changes in co-seismic slip were most rapid; in fact, most aftershocks locate where slip gradients are also moderate-to-low.

Also of interest in the Hayes *et al.* (2012b) study is that just 55% of aftershocks lie within regions of positive Coulomb stress (Lin & Stein, 2004) resulting from their favored co-seismic slip model, just slightly more than we might expect from a random distribution of aftershocks within the mainshock rupture area. This is likely an artifact of the high sensitivity of Coulomb stress transfer calculations on the precise distribution of co-seismic slip (which is calculated at a resolution of 25x18 km in the along-strike and down-dip directions, respectively), and uncertainties in aftershock locations (several kilometers horizontally and vertically); small changes in either can cause a switch from negative to positive Coulomb stress transfer (Ross Stein, pers. comm., 2012). In fact, considering just the range of vertical uncertainty of relocated aftershocks in Hayes *et al.* (2012b), the percentage of aftershocks locating in regions of positive stress transfer increases to approximately 70%. Incorporating horizontal uncertainties increases this further, to between 80% and 85%. This illustrates the care that must be taken in comparing aftershock distributions to models of co-seismic slip.

Cross-sections through the epicentral region of the mainshock and aftershock zone (Figure 8.8) show nicely the spatial distribution of the aftershock sequence, and the associated tectonic features they activate. RMTs indicate a dominance of thrust faulting close to the subduction zone interface. These cross-sections identify a set of events near the base of the seismogenic zone (e.g., A-A', B-B', D-D') that is spatially distinct from other thrust aftershocks, and helps to define the depth extent of faulting on the plate interface in this region (at the deep limit of these events), as well as the depth-extent of co-seismic slip (at the shallow limit of these events). Cross-section D-D' highlights a sequence of upper plate earthquakes near the northern end of the mainshock rupture zone, dominated by normal faulting. These earthquakes are associated with two large M 7.0 and M 6.9 aftershocks on March 11, 2010, near Pichilemu. The sequence branches upward from and oblique to the subduction zone interface (strikes of the largest two events are approximately 145° and 155°; www.globalcmt.org), and seems to promote subsequent aftershock activity on the up-dip portion of the megathrust plate boundary (since all of our RMTs are associated with earthquakes subsequent to the Pichilemu events), while possibly inhibiting activity on the portion of the megathrust directly beneath the upper plate normal faults (Figure 8.8). Also visible in both cross-section and in map view (Figure 8.6) is aftershock activity within the oceanic plate outboard of the subduction zone, in two clusters at the northern and southern ends of the mainshock rupture. While the more dominant of these clusters, in the north, lies directly up-dip of the main co-seismic asperity, the southern cluster aligns more closely with fracture zones at the south end of the rupture, further south than the asperity between 36°S-37°S.

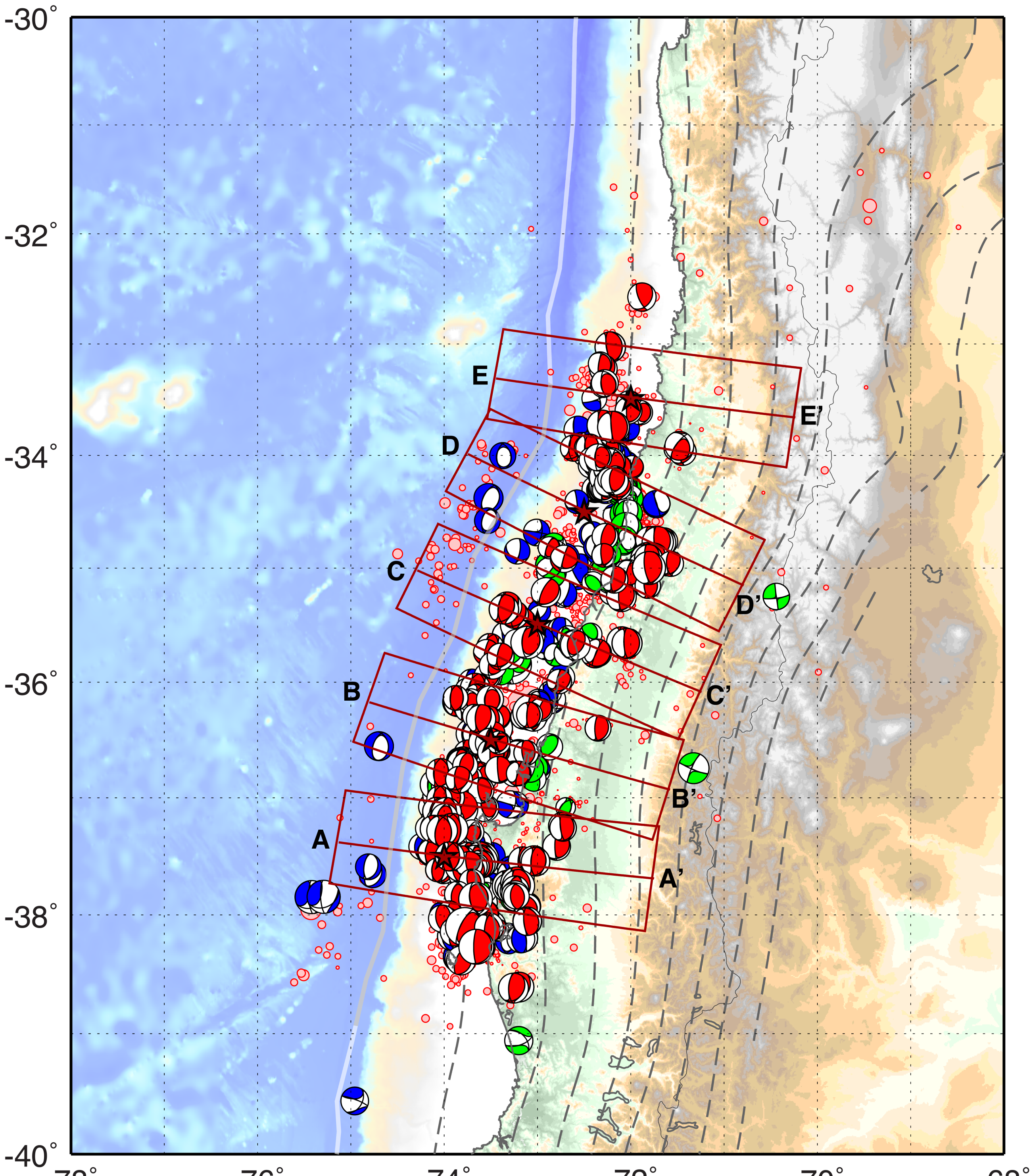

Figure 8.7: *Aftershock relocations and Regional Moment Tensors (RMTs), subdivided by their inferred tectonic environment (upper, lower, interplate; green, blue, red, respectively). Dark gray dashed contours represent the depth of the subducting Pacific slab in 20 km intervals, from Slab1.0 (Hayes et al., 2012a). The thick transparent white line represents the inferred location of the Nazca:South America plate boundary. Red lines show the boundaries of cross-sections in Figure 8.8.*

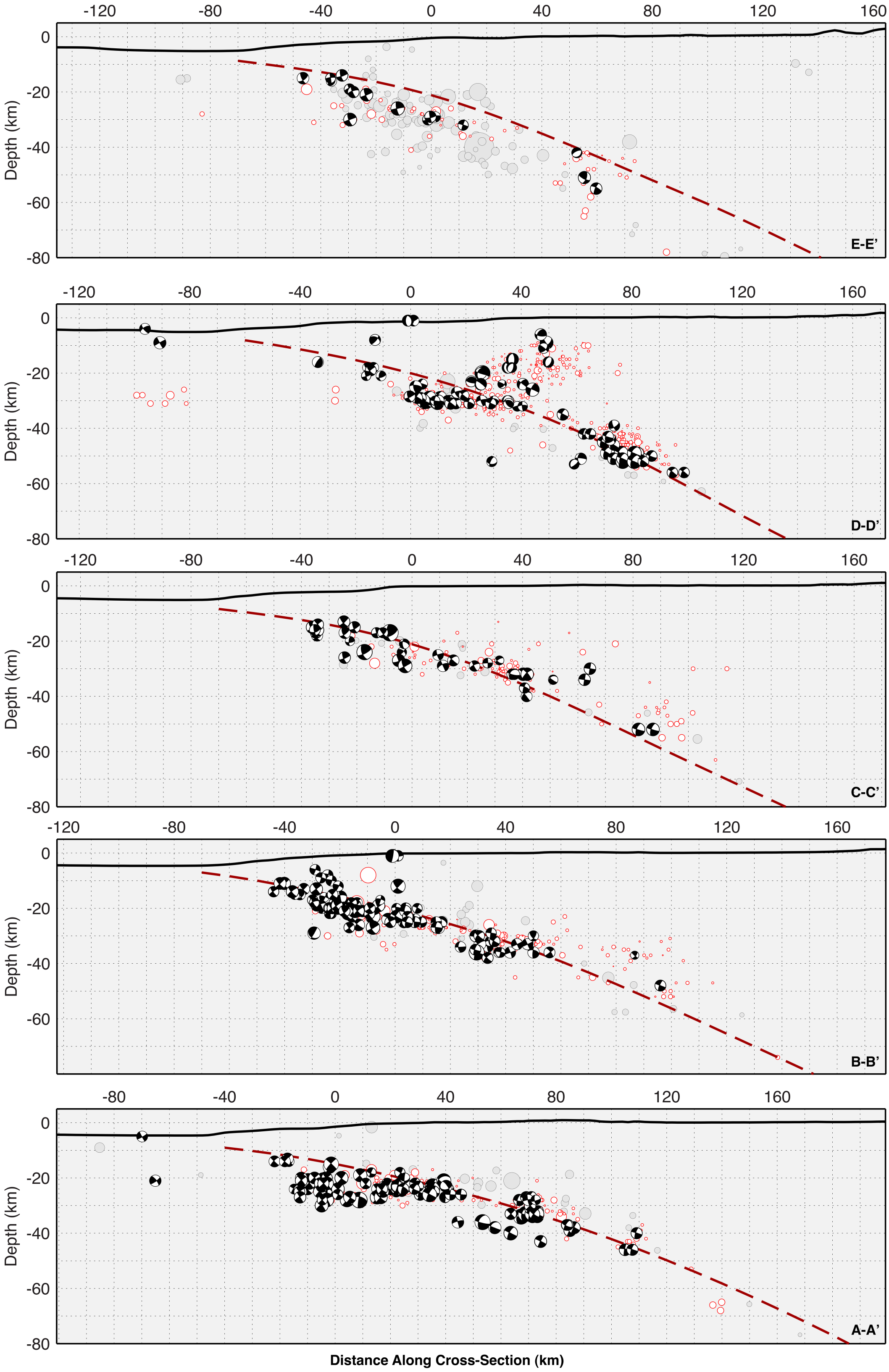

__Figure 8.8:__ Cross-sections through the aftershock sequence, showing the depth distribution of historic (light gray circles, thin black outlines) and aftershock (white circles, red outlines) seismicity, with symbols sized according to magnitude. RMTs of the aftershock sequence are also shown, as rear-hemisphere projections of the best fitting double-couple mechanism. Red dashed lines show the subduction zone interface location, from Slab1.0 (Hayes et al., 2012a). The black solid line near the surface shows bathymetry/topography, taken from GEBCO bathymetric data. Cross-sections are displayed from north (E-E') to south (A-A'). For cross-section locations, see Figure 8.7.

8.2.4 Discussion

In this paper I summarize some of the more prominent findings derived from studies of the 2010 Maule earthquake, with a specific focus on work related to inversions of co-seismic slip, and catalogs of subsequent aftershock distributions and moment tensor analyses.

Published co-seismic slip models are numerous, derived from various combinations of one or more of teleseismic, GPS, InSAR and tsunami datasets. Many of the more recent models, such as Vigny *et al.* (2011), Moreno *et al.* (2012), and Hayes *et al.* (2012b), indicate dominantly offshore slip in two-to-three major asperities: north of the hypocenter near 35°S, and in the south near 36°S-37°S. Co-seismic slips reached 15-20 m, and the northern and southern asperities were separated by a prominent minima in slip near the hypocenter, close to the location of the M8.0 1928 megathrust earthquake. Interestingly, while these and other teleseismic and geodetically derived slip models favor slip on the shallower, offshore portions of the subduction thrust, those models including tsunami data (e.g., Lorito *et al.*, 2011; Fujii and Satake, 2012) derive slip beneath the coastline, somewhat at odds with measurements of coastal subsidence and uplift (Farias *et al.*, 2010). This discrepancy has yet to be satisfactorily resolved.

Several catalogs of aftershocks and regional moment tensors for the Maule earthquake sequence have also been published to date, taking advantage of the unprecedented multi-national deployment and open access data of the IMAD network in the months following the mainshock rupture. The more dense catalogs of Lange *et al.* (2012) and Rietbrock *et al.* (2012), derived from automated picking algorithms, provide details of the tectonic settings activated by the aftershock sequence, and highlight dependencies in correlations between co-seismic and aftershock slip on the co-seismic model chosen for that comparison. Both studies favor slip inversions that derive slip in the shallower subduction thrust environment (e.g., Vigny *et al.*, 2011), and thus infer that slip in the largest aftershocks (M4+) occurs on the fringes of high slip, in regions of transition from high-to-low co-seismic slip environments. This is also the conclusion reached by Aguerto *et al.* (2012), which quantify patterns in aftershock slip distributions and their relationship to co-seismic slip by using a moment tensor catalog made up of their own regional moment tensors, and a relocated set of centroid moment tensors from the GCMT catalog. A detailed relocation of the largest aftershocks, as well as a more extensive set of regional moment tensors from Hayes *et al.* (2012b), provide similar results. However, Hayes *et al.* (2012b) find that overall a smaller fraction of the aftershock sequence is represented by interplate thrusting (55% versus 70% in Aguerto *et al.*, 2012), and that of those subduction interface events, most occur in regions of low slip and low slip gradient, rather than specifically where slip gradients are high and transitioning away from major asperities. Importantly, Hayes *et al.* (2012b) also demonstrate that comparisons of aftershock locations and co-seismic slip for the purposes of Coulomb stress transfer calculations are extremely dependent on uncertainties in both – particularly in earthquake location – and as such errors in even relocated earthquakes need to be taken into account in such studies.

8.2.5 Conclusions

The 2010 Maule earthquake was, at the time of the event, the fifth-largest earthquake ever recorded in the modern instrumental era. Owing to the expansions in global and regional seismic and geodetic networks over the past several years-to-decades, and in particular since the 2004 M 9.1 (Park *et al.*,

2005) Sumatra earthquake, data from this event and its aftershock sequence were perhaps also the best on record (since eclipsed by the 2011 M 9.0 Tohoku earthquake, offshore from Japan). Because of this, and owing also to the advancements of processing techniques and understanding of the earthquake source that have accompanied such data expansions, the Maule earthquake has been studied across multiple time and frequency scales, providing results that are helping to change the way we understand megathrust earthquake slip across the inter-, co-, and post-seismic spectrum. Such datasets for this and other similar earthquakes (including the Tohoku event) are likely to continue to provide insights into the behavior of megathrust plate boundaries, insights which will in turn help shape the way we characterize and respond to earthquake hazards and their associated societal risks in the future.

8.2.6 Acknowledgements

The author wishes to thank Harley Benz, Eric Bergman, Robert Herrmann, Andres Rietbrock, Chen Ji and Sergio Barrientos for discussions related to the Maule earthquake and subsequent data analyses, and Paul Earle and Wayne Richardson for thorough reviews of an initial manuscript. The Seismological Service National de Chile, Universidad de Chile, Universidad de Concepción, IRIS, the University of Liverpool, CNRS-INSU, and GFZ were all instrumental in the deployment, operation and recovery of the IMAD network; without their extensive efforts many of the studies discussed in this paper would not have been possible. Many of the figures were made using GMT, and I thank their developers and the many users of their support list. Thanks also to the global Centroid Moment Tensor project group for the maintenance of and open access to their catalog.

8.2.7 References

Agurto, H., Rietbrock, A., Ryder, I., and Miller, M., 2012. Seismic-afterslip characterization of the 2012 Mw 8.8 Maule, Chile, earthquake, based on moment tensor inversion, Geophys. Res. Lett. 39, doi:10.1029/2012GL053434.

Asano, Y., Saito, T., Ito, Y., Shiomi, K., Hirose, H., Matsumoto, T., Aoi, S., Hori, S., and Sekiguchi, S., 2010. Spatial distribution and focal mechanisms of aftershocks of the 2011 off the Pacific Coast of Tohoku Earthquake, Earth Planets Space 63, 669-673.

Beck, S., Barientos, S., Kausel, E., and Reyes, M., 1998. Source characteristics of historic earthquake along the central Chile subduction zone, J. South Am. Earth Sci. 11, 115–129, doi:10.1016/S0895-9811(98) 00005-4.

Delouis, B., Nocquet, J-M., and Vallée, M., 2010. Slip distribution of the February 27, 2010 Mw = 8.8 Maule earthquake, central Chile, from static and high-rate GPS, InSAR, and broadband teleseismic data, Geophys. J. Lett. 37, L17305, doi:10.1029/2010GL043899.

DeMets, C., Gordon, R.G., and Argus, D.F., 2010. Geologically current plate motions, Geophys. J. Int. 181, 1-80, doi: 10.1111/j.1365-246X.2009.04491.x.

Duputel, Z., Rivera, L., Kanamori, H., Hayes, G.P., Hirshorn, B., and Weinstein, S., 2011. Real-time W Phase inversion during the 2011 off the Pacific Coast of Tohoku Earthquake, Earth Planets Space 63, 535–539.

Duputel, Z., Rivera, L., Kanamori, H., and Hayes, G., 2012. W phase source inversion for moderate to large earthquakes (1990–2010). Geophys. J. Int. 189, 1125–1147.

Ekström, G., Nettles, M., and Dziewoński, A.M., 2012. The global CMT project 2004-2010: Centroid-moment tensors for 13,017 earthquakes, Phys. Ear. Planet. Int. 200-201, 1-9.

Engdahl, R., and A. Villaseñor (2002), Global seismicity: 1900–1999, in International Handbook of Earthquake and Engineering Seismology, Part A, edited by W. H. K. Lee *et al.*, chap. 41, pp. 665–690, Academic, Amsterdam, doi:10.1016/S0074-6142(02)80244-3.

Engdahl, E. R., R. D. Van Der Hilst, and R. P. Buland (1998), Global teleseismic earthquake relocation with improved travel times and procedures for depth determination, Bull. Seis. Soc. Am., 88, 722–743.

Farias, M., Vargas, G., Tassara, A., Carretier, S., Baize, S., Melnick, D., and Bataille, K., 2010. Land-Level Changes Produced by the Mw 8.8 2010 Chilean Earthquake, Science, 329(5994), 916–916.

Fujii, Y., and Satake, K., 2012. Slip distribution and seismic moment of the 2010 and 1960 Chilean earthquakes inferred from tsunami waveforms and coastal geodetic data, Pure Appl. Geophys., doi:10.1007/s00024-012-0524-2.

Fritz, H. M., Petroff, C. M., Catalan, P. A., Cienfuegos, R., Winckler, P., Kalligeris, N., Weiss, R., Barrientos, S. E., Meneses, G., Valderas-Bermejo, C., Ebeling, C., Papadopoulos, A., Contreras, M., Almar, R., Dominguez, J. C., and Synolakis, C. E., 2011. Field survey of the 27 February 2010 Chile tsunami, Pure Appl. Geophys., doi:10.1007/s00024-00011- 00283-00025.

Hayes, G., 2010. Finite fault model, updated results of the Feb. 27, 2010 Mw 8.8 Maule, Chile earthquake, http://earthquake.usgs.gov/earthquakes/eqinthenews/2010/us2010tfan/finite_fault.php.

Hayes, G.P., 2011. Rapid source characterization of the 2011 Mw 9.0 off the Pacific coast of Tohoku earthquake, Earth Planets Space 63, 529-534.

Hayes, G.P., Rivera, L., and Kanamori, H., 2009. Source inversion of the W-Phase: real- time implementation and extension to low magnitudes. Seismol. Res. Lett. 80, 817–822.

Hayes, G.P., Earle, P.S., Benz, H.M, Wald, D.J., Briggs, R.W., and the USGS/NEIC Earthquake Response Team, 2011. 88 Hours: The U.S. Geological Survey National Earthquake Information Center reponse to the 11 March 2011 Mw 9.0 Tohoku earthquake, Seismol. Res. Lett. 82, 481-493, doi: 10.1785/gssrl.82.4.481.

Hayes, G.P., Wald, D.J., and Johnson, R.L., 2012a. Slab1.0: A three-dimensional model of global subduction zone geometries, J. Geophys. Res. 117, B01302, doi:10.1029/2011JB008524.

Hayes, G.P., Bergman, E., Benz, H.M., Johnson, K.L., Brown, L., and Melzner, A., 2012b. Seismotectonic framework of the February 27, 2010 Mw 8.8 Maule, Chile earthquake sequence, submitted to Geophys. J. Int., 10/2012.

Kagan, Y., 1991. 3-D rotation of double-couple earthquake sources, Geophys. J. Int., 106, 709–716.

Kanamori, H., and Rivera, L., 2008. Source inversion of W phase: speeding up seismic tsunami warning. Geophys. J. Int. 175, 222–238.

Kiser, E., and Ishii, M., 2011. The 2010 Mw 8.8 Chile earthquake: Triggering on multiple segments and frequency-dependent rupture behavior. Geophys. Res. Lett., 38, doi:10.10129/2011GL047140.

Lange, D., Tilmann, F., Barrientos, S.E., Contreras-Reyes, E., Methe, P., Moreno, M., Heit, B., Agurto, H., Bernard, P., Vilotte, J-P., and Beck, S., 2012. Aftershock seismicity of the 27 February 2010 Mw 8.8 Maule earthquake rupture zone, Ear. Planet. Sci. Lett. 317-318, 413-425.

Lay, T., Ammon, C.J., Kanamori, H., Koper, K.D., Sufri, O., and Hutko, A.R., 2010. Teleseismic inversion for rupture process of the 27 February 2010 Chile (Mw 8.8) earthquake, Geophys. J. Lett. 37, L13301, doi:10.1029/2010GL043379.

Lay, T., Kanamori, H., Ammon, C.J., Koper, K.D., Hutko, A.R., Ye, L., Yue, H., and Rushing, T.M., 2012. Depth-varying rupture properties of subduction zone megathrust faults. J. Geophys. Res., 117, doi:10.1029/2011JB009133.

Lin, J., and Stein, R.S., 2004. Stress triggering in thrust and subduction earthquakes, and stress interaction between the southern San Andreas and nearby thrust and strike-slip faults, J. Geophys. Res. 109, doi:10.1029/2003JB002607.

Lorito, S., Romano, F., Atzori, S., Tong, X., Avallone, A., McCloskey, J., Cocco, M., Boschi, E., and Piatanesi, A., 2011. Limited overlap between the seismic gap and coseismic slip of the great 2010 Chile earthquake, Nature Geo. 4, doi: 10.1038/NGEO1073.

Moreno, M., Rosenau, M., and Oncken, O., 2010. 2010 Maule earthquake slip correlates with pre-seismic locking of Andean subduction zone, Nature 467, doi:10.1038/nature09349.

Moreno, M., *et al.*, 2012. Toward understanding tectonic control on the Mw 8.8 Maule Chile earthquake, Ear. Planet. Sci. Lett. 321-322, 152-165.

Pollitz. F., Brooks, B., Tong, X., Bevis, M.F., Foster, J.H., Bürgmann, R., Smalley, R. Jr., Vigny, C., Socquet, A., Ruegg, J-C., Campos, J., Barrientos, S., Parra, H., Baez Soto, J.C., Cimbaro, S., and Blanco, M., 2011. Coseismic slip distribution of the February 27, 2010 Mw 8.8 Maule, Chile earthquake, Geophys. Res. Lett. 38, L09309, doi:10.1029/2011GL047065.

Rietbrock, A., Ryder, I., Hayes, G., Haberland, C., Comte, D., Roecker, S., and Lyon-Caen, H., 2012. Aftershock seismicity of the 2010 Maule Mw=8.8, Chile, earthquake: Correlation between co-seismic slip models and aftershock distribution?, Geophys. Res. Lett. 39, L08310, doi:10.1029/2012GL051308.

Ruegg, J.C., Rudloff, A., Vigny, C., Madariaga, R., de Chabalier, J.B., Campos, J., Kausel, E., Barrientos, S., and Dimitrov, D., 2009. Interseismic strain accumulation measured by GPS in the seismic gap between Constitución and Concepción in Chile, Phys. Ear. Planet. Int. 175, 78-85.

Ryder, I., Rietbrock, A., Kelson, K., Bürgmann, R., Floyd, M., Socquet, A., Vigny, C., and Carrizo, D., 2012. Large extensional aftershocks in the continental forearc triggered by the 2010 Maule earthquake, Chile, Geophys. J. Int 188, 879-890.

Shao, G., Li, X., Liu, Q., Zhao, X., Yano, T., and Ji, C., 2010. Preliminary slip model of the Feb 27, 2010 Mw 8.9 Maule, Chile Earthquake,
http://www.geol.ucsb.edu/faculty/ji/big_earthquakes/2010/02/27/chile_2_27.html.

Sladen, A., 2010. Preliminary result 02/27/2010 (Mw 8.8), Chile, http://tectonics.caltech.edu/slip_history/2010_chile/index.html.

Tong, X., Sandwell, D., Luttrell, K., Brooks, B., Bevis, M., Shimada, M., Foster, J., Smalley, R. Jr., Parra, H., Báez Soto, J.C., Blanco, M., Kendrick, E., Genrich, J., and Cassamise II, D.J., 2010. The 2010 Maule Chile earthquake: Downdip rupture limit revealed by space geodesy, Geophys. Res. Lett. 37, L24311, doi:10.1029/2010GL045805.

Vigny, C., *et al.*, 2011. The 2010 Mw 8.8 Maule Megathrust Earthquake of Central Chile, Monitored by GPS, Science 332, doi: 10.1126/science.1204132.

Wang, D., and Mori, J., 2011. Frequency-dependent energy radiation and fault coupling for the 2010 Mw 8.8 Maule, Chile, and 2011 Mw 9.0 Tohoku, Japan, earthquakes. Geophys. Res. Lett., 38, doi:10.1029/2011GL049652.

9

Statistics of Collected Data

9.1 Introduction

The ISC Bulletin is based on the parametric data reports received from seismological agencies around the world. With rare exceptions, these reports include the results of waveform review done by analysts at network data centres and observatories. These reports include combinations of various bulletin elements such as event hypocentre estimates, moment tensors, magnitudes, event type and felt and damaging data as well as observations of the various seismic waves recorded at seismic stations.

Data reports are received in different formats that are often agency specific. Once an authorship is recognised, the data are automatically parsed into the ISC database and the original reports filed away to be accessed when necessary. Any reports not recognised or processed automatically are manually checked, corrected and re-processed. This chapter describes the data that are received at the ISC before the production of the reviewed Bulletin.

Notably, the ISC integrates all newly received data reports into the automatic ISC Bulletin (available on-line) soon after these reports are made available to ISC, provided it is done before the submission deadline that currently stands at 12 months following an event occurrence.

With data constantly being reported to the ISC, even after the ISC has published its review, the total data shown as collected, in this chapter, is limited to two years after the time of the associated reading or event, i.e. any hypocentre data collected two years after the event are not reflected in the figures below.

9.2 Summary of Agency Reports to the ISC

A total of 126 agencies have reported data for January 2010 to June 2010. The parsing of these reports into the ISC database is summarised in Table 9.1.

Table 9.1: *Summary of the parsing of reports received by the ISC from a total of 126 agencies, containing data for this summary period.*

	Number of reports
Total collected	2425
Automatically parsed	1814
Manually parsed	611

Data collected by the ISC consists of multiple data types. These are typically one of:

- Bulletin, hypocentres with associated phase arrival observations.
- Catalogue, hypocentres only.
- Unassociated phase arrival observations.

In Table 9.2, the number of different data types reported to the ISC by each agency is listed. The number of each data type reported by each agency is also listed. Agencies reporting indirectly have their data type additionally listed for the agency that reported it. The agencies reporting indirectly may also have 'hypocentres with associated phases' but with no associated phases listed - this is because the association is being made by the agency reporting directly to the ISC. Summary maps of the agencies and the types of data reported are shown in Figure 9.1 and Figure 9.2.

Table 9.2: *Agencies reporting to the ISC for this summary period. Entries in bold are for new or renewed reporting by agencies since the previous six-month period.*

Agency	Country	Directly, (D) or indirectly (I) reporting	Hypocentres with associated phases	Hypocentres only	Associated phases	Unassociated phases	Amplitudes
TIR	Albania	D	399	296	2498	234	0
CRAAG	Algeria	D	878	353	4592	879	0
LPA	Argentina	D	0	0	0	65	5
SJA	Argentina	D	1616	20	23448	0	2510
NSSP	Armenia	D	52	49	558	0	0
AUST	Australia	D	1978	5	29678	15	1
IDC	Austria	D	19203	0	368972	0	341345
VIE	Austria	D	2507	877	15102	104	11124
AZER	Azerbaijan	D	120	98	2577	0	0
BELR	Belarus	D	0	0	0	3681	849
UCC	Belgium	D	0	41	0	3108	888
VAO	Brazil	D	0	0	0	359	0
SOF	Bulgaria	D	191	185	1854	2547	0
OTT	Canada	D	1553	23	34097	0	5891
PGC	Canada	I OTT	961	0	12198	0	0
GUC	Chile	D	4737	144	72596	1241	14003
BJI	China	D	2829	56	167189	10296	77874
ASIES	Chinese Taipei	D	0	41	0	0	0
TAP	Chinese Taipei	D	11328	3	262011	0	0
RSNC	Colombia	I NEIC	0	5	0	0	0
CASC	Costa Rica	D	527	39	9935	0	165
HDC	Costa Rica	I NEIC	0	2	0	0	0
UCR	Costa Rica	I CASC	0	7	0	0	0
ZAG	Croatia	D	0	1	0	12697	0
SSNC	Cuba	D	6	0	74	63	27
NIC	Cyprus	D	250	202	1723	137	0
IPEC	Czech Republic	I CSEM	0	391	0	0	0
PRU	Czech Republic	D	5000	2448	45486	605	9202
WBNET	Czech Republic	D	90	0	1413	248	1563
DNK	Denmark	D	0	102	0	6652	3102
ARO	Djibouti	D	58	0	536	0	0
SDD	Dominican Republic	I NEIC	0	1	0	0	0
IGQ	Ecuador	D	1	99	0	3517	0
HLW	Egypt	D	248	182	2539	0	173
SNET	El Salvador	I NEIC	0	7	0	0	0
SSS	El Salvador	I CASC	0	2	0	0	0
EST	Estonia	I HEL	371	36	0	0	0
AAE	Ethiopia	D	9	0	18	401	0
SKO	FYR Macedonia	D	1380	671	7232	1376	3196
FIA0	Finland	I HEL	98	10	0	0	0
HEL	Finland	D	6455	6028	110179	2325	22319
CSEM	France	D	37354	56791	766408	0	141880
LDG	France	D	1862	1897	47187	3675	28713
STR	France	D	701	493	8579	3819	0

Table 9.2: *continued*

Agency	Country	Directly, (D) or indirectly (I) reporting	Hypocentres with associated phases	Hypocentres only	Associated phases	Unassociated phases	Amplitudes
PPT	French Polynesia	D	1524	0	11806	453	12212
TIF	Georgia	D	0	1349	0	17086	0
AWI	Germany	D	1332	0	3709	1313	0
BGR	Germany	D	839	495	16478	0	5829
BNS	Germany	I BGR	4	75	0	0	0
BRG	Germany	D	0	0	0	5261	4077
BUG	Germany	I BGR	50	0	0	0	0
CLL	Germany	D	0	0	0	8227	2876
GDNRW	Germany	I BGR	1	34	0	0	0
GFZ	Germany	I NEIC	9	1	0	0	0
LEDBW	Germany	I BGR	23	4	0	0	0
SZGRF	Germany	I BGR	476	2	0	0	0
ATH	Greece	D	8268	8042	162882	8740	0
THE	Greece	D	4598	4580	99663	6181	27616
UPSL	Greece	I CSEM	0	320	0	0	0
GCG	**Guatemala**	**I CASC**	**0**	**5**	**0**	**0**	**0**
HKC	Hong Kong	D	0	0	0	88	0
BUD	Hungary	D	0	19	0	4123	0
REY	Iceland	D	55	18	1527	0	0
HYB	India	D	1525	1	7830	37	1523
NDI	India	D	593	378	15151	7736	4740
DJA	Indonesia	D	3989	32	70102	0	78806
TEH	Iran	D	643	240	11108	0	2256
THR	Iran	D	146	163	1590	0	642
ISN	Iraq	D	187	108	1181	0	0
DIAS	Ireland	D	0	0	0	180	0
GII	Israel	D	50	49	1159	0	0
GEN	Italy	I CSEM	0	398	0	0	0
ROM	Italy	D	6895	4710	87096	0	36272
TRI	Italy	D	0	216	0	4916	0
LIC	Ivory Coast	D	989	0	3075	0	2752
JSN	Jamaica	D	252	3	1571	6	0
JMA	Japan	D	59400	3	432569	914	0
MAT	Japan	D	0	0	0	5276	0
NIED	Japan	D	0	744	0	0	0
SYO	Japan	D	0	0	0	1882	0
JSO	Jordan	D	32	11	239	0	0
NNC	Kazakhstan	D	9876	139	69872	0	55838
SIK	Kosovo	I CSEM	0	87	0	0	0
KNET	Kyrgyzstan	D	1608	0	13507	0	2030
KRNET	**Kyrgyzstan**	**D**	**1185**	**0**	**18316**	**0**	**0**
GRAL	Lebanon	D	239	203	1458	627	0
LIT	Lithuania	D	97	156	672	764	603
KLM	Malaysia	D	529	2	4205	0	0
ECX	Mexico	D	2138	135	48915	0	7311
MEX	Mexico	D	1910	536	16864	0	0
MOLD	Moldova	D	0	0	0	1919	611
PDG	Montenegro	D	400	334	7858	0	4258
CNRM	Morocco	I CSEM	0	131	0	0	0
MOZ	**Mozambique**	**D**	**135**	**0**	**540**	**0**	**0**
NAM	Namibia	D	1	0	8	0	0
DMN	Nepal	D	2188	2	23238	0	17291
DBN	Netherlands	D	0	0	0	1712	688
NOU	New Caledonia	D	105	0	812	866	205
WEL	New Zealand	D	4886	3	149812	8492	34423
BER	Norway	D	1707	1622	21943	383	4769
NAO	Norway	D	2870	1326	7109	1	2126
OMAN	Oman	D	408	88	3817	0	0
MSSP	Pakistan	D	0	0	0	1029	0
UPA	Panama	I CASC	0	4	0	0	0
ARE	Peru	I NEIC	0	16	0	0	0
MAN	Philippines	D	0	1002	0	19045	6201
QCP	Philippines	D	0	0	0	44	0
WAR	Poland	D	0	0	0	19535	90

Table 9.2: *continued*

Agency	Country	Directly, (D) or indirectly (I) reporting	Hypocentres with associated phases	Hypocentres only	Associated phases	Unassociated phases	Amplitudes
IGIL	Portugal	D	638	0	3242	0	1123
INMG	Portugal	D	1514	664	43428	2466	15626
PDA	Portugal	I SVSA	703	294	0	0	0
SVSA	Portugal	D	774	0	11634	2950	4109
KMA	Republic of Korea	D	589	0	7855	0	0
BUC	Romania	D	689	75	8891	37873	0
ASRS	Russia	D	15	0	198	0	0
BYKL	Russia	D	139	0	10282	0	3941
KOLA	**Russia**	**D**	**168**	**0**	**641**	**0**	**0**
KRSC	Russia	D	569	0	19732	0	0
MOS	Russia	D	2409	239	402406	0	152498
NERS	Russia	D	25	0	673	0	293
SKHL	Russia	D	446	448	13729	0	6520
YARS	**Russia**	**D**	**882**	**903**	**15753**	**0**	**0**
SGS	Saudi Arabia	D	102	80	550	0	0
BEO	Serbia	D	1304	1053	19028	12	0
BRA	Slovakia	D	0	0	0	10577	0
LJU	Slovenia	D	1609	1451	20505	4858	6141
HNR	**Solomon Islands**	**D**	**0**	**0**	**0**	**2000**	**0**
PRE	South Africa	D	1328	3	24556	72	8833
MDD	Spain	D	2310	4936	65784	0	50708
MRB	Spain	I CSEM	0	15	0	0	0
SFS	Spain	I CSEM	0	164	0	0	0
UPP	Sweden	D	590	3899	6408	0	0
ZUR	Switzerland	D	255	216	2152	0	1992
NSSC	Syria	D	1009	488	19308	184	9045
BKK	Thailand	D	963	24	8783	0	12086
TRN	Trinidad and Tobago	D	3	555	0	13187	0
TUN	Tunisia	I CSEM	0	10	0	0	0
DDA	Turkey	D	9185	6557	87312	8480	0
ISK	Turkey	D	9	11424	0	84807	0
AEIC	U.S.A.	I VIE	50	74	0	0	0
ANF	U.S.A.	I IRIS	2745	496	0	0	0
BRK	U.S.A.	I NEIC	0	0	0	0	0
BUT	U.S.A.	I IRIS	6	29	0	0	0
CERI	U.S.A.	I IRIS	4	0	0	0	0
GCMT	U.S.A.	D	0	3364	0	0	0
HON	U.S.A.	I NEIC	0	22	0	0	0
IRIS	U.S.A.	D	4738	4198	486005	0	0
LDO	U.S.A.	I NEIC	0	5	0	0	0
NCEDC	U.S.A.	I IRIS	60	26	0	0	0
NEIC	U.S.A.	D	17862	7479	646227	23	214086
PAS	U.S.A.	I IRIS	172	343	0	0	0
PMR	U.S.A.	I NEIC	0	32	0	0	0
PNSN	U.S.A.	D	3	124	0	0	0
REN	U.S.A.	I IRIS	6	9	0	0	0
RSPR	U.S.A.	D	1013	6	12954	0	0
SEA	U.S.A.	I NEIC	4	83	0	0	0
SIO	U.S.A.	D	1136	0	3532	0	3532
SLC	U.S.A.	I NEIC	34	3	0	0	0
SLM	U.S.A.	I IRIS	1	7	0	0	0
SNM	**U.S.A.**	**I NEIC**	**0**	**1**	**0**	**0**	**0**
TUL	**U.S.A.**	**I IRIS**	**34**	**4**	**0**	**0**	**0**
WES	**U.S.A.**	**I NEIC**	**0**	**3**	**0**	**0**	**0**
SIGU	**Ukraine**	**D**	**89**	**89**	**1602**	**13**	**0**
DSN	**United Arab Emirates**	**D**	**376**	**97**	**2008**	**0**	**0**
BGS	United Kingdom	D	209	141	7601	0	2919
UNK	Unknown	I IRIS	41	595	0	0	0
CAR	Venezuela	I VIE	2	2	0	0	0
FUNV	Venezuela	D	1648	0	21377	0	0
PLV	Vietnam	D	45	0	493	0	47
DHMR	Yemen	D	298	114	2694	9014	2268
BUL	Zimbabwe	D	177	0	748	362	0

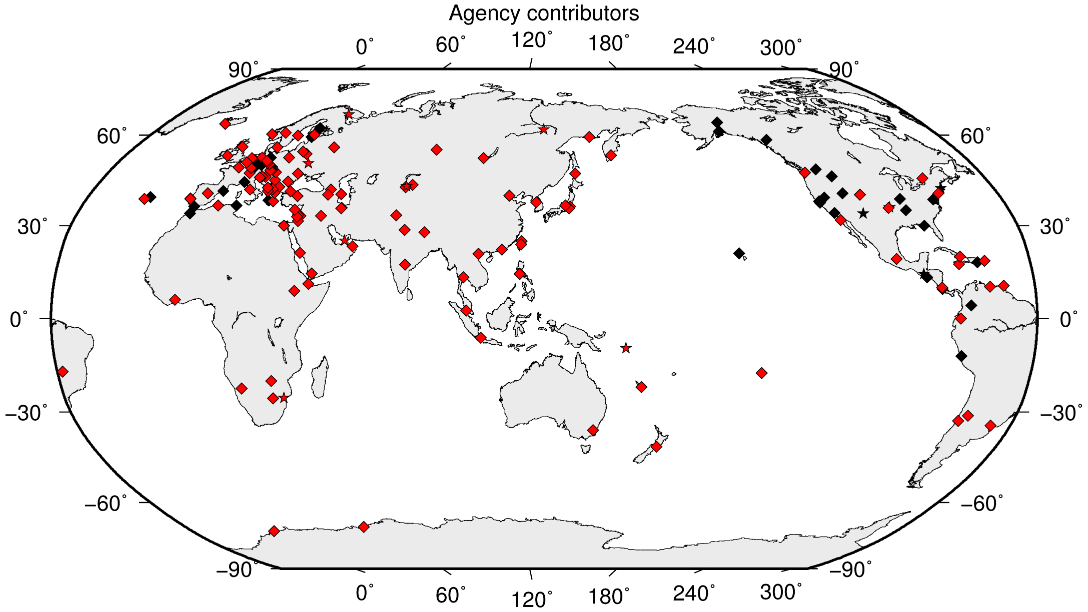

__Figure 9.1:__ Map of agencies that have contributed data to the ISC for this summary period. Agencies that have reported directly to the ISC are shown in red. Those that have reported indirectly (via another agency) are shown in black. Any new or renewed agencies, since the last six-month period, are shown by a star. Each agency is listed in Table 9.2.

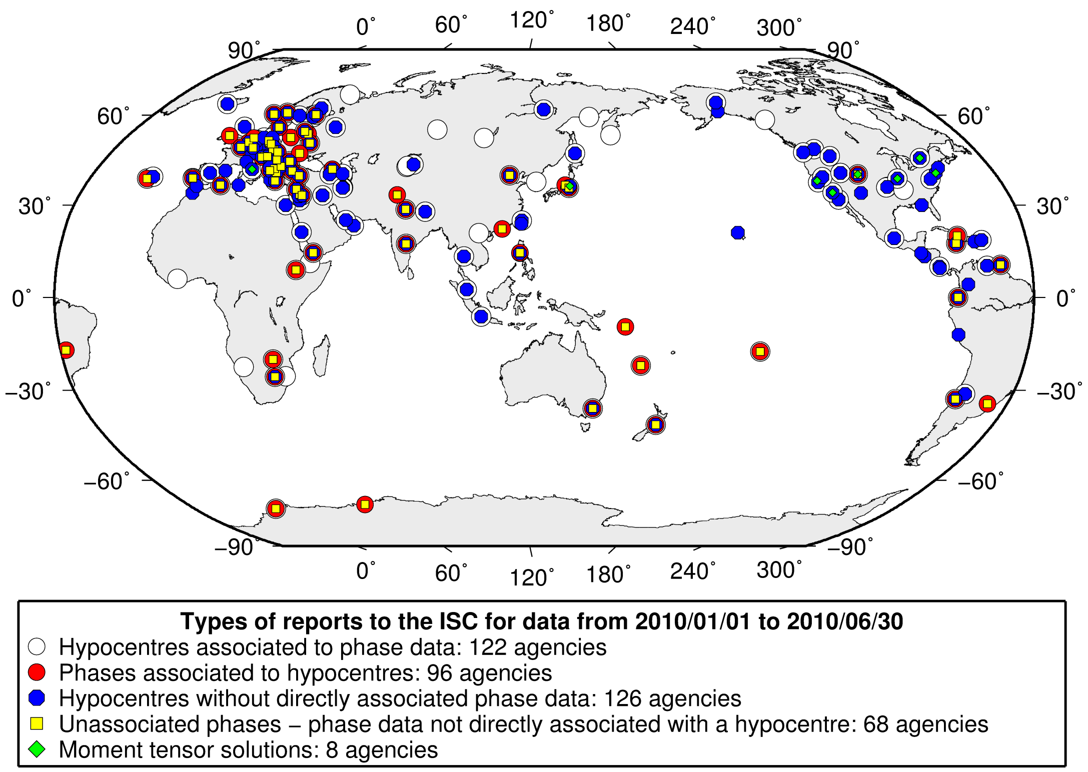

__Figure 9.2:__ Map of the different data types reported by agencies to the ISC. A full list of the data types reported by each agency is shown in Table 9.2.

9.3 Arrival Observations

The collection of phase arrival observations at the ISC has increased dramatically with time. The increase in reported phase arrival observations is shown in Figure 9.3.

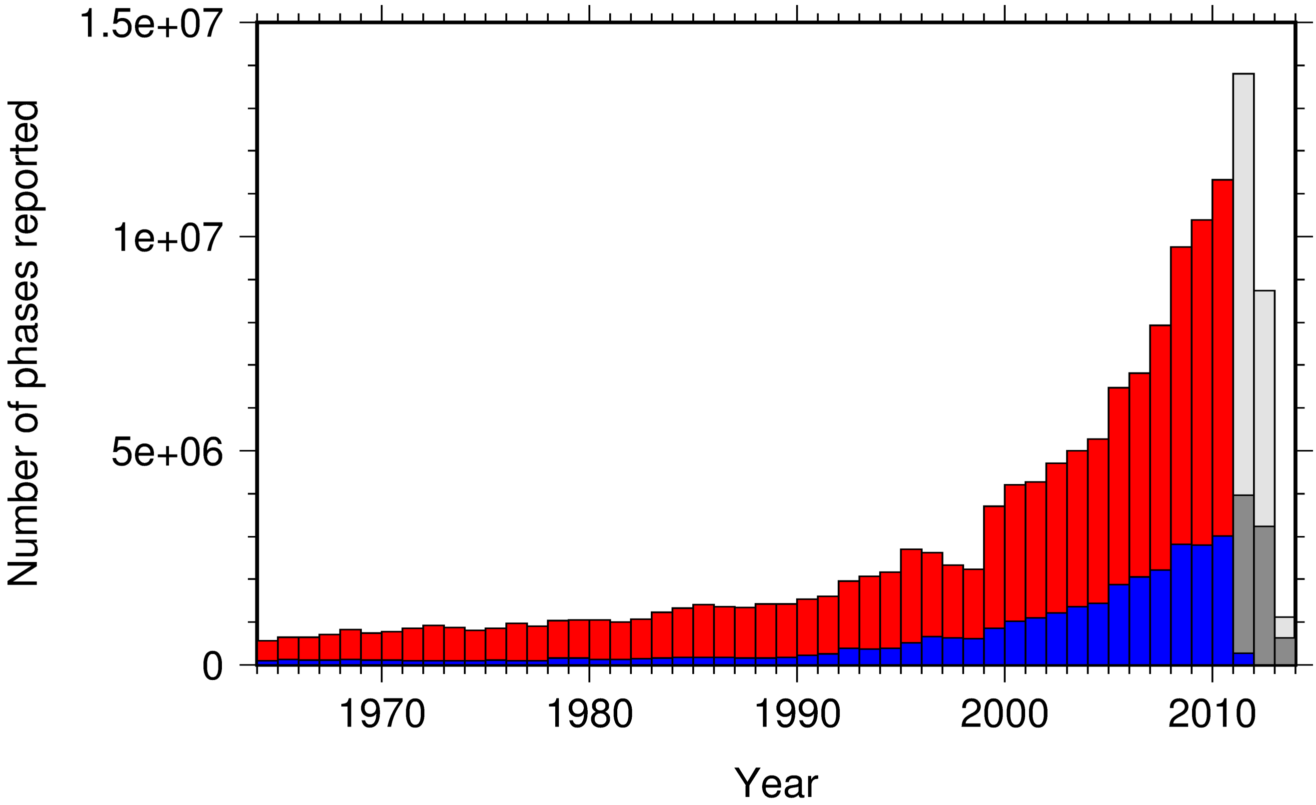

Figure 9.3: *Histogram showing the number of phases (red) and number of amplitudes (blue) collected by the ISC for events each year since 1964. The data in grey covers the current period where data are still being collected before the ISC review takes place and is accurate at the time of publication.*

The reports with phase data are summarised in Table 9.3. This table is split into three sections, providing information on the reports themselves, the phase data, and the stations reporting the phase data. A map of the stations contributing these phase data is shown in Figure 9.4.

The ISC encourages the reporting of phase arrival times together with amplitude and period measurements whenever feasible. Figure 9.5 shows the percentage of events reported by each station was accompanied with amplitude and period measurements.

Figure 9.6 indicates the number of amplitude and period measurement for each station.

Together with the increase in the number of phases (Figure 9.3), there has been an increase in the number of stations reported to the ISC. The increase in the number of stations is shown in Figure 9.7. This increase can also be seen on the maps for stations reported each decade in Figure 9.8.

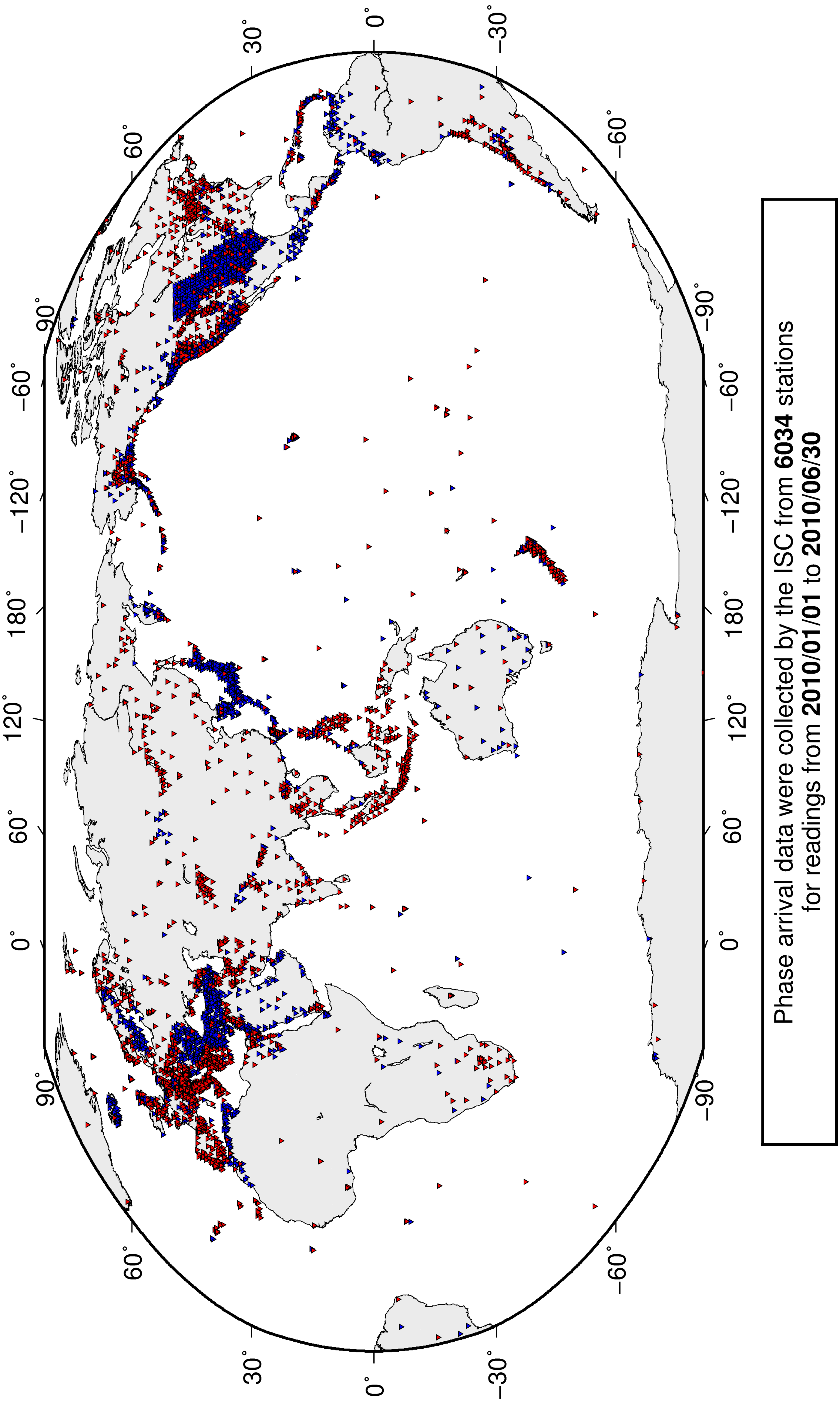

Figure 9.4: *Stations contributing phase data to the ISC for readings from January 2010 to the end of June 2010. Stations in blue provided phase arrival times only; stations in red provided both phase arrival times and amplitude data.*

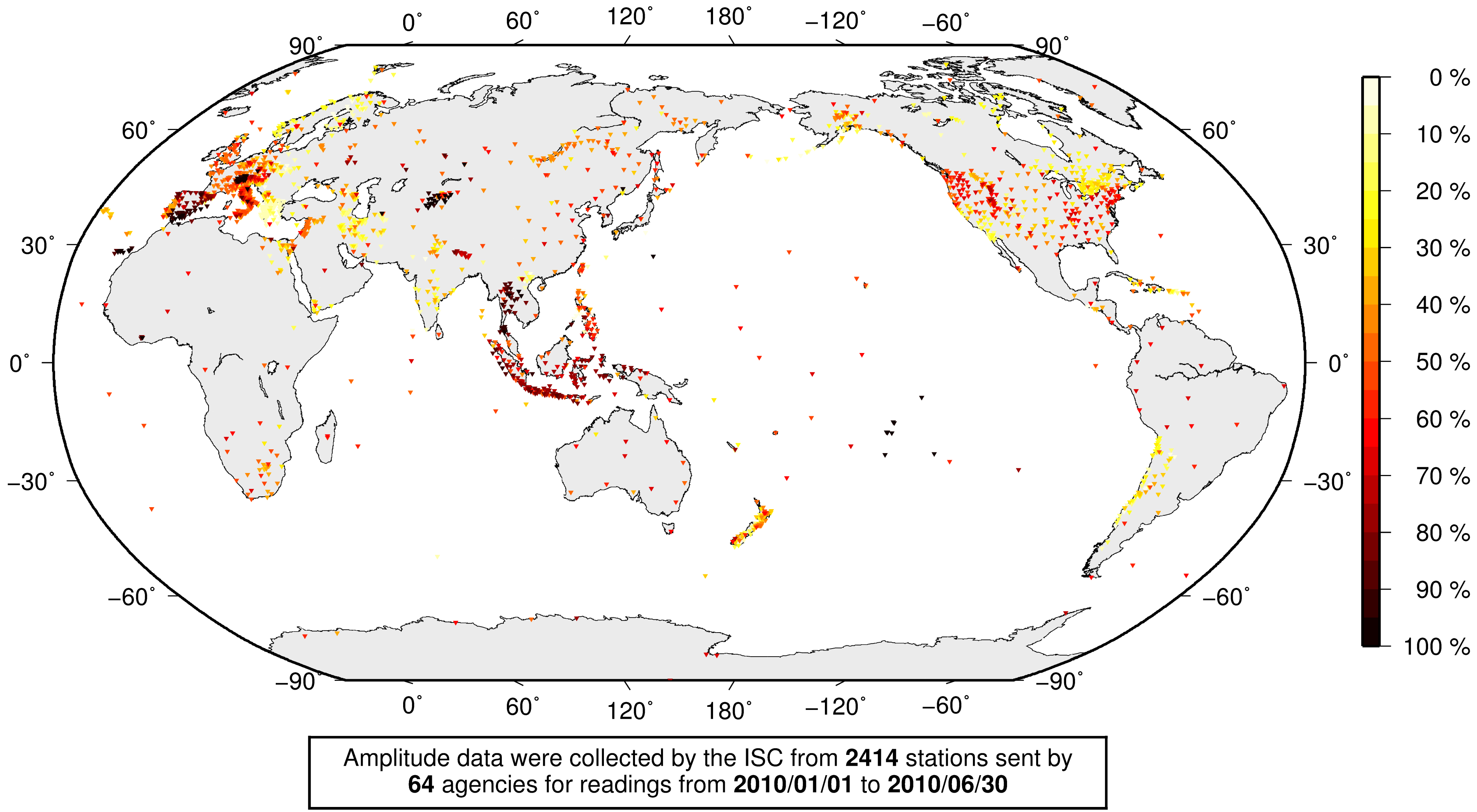

Figure 9.5: *Percentage of events for which phase arrival times from each station are accompanied with amplitude and period measurements.*

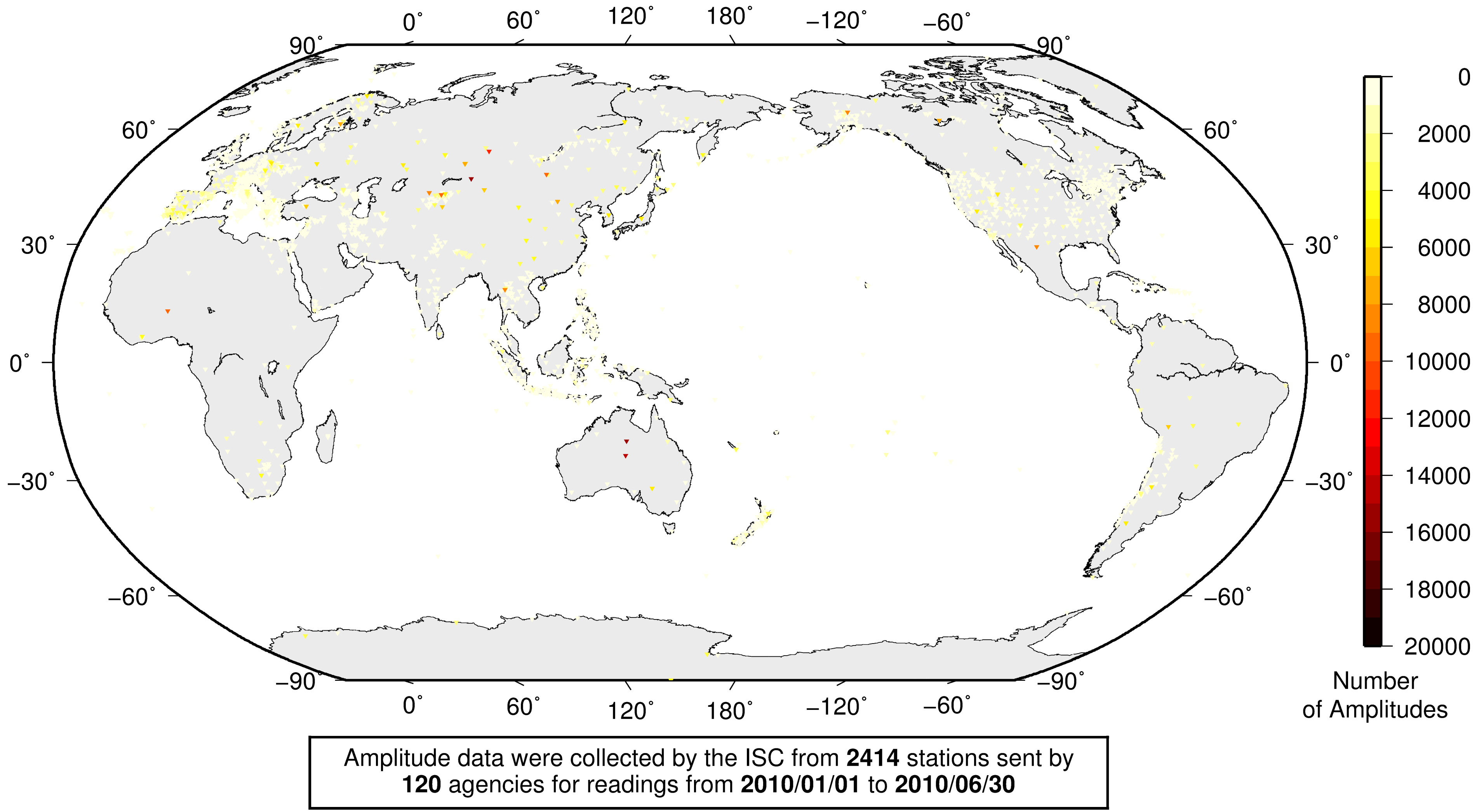

Figure 9.6: *Number of amplitude and period measurements for each station.*

Table 9.3: *Summary of reports containing phase arrival observations.*

Reports with phase arrivals	1775
Reports with phase arrivals including amplitudes	771
Reports with only phase arrivals (no hypocentres reported)	272
Total phase arrivals received	5644012
Total phase arrival-times received	5360793
Number of duplicate phase arrival-times	1174510 (21.9%)
Number of amplitudes received	1473461
Stations reporting phase arrivals	6034
Stations reporting phase arrivals with amplitude data	2449
Max number of stations per report	2010

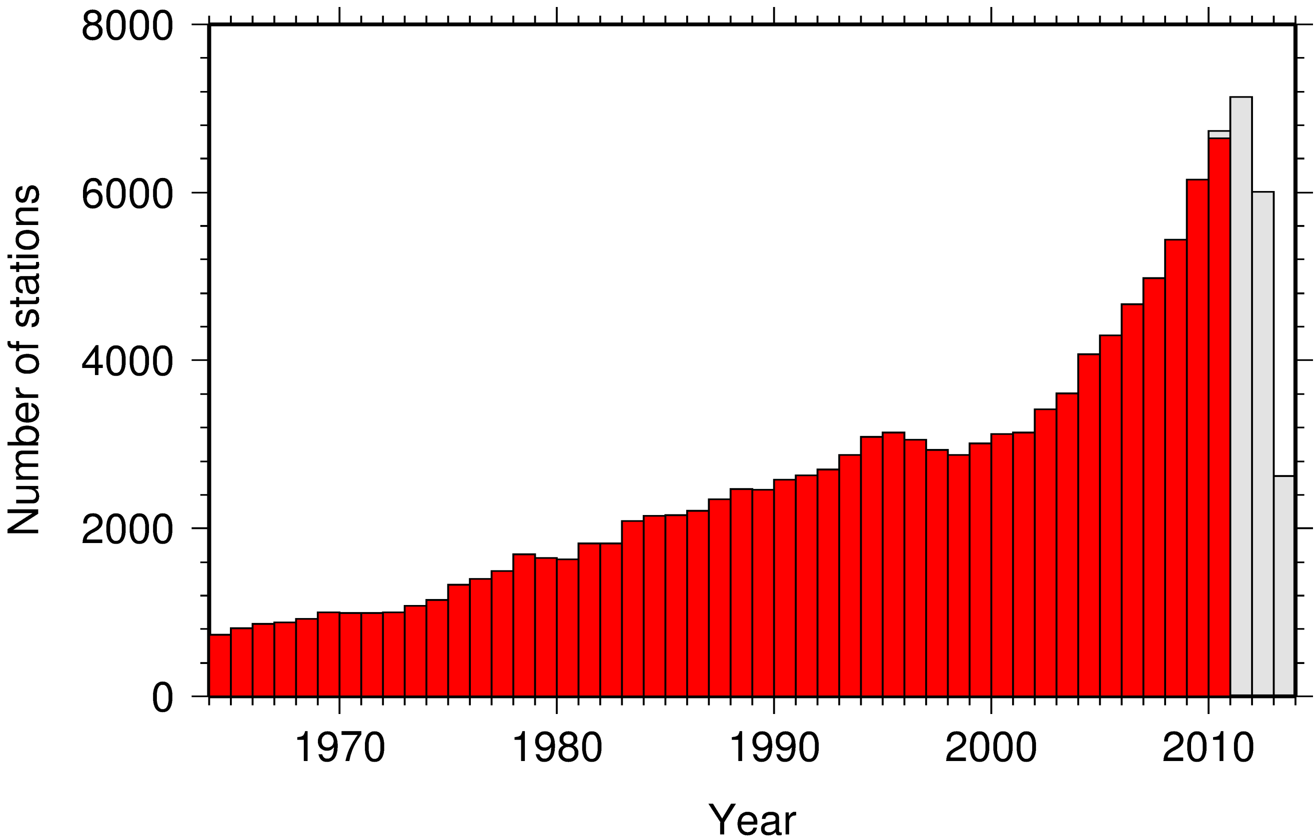

Figure 9.7: *Histogram showing the number of stations reporting to the ISC each year since 1964. The data in grey covers the current period where station information is still being collected before the ISC review of events takes place and is accurate at the time of publication.*

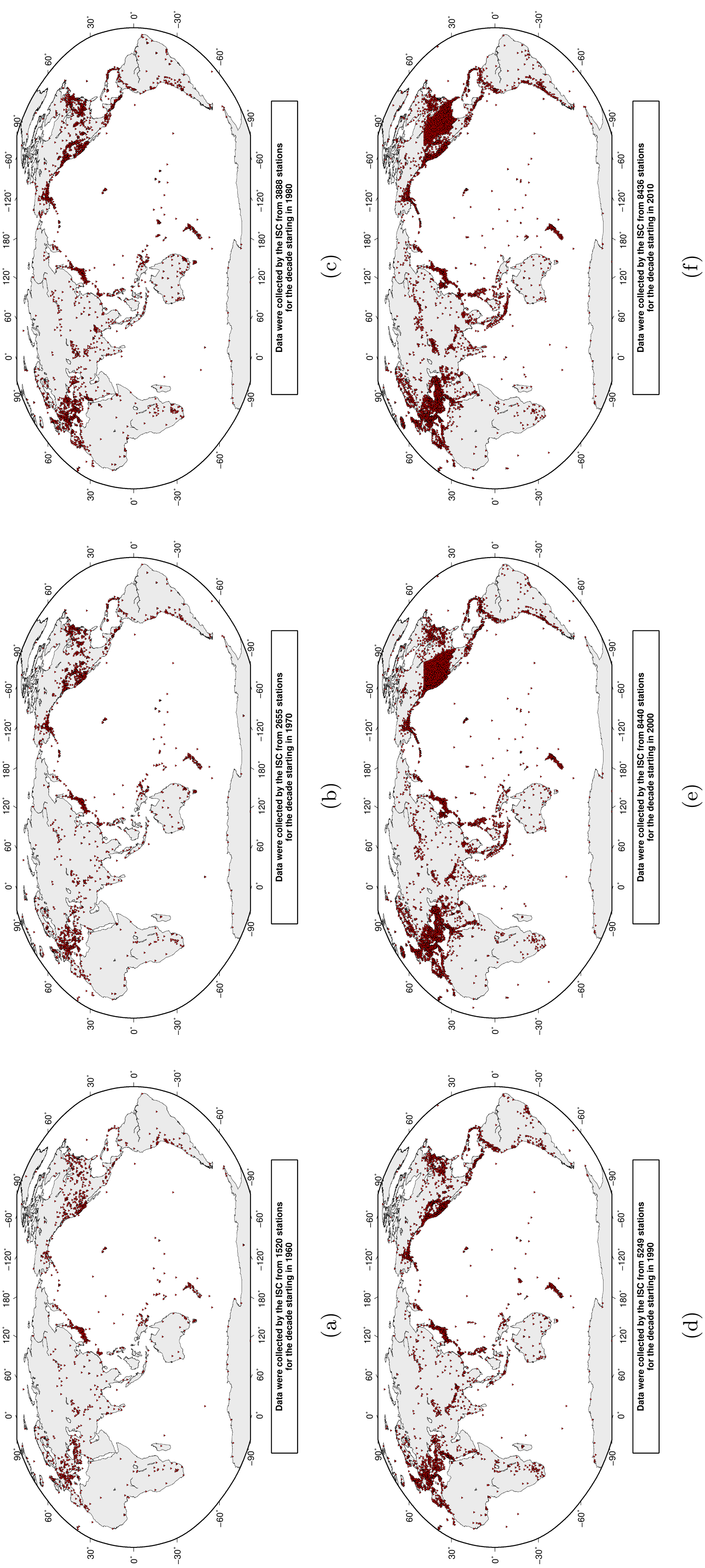

Figure 9.8: *Maps showing the stations reported to the ISC for each decade since 1960. Note that the last map covers a shorter time period.*

9.4 Hypocentres Collected

The ISC Bulletin groups multiple estimates of hypocentres into individual events, with an appropriate prime hypocentre solution selected. The collection of these hypocentre estimates are described in this section.

The reports containing hypocentres are summarised in Table 9.4. The number of hypocentres collected by the ISC has also increased significantly since 1964, as shown in Figure 9.9. A map of all hypocentres reported to the ISC for this summary period is shown in Figure 9.10. Where a network magnitude was reported with the hypocentre, this is also shown on the map, with preference given to reported values, first of M_W followed by M_S, m_b and M_L respectively (where more than one network magnitude was reported).

Table 9.4: *Summary of the reports containing hypocentres.*

Reports with hypocentres	2153
Reports of hypocentres only (no phase readings)	650
Total hypocentres received	351604
Number of duplicate hypocentres	77616 (22.1%)
Agencies determining hypocentres	151

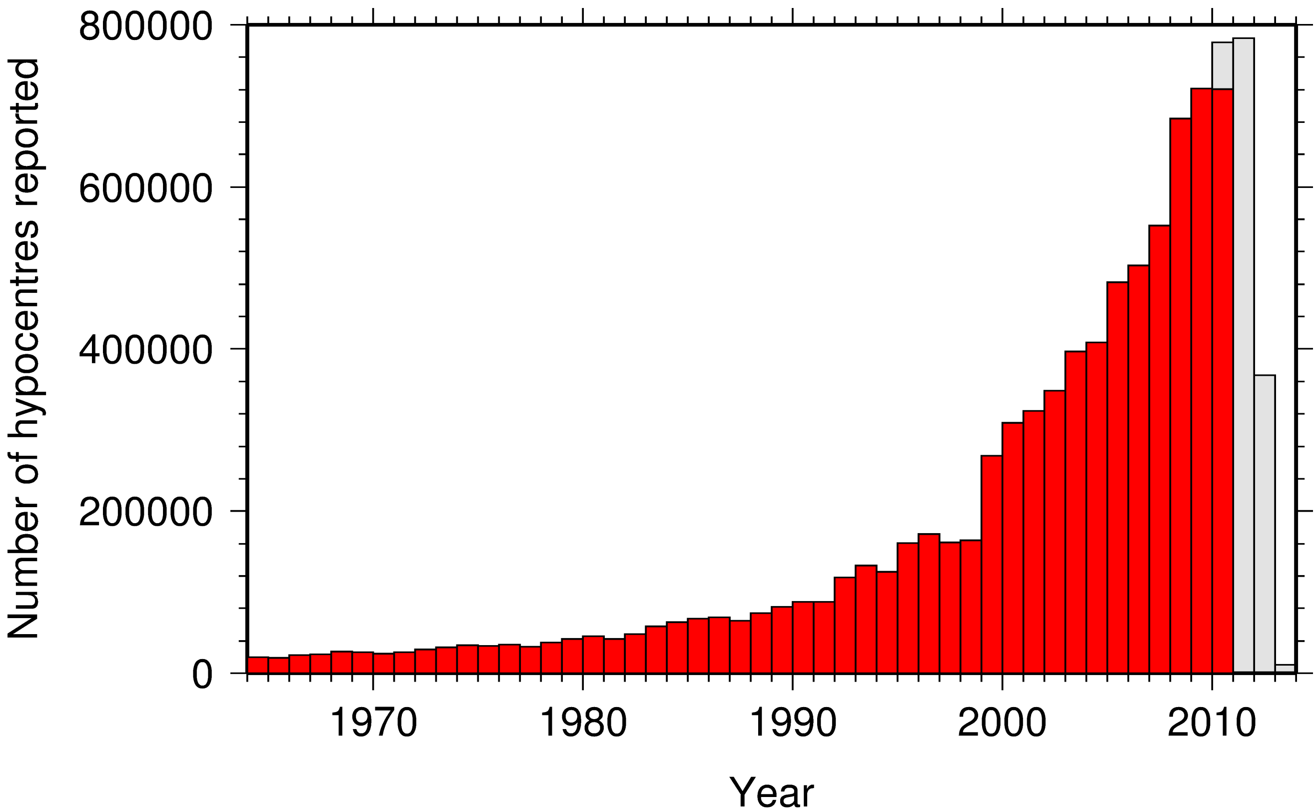

Figure 9.9: *Histogram showing the number of hypocentres collected by the ISC for events each year since 1964. For each event, multiple hypocentres may be reported.*

All the hypocentres that are reported to the ISC are automatically grouped into events, which form the basis of the ISC Bulletin. For this time period 383055 hypocentres (including ISC) were grouped

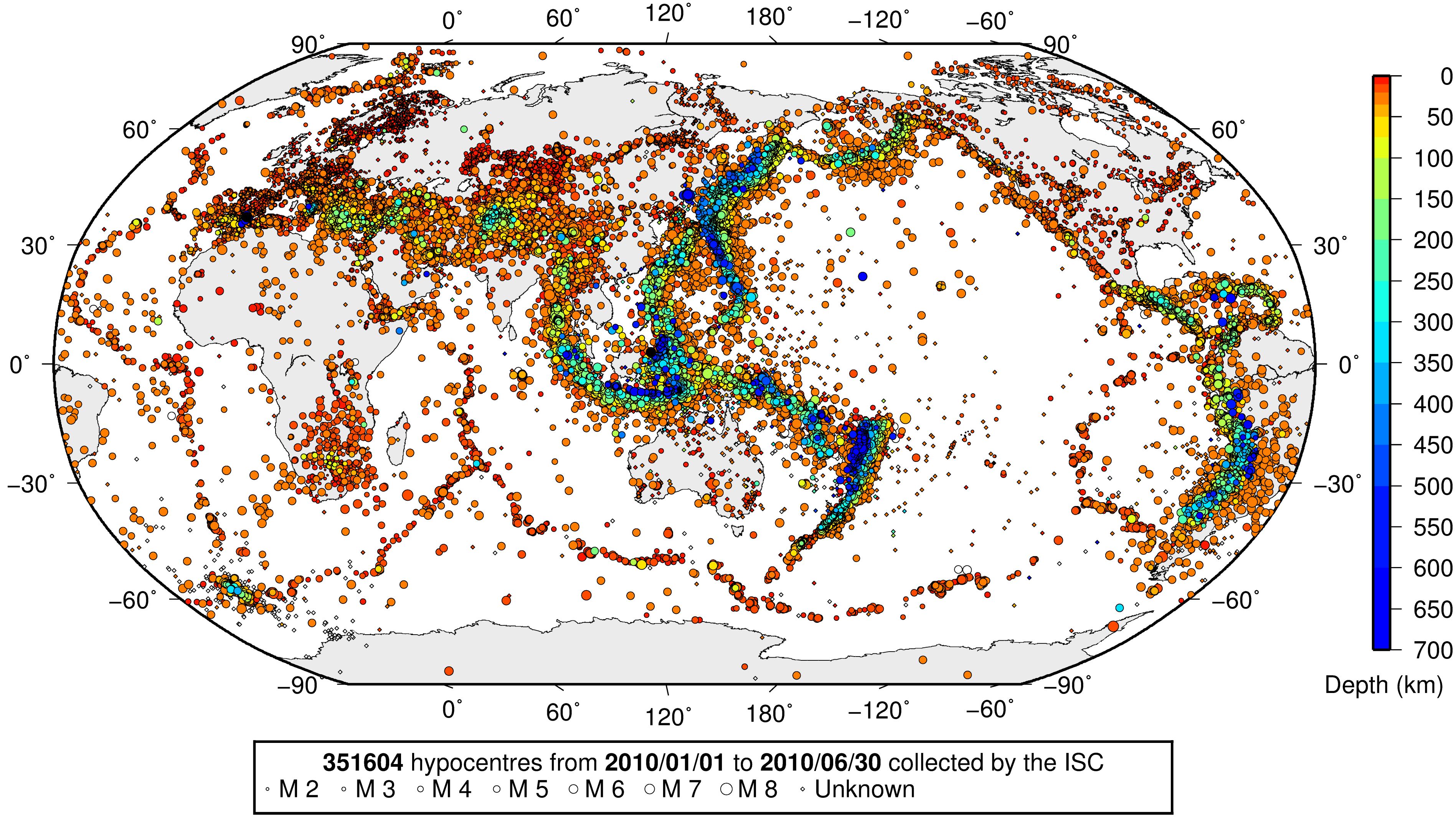

Figure 9.10: *Map of all hypocentres collected by the ISC. The scatter shows the large variation of the multiple hypocentres that are reported for each event. The magnitude corresponds with the reported network magnitude. If more than one network magnitude type was reported, preference was given to values of* M_W*,* M_S*,* m_b *and* M_L *respectively. Compare with Figure 10.2*

into 181754 events, the largest of these having 79 hypocentres in one event. The total number of events shown here is the result of an automatic grouping algorithm, and will differ from the total events in the published ISC Bulletin, where both the number of events and the number of hypocentre estimates will have changed due to further analysis. The process of grouping is detailed in Section 3.3.1. Figure 10.2 on page 129 shows a map of all prime hypocentres.

9.5 Collection of Network Magnitude Data

Data contributing agencies normally report earthquake hypocentre solutions along with magnitude estimates. For each seismic event, each agency may report one or more magnitudes of the same or different types. This stems from variability in observational practices at regional, national and global level in computing magnitudes based on a multitude of wave types. Differences in the amplitude measurement algorithm, seismogram component(s) used, frequency range, station distance range as well as the instrument type contribute to the diversity of magnitude types. Table 9.5 provides an overview of the complexity of reported network magnitudes reported for seismic events during current the period.

Table 9.5: *Statistics of magnitude reports to the ISC; M – average magnitude of estimates reported for each event.*

	M<3.0	3.0≤M<5.0	M≥5.0
Number of seismic events	128574	35888	561
Average number of magnitude estimates per event	1.9	5.3	27.9
Average number of magnitudes (by the same agency) per event	1.4	2.8	4.5
Average number of magnitude types per event	1.2	4.0	10.4
Number of magnitude types	21	28	23

Table 9.6 gives the basic description, main features and scientific paper references for the most commonly reported magnitude types.

Table 9.6: *Description of the most common magnitude types reported to the ISC.*

Magnitude type	Description	References	Comments
M	Unspecified		Often used in real or near-real time magnitude estimations
mB	Medium-period and Broad-band body-wave magnitude	*Gutenberg* (1945a); *Gutenberg* (1945b); *IASPEI* (2005); *IASPEI* (2013); *Bormann et al.* (2009); *Bormann and Dewey* (2012)	
mb	Short-period body-wave magnitude	*IASPEI* (2005); *IASPEI* (2013); *Bormann et al.* (2009); *Bormann and Dewey* (2012)	Classical mb based on stations between 21°-100° distance

Table 9.6: *continued*

Magnitude type	Description	References	Comments
mb1	Short-period body-wave magnitude	*IDC* (1999) and references therein	Reported only by the IDC; also includes stations at distances less than 21°
mb1mx	Maximum likelihood short-period body-wave magnitude	*Ringdal* (1976); *IDC* (1999) and references therein	Reported only by the IDC
mbtmp	short-period body-wave magnitude with depth fixed at the surface	*IDC* (1999) and references therein	Reported only by the IDC
mbLg	Lg-wave magnitude	*Nuttli* (1973); *IASPEI* (2005); *IASPEI* (2013); *Bormann and Dewey* (2012)	Also reported as MN
Mc	Coda magnitude		
MD (Md)	Duration magnitude	*Bisztricsany* (1958); *Lee et al.* (1972)	
ME (Me)	Energy magnitude	*Choy and Boatwright* (1995)	Reported only by NEIC
MJMA	JMA magnitude	*Tsuboi* (1954)	Reported only by JMA
ML (Ml)	Local (Richter) magnitude	*Richter* (1935); *Hutton and Boore* (1987); *IASPEI* (2005); *IASPEI* (2013)	
MLSn	Local magnitude calculated for Sn phases	*Balfour et al.* (2008)	Reported by PGC only for earthquakes west of the Cascadia subduction zone
MLv	Local (Richter) magnitude computed from the vertical component		Reported only by DJA and BKK
MN (Mn)	Lg-wave magnitude	*Nuttli* (1973); *IASPEI* (2005)	Also reported as mbLg
MS (Ms)	Surface-wave magnitude	*Gutenberg* (1945c); *Vaněk et al.* (1962); *IASPEI* (2005)	Classical surface-wave magnitude computed from station between 20°-160° distance
Ms1	Surface-wave magnitude	*IDC* (1999) and references therein	Reported only by the IDC; also includes stations at distances less than 20°
ms1mx	Maximum likelihood surface-wave magnitude	*Ringdal* (1976); *IDC* (1999) and references therein	Reported only by the IDC

Table 9.6: *continued*

Magnitude type	Description	References	Comments
Ms7	Surface-wave magnitude	*Bormann et al.* (2007)	Reported only by BJI and computed from records of a Chinese-made long-period seismograph in the distance range 3°-177°
MW (Mw)	Moment magnitude	*Kanamori* (1977); *Dziewonski et al.* (1981)	Computed according to the *IASPEI* (2005) and *IASPEI* (2013) standard formula
Mw(mB)	Proxy Mw based on mB	*Bormann and Saul* (2008)	Reported only by DJA and BKK
Mwp	Moment magnitude from P-waves	*Tsuboi et al.* (1995)	Reported only by DJA and BKK and used in rapid response
mbh	Unknown		
mbv	Unknown		
MG	Unknown		
Mm	Unknown		
msh	Unknown		
MSV	Unknown		

Table 9.7 lists all magnitude types reported, the corresponding number of events in the ISC Bulletin and the agency codes along with the number of earthquakes.

Table 9.7: *Summary of magnitude types in the ISC Bulletin for this summary period. The number of events with values for each magnitude type is listed. The agencies reporting these magnitude types are listed, together with the total number of values reported.*

Magnitude type	Events	Agencies reporting magnitude type (number of values)
M	4827	DJA (3513), SKO (948), FDF (227), BKK (176), TRN (48), PRU (16)
mB	2935	BJI (2275), DJA (1110), BKK (78)
mb	24801	IDC (18361), NEIC (5958), NNC (4183), MOS (2371), BJI (1852), DJA (1402), KRNET (1146), MAN (972), VIE (947), CSEM (455), SKHL (424), SZGRF (359), KLM (297), MDD (233), DSN (106), IGQ (93), BKK (81), SIGU (71), LDG (69), IASPEI (65), NIC (54), INMG (5), NDI (5), BGS (4), CRAAG (3), GII (2), DMN (2), IGIL (1), SSNC (1), CASC (1), LIC (1), STR (1)
mb1	19074	IDC (19074)
mb1mx	19074	IDC (19074)
mbh	27	SKHL (27)
mbLg	2061	MDD (2061)
mbtmp	19074	IDC (19074)
mbv	4	SKHL (4)
Mc	10	CSEM (10)

Table 9.7: *continued*

Magnitude type	Events	Agencies reporting magnitude type (number of values)
MD	33820	CSEM (16288), DDA (9004), ATH (7929), ROM (5996), ISK (5471), MEX (2236), ECX (2035), RSPR (1137), BER (1020), LDG (999), BUC (688), PDA (596), CASC (498), NSSC (429), TRN (391), SJA (328), GRAL (238), HLW (198), SOF (187), NCEDC (141), JSN (136), CNRM (130), PDG (130), PNSN (92), GUC (92), NOU (75), INMG (60), GII (50), TUL (36), SEA (26), HVO (20), SNET (20), PLV (18), IGQ (17), LDO (14), CERI (13), DHMR (12), TUN (10), BUL (9), GCG (5), SDD (4), UCR (4), BUT (3), WES (2), HDC (2), AAE (2), SSS (1), SSNC (1), INET (1)
ME	97	NEIC (97)
MG	362	AEIC (288), WEL (36), GUC (30), ARE (5), OTT (1), THE (1), RSPR (1)
MJMA	57682	JMA (57682)
ML	71743	CSEM (18399), TAP (11348), IDC (10823), ROM (6563), HEL (6220), GUC (4868), WEL (4745), THE (4532), UPP (3584), ECX (2492), PAS (1510), LJU (1498), SJA (1435), VIE (1317), BEO (1296), LDG (1247), PRE (1193), AEIC (1116), BER (1070), MAN (972), SKO (959), ATH (950), PGC (906), INMG (890), NSSC (863), NAO (809), CRAAG (743), PDA (682), KRSC (562), IGIL (456), STR (455), BJI (424), ISK (422), GEN (398), IPEC (391), TIR (354), PDG (335), DHMR (276), ZUR (251), DDA (248), NIC (247), TEH (196), KLM (191), HLW (177), ISN (171), THR (169), KNET (165), SFS (161), CASC (149), NEIC (139), BGR (137), NDI (124), PPT (110), FIA0 (108), SLC (97), OTT (89), WBNET (89), DSN (89), BNS (79), NOU (64), NCEDC (63), ARO (58), BGS (57), BUG (50), PLV (42), UCC (41), REY (36), REN (27), DMN (22), MRB (14), BUT (12), ARE (12), HVO (11), ALG (8), SZGRF (7), AUST (7), SGS (6), RSNC (4), SEA (3), NSSP (3), RSPR (3), UCR (3), LIS (2), LDO (2), SSS (2), SSNC (1), TIF (1), TTG (1), DJA (1), DNK (1), ZAG (1), ANF (1), GCG (1), BUC (1)
MLSn	53	PGC (53)
MLv	3597	DJA (3497), BKK (163)
Mm	10	GII (10)
MN	649	OTT (569), NEIC (77), TEH (43), CERI (7), OGSO (6), WES (4), TUL (2), MDD (2), PGC (1)
mpv	4595	NNC (4595)
MS	9277	IDC (8181), BJI (1861), MAN (979), MOS (505), NEIC (270), KLM (247), CSEM (160), SZGRF (132), LDG (63), SKHL (56), NSSP (53), VIE (46), DSN (43), IASPEI (20), ASRS (15), NOU (13), IGIL (3), GUC (2), SJA (2), INMG (1)
Ms1	8181	IDC (8181)
ms1mx	8181	IDC (8181)
Ms7	1857	BJI (1857)
msh	105	SKHL (105)

Table 9.7: *continued*

Magnitude type	Events	Agencies reporting magnitude type (number of values)
MSV	899	YARS (899)
MW	4369	FUNV (1644), NIED (918), GCMT (895), SJA (648), NEIC (475), PGC (408), BRK (44), CSEM (30), OTT (15), CAR (10), PAS (10), GUC (5), SLM (4), BER (4), UPA (3), NIC (2), ROM (2), CRAAG (1), LDO (1), NCEDC (1), UCR (1), GCG (1), ECX (1), MDD (1)
Mw(mB)	1152	DJA (1110), BKK (78)
Mwp	134	DJA (133), BKK (6)

The most commonly reported magnitude types are short-period body-wave, surface-wave, local (or Richter), moment, duration and JMA magnitude type. For a given earthquake, the number and type of reported magnitudes greatly vary depending on its size and location. The great Maule (Chile) earthquake of February 27, 2010 gives an example of the multitude of reported magnitude types for large earthquakes (Listing 9.1). Different magnitude estimates come from global monitoring agencies such as the IDC, NEIC and GCMT, a local agency (GUC) and other agencies, such as MOS and BJI, providing estimates based on the analysis of their networks. The same agency may report different magnitude types as well as several estimates of the same magnitude type, such as NEIC estimates of Mw obtained from W-phase, centroid and body-wave inversions.

Listing 9.1: *Example of reported magnitudes for a large event*

```
Event 14340585 Near coast of central Chile
   Date       Time        Err   RMS Latitude Longitude  Smaj  Smin  Az Depth   Err Ndef Nsta Gap  mdist  Mdist Qual   Author      OrigID
2010/02/27 06:34:13.33   0.45 2.199 -36.1485  -72.9327 5.560 4.098 120  28.1  2.80 2220 2384  10   0.92 177.40 m i se ISC       00198269
 (#PRIME)

Magnitude  Err Nsta Author      OrigID
ML      5.1 0.2    4 IDC        16659961
MS      8.3 0.1   23 IDC        16659961
Ms1     8.3 0.1   23 IDC        16659961
mb      5.9 0.1   34 IDC        16659961
mb1     5.9 0.1   37 IDC        16659961
mb1mx   5.9 0.1   37 IDC        16659961
mbtmp   5.9 0.1   37 IDC        16659961
ms1mx   8.1 0.1   32 IDC        16659961
ML      8.8          GUC        15669768
MW      8.8          NEIC       15669768
ME      8.3          NEIC       16818964
MS      8.5      299 NEIC       16818964
MW      8.8          NEIC       16818964
MW      8.8          NEIC       16818964
mb      7.2      245 NEIC       16818964
MS      8.5       60 MOS        14814964
mb      7.1       37 MOS        14814964
Ms      8.8       76 BJI        14395291
Ms7     8.7       63 BJI        14395291
mB      7.6       37 BJI        14395291
MW      8.8      136 GCMT       00123080
```

An example of a relatively small earthquake that occurred in northern Italy for which we received magnitude reports of mostly local and duration type from six agencies in Italy, France and Austria is given in Listing 9.2.

Listing 9.2: *Example of reported magnitudes for a small event*

```
Event 14297884 Northern Italy
   Date       Time        Err   RMS Latitude Longitude  Smaj  Smin  Az Depth   Err Ndef Nsta Gap  mdist  Mdist Qual   Author      OrigID
2010/02/05 02:36:10.06   0.75 1.087  44.3755    7.2710 1.959 1.638  72  15.4  4.49  313  168  30   0.13   9.09 m i ke ISC       00196259
 (#PRIME)

Magnitude  Err Nsta Author      OrigID
Md      2.8 0.3   16 ROM        16318041
Ml      3.0 0.4   11 ROM        16318041
ML      3.5 0.5   36 CSEM       17115576
ML      2.9          GEN        17115577
Md      3.2 0.1    3 LDG        13652662
Ml      3.3 0.4   40 LDG        13652662
ML      2.9 0.3    5 VIE        15917307
mb      2.6 0.1    4 VIE        15917307
Ml      3.1 0.0      STR        16033989
```

Figure 9.11 shows a distribution of the number of agencies reporting magnitude estimates to the ISC according to the magnitude value. The peak of the distribution corresponds to small earthquakes where many local agencies report local and/or duration magnitudes. The number of contributing agencies rapidly decreases for earthquakes of approximately magnitude 5.5 and above, where magnitudes are mostly given by global monitoring agencies.

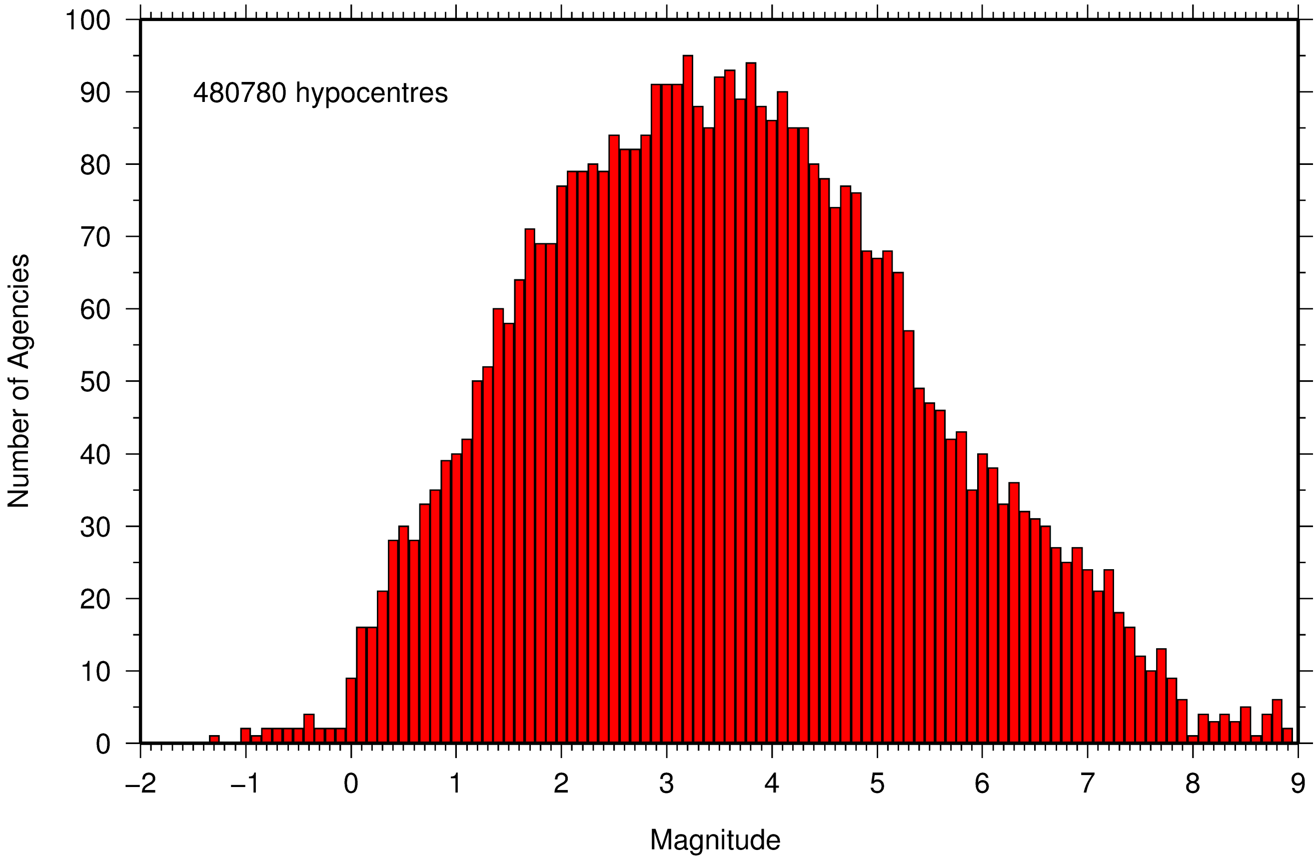

Figure 9.11: *Histogram showing the number of agencies that reported network magnitude values. All magnitude types are included.*

9.6 Moment Tensor Solutions

The ISC Bulletin publishes moment tensor solutions, which are reported to the ISC by other agencies. The collection of moment tensor solutions is summarised in Table 9.8. A histogram showing all moment tensor solutions collected throughout the ISC history is shown in Figure 9.12. Several moment tensor solutions from different authors and different moment tensor solutions calculated by different methods from the same agency may be present for the same event.

Table 9.8: *Summary of reports containing moment tensor solutions.*

Reports with Moment Tensors	12
Total moment tensors received	4644
Agencies reporting moment tensors	8

The number of moment tensors for this summary period, reported by each agency, is shown in Table 9.9. The moment tensor solutions are plotted in Figure 9.13.

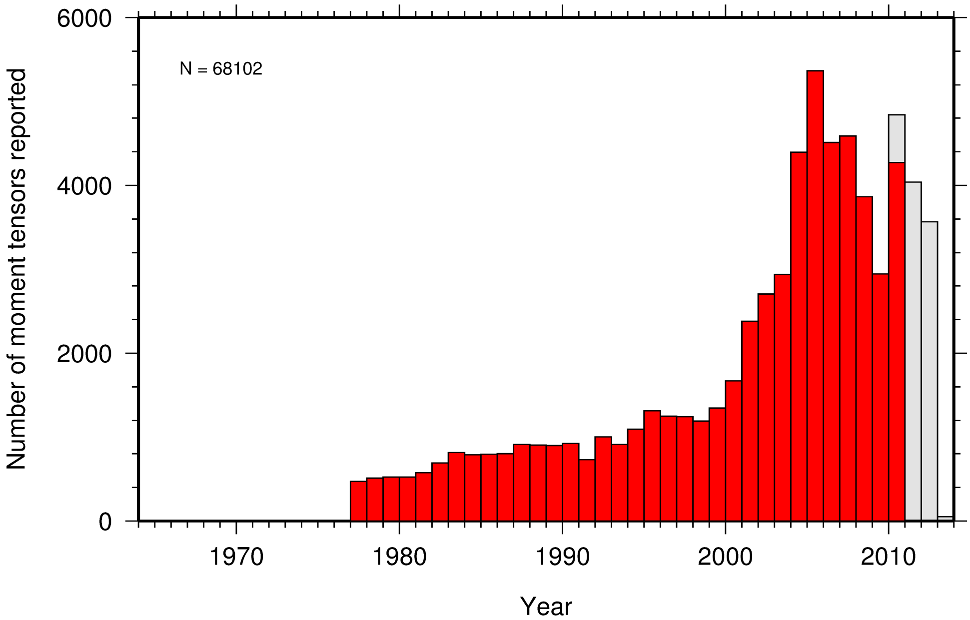

Figure 9.12: *Histogram showing the number of moment tensors reported to the ISC since 1964. The regions in grey represent data that are still being actively collected.*

Table 9.9: *Summary of moment tensor solutions in the ISC Bulletin reported by each agency.*

Agency	Number of moment tensor solutions
GCMT	895
NEIC	319
NIED	160
BRK	41
OTT	8
PAS	7
SLM	3
ROM	2

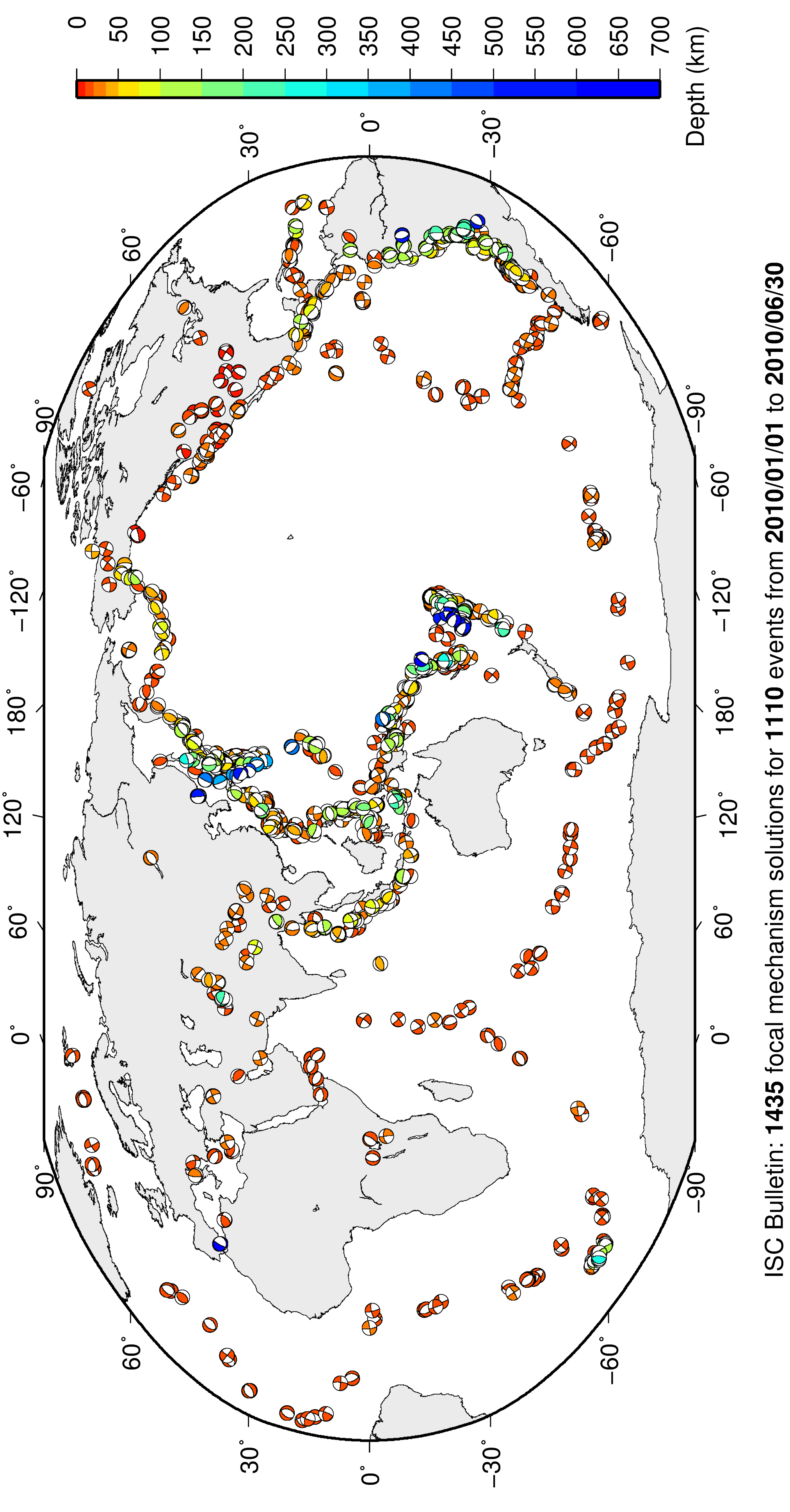

Figure 9.13: *Map of all moment tensor solutions in the ISC Bulletin for this summary period.*

9.7 Timing of Data Collection

Here we present the timing of reports to the ISC. Please note, this does not include provisional alerts, which are replaced at a later stage. Instead, it reflects the final data sent to the ISC. The absolute timing of all hypocentre reports, regardless of magnitude, is shown in Figure 9.14. In Figure 9.15 the reports are grouped into one of six categories - from within three days of an event origin time, to over one year. The histogram shows the distribution with magnitude (for hypocentres where a network magnitude was reported) for each category, whilst the map shows the geographic distribution of the reported hypocentres.

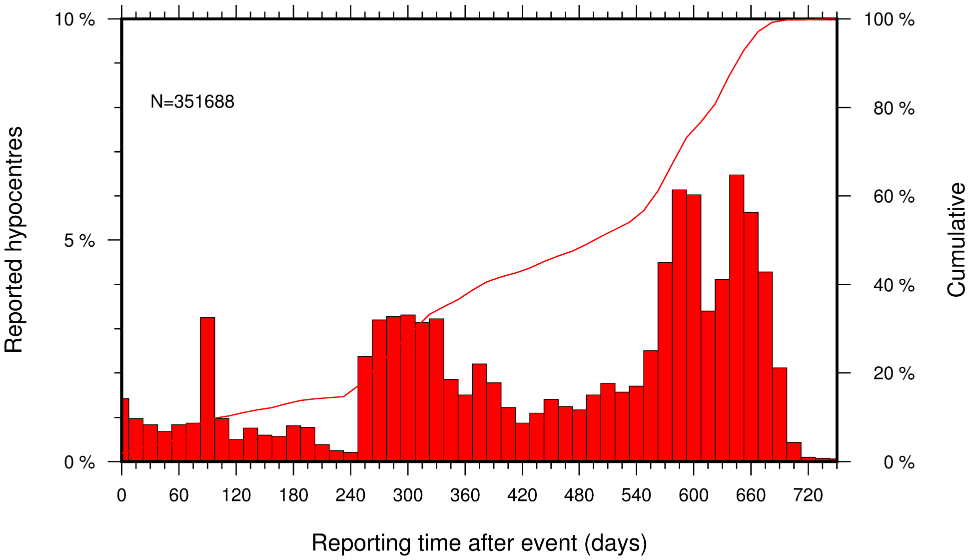

Figure 9.14: *Histogram showing the timing of final reports of the hypocentres (total of N) to the ISC. The cumulative frequency is shown by the solid line.*

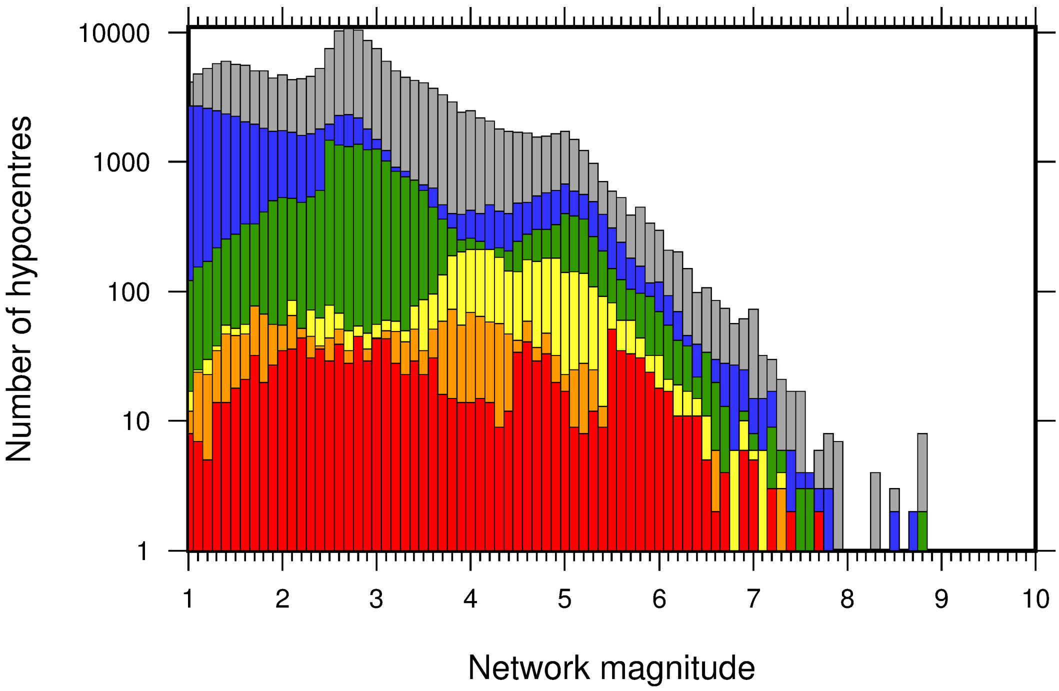

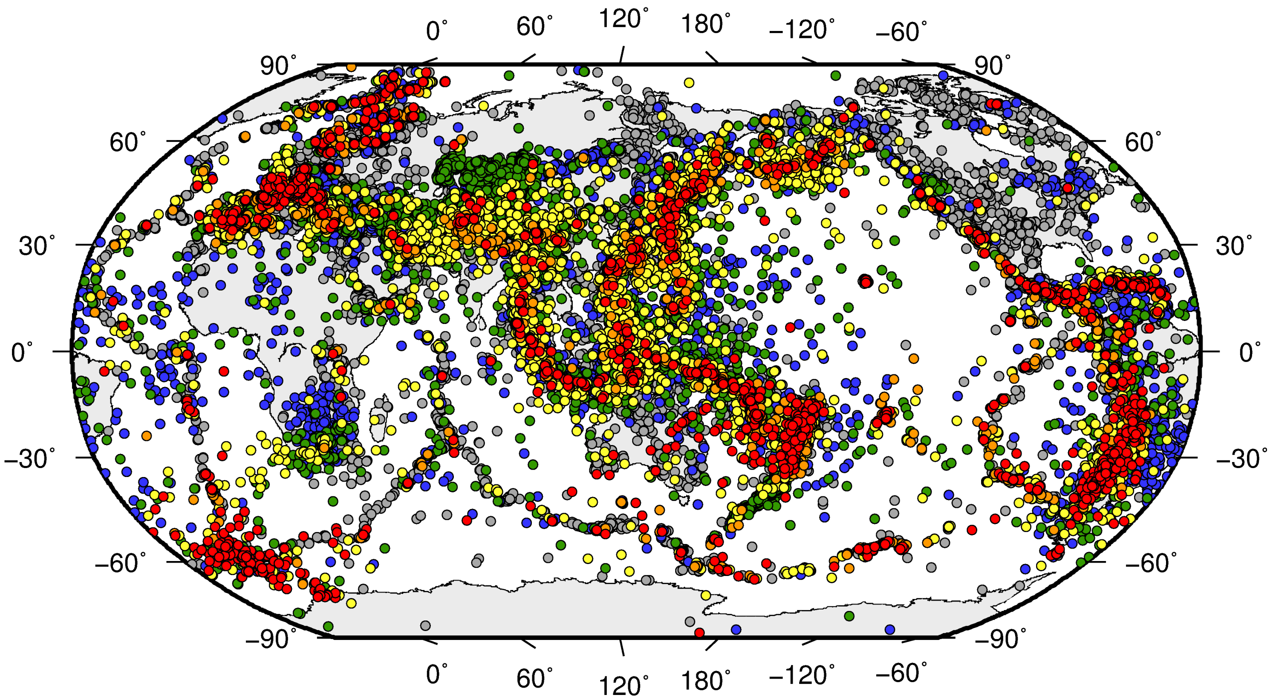

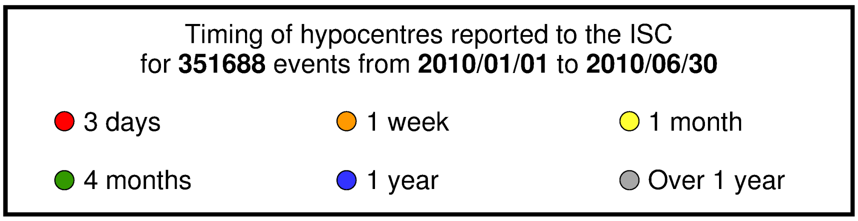

Figure 9.15: *Timing of hypocentres reported to the ISC. The colours show the time after the origin time that the corresponding hypocentre was reported. The histogram shows the distribution with magnitude. If more than one network magnitude was reported, preference was given to a value of M_W followed by M_S, m_b and M_L respectively; all reported hypocentres are included on the map. Note: early reported hypocentres are plotted over later reported hypocentres, on both the map and histogram.*

10

Overview of the ISC Bulletin

This section provides an overview of the seismic event data in the ISC Bulletin. We indicate the differences between all ISC events and those ISC events that are reviewed or located. We describe the wealth of phase arrivals and phase amplitudes and periods observed at seismic stations worldwide, reported in the ISC Bulletin and often used in the ISC location and magnitude determination. Finally, we make some comparisons of the ISC magnitudes with those reported by other agencies, and discuss magnitude completeness of the ISC Bulletin.

10.1 Events

Altogether 169,296 events occurred during the summary period between 2010/01/01 and 2010/07/01. Some 90% (153,119) of the events were identified as earthquakes, the rest (16,177) were of anthropogenic (rockbursts, induced events, mine and other chemical explosions) origin. As discussed in Section 3.3.3, typically about 20% of the events are selected for ISC review, and about half of the events selected for review are located by the ISC. In this summary period 17% of the events were reviewed and 10% of the events were located by the ISC. For events that are not located by the ISC, the prime hypocentre is identified according to the rules described in Section 3.3.1.

Out of the 5,000,000 reported seismic phase arrivals as many as 54% correspond to ISC-reviewed events, and 50% of the reported observations are associated to events selected for ISC location. Note that all large events are reviewed and located by the ISC. Since large events are globally recorded and thus reported by stations worldwide, they will provide the bulk of observations. This explains why only about one-fifth of the events in any given month is reviewed although the number of phases associated to reviewed events has increased nearly exponentially in the past decades.

Figure 10.1 shows the daily number of events throughout the summary period. The large increase in event numbers in February relates to the aftershocks of the Mw 8.8 Maule, Chile, earthquake on 27th February. Other peaks correspond to large events such as the Mw 7.2 earthquake near Mexicali, Mexico, on 4th April, the Mw 7.8 earthquake in northern Sumatra, Indonesia, on 6th April, and the Mw 7.0 earthquake to the north of Papua, Indonesia, on 16th June. Figure 10.2 shows the locations of the events in the ISC Bulletin; the locations of ISC-reviewed and ISC-located events are shown in Figures 10.3 and 10.4, respectively.

Figure 10.5 shows the hypocentral depth distributions of events in the ISC Bulletin for the summary period. The vast majority of events occur in the Earth's crust. Note that the peaks at 0, 10, 35 km, and at every 50 km intervals deeper than 100 km are artifacts of analyst practices of fixing the depth to a nominal value when the depth cannot be reliably resolved.

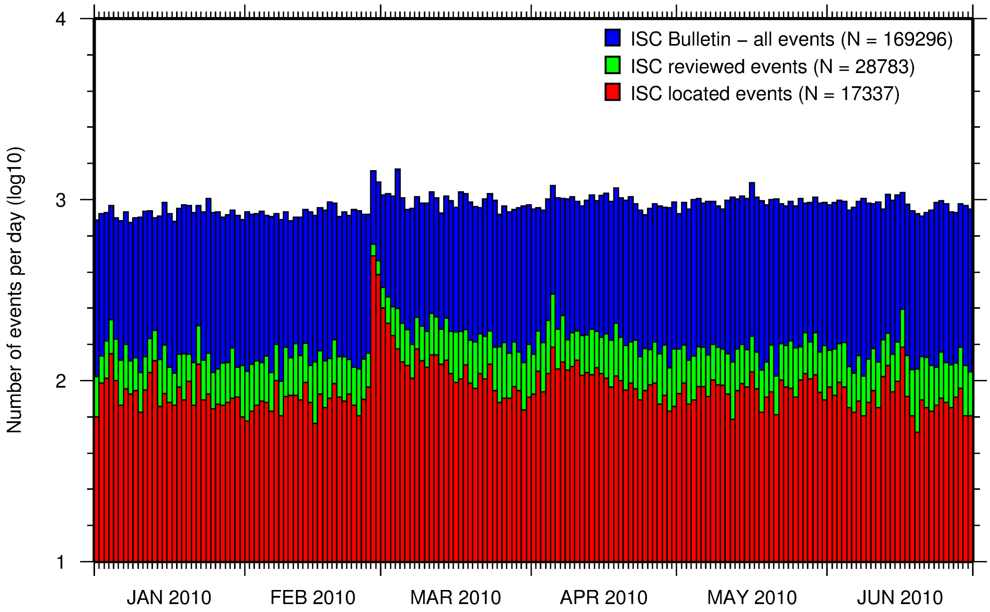

Figure 10.1: *Histogram showing the number of events in the ISC Bulletin for the current summary period. The vertical scale is logarithmic.*

Figure 10.6 shows the depth distribution of free-depth solutions in the ISC Bulletin. The depth of a hypocentre reported to the ISC is assumed to be determined as a free parameter, unless it is explicitly labelled as a fixed-depth solution. On the other hand, as described in Section 3.3, the ISC locator attempts to get a free-depth solution if, and only if, there is resolution for the depth in the data, i.e. if there is a local network and/or sufficient depth-sensitive phases are reported.

Figure 10.7 shows the depth distribution of fixed-depth solutions in the ISC Bulletin. Except for a fraction of events whose depth is fixed to a shallow depth, this set constitutes mostly ISC-located events. If there is no resolution for depth in the data, the ISC locator fixes the depth to a value obtained from the ISC default depth grid file, or if no default depth exists for that location, to a nominal default depth assigned to each Flinn-Engdahl region (see details in Section 3.3). During the ISC review the analysts usually accept the depth obtained from the default depth grid, but may alternatively fix the depth to a round number, preferably divisible by 50.

For events selected for ISC location, the number of stations typically increases as arrival data reported by several agencies are grouped together and associated to the prime hypocentre. Consequently, the network geometry, characterised by the secondary azimuthal gap (the largest azimuthal gap a single station closes), is typically improved. Figure 10.8 illustrates that the secondary azimuthal gap is indeed generally smaller for ISC-located events than that for all events in the ISC Bulletin. Figure 10.9 shows the distribution of the number of associated stations. For large events the number of associated stations is usually larger for ISC-located events than for any of the reported event bulletins. On the other hand, events with just a few reporting stations are rarely selected for ISC location. The same is true for the number of defining stations (stations with at least one defining phase that were used in the location). Figure 10.10 indicates that because the reported observations from multiple agencies are associated to the prime, large ISC-located events typically have a larger number of defining stations than any of the reported event bulletins.

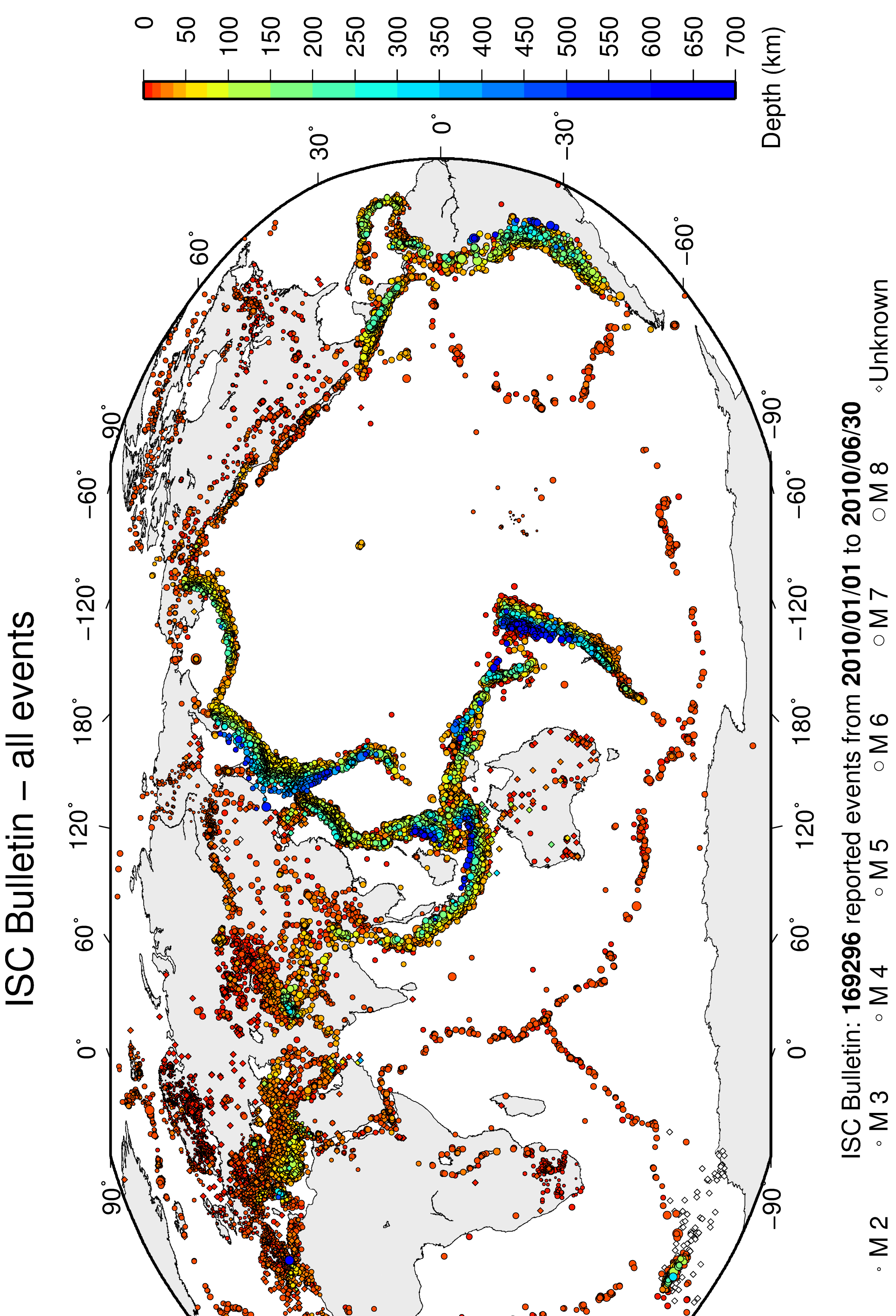

Figure 10.2: *Map of all events in the ISC Bulletin. Prime hypocentre locations are shown. Compare with Figure 9.10.*

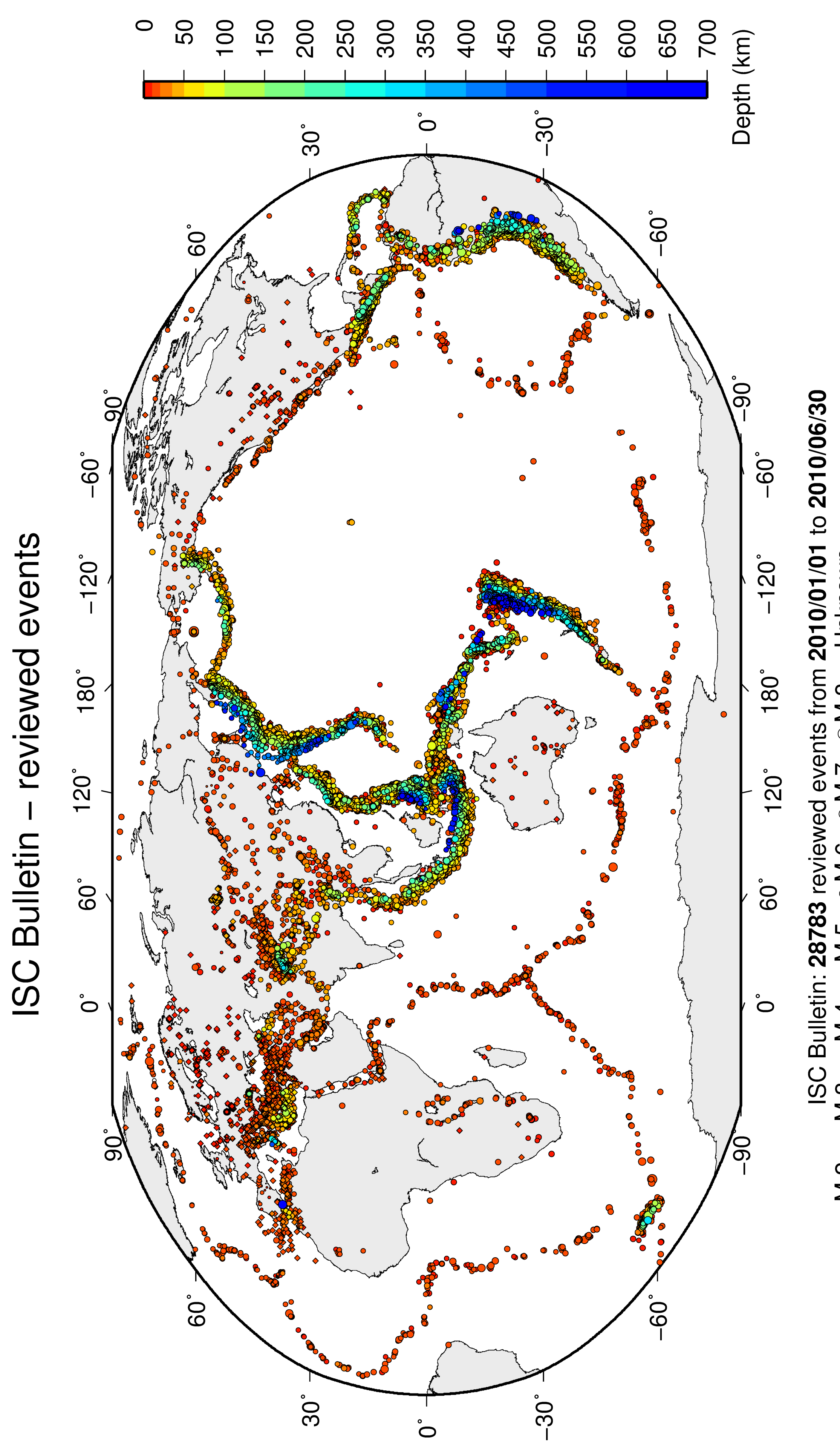

Figure 10.3: Map of all events reviewed by the ISC for this time period. Prime hypocentre locations are shown.

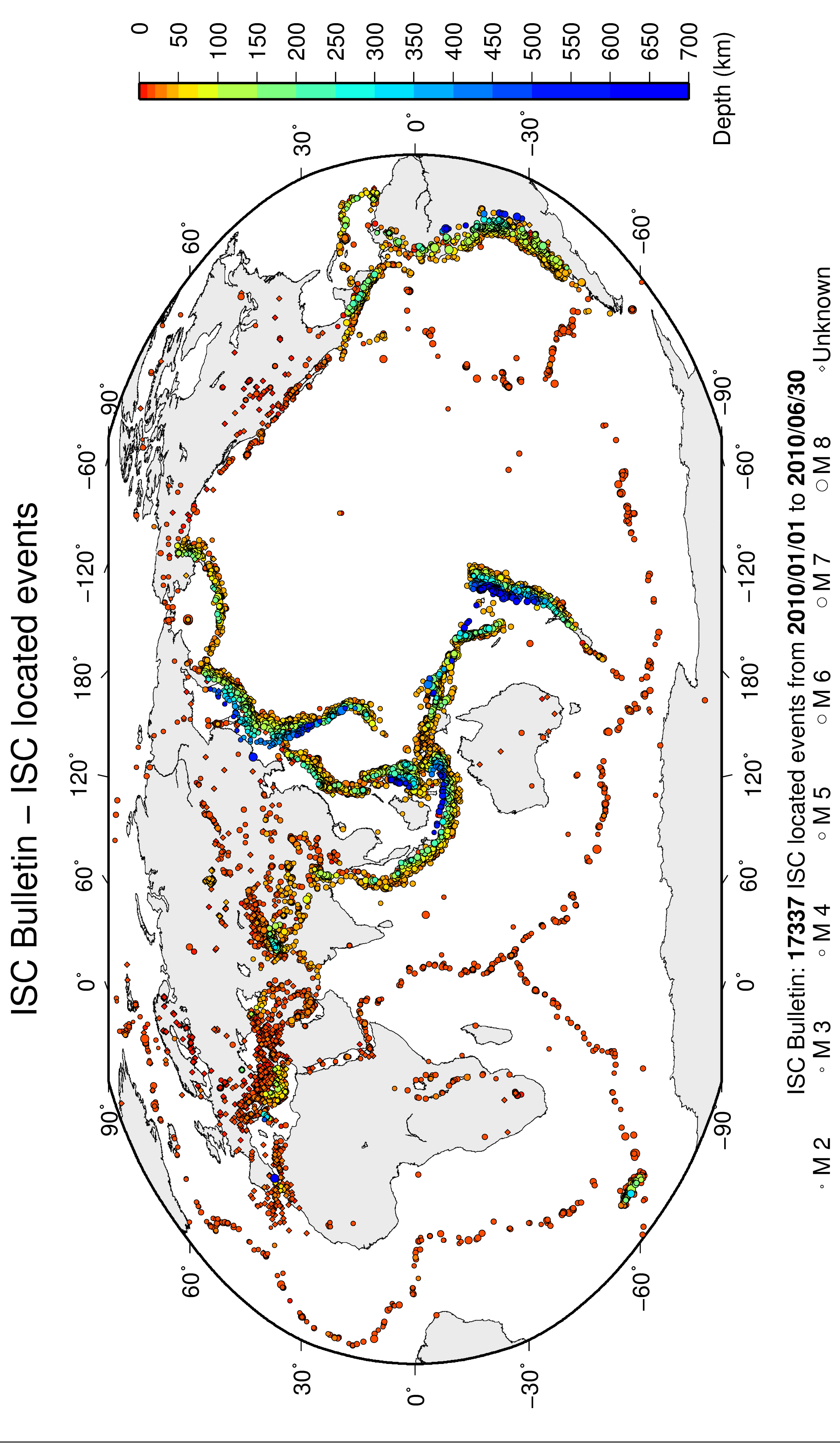

Figure 10.4: Map of all events located by the ISC for this time period. ISC determined hypocentre locations are shown.

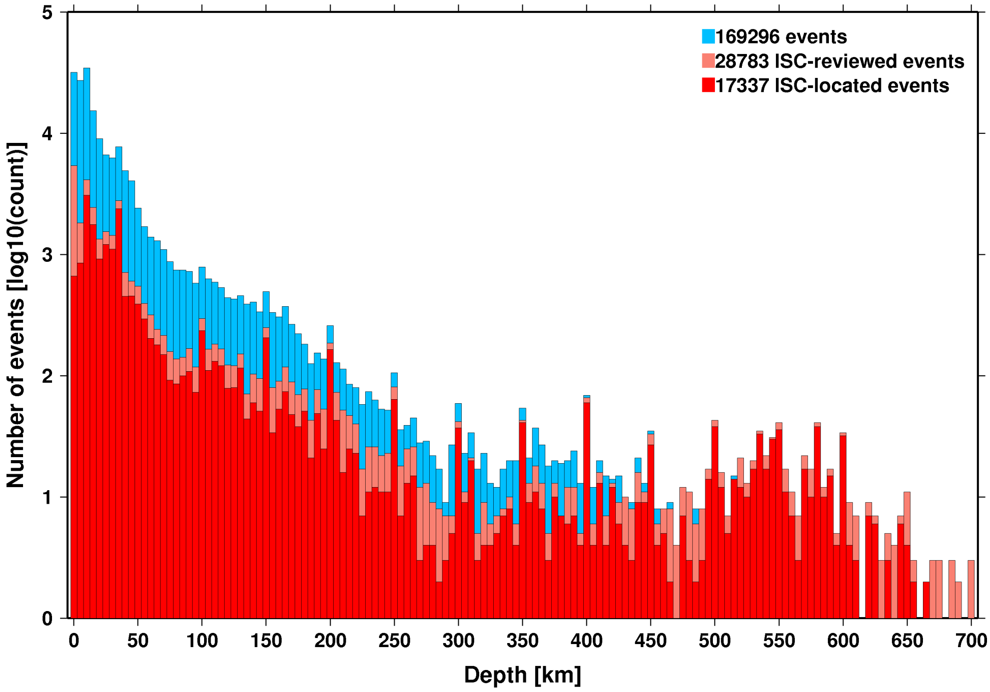

Figure 10.5: *Distribution of event depths in the ISC Bulletin (blue) and for the ISC-reviewed (pink) and the ISC-located (red) events during the summary period. All ISC-located events are reviewed, but not all reviewed events are located by the ISC. The vertical scale is logarithmic.*

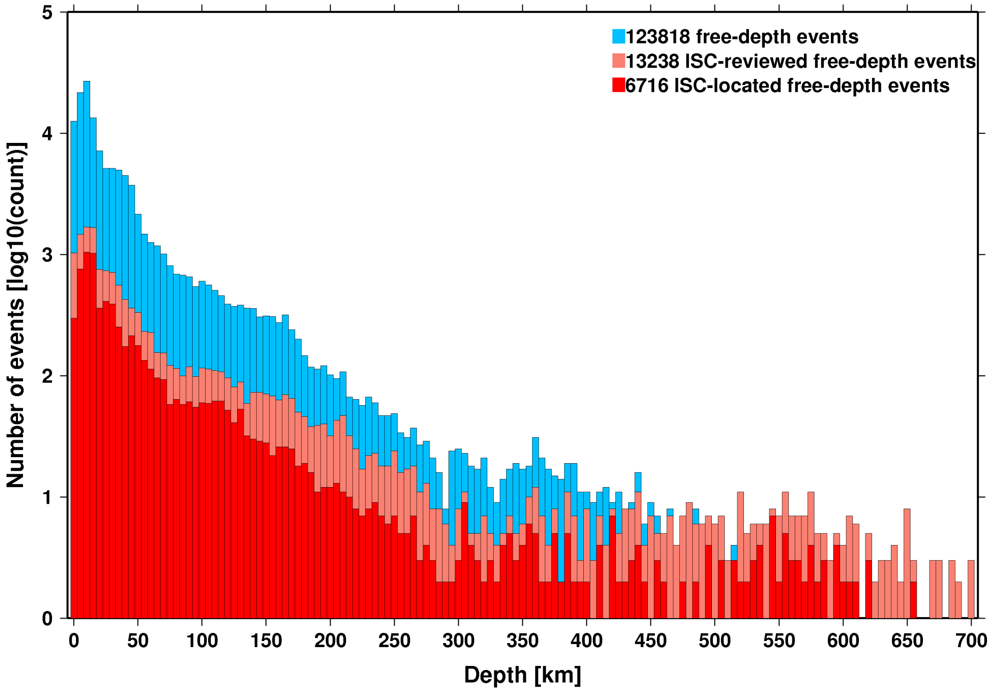

Figure 10.6: *Hypocentral depth distribution of events where the prime hypocentres are reported/located with a free-depth solution in the ISC Bulletin. The vertical scale is logarithmic.*

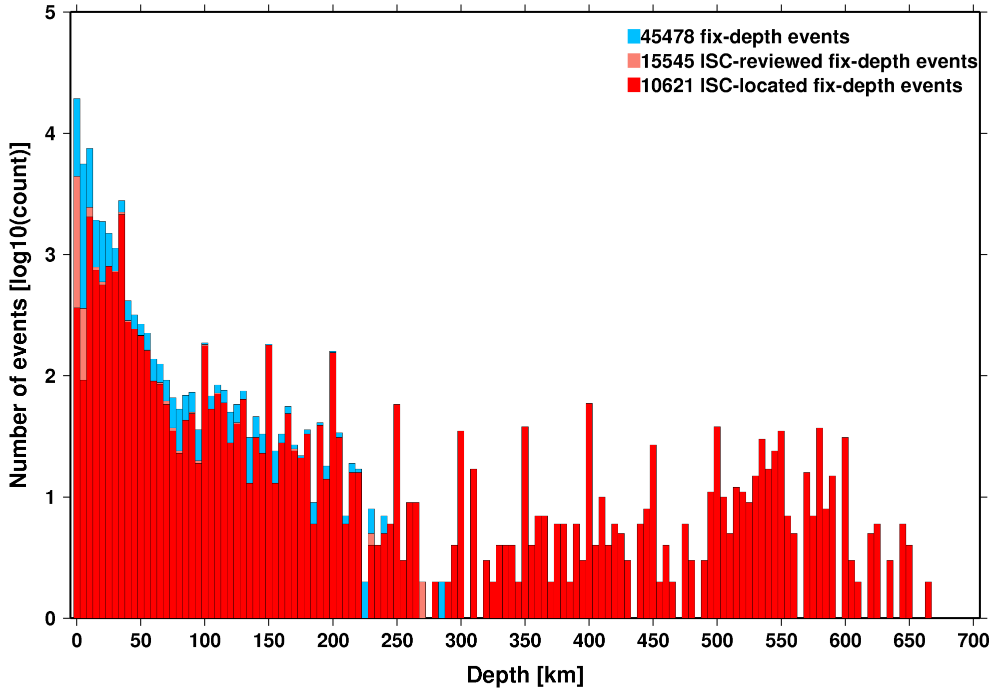

Figure 10.7: *Hypocentral depth distribution of events where the prime hypocentres are reported/located with a fixed-depth solution in the ISC Bulletin. The vertical scale is logarithmic.*

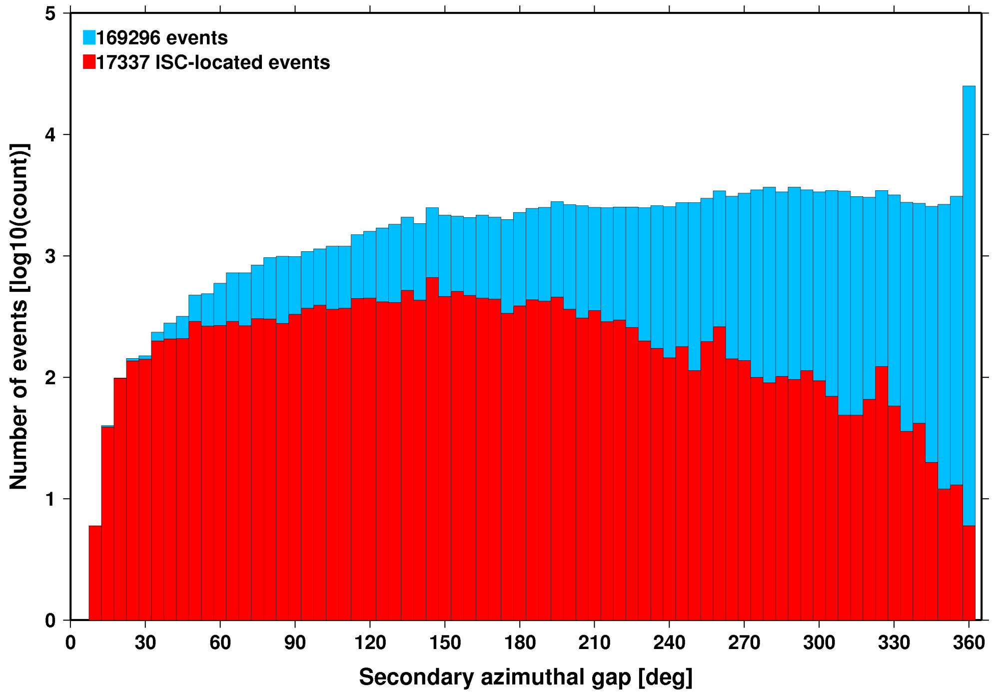

Figure 10.8: *Distribution of secondary azimuthal gap for events in the ISC Bulletin (blue) and those selected for ISC location (red). The vertical scale is logarithmic.*

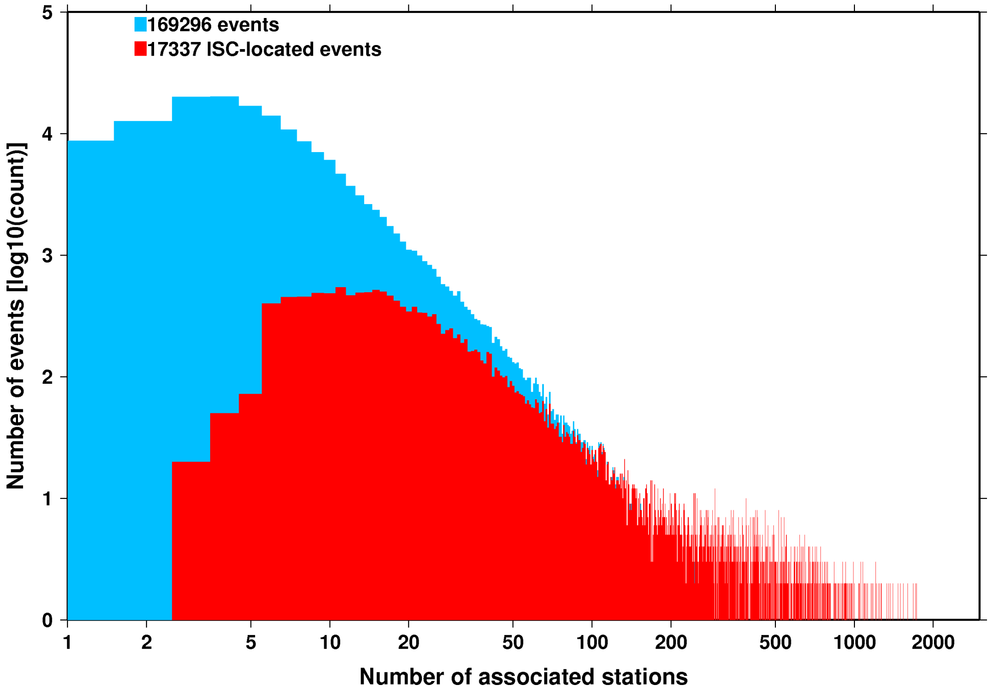

Figure 10.9: *Distribution of the number of associated stations for events in the ISC Bulletin (blue) and those selected for ISC location (red). The vertical scale is logarithmic.*

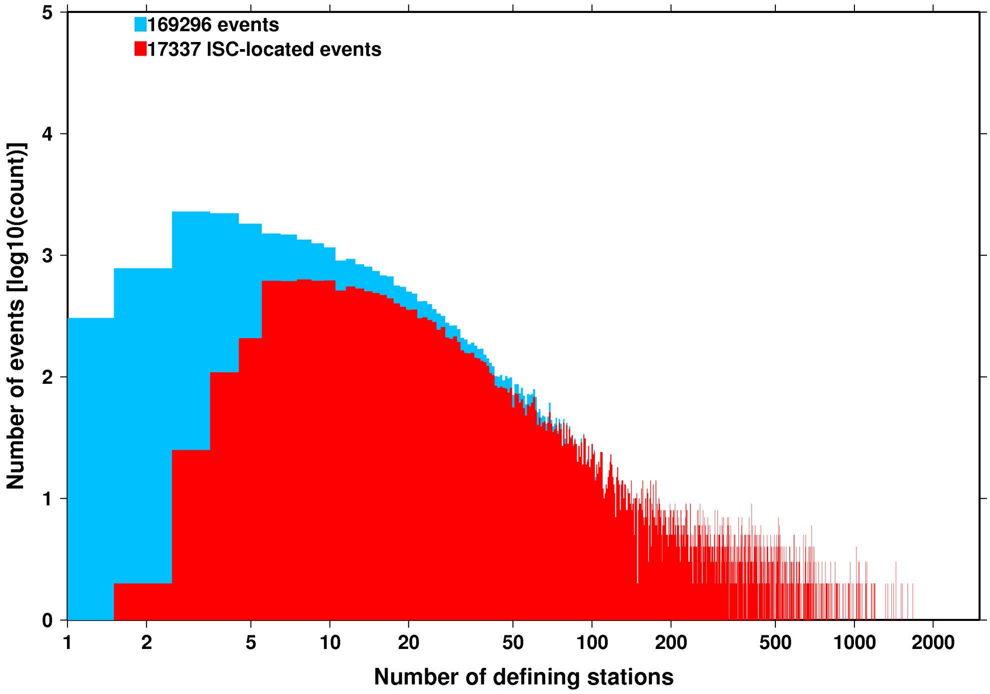

Figure 10.10: *Distribution of the number of defining stations for events in the ISC Bulletin (blue) and those selected for ISC location (red). The vertical scale is logarithmic.*

The formal uncertainty estimates are also typically smaller for ISC-located events. Figure 10.11 shows the distribution of the area of the 90% confidence error ellipse for ISC-located events during the summary period. The distribution suffers from a long tail indicating a few poorly constrained event locations. Nevertheless, half of the events are characterised by an error ellipse with an area less than 278 km^2, 90% of the events have an error ellipse area less than 1,800 km^2, and 95% of the events have an error ellipse area less than 2,900 km^2.

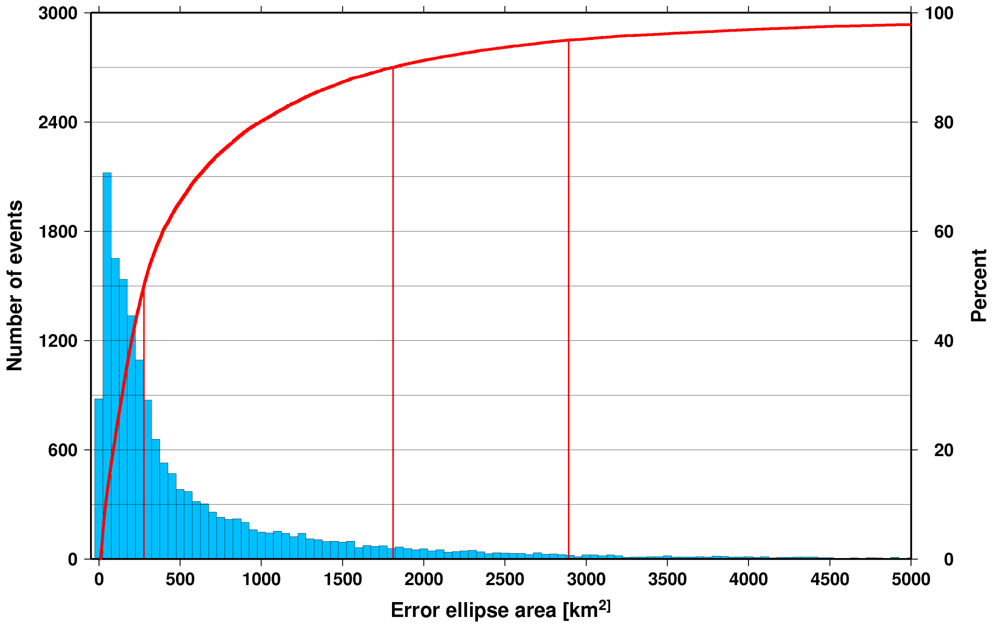

Figure 10.11: *Distribution of the area of the 90% confidence error ellipse of the ISC-located events. Vertical red lines indicate the 50th, 90th and 95th percentile values.*

Figure 10.12 shows one of the major characteristic features of the ISC location algorithm (Bondár and Storchak, 2011). Because the ISC locator accounts for correlated travel-time prediction errors due to unmodelled velocity heterogeneities along similar ray paths, the area of the 90% confidence error ellipse does not decrease indefinitely with increasing number of stations, but levels off once the information carried by the network geometry is exhausted, thus providing more realistic uncertainty estimates.

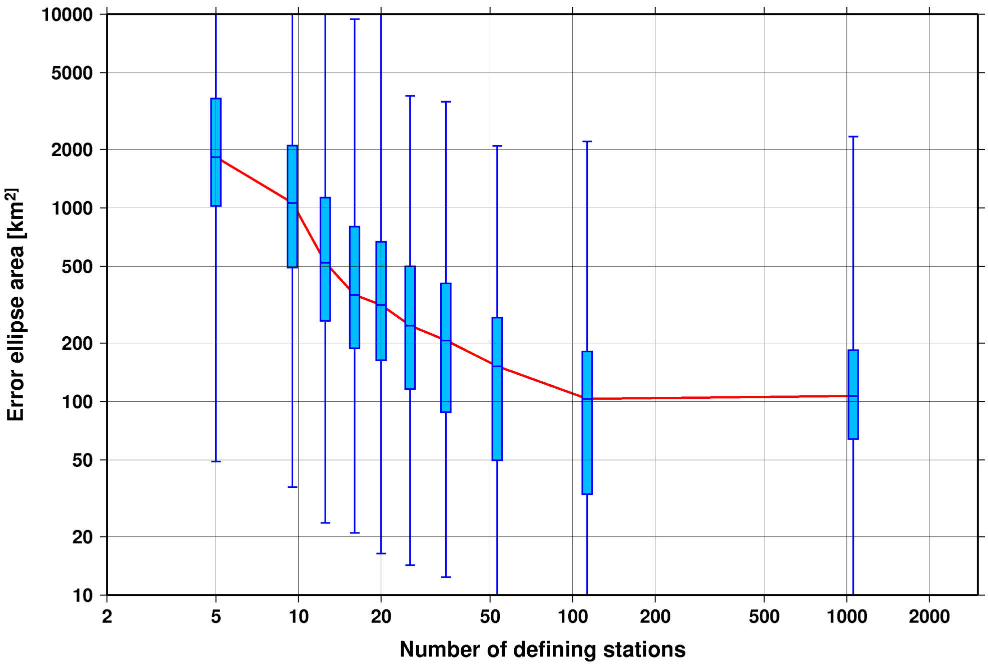

Figure 10.12: *Box-and-whisker plot of the area of the 90% confidence error ellipse of the ISC-located events as a function of the number of defining stations. Each box represents one-tenth-worth of the total number of data. The red line indicates the median 90% confidence error ellipse area.*

10.2 Seismic Phases and Travel-Time Residuals

The number of phases that are associated to events over the summary period in the ISC Bulletin is shown in Figure 10.13. Phase types and their total number in the ISC Bulletin is shown in the Appendix, Table 12.2. A summary of phase types is indicated in Figure 10.14.

In computing ISC locations, the current (for events since 2009) ISC location algorithm (*Bondár and Storchak*, 2011) uses all *ak135* phases where possible. Within the Bulletin, the phases that contribute to an ISC location are labelled as *time defining*. In this section, we summarise these time defining phases.

In Figure 10.15, the number of defining phases is shown in a histogram over the summary period. Each defining phase is listed in Table 10.1, which also provides a summary of the number of defining phases per event. A pie chart showing the proportion of defining phases is shown in Figure 10.16. Figure 10.17 shows travel times of seismic waves. The distribution of residuals for these defining phases is shown for the top five phases in Figures 10.18 through 10.22.

Table 10.1: *Numbers of 'time defining' phases (N) in the ISC Bulletin for 17337 ISC located events.*

Phase	Number of 'defining' phases	Number of events	Max per event	Median per event
P	968870	14291	3330	10
Pn	377559	15568	983	11
Sn	113944	12731	246	5
PKPdf	108345	6064	795	3
Pg	49682	4256	144	7
Pb	48598	6086	131	4
Sg	38008	4276	145	5
Sb	35180	5919	85	4
PKPbc	35125	5071	289	2
S	31624	3320	654	4
pP	25555	2669	365	4
PKPab	24850	4558	221	2

Table 10.1: *continued*

Phase	Number of 'defining' phases	Number of events	Max per event	Median per event
Pdif	15904	1524	519	1
PcP	15535	3433	147	2
PKiKP	15165	1499	553	2
PP	14667	2211	386	3
sP	7473	1569	58	4
SS	6982	1938	54	2
ScP	5445	1223	350	2
pPKPdf	3633	919	59	3
sS	3544	1016	19	3
PKKPbc	3278	580	108	2
SKSac	2780	692	54	2
SKSdf	2009	887	11	2
PnPn	1885	776	11	2
ScS	1828	819	99	1
PKSdf	1734	833	11	2
SKKSac	1722	902	22	1
PKKPab	1631	301	350	2
SnSn	1568	644	11	2
SKPbc	1242	301	56	2
PcS	1036	640	6	1
P'P'df	792	140	96	2
PKKPdf	751	256	32	2
SKiKP	721	312	66	1
PS	643	201	20	2
pPKPbc	516	251	31	1
SKPab	506	153	49	2
SP	317	92	32	2
pPKPab	312	164	20	1
Sdif	291	163	16	1
SKPdf	247	65	42	1
PnS	236	137	6	1
pPKiKP	100	56	7	1
SKKPbc	88	28	12	2
pPdif	60	23	12	1
sPKPdf	43	22	9	1
SPn	42	26	8	1
PKSab	42	12	20	1
P'P'bc	35	11	18	1
P'P'ab	30	10	13	1
SKKPab	25	14	6	1
pwP	23	19	2	1
PbPb	23	18	3	1
PKSbc	19	11	7	1
pS	17	8	6	1
SKKSdf	16	14	3	1
sPKPbc	14	11	3	1
SbSb	13	10	2	1
pPn	9	6	4	1
S'S'ac	8	3	6	1
sPKPab	7	6	2	1
sSdif	5	5	1	1
sPKiKP	4	4	1	1
SKKPdf	3	3	1	1
PKKSdf	2	1	2	2
sPn	2	1	2	2
PKKSbc	2	1	2	2
sSKSac	2	2	1	1
pSKSac	2	2	1	1
sSKSdf	1	1	1	1
PgPg	1	1	1	1

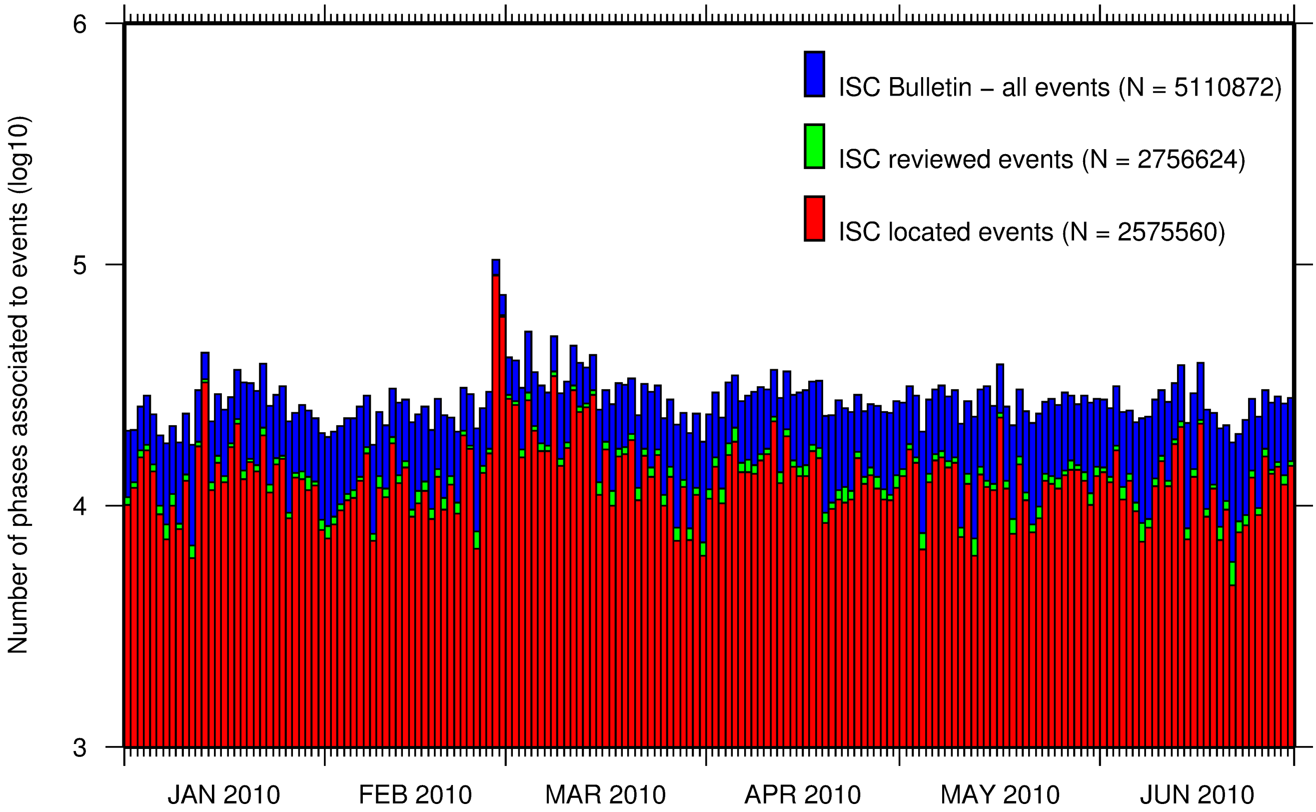

Figure 10.13: Histogram showing the number of phases (N) that the ISC has associated to events in the ISC Bulletin for the current summary period.

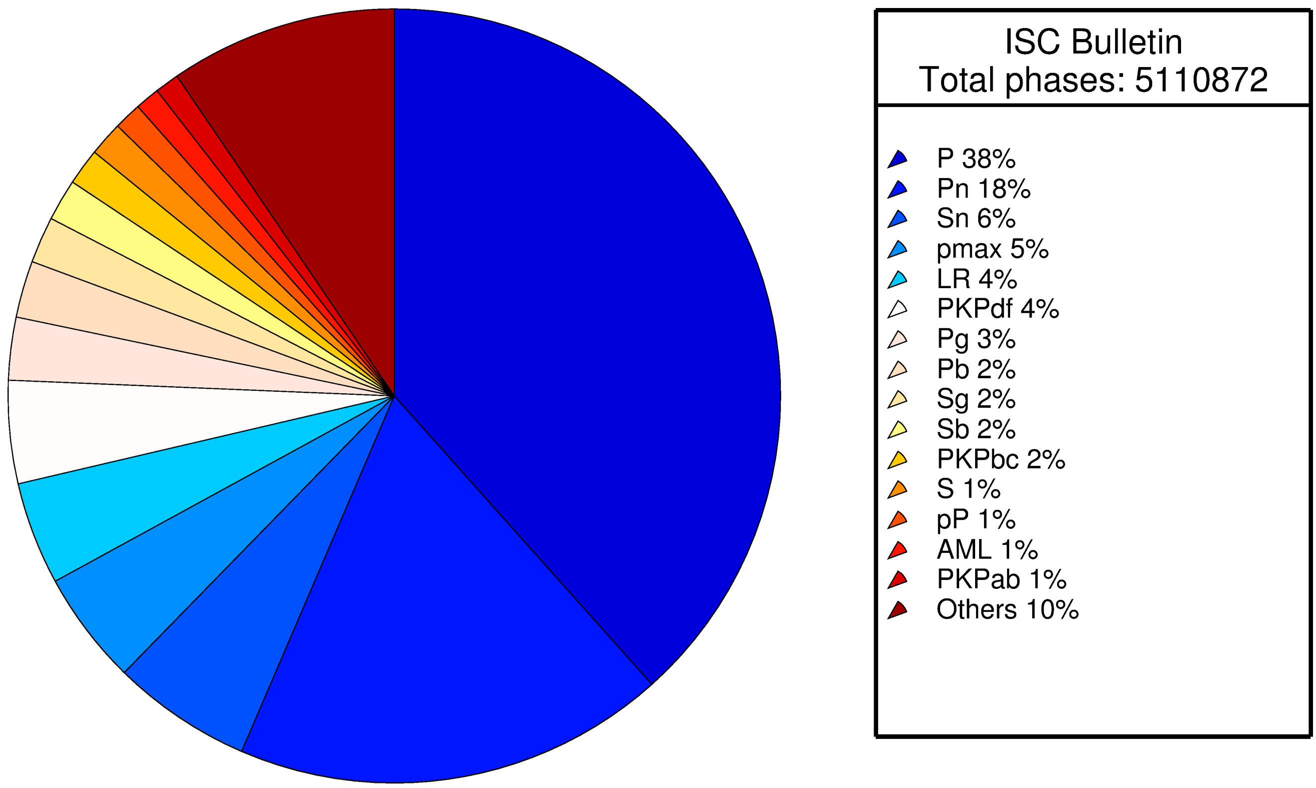

Figure 10.14: Pie chart showing the fraction of various phase types in the ISC Bulletin for this summary period.

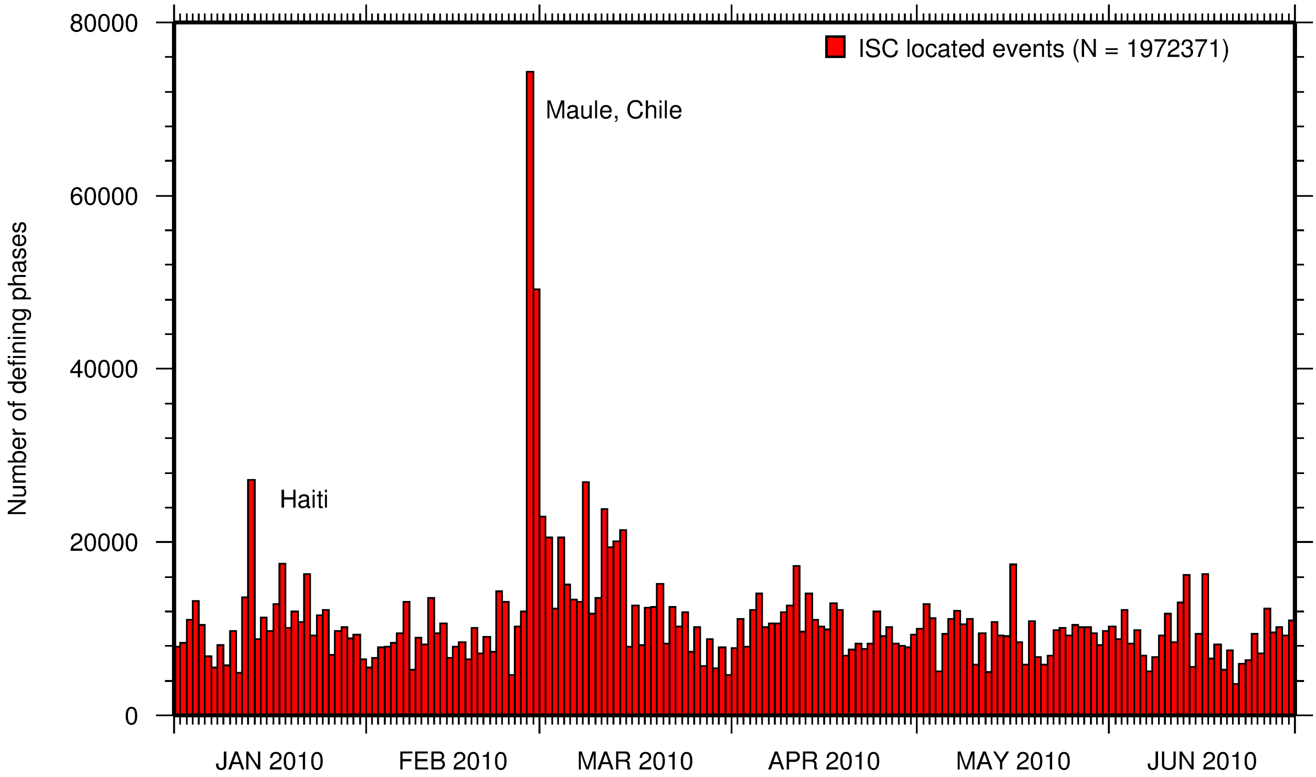

Figure 10.15: *Histogram showing the number of defining phases in the ISC Bulletin, for events located by the ISC.*

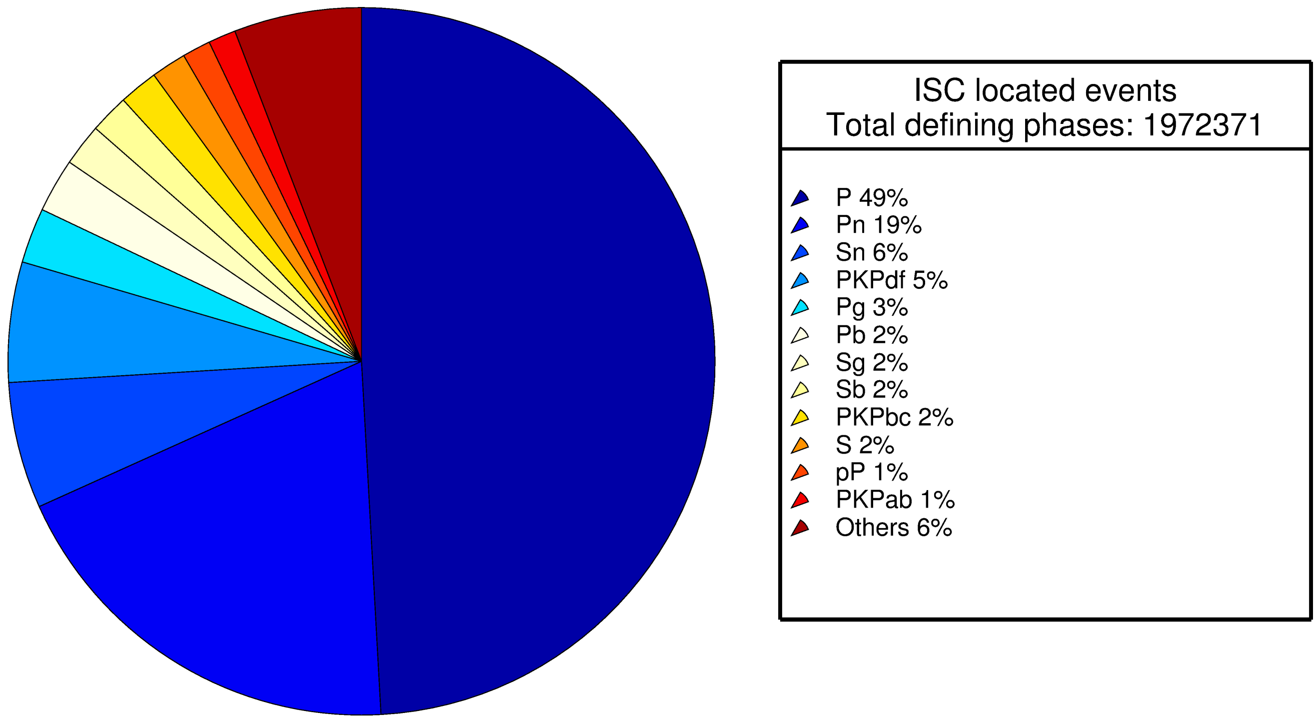

Figure 10.16: *Pie chart showing the defining phases in the ISC Bulletin, for events located by the ISC. A complete list of defining phases is shown in Table 10.1.*

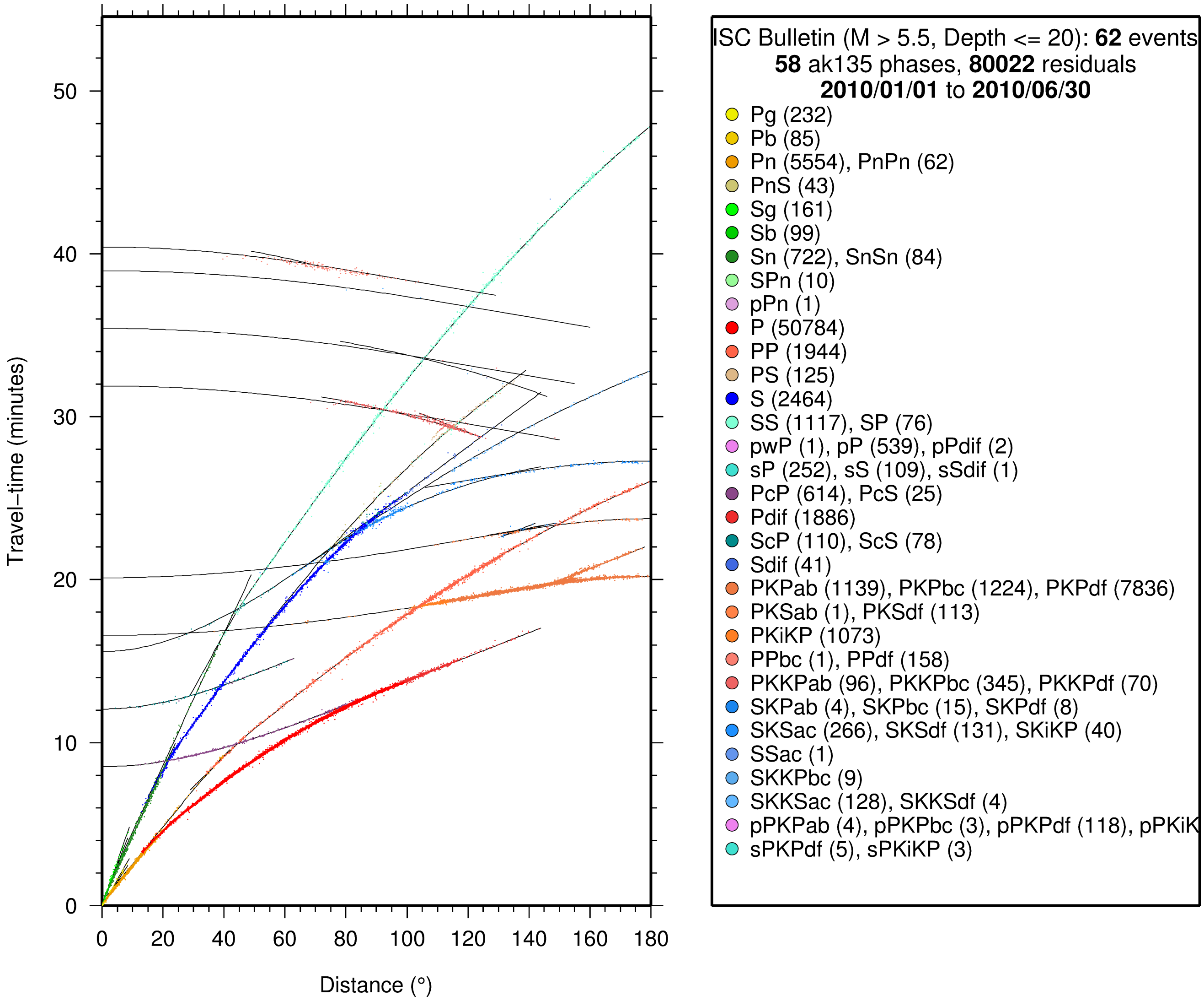

Figure 10.17: *Distribution of travel-time observations in the ISC Bulletin for events with M > 5.5 and depth less than 20 km. The travel-time observations are shown relative to a 0 km source and compared with the theoretical ak135 travel-time curves (solid lines). The legend lists the number of each phase plotted.*

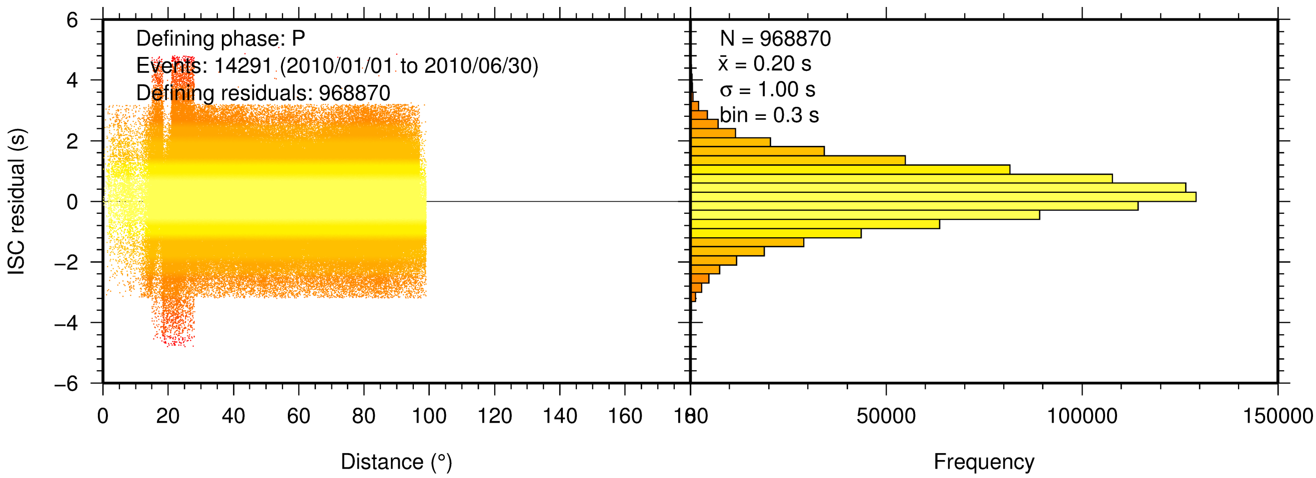

Figure 10.18: *Distribution of travel-time residuals for the defining P phases used in the computation of ISC located events in the Bulletin.*

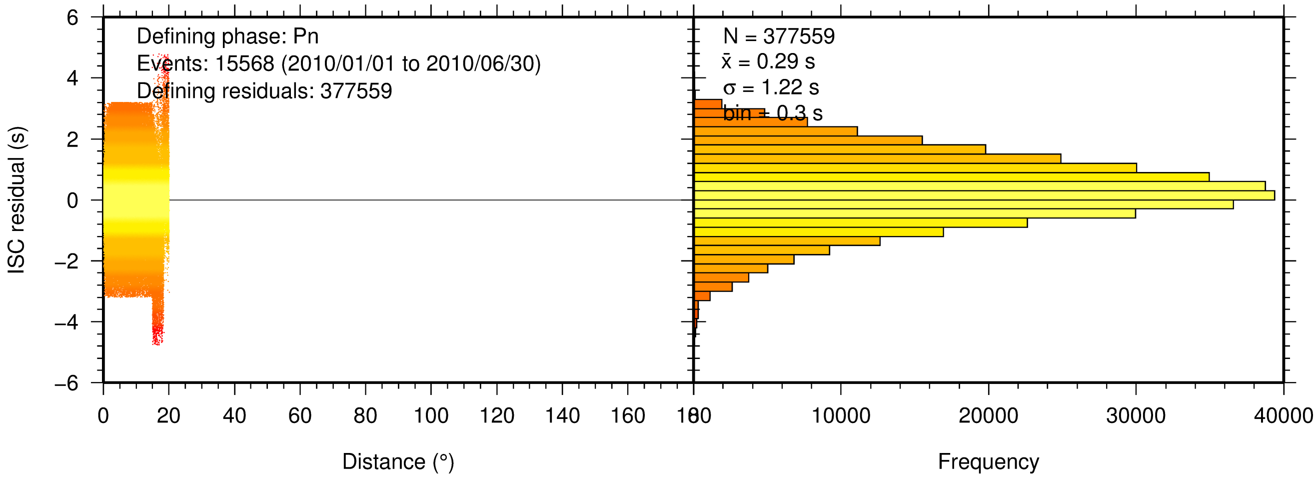

Figure 10.19: *Distribution of travel-time residuals for the defining Pn phases used in the computation of ISC located events in the Bulletin.*

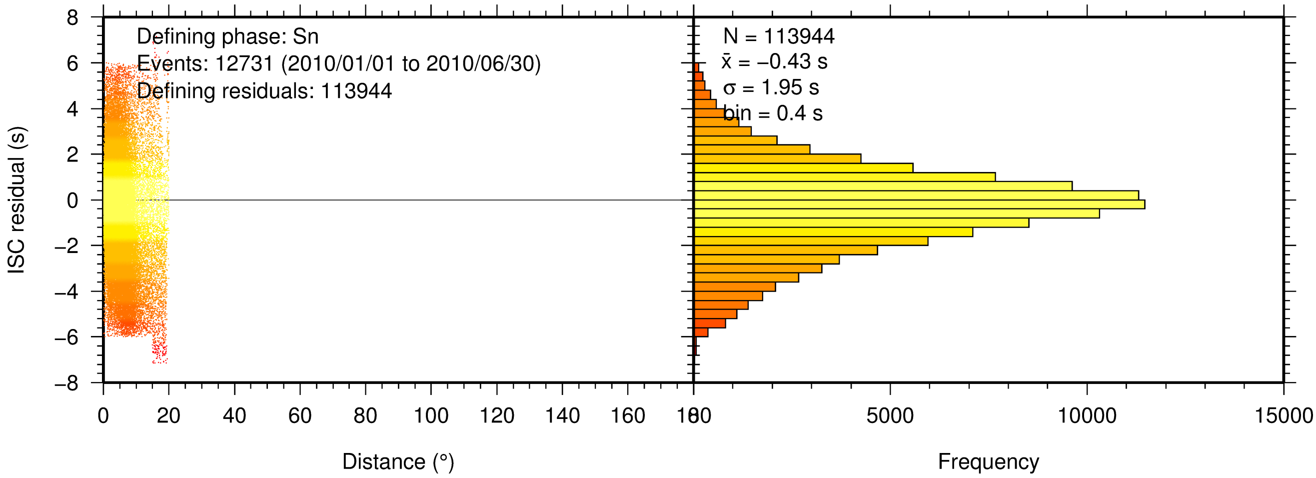

Figure 10.20: *Distribution of travel-time residuals for the defining Sn phases used in the computation of ISC located events in the Bulletin.*

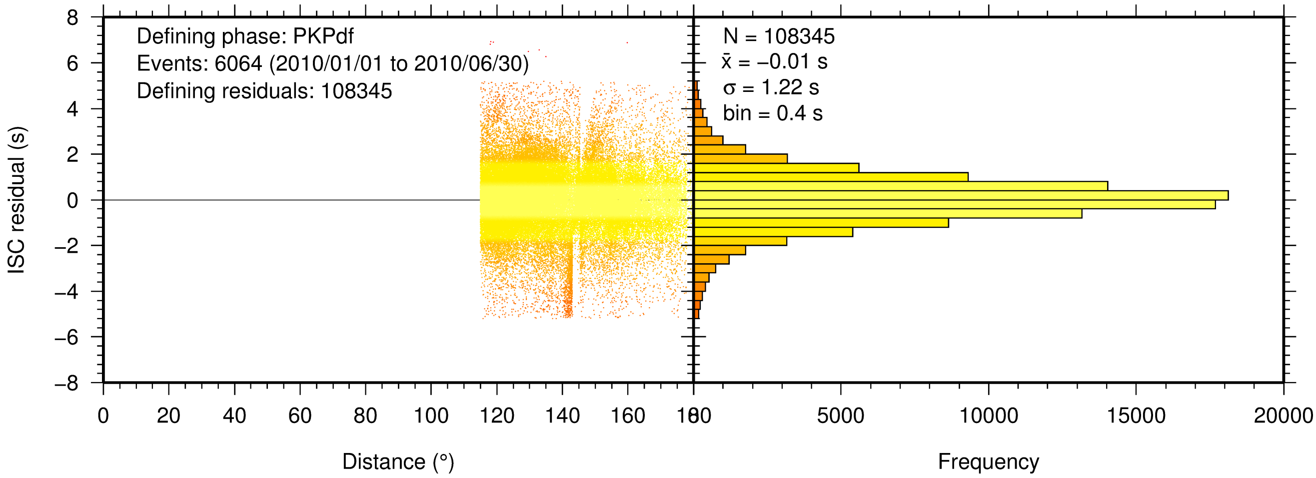

Figure 10.21: *Distribution of travel-time residuals for the defining PKPdf phases used in the computation of ISC located events in the Bulletin.*

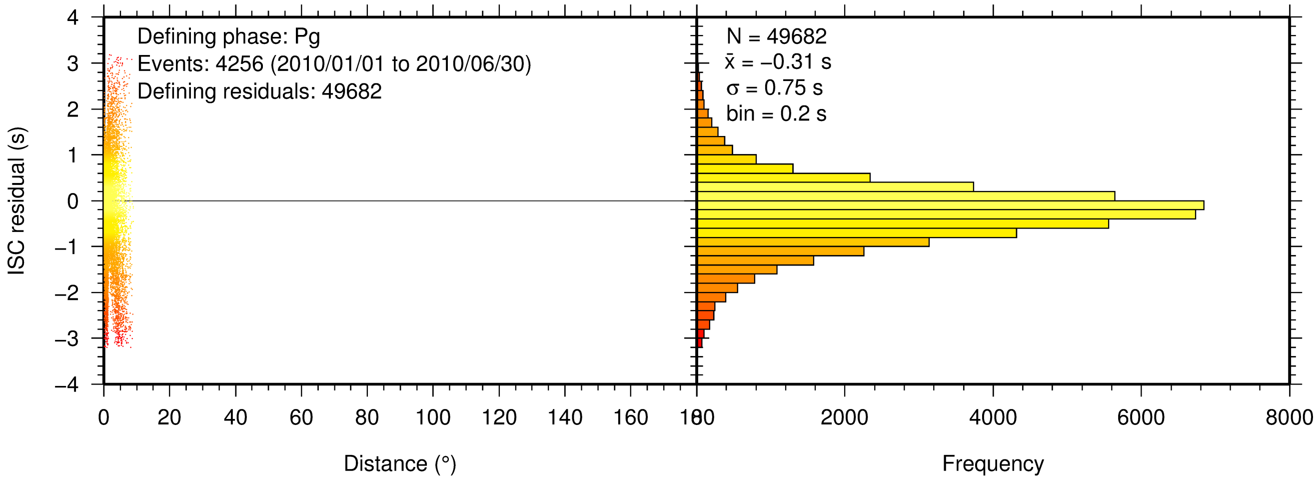

Figure 10.22: *Distribution of travel-time residuals for the defining Pg phases used in the computation of ISC located events in the Bulletin.*

10.3 Seismic Wave Amplitudes and Periods

The ISC Bulletin contains a variety of seismic wave amplitudes and periods measured by reporting agencies. For this Bulletin Summary, the total of collected amplitudes and periods is 1,482,924 (see Section 9.3). For the determination of the ISC magnitudes MS and mb, only a fraction of such data can be used. Indeed, the ISC network magnitudes are computed only for ISC located events. Here we recall the main features of the ISC procedure for MS and mb computation (see detailed description in Section 3.4). For each amplitude-period pair in a reading the ISC algorithm computes the magnitude (a reading can include several amplitude-period measurements) and the reading magnitude is assigned to the maximum A/T in the reading. If more than one reading magnitude is available for a station, the station magnitude is the median of the reading magnitudes. The network magnitude is computed then as the 20% alpha-trimmed median of the station magnitudes (at least three required). MS is computed for shallow earthquakes (depth $\leq$ 60 km) only and using amplitudes and periods on all three components (when available) if the period is within 10-60 s and the epicentral distance is between 20° and 160°. mb is computed also for deep earthquakes (depth down to 700 km) but only with amplitudes on the vertical component measured at periods $\leq$ 3 s in the distance range 21°-100°.

Table 10.2 is a summary of the amplitude and period data that contributed to the computation of station and ISC MS and mb network magnitudes for this Bulletin Summary.

Table 10.2: *Summary of the amplitude-period data used by the ISC locator to compute MS and mb.*

	MS	mb
Number of amplitude-period data	102720	422791
Number of readings	94221	421567
Percentage of readings in the ISC located events with qualifying data for magnitude computation	10.1	41.8
Number of station magnitudes	86235	339810
Number of network magnitudes	3181	12854

A small percentage of the readings with qualifying data for MS and mb calculation have more than one amplitude-period pair. Notably, only 10.1% of the readings for the ISC located (shallow) events included qualifying data for MS computation, whereas for mb the percentage is much higher. This is due to the seismological practice of reporting agencies. Agencies contributing systematic reports of amplitude and period data are listed in Appendix Table 12.3. Obviously the ISC Bulletin would benefit if more agencies included surface wave amplitude-period data in their reports.

Figure 10.23 shows the distribution of the number of station magnitudes versus distance. For mb there is a significant increase in the distance range 70°-90°, whereas for MS most of the contributing stations are below 100°. The increase in the number of station magnitude between 70°-90° for mb is partly due to the very dense distribution of seismic stations in North America and Europe with respect to earthquake occurring in various subduction zones around the Pacific Ocean.

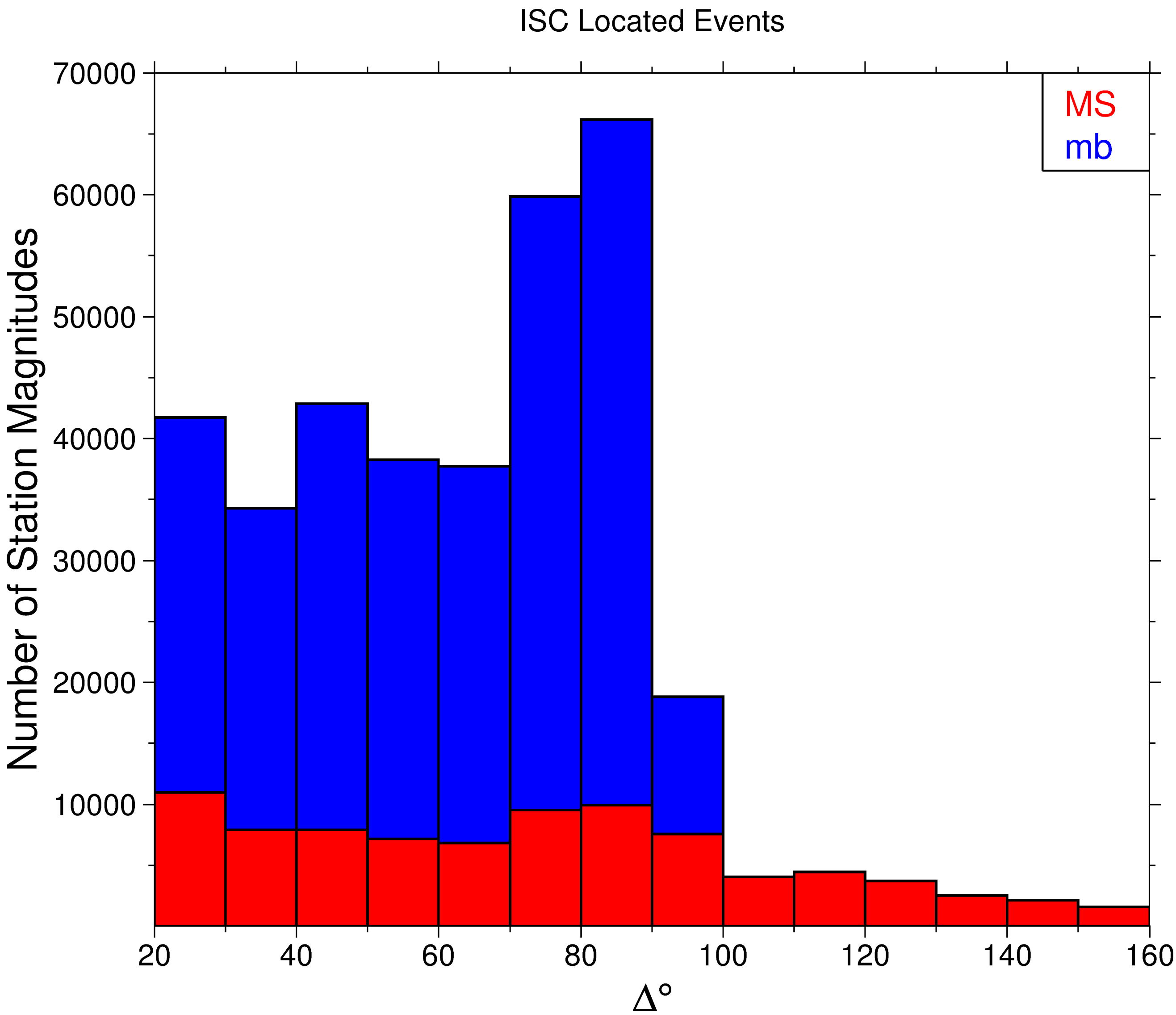

Figure 10.23: *Distribution of the number of station magnitudes computed by the ISC locator for mb (blue) and MS (red) versus distance.*

Finally, Figure 10.24 shows the distribution of network MS and mb as well as the median number of stations for magnitude bins of 0.2. Clearly with increasing magnitude the number of events is smaller but with a general tendency of having more stations contributing to the network magnitude.

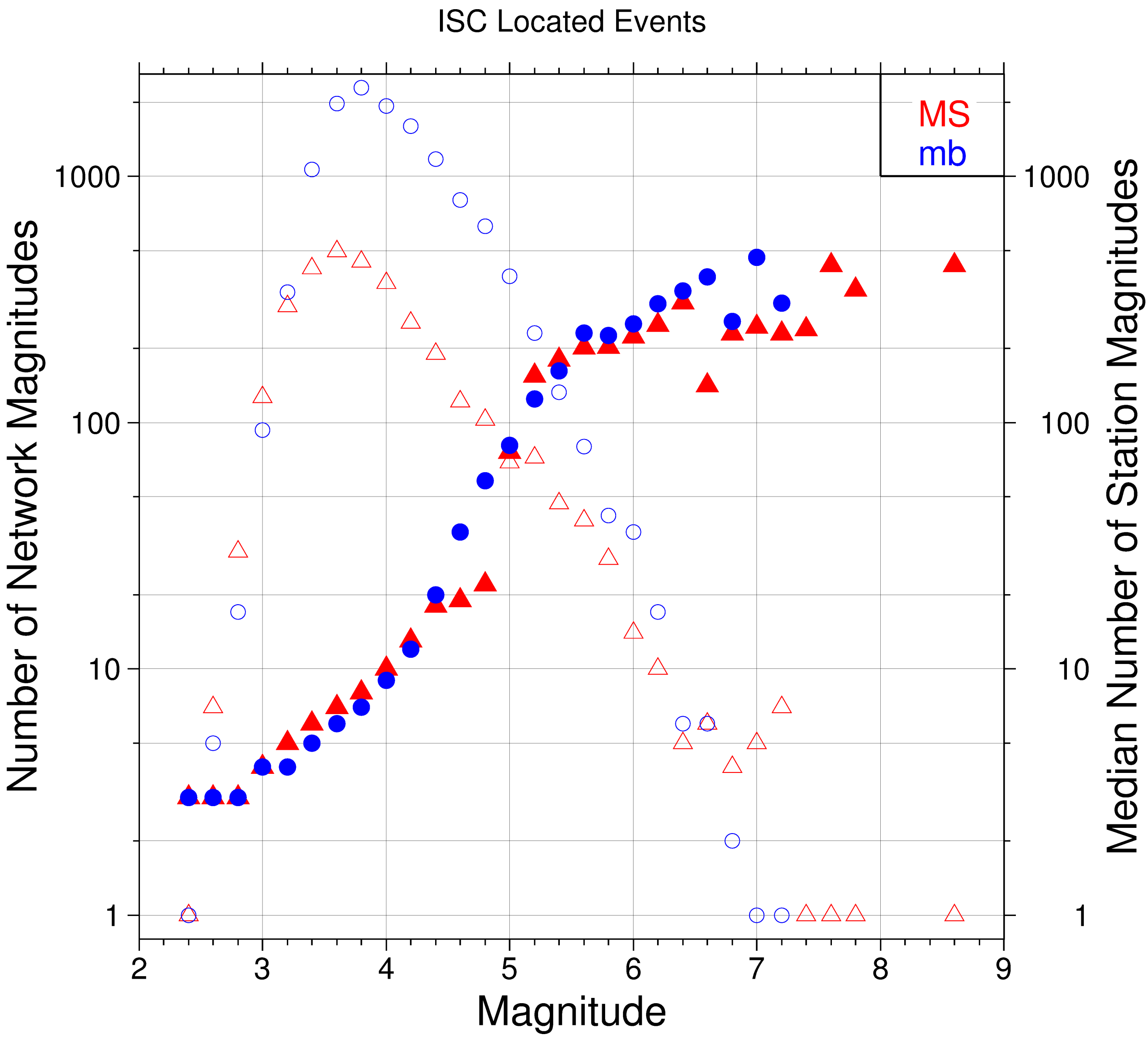

Figure 10.24: *Number of network magnitudes (open symbols) and median number of stations magnitudes (filled symbols). Blue circles refer to mb and red triangles to MS. The width of the magnitude interval δM is 0.2, and each symbol includes data with magnitude in $M \pm \delta M/2$.*

10.4 Completeness of the ISC Bulletin

The completeness of the ISC Bulletin can be expressed as a magnitude value, above which we expect the Bulletin to contain 100% of events. This magnitude of completeness, M_C, can be measured as the point where the seismicity no longer follows the Gutenberg-Richter relationship. We compute an estimate of M_C using the maximum curvature technique of *Woessner and Wiemer* (2005).

The completeness of the ISC Bulletin for this summary period is shown in Figure 10.25. A history of completeness for the ISC Bulletin is shown in Figure 10.26. The step change in 1996 corresponds with the inclusion of the Prototype IDC (EIDC) Bulletin, followed by the Reviewed Event Bulletin (REB) of the IDC.

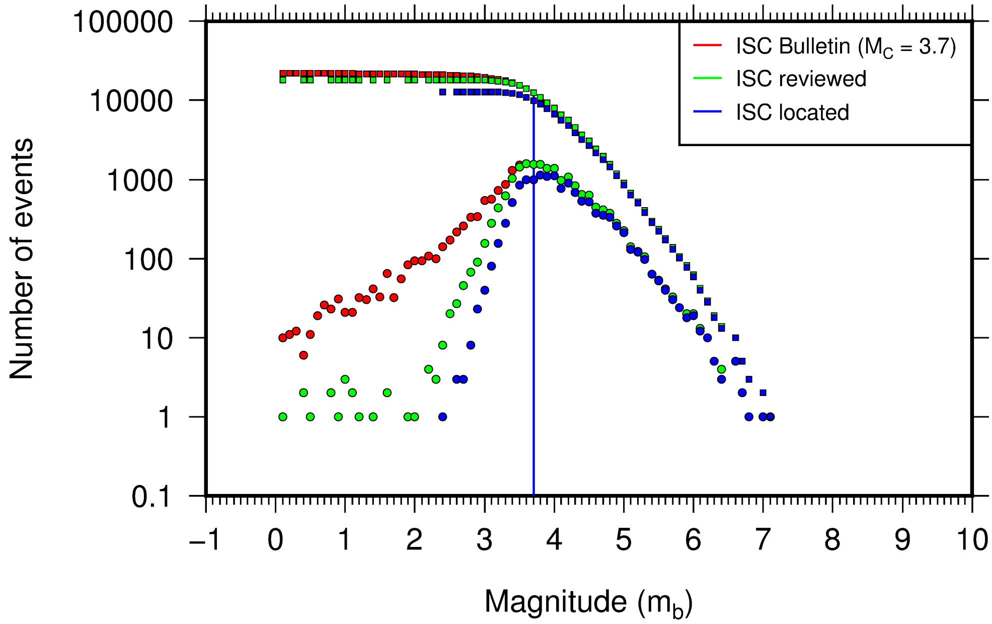

Figure 10.25: *Frequency and cumulative frequency magnitude distribution for all events in the ISC Bulletin, ISC reviewed events and events located by the ISC. The magnitude of completeness (M_C) is shown for the ISC Bulletin. Note: only events with values of m_b are represented in the figure.*

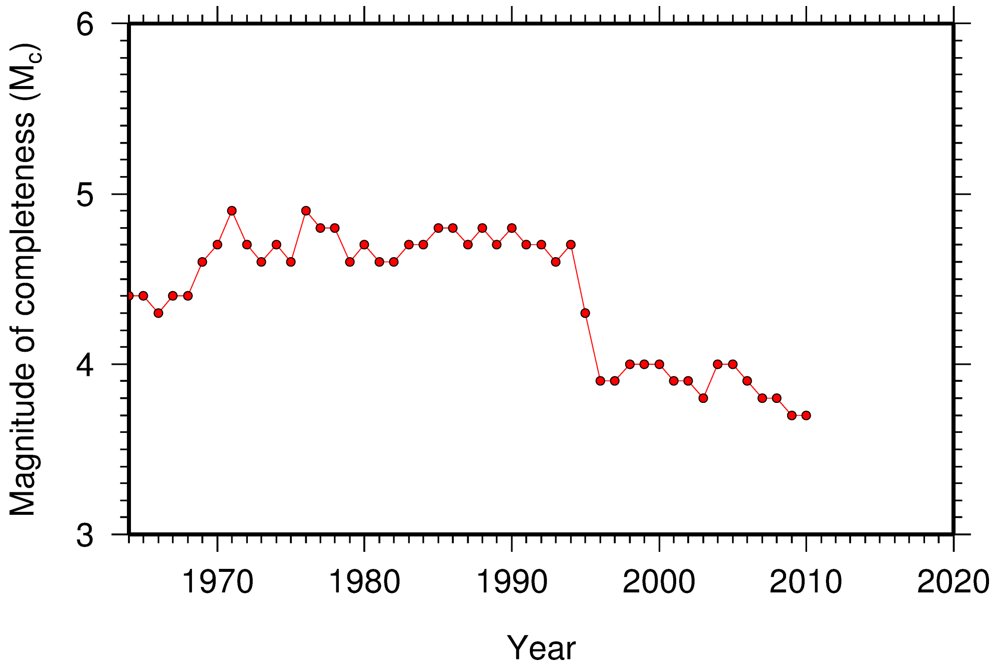

Figure 10.26: *Variation of magnitude of completeness (M_C) for each year in the ISC Bulletin. Note: M_C is calculated only using those events with values of m_b.*

10.5 Magnitude Comparisons

The ISC Bulletin publishes network magnitudes reported by multiple agencies to the ISC. For events that have been located by the ISC, where enough amplitude data has been collected, the MS and mb magnitudes are calculated by the ISC (MS is computed only for depths ≤ 60 km). In this section, ISC magnitudes and some other reported magnitudes in the ISC Bulletin are compared.

The comparison between MS and mb computed by the ISC locator for events in this summary period is shown in Figure 10.27, where the large number of data pairs allows a colour coding of the data density. The scatter in the data reflects the fundamental differences between these magnitude scales.

Similar plots are shown in Figure 10.28 and 10.29, respectively, for comparisons of ISC mb and ISC MS with Mw from the GCMT catalogue. Since Mw is not often available below magnitude 5, these distributions are mostly for larger, global events. Not surprisingly, the scatter between mb and Mw is larger than the scatter between MS and Mw. Also, the saturation effect of mb is clearly visible for earthquakes with Mw > 6.5. In contrast, MS scales well with Mw > 6, whereas for smaller magnitudes MS appears to be systematically smaller than Mw.

In Figure 10.30 ISC values of mb are compared with all reported values of mb, values of mb reported by NEIC and values of mb reported by IDC. Similarly in Figure 10.31, ISC values of MS are compared with all reported values of MS, values of MS reported by NEIC and values of MS reported by IDC. There is a large scatter between the ISC magnitudes and the mb and MS reported by all other agencies.

The scatter decreases both for mb and MS when ISC magnitudes are compared just with NEIC and IDC magnitudes. This is not surprising as the latter two agencies provide most of the amplitudes and periods used by the ISC locator to compute MS and mb. However, ISC mb appears to be smaller than NEIC mb for mb < 4 and larger than IDC mb for mb > 4. Since NEIC does not include IDC amplitudes, it seems these features originate from observations at the high-gain, low-noise sites reported by the IDC. For the MS comparisons between ISC and NEIC a similar but smaller effect is observed for MS < 4.5, whereas a good scaling is generally observed for the MS comparisons between ISC and IDC.

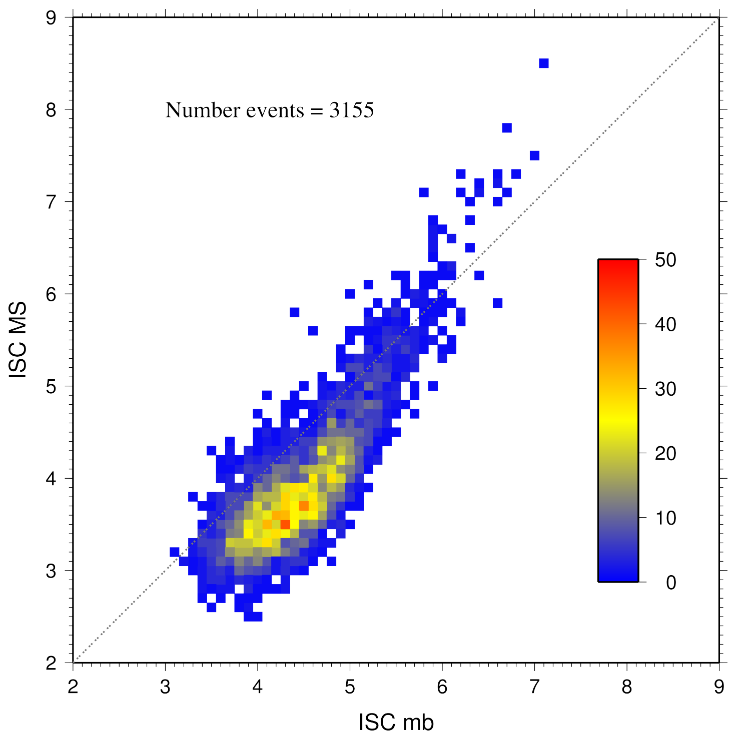

Figure 10.27: *Comparison of ISC values of MS with mb for common event pairs.*

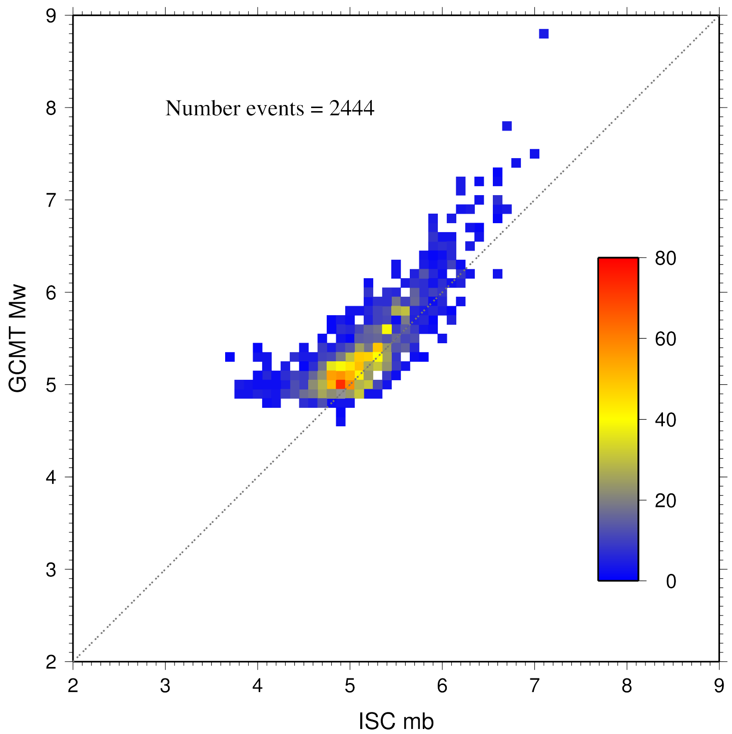

Figure 10.28: *Comparison of ISC values of mb with GCMT Mw for common event pairs.*

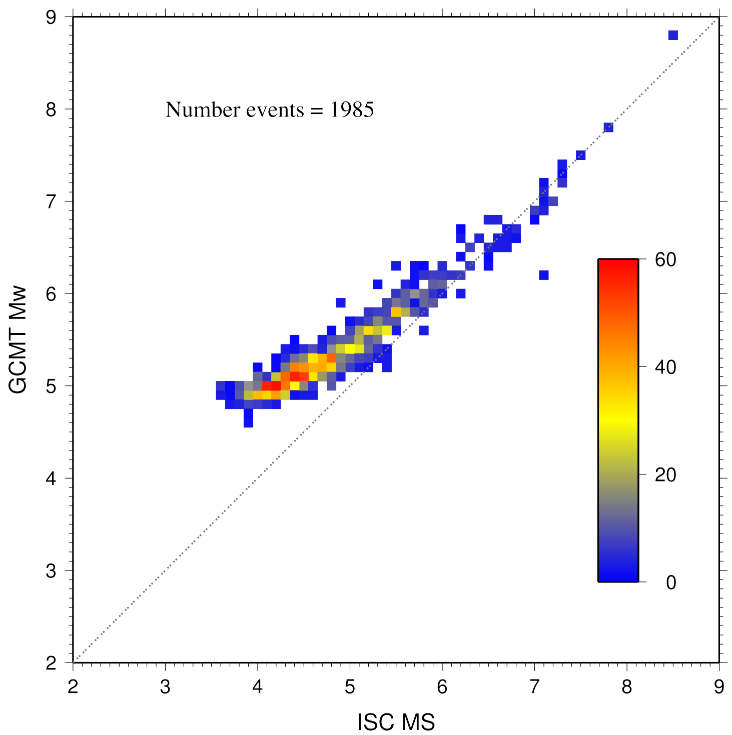

Figure 10.29: *Comparison of ISC values of MS with GCMT Mw for common event pairs.*

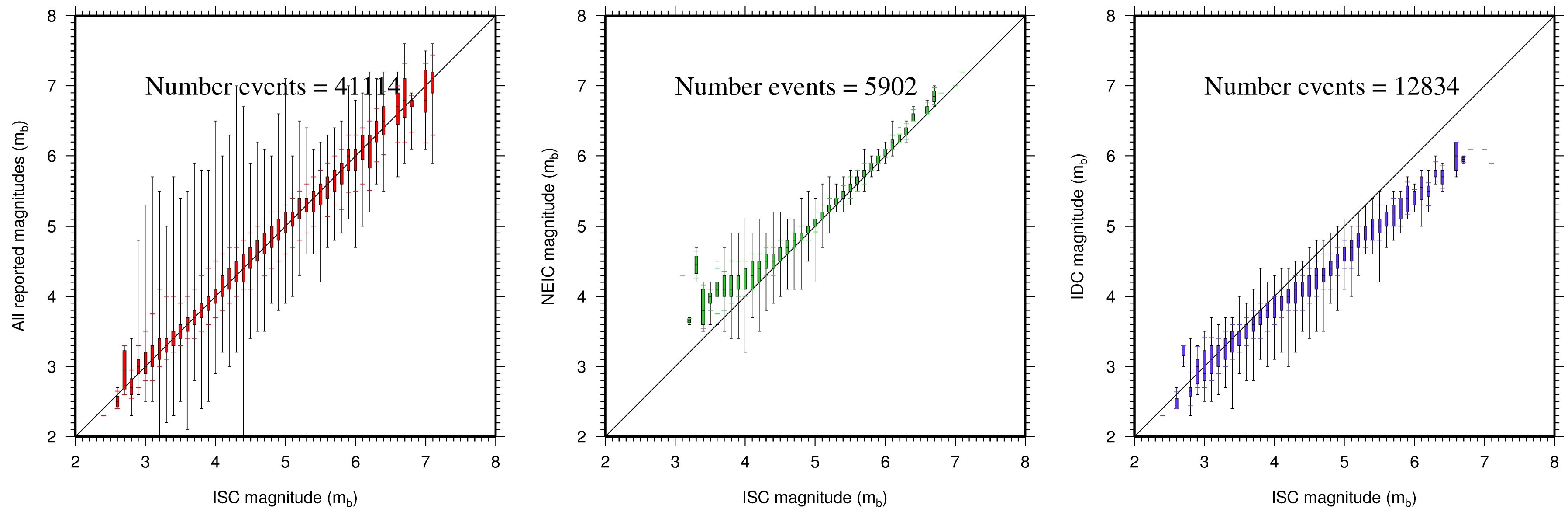

(a) (b) (c)

Figure 10.30: *Comparison of ISC magnitude data (mb) with other agency magnitudes (mb). The statistical summary is shown in box-and-whisker plots where the 10th and 90th percentiles are shown in addition to the max and min values. (a): All magnitudes reported; (b): NEIC magnitudes; (c): IDC magnitudes.*

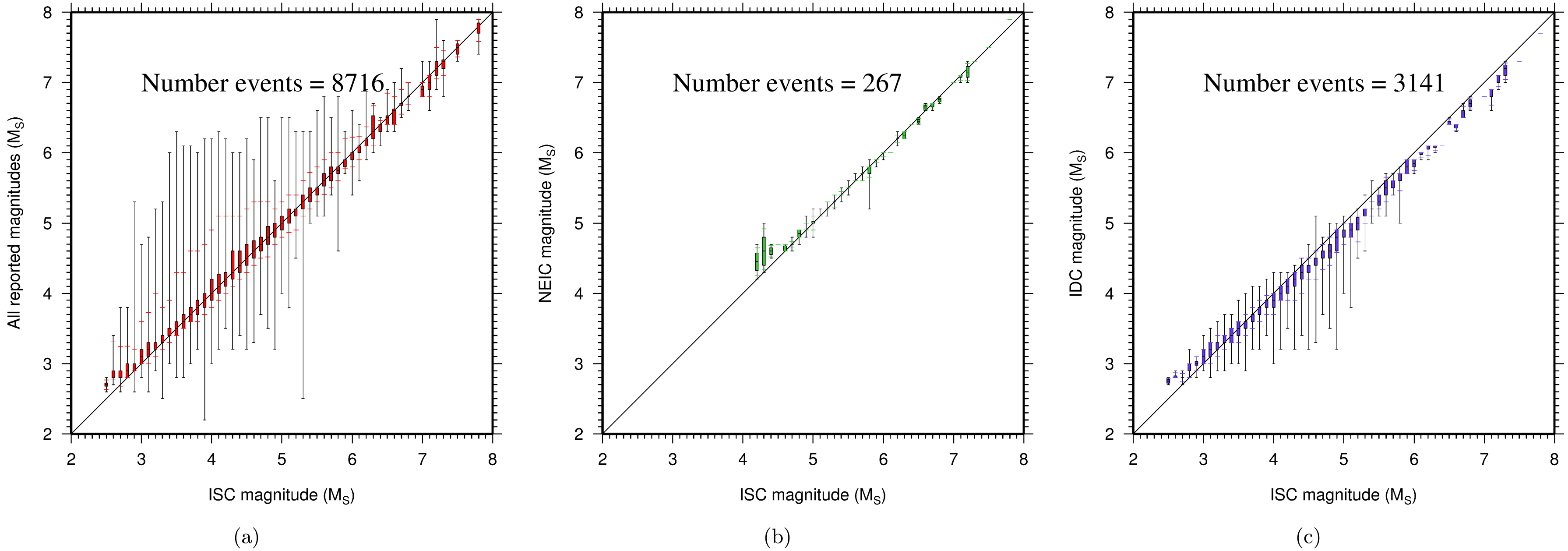

Figure 10.31: *Comparison of ISC magnitude data (MS) with other agency magnitudes (MS). The statistical summary is shown in the box-and-whisker plots where the 10th and 90th percentiles are shown in addition to the max and min values. (a): All magnitudes reported; (b): NEIC magnitudes; (c): IDC magnitudes.*

11

The Leading Data Contributors

As many as 126 agencies reported bulletin data related to the current six month period. Although we are grateful for every report, we nevertheless would like to acknowledge those agencies that made the most useful or distinct contributions to the contents of the ISC Bulletin. Here we note those agencies that:

- provided a comparatively large volume of parametric data (see 11.1),
- reported data that helped quite considerably to improve the quality of the ISC locations or magnitude determinations (see 11.2),
- helped the ISC by consistently reporting data in one of the standard recognised formats and in-line with the ISC data collection schedule (see 11.3).

We do not aim to discourage those numerous small networks who provide comparatively smaller yet still most essential volumes of regional data regularly, consistently and accurately. Without these reports the ISC Bulletin would not be as comprehensive and complete as it is today.

11.1 The Largest Data Contributors

We commend the contribution of those agencies that submitted information for a large portion of seismic events. We acknowledge the contribution of NEIC, IDC, MOS, BJI, USArray and a few others (Figure 11.1) that reported the majority of moderate to large events recorded at teleseismic distances. The contributions of JMA, NEIC, IDC, CSEM, and a number of others are also acknowledged with respect to small seismic events. Note that the NEIC bulletin accumulates a contribution of all regional networks in the USA. Similarly, the CSEM communicates contributions of many tens of European and Mediterranean networks that the ISC does not always receive directly. Several agencies monitoring highly seismic regions routinely report large volumes of small to moderate magnitude events, such as those in Japan, Chinese Taipei, Turkey, Chile, Italy, Indonesia, Greece, New Zealand and southern Kazakhstan. Contributions of small magnitude events by agencies in regions of low seismicity, such as Finland, Czech Republic and central and northern Kazakhstan are also gratefully received.

We also would like to acknowledge contributions of those agencies that report a large portion of arrival time and amplitude data (Figure 11.2). For small magnitude events, these are local agencies in charge of monitoring local and regional seismicity. For moderate to large events, contributions of IDC, USArray, NEIC, MOS are especially acknowledged. Notably, three agencies (IDC, NEIC and MOS) reported together as much as 70-75% of all amplitude measurements made for teleseismically recorded events; 82-88% of all amplitudes were reported by seven agencies (those above plus BJI, DJA, DMN and LDG).

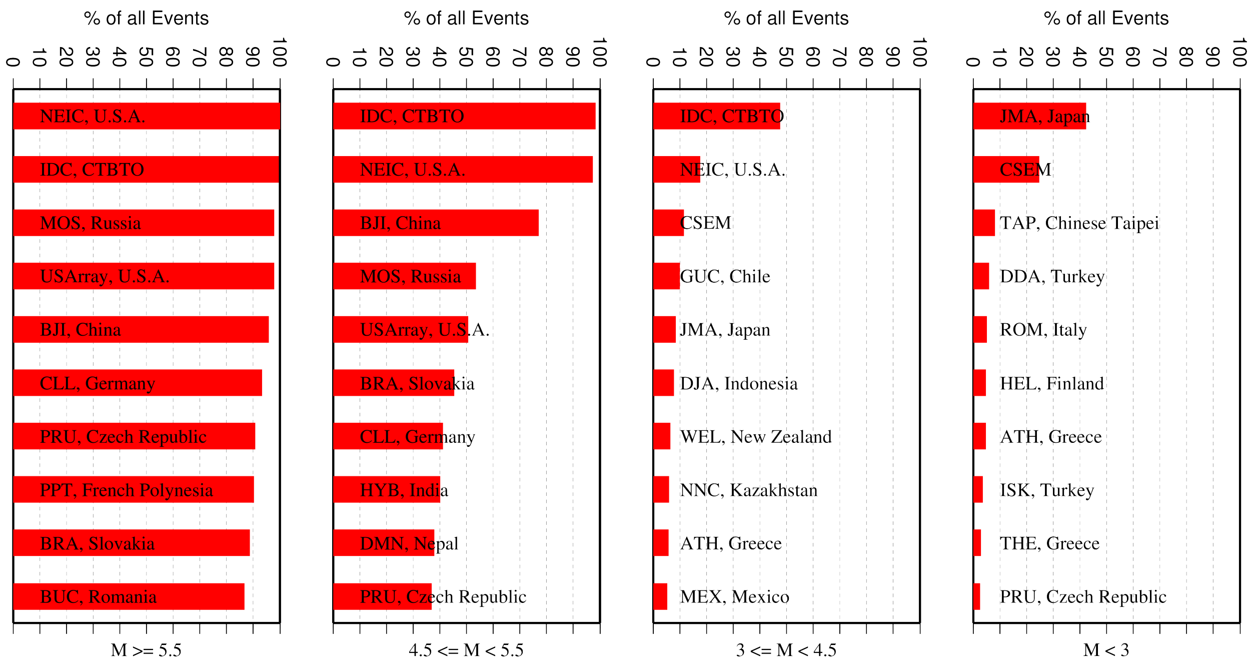

Figure 11.1: *Frequency of events in the ISC Bulletin for which an agency reported at least one item of data: a moment tensor, a hypocentre, a station arrival time or an amplitude. The top ten agencies are shown for four magnitude intervals.*

We hope that other agencies would also be able to update their monitoring routines in the future to include the amplitude reports for teleseismic events compliant with the IASPEI standards.

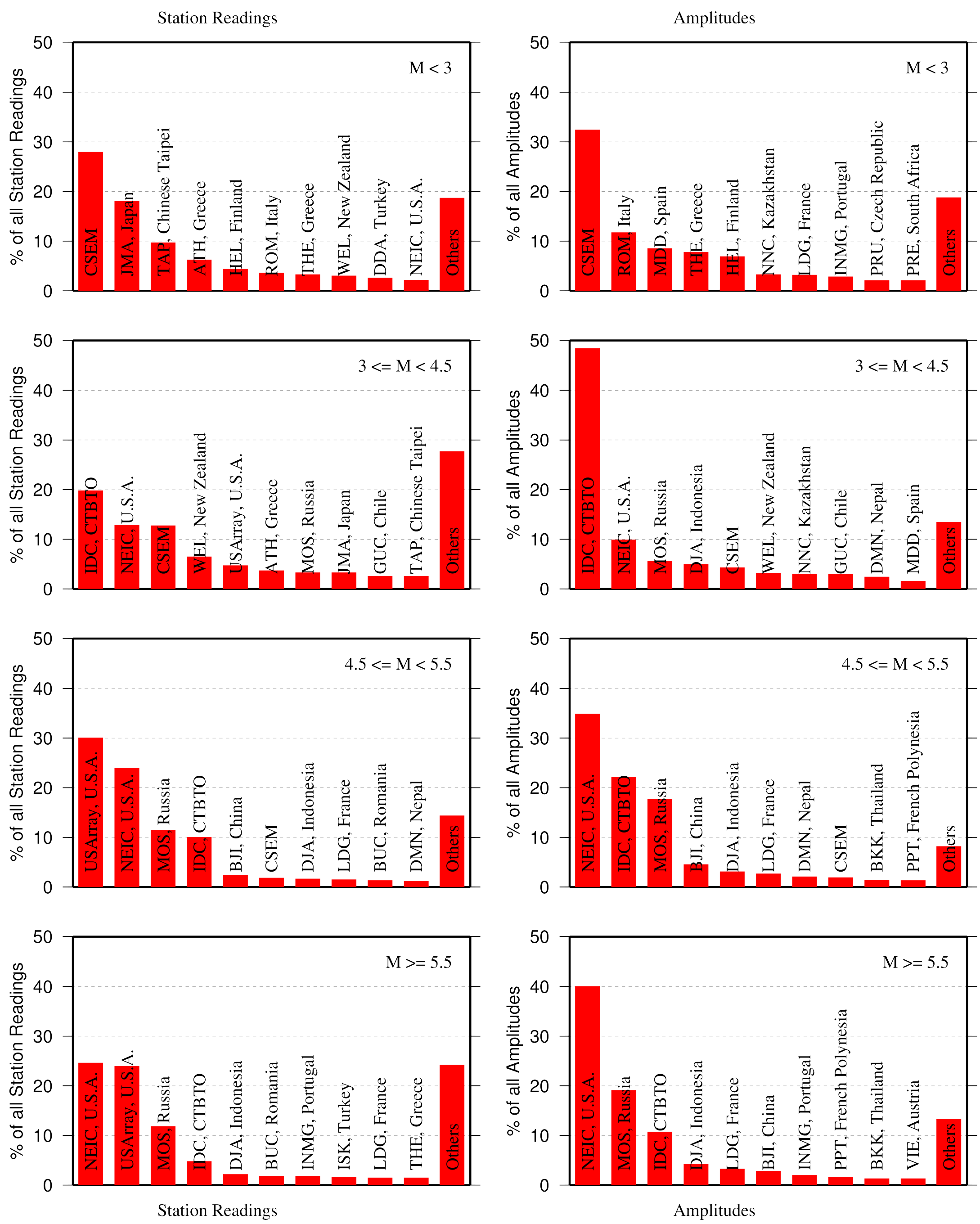

Figure 11.2: *Contributions of station arrival time readings (left) and amplitudes (right) of agencies to the ISC Bulletin. Top ten agencies are shown for four magnitude intervals.*

11.2 Contributors Reporting the Most Valuable Parameters

One of the main ISC duties is to re-calculate hypocentre estimates for those seismic events where a collective wealth of all station reports received from all agencies is likely to improve either the event location or depth compared to the hypocentre solution from each single agency. For areas with a sparse local seismic network or an unfavourable station configuration, readings made by other networks at teleseismic distances are very important. All events near mid-oceanic ridges as well as those in the majority of subduction zones around the world fall into this category. Hence we greatly appreciate the effort made by many agencies that report data for remote earthquakes (Figure 11.3). For some agencies, such as the IDC and the NEIC, it is part of their mission. For instance, the IDC reports almost every seismic event that is large enough to be recorded at teleseismic distance (20 degrees and beyond). This is largely because the International Monitoring System of primary arrays and broadband instruments is distributed at quiet sites around the world in order to be able to detect possible violations of the Comprehensive Test Ban Treaty. The NEIC reported over 30% of those events as their mission requires them to report events above magnitude 4.5 outside the United States of America. For other agencies reporting distant events it is an extra effort that they undertake to notify their governments and relief agencies as well as to help the ISC and academic research in general. Hence these agencies usually report on the larger magnitude events. Notably, the US Array Network Facility reports manually picked individual station arrivals for 8% of all events worldwide that are recorded at teleseismic distances. BJI, MOS, NAO, DMN, CLL, BRA and PPT each reported on several percent of all relevant events. We encourage other agencies to report distant events to us.

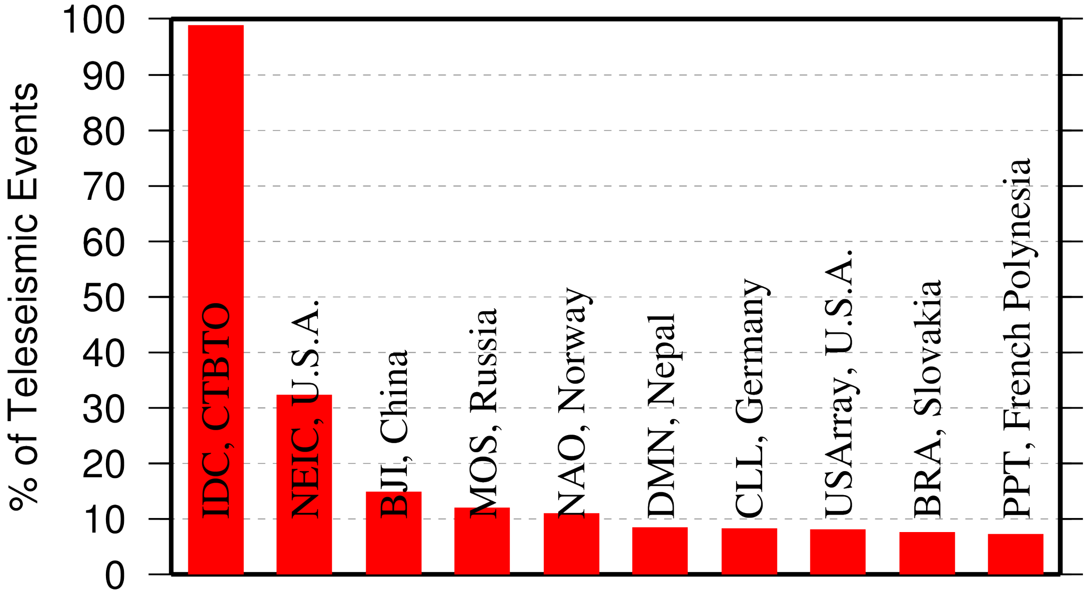

Figure 11.3: *Top ten agencies that reported teleseismic phase arrivals for a large portion of ISC events.*

In addition to the first arriving phase we encourage reporters to contribute observations of secondary seismic phases that help constrain the event location and depth: S, Sn, Sg and pP, sP, PcP (Figure 11.4). We expect though that these observations are actually made from waveforms, rather than just predicted by standard velocity models and modern software programs. It is especially important that these arrivals are manually reviewed by an operator (as we know takes place at the IDC and NEIC), as opposed to some lesser attempts to provide automatic phase readings that are later rejected by the ISC due to a generally poor quality of unreviewed picking.

Another important long-term task that the ISC performs is to compute the most definitive values of MS and mb network magnitudes that are considered reliable due to removal of outliers and consequent averaging (using alpha-trimmed median) across the largest network of stations, generally not feasible for a single agency. Despite concern over the bias at the lower end of mb introduced by the body wave amplitude data from the IDC, other agencies are also known to bias the results. This topic is further discussed in Section 10.5.

Notably, the IDC reports almost 100% of all events for which MS and mb are estimated. This is due

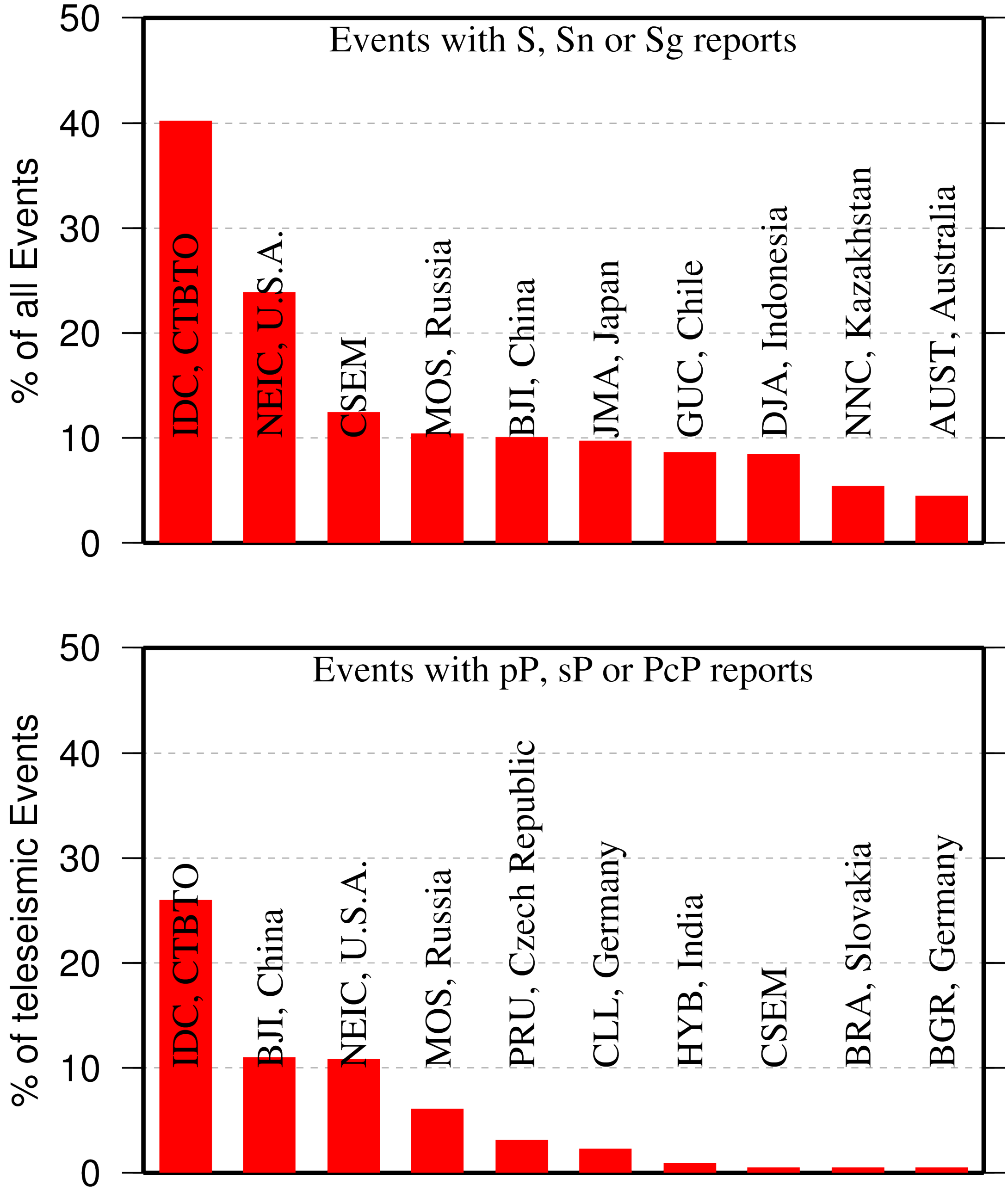

Figure 11.4: *Top ten agencies that report secondary phases important for an accurate epicentre location (top) and focal depth determination (bottom).*

to the standard routine that requires determination of body and surface wave magnitudes useful for discrimination purposes. NEIC, MOS, BJI, NAO, PRU and a few other agencies (Figure 11.5) are also responsible for the majority of the amplitude and period reports that contribute towards the ISC magnitudes.

Since the ISC does not routinely process waveforms, we rely on other agencies to report moment magnitudes as well as moment tensor determinations (Figure 11.6).

Among other event parameters the ISC Bulletin also contains information on event type. We cannot independently verify the type of each event in the Bulletin and thus rely on other agencies to report the event type to us. Practices of reporting non-tectonic events vary greatly from country to country.

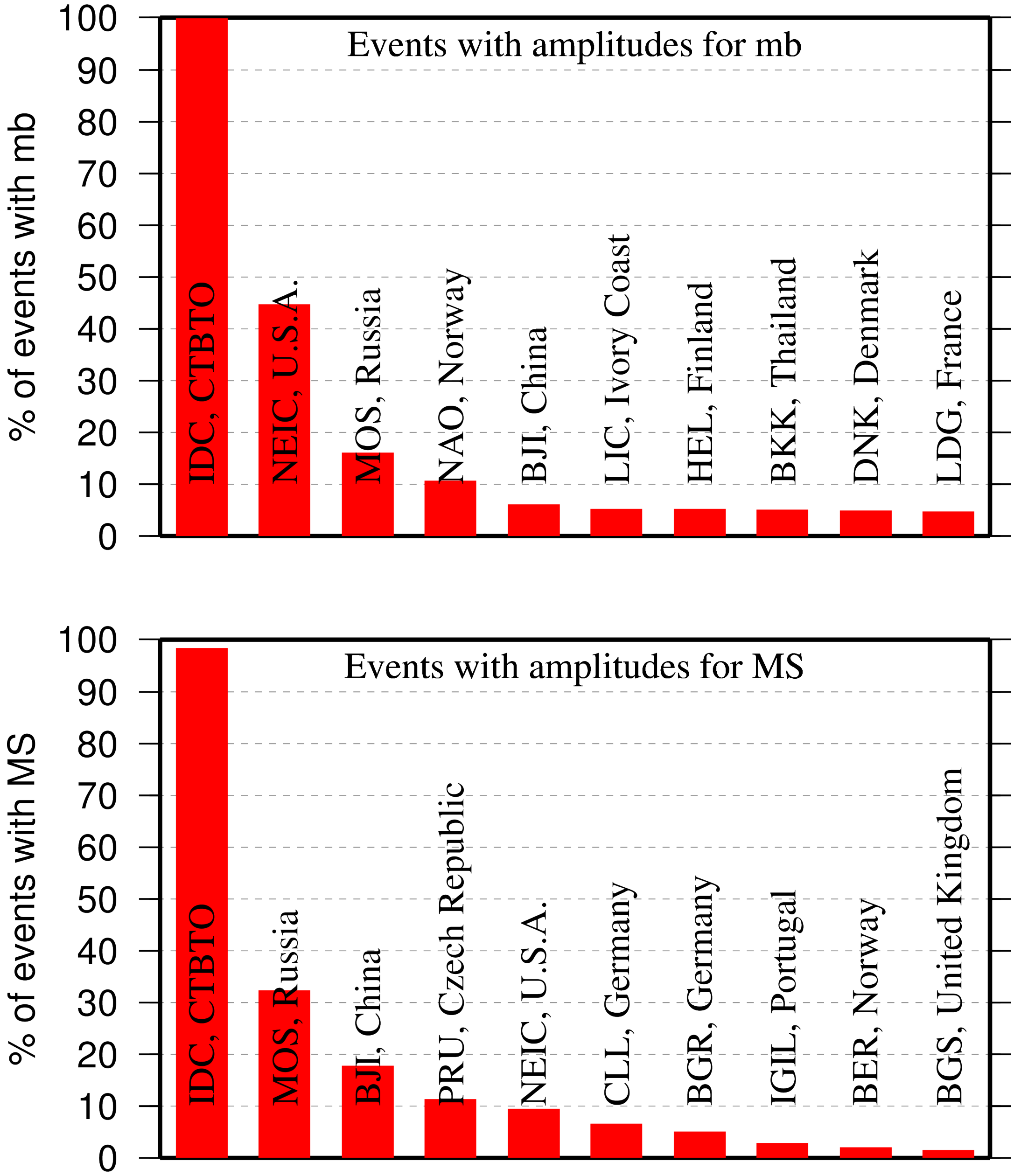

Figure 11.5: *Agencies that report defining body (top) and surface (bottom) wave amplitudes and periods for the largest fraction of those ISC Bulletin events with MS/mb determinations.*

Many agencies do not include anthropogenic events in their reports. Suppression of such events from reports to the ISC may lead to a situation where a neighbouring agency reports the anthropogenic event as an earthquake for which expected data are missing. This in turn is detrimental to ISC Bulletin users studying natural seismic hazard. Hence we encourage all agencies to join the agencies listed on Figure 11.7 and several others in reporting both natural and anthropogenic events to the ISC.

The ISC Bulletin also contains felt and damaging information when local agencies have reported it to us. Agencies listed on Figure 11.8 provide such information for the majority of all felt or damaging events in the ISC Bulletin.

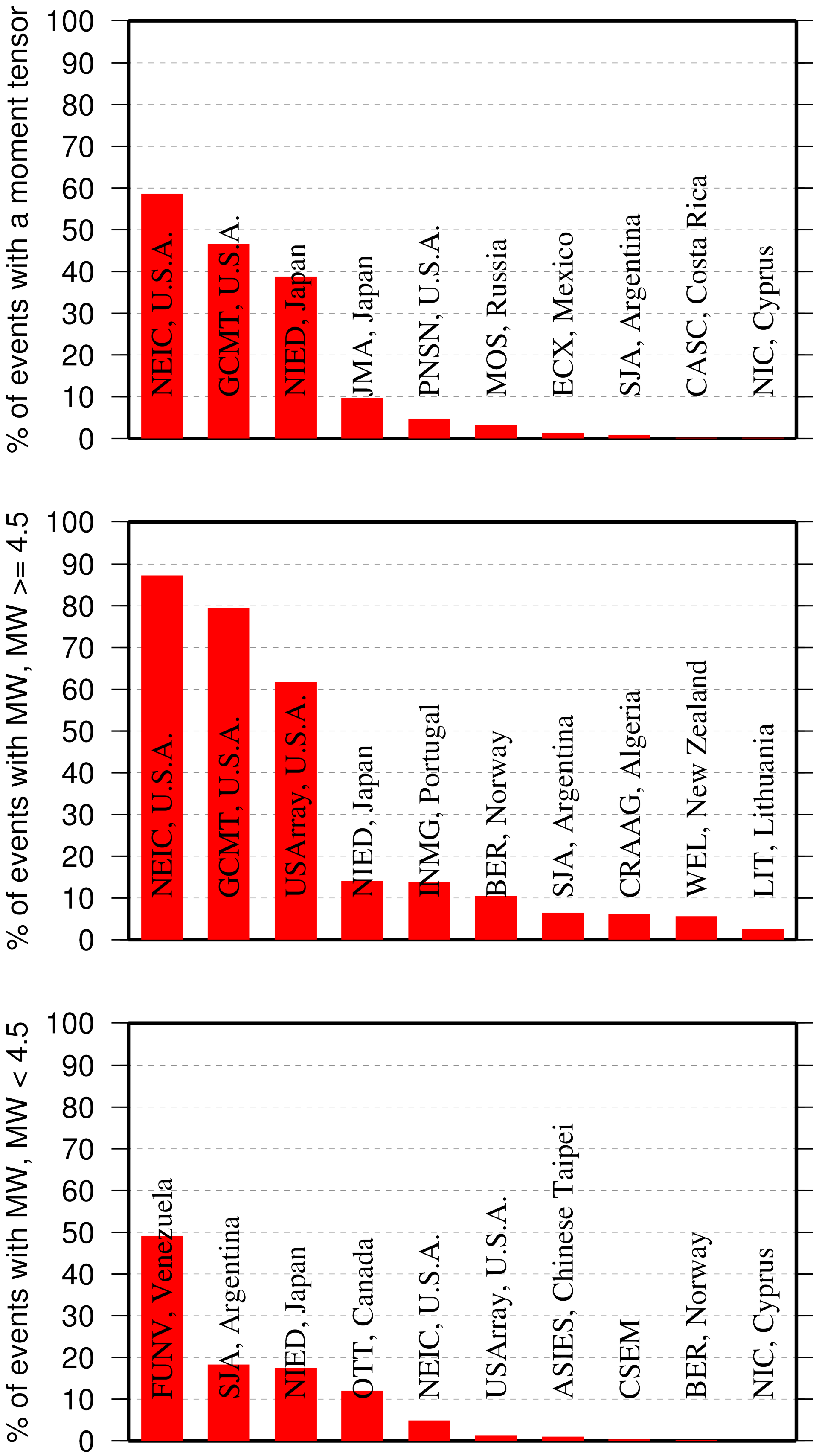

Figure 11.6: *Top ten agencies that most frequently report determinations of seismic moment tensor (top) and moment magnitude (middle/bottom for M greater/smaller than 4.5).*

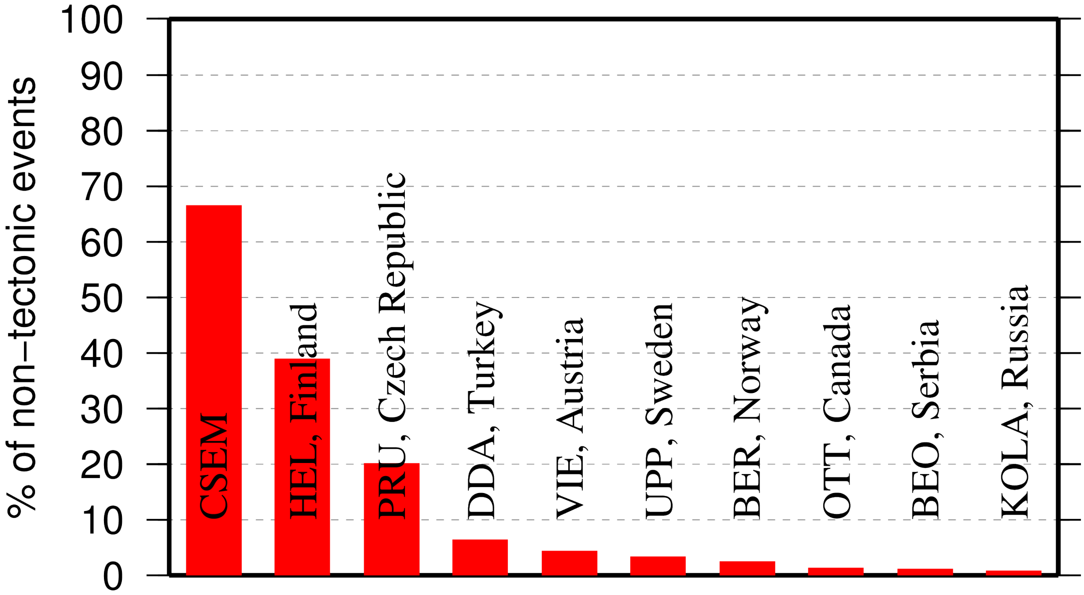

Figure 11.7: *Top ten agencies that most frequently report non-tectonic seismic events to the ISC.*

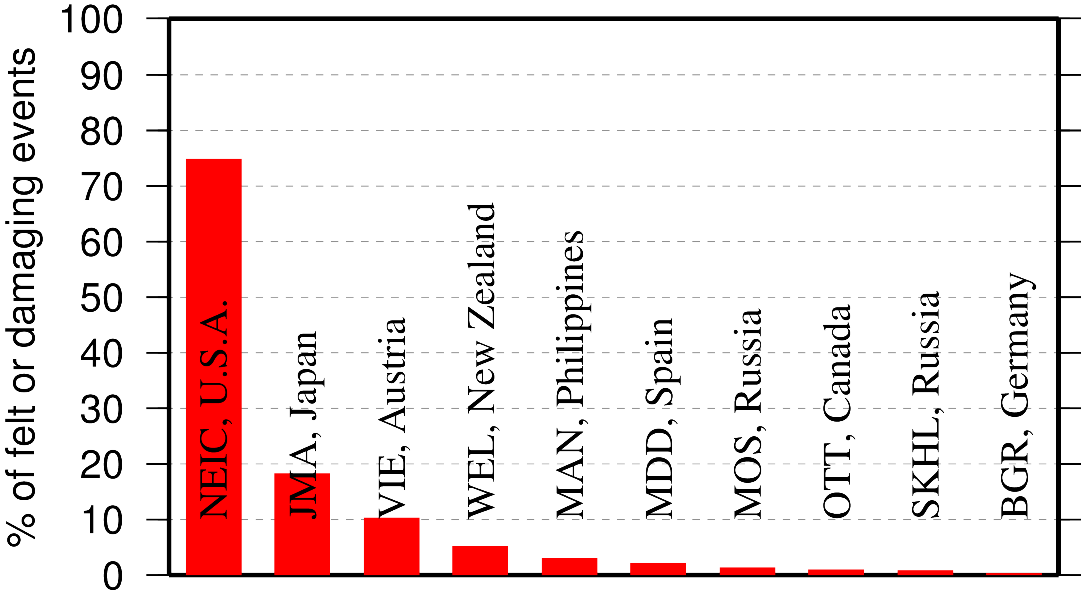

Figure 11.8: *Top ten agencies that most frequently report macroseismic information to the ISC.*

11.3 The Most Consistent and Punctual Contributors

During this six month period, 29 agencies reported their bulletin data in one of the standard seismic formats (ISF, IMS, GSE or Nordic) and within the current 12 month deadline. Here we must reiterate that the ISC accepts reviewed bulletin data after a final analysis as soon as they are ready. These data, even if they arrive before the deadline, are immediately parsed into the ISC database, grouped with other data and become available to the ISC users on-line as part of the preliminary ISC Bulletin. There is no reason to wait until the deadline to send the data to the ISC. Table 11.1 lists all agencies that have been helpful to the ISC in this respect during the six month period.

Table 11.1: *Agencies that contributed reviewed bulletin data to the ISC in one of the standard international formats before the submission deadline.*

Agency Code	Country	Average Delay from real time (days)
SSNC	Cuba	15
LDG	France	19
PPT	French Polynesia	22
NAO	Norway	23
IGIL	Portugal	32
PDG	Montenegro	37
UCC	Belgium	47
TIR	Albania	50
SVSA	Portugal	50
DMN	Nepal	51
INMG	Portugal	76
BGR	Germany	106
BJI	China	111
SIO	U.S.A.	115
ISN	Iraq	118
IDC	CTBTO	122
PRE	South Africa	126
THE	Greece	142
KNET	Kyrgyzstan	158
LIC	Ivory Coast	169
BGS	United Kingdom	171
BER	Norway	235
KRSC	Russia	261
LIT	Lithuania	263
BYKL	Russia	294
ASRS	Russia	303
VIE	Austria	330
AUST	Australia	332
HYB	India	365

12

Appendix

Table 12.1: *Listing of all 304 agencies that have directly reported to the ISC. The 126 agencies highlighted in bold have reported data to the ISC Bulletin for the period of this Bulletin Summary.*

Agency Code	Agency Name
AAA	Alma-ata, Kazakhstan
AAE	**University of Addis Ababa, Ethiopia**
AAM	University of Michigan, USA
ADE	Primary Industries and Resources SA, Australia
ADH	Observatorio Afonso Chaves, Portugal
AEIC	Alaska Earthquake Information Center, USA
AFAR	Afar Depression: interpretation of the 1960-2000 earthquakes, Israel
ALG	Algiers University, Algeria
ANF	USArray Array Network Facility, USA
ANT	Antofagasta, Chile
ARE	Instituto Geofisico del Peru, Peru
ARO	**Observatoire Géophysique d'Arta, Djibouti**
ASIES	**Institute of Earth Sciences, Academia Sinica, Chinese Taipei**
ASL	Albuquerque Seismological Laboratory, USA
ASM	University of Asmara, Eritrea
ASRS	**Altai-Sayan Seismological Centre, GS SB RAS, Russia**
ATA	The Earthquake Research Center Ataturk University, Turkey
ATH	**National Observatory of Athens, Greece**
AUST	**Geoscience Australia, Australia**
AWI	**Alfred Wegener Institute for Polar and Marine Research, Germany**
AZER	**Republic Center of Seismic Survey, Azerbaijan**
BCIS	Bureau Central International de Sismologie, France
BDF	Observatório Sismológico da Universidade de Brasília, Brazil
BELR	**Centre of Geophysical Monitoring, Belarus**
BEO	**Seismological Survey of Serbia, Serbia**
BER	**University of Bergen, Norway**
BERK	Berkheimer H, Germany
BGR	**Bundesanstalt für Geowissenschaften und Rohstoffe, Germany**
BGS	**British Geological Survey, United Kingdom**
BHUJ2	Study of Aftershocks of the Bhuj Earthquake by Japanese Research Team, Japan
BIAK	Biak earthquake aftershocks (17-Feb-1996), USA
BJI	**China Earthquake Networks Center, China**
BKK	**Thai Meteorological Department, Thailand**
BNS	Erdbebenstation, Geologisches Institut der Universität, Köln, Germany
BOG	Universidad Javeriana, Colombia
BRA	**Geophysical Institute, Slovak Academy of Sciences, Slovakia**

Table 12.1: *continued*

Agency Code	Agency Name
BRG	**Seismological Observatory Berggießhübel, TU Bergakademie Freiberg**, **Germany**
BRK	Berkeley Seismological Laboratory, USA
BRS	Brisbane Seismograph Station, Australia
BUC	**National Institute for Earth Physics**, **Romania**
BUD	**Geodetic and Geophysical Research Institute**, **Hungary**
BUG	Institute of Geology, Mineralogy & Geophysics, Germany
BUL	**Goetz Observatory**, **Zimbabwe**
BUT	Montana Bureau of Mines and Geology, USA
BYKL	**Baykal Regional Seismological Centre, GS SB RAS**, **Russia**
CADCG	Central America Data Centre, Costa Rica
CAN	Australian National University, Australia
CANSK	Canadian and Scandinavian Networks, Sweden
CAR	Instituto Sismologico de Caracas, Venezuela
CASC	**Central American Seismic Center**, **Costa Rica**
CERI	Center for Earthquake Research and Information, USA
CLL	**Geophysikalisches Observatorium Collm**, **Germany**
CNG	Seismographic Station Changalane, Mozambique
CNRM	Centre National de Recherche, Morocco
COSMOS	Consortium of Organizations for Strong Motion Observations, USA
CRAAG	**Centre de Recherche en Astronomie, Astrophysique et Géophysique**, **Algeria**
CSC	University of South Carolina, USA
CSEM	**Centre Sismologique Euro-Méditerranéen (CSEM/EMSC)**, **France**
DASA	Defense Atomic Support Agency, USA
DBN	**Koninklijk Nederlands Meteorologisch Instituut**, **Netherlands**
DDA	**Disaster and Emergency Management Presidency**, **Turkey**
DHMR	**Yemen National Seismological Center**, **Yemen**
DIAS	**Dublin Institute for Advanced Studies**, **Ireland**
DJA	**Badan Meteorologi, Klimatologi dan Geofisika**, **Indonesia**
DMN	**Department of Mines and Geology, Ministry of Industry of Nepal**, **Nepal**
DNK	**Geological Survey of Denmark and Greenland**, **Denmark**
DSN	**Dubai Seismic Network**, **United Arab Emirates**
DUSS	Damascus University, Syria
EAF	East African Network, Unknown
EBR	Observatori de l'Ebre, Spain
ECX	**Red Sismica del Noroeste de Mexico (RESOM)**, **Mexico**
EFATE	OBS Experiment near Efate, Vanuatu, USA
EHB	Engdahl, van der Hilst and Buland, USA
EIDC	Experimental (GSETT3) International Data Center, USA
EKA	Eskdalemuir Array Station, United Kingdom
ENT	Geological Survey and Mines Department, Uganda
EPSI	Reference events computed by the ISC for EPSI project, United Kingdom
ERDA	Energy Research and Development Administration, USA
EST	Geological Survey of Estonia, Estonia

Table 12.1: *continued*

Agency Code	Agency Name
FBR	Fabra Observatory, Spain
FDF	Fort de France, Martinique
FIA0	Finessa Array, Finland
FOR	Unknown Historical Agency, Unknown - historical agency
FUNV	**Fundación Venezolana de Investigaciones Sismológicas**, **Venezuela**
FUR	Geophysikalisches Observatorium der Universität München, Germany
GBZT	Marmara Research Center, Turkey
GCG	INSIVUMEH, Guatemala
GCMT	**The Global CMT Project**, **USA**
GDNRW	Geologischer Dienst Nordrhein-Westfalen, Germany
GEN	Dipartimento per lo Studio del Territorio e delle sue Risorse (RSNI), Italy
GFZ	Helmholtz Centre Potsdam GFZ German Research Centre For Geosciences, Germany
GII	**The Geophysical Institute of Israel**, **Israel**
GRAL	**National Council for Scientific Research**, **Lebanon**
GTFE	German Task Force for Earthquakes, Germany
GUC	**Departamento de Geofísica, Universidad de Chile**, **Chile**
HAN	Hannover, Germany
HDC	Observatorio Vulcanológico y Sismológico de Costa Rica, Costa Rica
HEL	**Institute of Seismology, University of Helsinki**, **Finland**
HFS	Hagfors Observatory, Sweden
HFS1	Hagfors Observatory, Sweden
HFS2	Hagfors Observatory, Sweden
HKC	**Hong Kong Observatory**, **Hong Kong**
HLUG	Hessisches Landesamt für Umwelt und Geologie, Germany
HLW	**National Research Institute of Astronomy and Geophysics**, **Egypt**
HNR	**Ministry of Mines, Energy and Rural Electrification**, **Solomon Islands**
HON	Pacific Tsunami Warning Center - NOAA, USA
HRVD	Harvard University, USA
HRVD_LR	Department of Geological Sciences, Harvard University, USA
HVO	Hawaiian Volcano Observatory, USA
HYB	**National Geophysical Research Institute**, **India**
HYD	National Geophysical Research Institute, India
IAG	Instituto Andaluz de Geofisica, Spain
IASPEI	IASPEI Working Group on Reference Events, USA
ICE	Instituto Costarricense de Electricidad, Costa Rica
IDC	**International Data Centre**, **CTBTO**, **Austria**
IGIL	**Instituto Geofisico do Infante Dom Luiz**, **Portugal**
IGQ	**Servicio Nacional de Sismología y Vulcanología**, **Ecuador**
IGS	Institute of Geological Sciences, United Kingdom
INET	Instituto Nicaragüense de Estudios Territoriales, Nicaragua
INMG	**Instituto Português do Mar e da Atmosfera, I.P.**, **Portugal**
IPEC	Ústav fyziky Země, Czech Republic

Table 12.1: continued

Agency Code	Agency Name
IPRG	Institute for Petroleum Research and Geophysics, Israel
IRIS	**IRIS Data Management Center**, **USA**
IRSM	Institute of Rock Structure and Mechanics, Czech Republic
ISK	**Kandilli Observatory and Research Institute**, **Turkey**
ISN	**Iraqi Meteorological and Seismology Organisation**, **Iraq**
ISS	International Seismological Summary, United Kingdom
IST	Institute of Physics of the Earth, Technical University of Istanbul, Turkey
JEN	Geodynamisches Observatorium Moxa, Germany
JMA	**Japan Meteorological Agency**, **Japan**
JOH	Bernard Price Institute of Geophysics, South Africa
JSN	**Jamaica Seismic Network**, **Jamaica**
JSO	**Jordan Seismological Observatory**, **Jordan**
KBC	Institut de Recherches Géologiques et Minières, Cameroon
KEW	Kew Observatory, United Kingdom
KHC	Geofysikalni Ustav, Ceske Akademie Ved, Czech Republic
KISR	Kuwait Institute for Scientific Research, Kuwait
KLM	**Malaysian Meteorological Service**, **Malaysia**
KMA	**Korea Meteorological Administration**, **Republic of Korea**
KNET	**Kyrgyz Seismic Network**, **Kyrgyzstan**
KOLA	**Kola Regional Seismic Centre, GS RAS**, **Russia**
KRL	Geodätisches Institut der Universität Karlsruhe, Germany
KRNET	**Institute of Seismology, Academy of Sciences of Kyrgyz Republic**, **Kyrgyzstan**
KRSC	**Kamchatkan Experimental and Methodical Seismological Department**, **GS RAS**, **Russia**
KSA	Observatoire de Ksara, Lebanon
KUK	Geological Survey Department of Ghana, Ghana
LAO	Large Aperture Seismic Array, USA
LDG	**Laboratoire de Détection et de Géophysique/CEA**, **France**
LDN	University of Western Ontario, Canada
LDO	Lamont-Doherty Earth Observatory, USA
LED	Landeserdbebendienst Baden-Württemberg, Germany
LEDBW	Landeserdbebendienst Baden-Württemberg, Germany
LER	Besucherbergwerk Binweide Station, Germany
LIB	Tripoli, Libya
LIC	**Station Géophysique de Lamto**, **Ivory Coast**
LIM	Lima, Peru
LIS	Instituto de Meteorologia, Portugal
LIT	**Geological Survey of Lithuania**, **Lithuania**
LJU	**Environmental Agency of the Republic of Slovenia**, **Slovenia**
LPA	**Universidad Nacional de La Plata**, **Argentina**
LSZ	Geological Survey Department of Zambia, Zambia
LVSN	Latvian Seismic Network, Latvia
MAN	**Philippine Institute of Volcanology and Seismology**, **Philippines**
MAT	**The Matsushiro Seismological Observatory**, **Japan**
MCO	Macao Meteorological and Geophysical Bureau, Macao, China
MDD	**Instituto Geográfico Nacional**, **Spain**

Table 12.1: continued

Agency Code	Agency Name
MED_RCMT	MedNet Regional Centroid - Moment Tensors, Italy
MES	Messina Seismological Observatory, Italy
MEX	**Instituto de Geofísica de la UNAM, Mexico**
MOLD	**Institute of Geophysics and Geology, Moldova**
MOS	**Geophysical Survey of Russian Academy of Sciences, Russia**
MOZ	**Direccao Nacional de Geologia, Mozambique**
MRB	Institut Cartogràfic de Catalunya, Spain
MSI	Messina Seismological Observatory, Italy
MSSP	**Micro Seismic Studies Programme, PINSTECH, Pakistan**
MUN	Mundaring Observatory, Australia
NAI	University of Nairobi, Kenya
NAM	**The Geological Survey of Namibia, Namibia**
NAO	**Stiftelsen NORSAR, Norway**
NCEDC	Northern California Earthquake Data Center, USA
NDI	**India Meteorological Department, India**
NEIC	**National Earthquake Information Center, USA**
NEIS	National Earthquake Information Service, USA
NERS	**North Eastern Regional Seismological Centre, GS RAS, Russia**
NIC	**Cyprus Geological Survey Department, Cyprus**
NIED	**National Research Institute for Earth Science and Disaster Prevention, Japan**
NNC	**National Nuclear Center, Kazakhstan**
NOU	**IRD Centre de Nouméa, New Caledonia**
NSSC	**National Syrian Seismological Center, Syria**
NSSP	**National Survey of Seismic Protection, Armenia**
OGSO	Ohio Geological Survey, USA
OMAN	**Sultan Qaboos University, Oman**
ORF	Orfeus Data Center, Netherlands
OTT	**Canadian Hazards Information Service, Natural Resources Canada, Canada**
PAL	Palisades, USA
PAS	California Institute of Technology, USA
PDA	Universidade dos Açores, Portugal
PDG	**Seismological Institute of Montenegro, Montenegro**
PEK	Peking, China
PGC	Pacific Geoscience Centre, Canada
PLV	**National Center for Scientific Research, Vietnam**
PMEL	Pacific seismicity from hydrophones, USA
PMR	Alaska Tsunami Warning Center,, USA
PNSN	**Pacific Northwest Seismic Network, USA**
PPT	**Laboratoire de Géophysique/CEA, French Polynesia**
PRE	**Council for Geoscience, South Africa**
PRU	**Geophysical Institute, Academy of Sciences of the Czech Republic, Czech Republic**
PTO	Instituto Geofísico da Universidade do Porto, Portugal
QCP	**Manila Observatory, Philippines**
QUE	Pakistan Meteorological Department, Pakistan

Table 12.1: *continued*

Agency Code	Agency Name
QUI	Escuela Politécnica Nacional, Ecuador
RAB	Rabaul Volcanological Observatory, Papua New Guinea
RBA	Université Mohammed V, Morocco
REN	MacKay School of Mines, USA
REY	**Icelandic Meteorological Office, Iceland**
RMIT	Royal Melbourne Institute of Technology, Australia
ROC	Odenbach Seismic Observatory, USA
ROM	**Istituto Nazionale di Geofisica e Vulcanologia, Italy**
RRLJ	Regional Research Laboratory Jorhat, India
RSMAC	Red Sísmica Mexicana de Apertura Continental, Mexico
RSNC	Red Sismológica Nacional de Colombia, Colombia
RSPR	**Red Sísmica de Puerto Rico, USA**
RYD	King Saud University, Saudi Arabia
SAPSE	Southern Alps Passive Seismic Experiment, New Zealand
SAR	Sarajevo Seismological Station, Bosnia and Herzegovina
SCB	Observatorio San Calixto, Bolivia
SCEDC	Southern California Earthquake Data Center, USA
SDD	Universidad Autonoma de Santo Domingo, Dominican Republic
SEA	Geophysics Program AK-50, USA
SEPA	Seismic Experiment in Patagonia and Antarctica, USA
SET	Setif Observatory, Algeria
SFS	Real Instituto y Observatorio de la Armada, Spain
SGS	**Saudi Geological Survey, Saudi Arabia**
SHL	Central Seismological Observatory, India
SIGU	**Subbotin Institute of Geophysics, National Academy of Sciences, Ukraine**
SIK	Seismic Institute of Kosovo, Kosovo
SIO	**Scripps Institution of Oceanography, USA**
SJA	**Instituto Nacional de Prevención Sísmica, Argentina**
SJS	Instituto Costarricense de Electricidad, Costa Rica
SKHL	**Sakhalin Experimental and Methodological Seismological Expedition, GS RAS, Russia**
SKL	Sakhalin Complex Scientific Research Institute, Russia
SKO	**Seismological Observatory Skopje, FYR Macedonia**
SLC	Salt Lake City, USA
SLM	Saint Louis University, USA
SNET	Servicio Nacional de Estudios Territoriales, El Salvador
SNM	New Mexico Institute of Mining and Technology, USA
SNSN	Saudi National Seismic Network, Saudi Arabia
SOF	**Geophysical Institute, Bulgarian Academy of Sciences, Bulgaria**
SOME	Seismological Experimental Methodological Expedition, Kazakhstan
SPA	USGS - South Pole, Antarctica
SPGM	Service de Physique du Globe, Morocco
SRI	Stanford Research Institute, USA
SSN	Sudan Seismic Network, Sudan
SSNC	**Servicio Sismológico Nacional Cubano, Cuba**

Table 12.1: continued

Agency Code	Agency Name
SSS	Centro de Estudios y Investigaciones Geotecnicas del San Salvador, El Salvador
STK	Stockholm Seismological Station, Sweden
STR	**Institut de Physique du Globe, France**
STU	Stuttgart Seismological Station, Germany
SVSA	**Sistema de Vigilância Sismológica dos Açores, Portugal**
SYO	**National Institute of Polar Research, Japan**
SZGRF	Seismologisches Zentralobservatorium Gräfenberg, Germany
TAC	Estación Central de Tacubaya, Mexico
TAN	Antananarivo, Madagascar
TANZANIA	Tanzania Broadband Seismic Experiment, USA
TAP	**CWB, Chinese Taipei**
TAU	University of Tasmania, Australia
TEH	**Tehran University, Iran**
TEIC	Center for Earthquake Research and Information, USA
THE	**Department of Geophysics, Aristotle University of Thessaloniki, Greece**
THR	**International Institute of Earthquake Engineering and Seismology (IIEES), Iran**
TIF	**Seismic Monitoring Centre of Georgia, Georgia**
TIR	**The Institute of Seismology, Academy of Sciences of Albania, Albania**
TRI	**Osservatorio Geofisico Sperimentale, Italy**
TRN	**University of the West Indies, Trinidad and Tobago**
TTG	Titograd Seismological Station, Montenegro
TUL	Oklahoma Geological Survey, USA
TUN	Institut National de la Météorologie, Tunisia
TVA	Tennessee Valley Authority, USA
TZN	University of Dar Es Salaam, Tanzania
UAV	Red Sismológica de Los Andes Venezolanos, Venezuela
UCC	**Royal Observatory of Belgium, Belgium**
UCR	Universidad de Costa Rica, Costa Rica
UGN	Institute of Geonics AS CR, Czech Republic
ULE	University of Leeds, United Kingdom
UNAH	Universidad Nacional Autonoma de Honduras, Honduras
UPA	Universidad de Panama, Panama
UPP	**University of Uppsala, Sweden**
UPSL	University of Patras, Department of Geology, Greece
USAEC	United States Atomic Energy Commission, USA
USCGS	United States Coast and Geodetic Survey, USA
USGS	**United States Geological Survey, USA**
UVC	Universidad del Valle, Colombia
VAO	**Instituto Astronomico e Geofísico, Brazil**
VIE	**Österreichischer Geophysikalischer Dienst, Austria**
VSI	University of Athens, Greece
WAR	**Institute of Geophysics, Polish Academy of Sciences, Poland**
WBNET	**West Bohemia Seismic Network, Czech Republic**

Table 12.1: *continued*

Agency Code	Agency Name
WEL	**Institute of Geological and Nuclear Sciences**, **New Zealand**
WES	Weston Observatory, USA
YARS	**Yakutiya Regional Seismological Center, GS SB RAS**, **Russia**
ZAG	**Seismological Survey of the Republic of Croatia**, **Croatia**
ZUR	**Swiss Seismological Sevice (SED)**, **Switzerland**
ZUR_RMT	Zurich Moment Tensors, Switzerland

Table 12.2: *Phases reported to the ISC. These include phases that could not be matched to an appropriate* ak135 *phase. Those agencies that reported at least 10% of a particular phase are also shown.*

Reported Phase	Total	Agencies reporting
P	2322395	IRIS (18%), NEIC (15%)
S	839227	JMA (25%), TAP (14%), CSEM (12%)
Pg	290068	CSEM (53%), ROM (17%)
Pn	259504	CSEM (41%), NEIC (25%)
Sg	203573	CSEM (49%), ROM (19%)
PN	182404	WEL (46%), ATH (24%), ISK (20%)
pmax	131783	MOS (92%)
LR	114800	IDC (45%), NEIC (35%), BJI (14%)
Sn	101110	CSEM (33%), NEIC (16%), NNC (13%)
Lg	81867	CSEM (44%), MDD (23%), NNC (13%)
PG	79414	ISK (34%), ATH (28%), HEL (15%), PRU (12%)
AML	69778	WEL (44%), GUC (17%), NSSC (13%)
NULL	63483	MOS (51%), ECX (11%)
SG	57288	HEL (28%), PRU (24%), ISK (21%), ATH (13%)
PKP	54474	IDC (40%), NEIC (31%), BJI (12%)
Pb	49544	CSEM (73%), IRIS (27%)
SN	47550	WEL (36%), ATH (31%), HEL (14%)
PB	47067	ATH (88%), HEL (12%)
Sb	44190	CSEM (64%), IRIS (35%)
SB	34816	ATH (80%), HEL (20%)
PKIKP	31117	MOS (91%)
PKPbc	30698	NEIC (47%), IDC (38%)
pP	29550	NEIC (35%), BJI (30%), IDC (18%)
PKPdf	28426	NEIC (83%)
T	25335	IDC (89%), PPT (11%)
MLR	24882	MOS (100%)
PP	22874	BJI (43%), NEIC (22%), IDC (12%)
PFAKE	21672	NEIC (100%)
PKPab	20368	NEIC (46%), IDC (38%)
MSG	19921	HEL (100%)
PcP	18812	NEIC (43%), IDC (39%)
P*	18199	WEL (96%)
A	17649	INMG (62%), SVSA (21%), SKHL (16%)
PMZ	17034	BJI (100%)
PKiKP	15560	IRIS (67%), NEIC (14%)
SS	13029	BJI (55%), MOS (26%)
x	9769	NDI (61%), PRU (39%)
sP	9614	BJI (82%)
LZ	9536	BJI (100%)
AMB	9386	SKHL (31%), PRE (19%), NDI (18%), BJI (15%), BGS (12%)
LN	9300	BJI (100%)
IAML	9225	BER (37%), ECX (30%), GUC (25%)
LE	9095	BJI (100%)
smax	7332	MOS (87%), BJI (13%)
ScP	6669	NEIC (41%), IDC (37%), BJI (13%)
S*	6383	WEL (97%)

Table 12.2: continued

Reported Phase	Total	Agencies reporting
Pdiff	6236	IRIS (79%), IDC (12%)
Trac	5885	OTT (100%)
PKKPbc	5457	NEIC (51%), IDC (47%)
AMS	5158	PRU (57%), BGS (16%), SKHL (12%)
*PP	4960	MOS (100%)
sS	4803	BJI (99%)
pPKP	4491	BJI (49%), IDC (20%), NEIC (15%), PRU (14%)
Sm	4457	YARS (98%)
SKS	4097	BJI (80%)
PKP2	3904	MOS (96%)
R	3019	LDG (59%), STR (41%)
sPKP	2652	BJI (96%)
SKKS	2584	BJI (91%)
Pdif	2525	NEIC (80%), BJI (11%)
SKPbc	2312	NEIC (53%), IDC (44%)
Pm	2309	YARS (98%)
PKPpre	2283	NEIC (98%)
PPMZ	2250	BJI (100%)
LG	2189	OTT (83%), BRA (14%)
p	2138	HEL (100%)
PKHKP	2103	MOS (100%)
PKhKP	2003	IDC (100%)
PKS	1897	BJI (97%)
ScS	1871	BJI (78%)
Smax	1779	BYKL (100%)
PPP	1777	MOS (82%)
S1	1660	GUC (99%)
IAmb	1581	HYB (55%), BER (41%)
P9	1574	ECX (52%), GUC (41%)
LQ	1549	PPT (52%), INMG (26%), BELR (16%)
PS	1416	MOS (51%), CLL (13%)
Pmax	1323	BYKL (96%)
L	1297	STR (40%), BGR (37%)
P1	1279	GUC (98%)
SSS	1243	MOS (65%), CLL (19%), BELR (12%)
PcS	1186	BJI (99%)
pPKPbc	1181	IDC (43%), NEIC (27%), BGR (23%)
Rg	1116	NNC (69%), NAO (11%)
PKKPab	1008	NEIC (48%), IDC (44%)
PKKP	987	IDC (43%), NEIC (34%), PRU (13%)
SKP	961	NEIC (29%), IDC (26%), IRIS (26%), PRU (15%)
SP	917	MOS (35%), PRU (30%)
PKPPKP	875	IDC (85%), PRU (11%)
LRM	839	BELR (51%), MOLD (49%)
pPKPdf	764	NEIC (69%)
SKSac	679	BER (21%), WAR (15%), INMG (12%), HYB (12%), CLL (11%)
IVMs_BB	665	HYB (65%), BER (35%)

Table 12.2: *continued*

Reported Phase	Total	Agencies reporting
S4	636	GUC (75%), SJA (21%)
PKPAB	628	PRU (99%)
P'P'	623	NEIC (100%)
*SP	590	MOS (100%)
SME	578	BJI (100%)
SMN	577	BJI (100%)
max	563	BYKL (100%)
Lm	545	CLL (100%)
P4	507	SJA (47%), GUC (40%)
LMZ	501	WAR (100%)
P2	480	ECX (98%)
pPKPab	466	NEIC (41%), IDC (41%)
*SS	448	MOS (100%)
IAMs_20	443	BER (84%), HYB (16%)
AMP	398	NOU (51%), HLW (43%)
LmV	354	CLL (100%)
PCP	348	PRU (67%), BRA (22%)
SKKPbc	348	IDC (52%), NEIC (45%)
PPS	310	CLL (57%), MOS (30%)
PKP2bc	300	IDC (100%)
PDIFF	275	PRU (89%), BRG (11%)
H	273	IDC (100%)
PM	271	BELR (100%)
PDIF	259	BRA (91%)
PKP1	254	LIC (96%)
P'P'df	239	NEIC (98%)
(P)	231	BRG (70%), CLL (22%)
PKPDF	218	PRU (100%)
LmH	212	CLL (100%)
Sgm	204	SIGU (100%)
SKPdf	201	NEIC (61%), BGR (16%)
PKKPdf	200	NEIC (67%), BGR (15%)
pkp	193	HEL (100%)
pPcP	184	IDC (57%), NEIC (41%)
PKPdiff	180	IRIS (97%)
Sgmax	174	NERS (100%)
RG	163	HEL (100%)
pg	148	BUD (100%)
P3KPbc	145	IDC (100%)
sg	139	BUD (100%)
rx	129	SKHL (100%)
AMb	128	IGIL (77%), DHMR (20%)
Sdif	124	CLL (55%), PPT (19%), INMG (13%)
PKPdif	124	IRIS (85%), NEIC (15%)
X	121	SYO (88%)
pPKiKP	119	CLL (29%), HYB (20%), VIE (20%), BUD (20%)
SSSS	117	CLL (99%)

Table 12.2: *continued*

Reported Phase	Total	Agencies reporting
AP	116	UCC (95%)
MSN	115	HEL (100%)
SKPab	115	NEIC (50%), IDC (37%)
P4KPbc	114	IDC (100%)
Snm	107	SIGU (100%)
Pgm	103	SIGU (100%)
Pgmax	91	NERS (100%)
SKKSac	82	CLL (55%), BGR (23%), WAR (15%)
PKP2ab	81	IDC (100%)
E	79	UCC (81%), WAR (16%)
SKKP	73	IDC (38%), NEIC (37%), PRU (21%)
P3	71	ECX (39%), NDI (39%)
LQM	67	BELR (94%)
P'P'ab	65	NEIC (100%)
pPn	63	BUD (73%), HYB (19%)
IVmB_BB	61	BER (98%)
(sP)	59	CLL (100%)
PmP	57	BGR (96%)
APKP	57	UCC (100%)
XS	56	PRU (100%)
PN4	56	ISN (100%)
sPKPdf	56	VIE (39%), HYB (21%), CLL (20%), BGR (16%)
pPdiff	55	BGR (60%), VIE (18%), IDC (13%)
SmS	53	BGR (96%)
Pu	53	NEIC (100%)
mb	52	OMAN (62%), KMA (21%), OTT (17%)
PgPg	52	BYKL (94%)
Pnm	51	SIGU (100%)
P3KP	46	IDC (100%)
SN4	44	ISN (100%)
SM	43	BELR (100%)
PKKKP	39	NEIC (100%)
SDIF	39	PRU (79%), BRG (15%)
sPP	37	CLL (100%)
Lmax	36	CLL (100%)
PKPPKPdf	36	BUD (72%), CLL (28%)
PSKS	36	CLL (97%)
SKSP	35	MOLD (29%), BELR (29%), CLL (23%), DBN (17%)
PA	35	JSN (100%)
ml	35	OMAN (100%)
SgSg	35	BYKL (100%)
SKKPdf	32	BUD (91%)
pPP	32	CLL (91%)
sPKiKP	32	CLL (47%), HYB (34%), VIE (16%)
(SS)	32	CLL (100%)
PKPM	28	BELR (100%)
IVMsBB	28	HYB (100%)

Table 12.2: *continued*

Reported Phase	Total	Agencies reporting
pScP	27	IDC (56%), NEIC (44%)
SH	27	SYO (100%)
sn	27	BUD (100%)
pPdif	27	CLL (74%), HYB (26%)
SDIFF	26	BRG (100%)
SCP	26	PRU (38%), UCC (27%), BRA (19%), BRG (12%)
(SSS)	25	CLL (100%)
SKSdf	25	BUD (36%), WAR (32%), HYB (12%), CLL (12%)
(PP)	24	CLL (100%)
S3	23	MEX (39%), SJA (35%), NDI (22%)
PXPXdf	22	BGR (100%)
SCS	22	NDI (41%), PRU (27%), BRA (18%)
PKdiff	22	IRIS (100%)
(pP)	22	CLL (100%)
pn	21	BUD (100%)
e	20	WAR (100%)
SKKKS	20	BELR (100%)
PKKS	20	PRU (80%)
sPKPbc	20	HYB (40%), CLL (35%), VIE (20%)
S2	20	GUC (45%), SJA (30%), MEX (20%)
sPn	20	NEIC (40%), HYB (35%), SKHL (15%)
PPM	20	BELR (95%)
XP	20	UCC (100%)
PKPc	18	WAR (100%)
SKiKP	18	IDC (39%), PPT (33%), UCC (28%)
PPPP	18	CLL (100%)
Sdiff	18	BUD (50%), LJU (22%), WAR (17%), IDC (11%)
(PKiKP)	18	CLL (100%)
sSS	17	CLL (100%)
LV	17	CLL (100%)
sPdif	17	HYB (53%), CLL (47%)
PN5	17	THR (100%)
pS	15	WAR (40%), SVSA (40%), LJU (13%)
Sg4	14	SJA (93%)
TT	14	NEIC (100%)
SPP	14	CLL (36%), HYB (21%), MOS (21%), BELR (14%)
sPg	14	SKHL (86%), NEIC (14%)
Pg4	14	SJA (93%)
(SSSS)	13	CLL (100%)
PSS	13	CLL (100%)
Plp	13	CLL (100%)
PsP	13	MOLD (100%)
Li	13	MOLD (100%)
pPg	12	SKHL (100%)
PPPrev	12	CLL (100%)
M	11	MOLD (91%)
P4KP	11	IDC (64%), NEIC (36%)

Table 12.2: *continued*

Reported Phase	Total	Agencies reporting
MPN	10	HEL (100%)
APKPbc	10	UCC (100%)
PnPn	10	HYB (100%)
SKPa	10	NAO (80%), BER (20%)
PX	10	WAR (90%)
PCS	10	NDI (70%), BRG (20%)
sPS	10	CLL (100%)
AMPN	10	SJA (60%), GUC (30%)
PKSdf	10	CLL (100%)
XSKS	9	PRU (100%)
SKKSdf	9	NEIC (78%), CLL (22%)
PSPS	9	CLL (100%)
sPPS	9	CLL (100%)
PC	9	BER (67%), ECX (11%), NDI (11%), CASC (11%)
(S)	9	CLL (89%), BRG (11%)
Lg1	8	MOLD (100%)
(Pg)	8	CLL (100%)
Lg2	8	MOLD (100%)
XM	8	MOLD (100%)
PKKSdf	8	NEIC (75%), CLL (25%)
SMZ	8	BJI (100%)
(PPP)	7	CLL (100%)
PPlp	7	CLL (100%)
(pPKiKP)	7	CLL (100%)
PKPlp	7	CLL (100%)
sPPP	7	CLL (100%)
(PPS)	7	CLL (100%)
SPKiKP	7	UCC (100%)
P(2)	7	CLL (100%)
PKKP2	7	BGR (100%)
PPmax	7	CLL (100%)
SKPpB	7	BRA (100%)
(pPKPdf)	7	CLL (100%)
sSdiff	7	CLL (100%)
PPKP	6	UCC (100%)
APKPab	6	UCC (100%)
(PcP)	6	CLL (100%)
sPKPab	6	HYB (83%), CLL (17%)
AMSN	6	SJA (100%)
sSSS	6	CLL (100%)
sSKSac	6	CLL (50%), WAR (33%), LJU (17%)
PPKiKP	6	UCC (100%)
PKSbc	6	CLL (100%)
Lg4	6	BER (100%)
PKPPKPbc	5	BUD (60%), CLL (40%)
PGS	5	NDI (100%)
PKSab	5	CLL (100%)

Table 12.2: *continued*

Reported Phase	Total	Agencies reporting
PKKPB	5	BRA (80%), BRG (20%)
Pdi	5	SKO (100%)
SKPPKPbc	5	CLL (100%)
(PKPdf)	5	CLL (100%)
pPDIF	5	BRG (60%), BRA (40%)
SKPDF	5	BRA (100%)
(PKPab)	5	CLL (100%)
SKPB	5	BRA (100%)
(sPKiKP)	4	CLL (100%)
PCN	4	NDI (100%)
PPPPrev	4	CLL (100%)
sSKKSac	4	CLL (100%)
SKKPab	4	IDC (75%), NEIC (25%)
sPcP	4	CLL (100%)
SKSp	4	BRA (100%)
(sPP)	4	CLL (100%)
PKKSbc	4	CLL (100%)
(Sn)	4	CLL (100%)
W	4	CLL (100%)
(SP)	4	CLL (100%)
(pPKPbc)	3	CLL (100%)
sPKKPdf	3	CLL (100%)
PKPmax	3	CLL (100%)
sPKKPbc	3	CLL (100%)
PKPd4	3	BER (100%)
(Sdif)	3	CLL (100%)
pSKSac	3	CLL (100%)
(PPPP)	3	CLL (100%)
(PSS)	3	CLL (100%)
(Pdif)	3	CLL (100%)
(sSS)	3	CLL (100%)
PKiK	3	HYB (33%), NAO (33%), BER (33%)
pPS	3	CLL (100%)
sPDIF	3	BRA (100%)
SKSSKSac	3	CLL (100%)
pPPS	3	CLL (100%)
IVmBBB	3	BER (100%)
pwP	3	NEIC (100%)
IAML4	3	GUC (67%), BER (33%)
(pPKPab)	3	CLL (100%)
PKKPpB	3	BRA (100%)
(PKPbc)	3	CLL (100%)
SKKSp	3	BRA (100%)
pPKKPdf	3	CLL (100%)
PKPP	3	NDI (100%)
(Sg)	2	CLL (100%)
(PS)	2	CLL (100%)

Table 12.2: *continued*

Reported Phase	Total	Agencies reporting
sPKSdf	2	CLL (100%)
SnSn	2	HYB (100%)
PSP	2	LPA (50%), MOLD (50%)
UNK	2	CSEM (50%), MDD (50%)
PP2	2	LIT (100%)
SSP	2	CLL (100%)
AMPG	2	SJA (100%)
[	2	ECX (100%)
pPKKPbc	2	CLL (100%)
(SKSac)	2	CLL (100%)
Pn9	2	BER (100%)
-MS	2	INMG (100%)
SPKP	2	UCC (100%)
LmV(360	2	CLL (100%)
sSKS	2	HYB (100%)
PKP3	2	NDI (100%)
SKKSacre	2	CLL (100%)
pPKKPab	2	CLL (100%)
sPdiff	2	VIE (100%)
AMSG	2	SJA (100%)
PKPBC	2	PRU (100%)
SKIKP	2	LPA (100%)
s	2	NDI (50%), BUD (50%)
(PKSdf)	2	CLL (100%)
(PPPrev)	2	CLL (100%)
RAY	2	STR (100%)
(pPP)	2	CLL (100%)
PGN	2	HEL (50%), NDI (50%)
SX	2	WAR (50%), NDI (50%)
(sPKPab)	2	CLL (100%)
PSSrev	2	CLL (100%)
(SKPdf)	2	CLL (100%)
PKPbc(2)	2	CLL (100%)
sSKSdf	2	NEIC (50%), CLL (50%)
sPb	2	BUD (100%)
(SKKSac)	2	CLL (100%)
PD	2	NDI (100%)
(Pn)	2	CLL (100%)
PKPS	2	NDI (100%)
f	2	BUD (100%)
sPKKPab	1	CLL (100%)
pSKPdf	1	CLL (100%)
(sPSPS)	1	CLL (100%)
AML1	1	GUC (100%)
(PKKPab)	1	CLL (100%)
Lq2	1	MOLD (100%)
PN3	1	SJA (100%)

Table 12.2: *continued*

Reported Phase	Total	Agencies reporting
P*P	1	ZUR (100%)
sPSPS	1	CLL (100%)
PP(2)	1	CLL (100%)
PP4	1	BER (100%)
pPPPrev	1	CLL (100%)
PcPPKPre	1	CLL (100%)
SS(2)	1	LPA (100%)
Px	1	WAR (100%)
Lm(360	1	CLL (100%)
SSSSS	1	DBN (100%)
PGT	1	TIR (100%)
SSPrev	1	CLL (100%)
(sPKPdf)	1	CLL (100%)
SKSSKS	1	PRU (100%)
Sn2	1	BER (100%)
pP(2)	1	CLL (100%)
sPKKSbc	1	CLL (100%)
Pn4	1	BER (100%)
PFIF	1	BRG (100%)
sPKSbc	1	CLL (100%)
SSSmax	1	CLL (100%)
(sSSS)	1	CLL (100%)
Lq1	1	MOLD (100%)
PGCN	1	NDI (100%)
SG3	1	NDI (100%)
IAMSBB	1	BER (100%)
SKPPKPdf	1	CLL (100%)
AnL	1	INMG (100%)
(pPKSbc)	1	CLL (100%)
PGDN	1	NDI (100%)
(PKP)	1	CLL (100%)
(PSKS)	1	CLL (100%)
PG9	1	ECX (100%)
P'P'bc	1	HYB (100%)
(pPcP)	1	CLL (100%)
PKPab(2)	1	CLL (100%)
PKKPdfm	1	CLL (100%)
sSKPbc	1	CLL (100%)
KSP	1	BELR (100%)
pPmax	1	CLL (100%)
PE	1	NDI (100%)
PPPmax	1	CLL (100%)
PKIKS	1	LPA (100%)
Rq	1	MOLD (100%)
sSKPab	1	CLL (100%)
(ScP)	1	CLL (100%)
PKKPDF	1	BRG (100%)

Table 12.2: *continued*

Reported Phase	Total	Agencies reporting
(sS)	1	CLL (100%)
SPKKP	1	BRG (100%)
pPPPP	1	CLL (100%)
pSdiff	1	CLL (100%)
PKiKPmax	1	CLL (100%)
sSP	1	CLL (100%)
PcZP	1	SYO (100%)
SKSac(2)	1	CLL (100%)
sPPPrev	1	CLL (100%)
SSSrev	1	CLL (100%)
D	1	MSSP (100%)
(sPcP)	1	CLL (100%)
PPPS	1	DBN (100%)
PPS(2)	1	CLL (100%)
SN3	1	NDI (100%)
(SKKSdf)	1	CLL (100%)
pSKKPbc	1	CLL (100%)
PKiKP(2)	1	CLL (100%)
Pdiffmax	1	CLL (100%)
(SSSm)	1	CLL (100%)
sScP	1	CLL (100%)
P'P'P'	1	BRG (100%)
PKPdf(2)	1	CLL (100%)
IP	1	ECX (100%)
(pSP)	1	CLL (100%)
S(2)	1	LPA (100%)
PSKSmax	1	CLL (100%)
Sg9	1	BER (100%)
(sPdif)	1	CLL (100%)
Sglp	1	CLL (100%)
PN2	1	ISN (100%)
PKSP	1	NDI (100%)
T(MAX)	1	WEL (100%)
SSmax	1	CLL (100%)
PKPdflp	1	CLL (100%)
(SN)	1	BRG (100%)
AMS4	1	SJA (100%)
Sn3	1	BER (100%)
(sPKPbc)	1	CLL (100%)
SN2	1	ISN (100%)
(sPSS)	1	CLL (100%)
Pn2	1	BER (100%)
AMB4	1	SJA (100%)
LgX	1	CSEM (100%)
PPSmax	1	CLL (100%)
SKPPKP	1	BRG (100%)
PKSB	1	BRA (100%)

Table 12.2: *continued*

Reported Phase	Total	Agencies reporting
pSKPbc	1	CLL (100%)
pSKPab	1	CLL (100%)
-ML	1	INMG (100%)
PSKS(2)	1	CLL (100%)
PKPdfc	1	WAR (100%)
pPKSdf	1	CLL (100%)
h	1	KRSC (100%)
O	1	SYO (100%)
PK	1	BRG (100%)
3	1	NDI (100%)
SSSSmax	1	CLL (100%)
IAmB	1	BER (100%)
SPS	1	CLL (100%)

Table 12.3: Reporters of amplitude data.

Agency	Number of reported amplitudes	Number of amplitudes in ISC located events	Number used for ISC mb	Number used for ISC MS
IDC	341341	317241	133851	31918
NEIC	214086	213413	139562	38072
MOS	152498	144189	61091	16544
CSEM	141880	25984	7064	0
DJA	78806	49849	7401	0
BJI	77874	75286	5060	8178
NNC	55838	13121	97	0
MDD	50708	9991	0	0
ROM	36272	2594	0	0
WEL	34423	3756	0	0
LDG	28713	19594	4127	0
THE	27616	4554	0	0
HEL	22319	2718	1464	0
DMN	17291	16767	845	0
INMG	15626	6973	3239	0
GUC	14003	5273	2	0
PPT	12212	10414	1306	0
BKK	12086	11540	5120	0
VIE	11124	6744	3261	0
PRU	9202	3103	0	1803
NSSC	9045	1749	0	0
PRE	8833	2326	923	251
ECX	7311	2107	0	0
YARS	6651	219	0	0
SKHL	6520	5795	0	0
MAN	6201	2683	0	0
LJU	6141	206	0	0
OTT	5891	334	0	0
BGR	5829	5611	4438	355
BER	4769	1743	521	335
NDI	4740	3629	1074	122
PDG	4258	2315	0	0
SVSA	4109	463	249	0
BRG	4077	2607	370	0
BYKL	3941	2317	0	0
SIO	3532	3513	1215	0
SKO	3196	535	25	0
DNK	3102	2689	1615	0
BGS	2919	1957	860	620
CLL	2876	2581	419	397
LIC	2752	2571	1908	0
SJA	2510	1029	0	0
DHMR	2268	174	20	0
TEH	2256	2156	0	0

Table 12.3: continued

Agency	Number of reported amplitudes	Number of amplitudes in ISC located events	Number used for ISC mb	Number used for ISC MS
NAO	2126	2077	1372	0
KNET	2030	476	0	0
ZUR	1992	341	113	0
WBNET	1563	0	0	0
HYB	1523	1514	667	45
IGIL	1123	536	70	228
UCC	888	783	511	0
DBN	688	382	191	0
THR	642	626	0	0
MOLD	611	361	60	0
LIT	603	553	354	0
NERS	293	104	0	0
BELR	239	0	0	0
NOU	205	108	0	0
HLW	173	95	0	0
CASC	165	121	0	0
MOZ	135	2	0	0
SIGU	110	10	0	0
WAR	90	90	0	46
PLV	47	14	0	0
SSNC	27	27	0	4
LPA	5	5	0	0
AUST	1	1	0	0

13

Glossary of ISC Terminology

- Agency/ISC data contributor

  An academic or government institute, seismological organisation or company, geological/meteorological survey, station operator or author that reports or contributed data in the past to the ISC or one of its predecessors. Agencies may contribute data to the ISC directly, or indirectly through other ISC data contributors.

- Agency code

  A unique, maximum eight-character code for a data reporting agency (e.g. NEIC, GFZ, BUD) or author (e.g. ISC, EHB, IASPEI). Often the agency code is the commonly used acronym of the reporting agency or contributor.

- Arrival

  A phase observation at a station is characterised by a phase name and an arrival time.

- Associated phase

  Associated phase arrival or amplitude measurements represent a collection of observations belonging to (i.e. generated by) an event. The complete set of observations are associated to the prime hypocentre.

- Azimuthal gap/Secondary azimuthal gap

  The azimuthal gap for an event is defined as the largest angle between two stations with defining phases when the stations are ordered by their event-to-station azimuths. The secondary azimuthal gap is the largest azimuthal gap that a single station closes.

- BAAS

  Seismological bulletins published by the British Association for the Advancement of Science (1913-1917) under the leadership of H.H. Turner. These bulletins are the predecessors of the ISS Bulletins and include reports from stations distributed worldwide.

- Bulletin

  An ordered list of event hypocentres, uncertainties, focal mechanisms, network magnitudes, as well as phase arrival and amplitude observations associated to each event. An event bulletin may list all the reported hypocentres for an event. The convention in the ISC Bulletin is that the preferred (prime) hypocentre appears last in the list of reported hypocentres for an event.

- Catalogue

  An ordered list of event hypocentres, uncertainties and magnitudes. An event catalogue typically lists only the preferred (prime) hypocentres and network magnitudes.

- CoSOI/IASPEI

  Commission on Seismological Observation and Interpretation, a commission of IASPEI that prepares and discusses international standards and procedures in seismological observation and interpretation.

- Defining/Non-defining phase

  A defining phase is used in the location of the event (time-defining) or in the calculation of the network magnitude (magnitude-defining). Non-defining phases are not used in the calculations because they suffer from large residuals or could not be identified.

- Direct/Indirect report

  A data report sent (e-mailed) directly to the ISC, or indirectly through another ISC data contributor.

- Duplicates

  Nearly identical phase arrival time data reported by one or more agencies for the same station. Duplicates may be created by agencies reporting observations from other agencies, or several agencies independently analysing the waveforms from the same station.

- Event

  A natural (e.g. earthquake, landslide, asteroid impact) or anthropogenic (e.g. explosion) phenomenon that generates seismic waves and its source can be identified by an event location algorithm.

- Grouping

  The ISC algorithm that organises reported hypocentres into groups of events. Phases associated to any of the reported hypocentres will also be associated to the preferred (prime) hypocentre. The grouping algorithm also attempts to associate phases that were reported without an accompanying hypocentre to events.

- Ground Truth

  An event with a hypocentre known to certain accuracy at a high confidence level. For instance, GT0 stands for events with exactly known location, depth and origin time (typically explosions); GT5 stands for events with their epicentre known to 5 km accuracy at the 95% confidence level, while their depth and origin time may be known with less accuracy.

- Ground Truth database

  On behalf of IASPEI, the ISC hosts and maintains the IASPEI Reference Event List, a bulletin of ground truth events.

- IASPEI

  International Association of Seismology and Physics of the Earth Interior, www.iaspei.org.

- International Registry of Seismograph Stations (IR)

  Registry of seismographic stations, jointly run by the ISC and the World Data Center for Seismology, Denver (NEIC). The registry provides and maintains unique five-letter codes for stations participating in the international parametric and waveform data exchange.

- ISC Bulletin

  The comprehensive bulletin of the seismicity of the Earth stored in the ISC database and accessible through the ISC website. The bulletin contains both natural and anthropogenic events. Currently the ISC Bulletin spans more than 50 years (1960-to date) and it is constantly extended by adding both recent and past data. Eventually the ISC Bulletin will contain all instrumentally recorded events since 1900.

- ISC Governing Council

  According to the ISC Working Statutes the Governing Council is the governing body of the ISC, comprising one representative for each ISC Member.

- ISC-located events

  A subset of the events selected for ISC review are located by the ISC. The rules for selecting an event for location are described in Section 3.3.4; ISC-located events have a prime hypocentral estimate with the author ISC.

- ISC Member

  An academic or government institute, seismological organisation or company, geological/meteorological survey, station operator, national/international scientific organisation that contribute to the ISC budget by paying membership fees. ISC members have voting rights in the ISC Governing Council.

- ISC-reviewed events

  A subset of the events reported to the ISC are selected for ISC analyst review. These events may or may not be located by the ISC. The rules for selecting an event for review are described in Section 3.3.3. Non-reviewed events are explicitly marked in the ISC Bulletin by the comment following the prime hypocentre "Event not reviewed by the ISC".

- ISF

  International Seismic Format (www.isc.ac.uk/standards/isf). A standard bulletin format approved by IASPEI. The ISC Bulletin is presented in this format at the ISC website.

- ISS

  International Seismological Summary (1918-1963). These bulletins are the predecessors of the ISC Bulletin and represent the major source of instrumental seismological data before the digital era. The ISS contains regionally and teleseismically recorded events from several hundreds of globally distributed stations.

- Network magnitude

The event magnitude reported by an agency or computed by the ISC locator. An agency can report several network magnitudes for the same event and also several values for the same magnitude type. The network magnitude obtained with the ISC locator is defined as the median of station magnitudes of the same magnitude type.

- Phase

  A maximum eight-character code for a seismic, infrasonic, or hydroacoustic phase. During the ISC processing, reported phases are mapped to standard IASPEI phase names. Amplitude measurements are identified by specific phase names to facilitate the computation of body-wave and surface-wave magnitudes.

- Prime hypocentre

  The preferred hypocentre solution for an event from a list of hypocentres reported by various agencies or calculated by the ISC.

- Reading

  Parametric data that are associated to a single event and reported by a single agency from a single station. A reading typically includes one or more phase names, arrival times and/or amplitude/period measurements.

- Report/Data report

  All data that are reported to the ISC are parsed and stored in the ISC database. These may include event bulletins, focal mechanisms, moment tensor solutions, macroseismic descriptions and other event comments, as well as phase arrival data that are not associated to events. Every single report sent to the ISC can be traced back in the ISC database via its unique report identifier.

- Shide Circulars

  Collections of station reports for large earthquakes occurring in the period 1899-1912. These reports were compiled through the efforts of J. Milne. The reports are mainly for stations of the British Empire equipped with Milne seismographs. After Milne's death, the Shide Circulars were replaced by the Seismological Bulletins of the BAAS.

- Station code

  A unique, maximum six-character code for a station. The ISC Bulletin contains data exclusively from stations registered in the International Registry of Seismograph Stations.

14

Acknowledgements

We thank Allison Bent and Gavin Hayes for their review articles on notable events in the time interval covered by this Bulletin Summary.

We thank also Peter Bormann for his contribution to the section on IASPEI standards for magnitudes, Johannes Schweitzer for the updated ray-path figures for seismic phases, and Robin Adams and Johannes Schweitzer for input on the background history for the ISC.

Thanks are due also to John Adams, Johannes Schweitzer and Gary Gibson for suggestions and for their reviews of drafts for this issue of the Bulletin Summary.

We are also grateful to all the developers of the Generic Mapping Tools (GMT) suite of software (*Wessel and Smith*, 1998), used extensively here in producing the graphical figures.

Finally, we thank the ISC Member Institutions, Data Contributors, Funding Agencies (including NSF Award 0949072) and Sponsors for supporting the ISC long-term operations.

References

Adams, R. D., A. A. Hughes, and D. M. McGregor (1982), Analysis procedures at the International Seismological Centre, *Physics of the Earth and Planetary Interiors*, *30*, 85–93.

Amante, C., and B. W. Eakins (2009), ETOPO1 1 arc-minute global relief model: procedures, data sources and analysis, *NOAA Technical Memorandum NESDIS NGDC-24*, NOAA.

Balfour, N., R. Baldwin, and A. Bird (2008), Magnitude calculations in Antelope 4.10, *Analysis Group Note of Geological Survey of Canada*, pp. 1–13.

Bennett, T. J., V. Oancea, B. W. Barker, Y.-L. Kung, M. Bahavar, B. C. Kohl, J. . Murphy, and I. K. Bondár (2010), The nuclear explosion database NEDB: a new database and web site for accessing nuclear explosion source information and waveforms, *Seismological Research Letters*, *81*, doi:10.1785/gssrl.81.1.12.

Bisztricsany, E. A. (1958), A new method for the determination of the magnitude of earthquakes, *Geofiz. Kozl*, pp. 69–76.

Bolt, B. A. (1960), The revision of earthquake epicentres, focal depths and origin time using a high-speed computer, *Geophysical Journal of the Royal Astronomical Society*, *3*, 434–440.

Bondár, I., and K. McLaughlin (2009a), A new ground truth data set for seismic studies, *Seismological Research Letters*, *80*, 465–472.

Bondár, I., and K. McLaughlin (2009b), Seismic location bias and uncertainty in the presence of correlated and non-Gaussian travel-time errors, *Bulletin of the Seismological Society of America*, *99*, 172–193.

Bondár, I., and D. Storchak (2011), Improved location procedures at the International Seismological Centre, *Geophysical Journal International*, *186*, 1220–1244.

Bondár, I., E. R. Engdahl, X. Yang, H. A. A. Ghalib, A. Hofstetter, V. Kirchenko, R. Wagner, I. Gupta, G. Ekström, E. Bergman, H. Israelsson, and K. McLaughlin (2004), Collection of a reference event set for regional and teleseismic location calibration, *Bulletin of the Seismological Society of America*, *94*, 1528–1545.

Bondár, I., E. Bergman, E. R. Engdahl, B. Kohl, Y.-L. Kung, and K. McLaughlin (2008), A hybrid multiple event location technique to obtain ground truth event locations, *Geophysical Journal International*, *175*, doi:10.1111/j.1365,246X.2008.03,867x.

Bormann, P., and J. W. Dewey (2012), The new IASPEI standards for determining magnitudes from digital data and their relation to classical magnitudes, IS 3.3, *New Manual of Seismological Observatory Practice 2 (NMSOP-2), P. Bormann (Ed.)*, pp. 1–44, doi:10.2312/GFZ.NMSOP-2_IS_3.3,10.2312/GFZ.NMSOP-2, `http://nmsop.gfz-postsdam.de`.

Bormann, P., and J. Saul (2008), The new IASPEI standard broadband magnitude mB, *Seism. Res. Lett*, *79*(5), 698–705.

Bormann, P., R. Liu, X. Ren, R. Gutdeutsch, D. Kaiser, and S. Castellaro (2007), Chinese national network magnitudes, their relation to NEIC magnitudes and recommendations for new IASPEI magnitude standards, *Bulletin of the Seismological Society of America*, *97*(1B), 114–127, doi:10.1785/012006007835.

Bormann, P., R. Liu, Z. Xu, R. Ren, and S. Wendt (2009), First application of the new IASPEI teleseismic magnitude standards to data of the China National Seismographic Network, *Bulletin of the Seismological Society of America*, *99*, 1868–1891, doi:10.1785/0120080010.

Chang, A. C., R. H. Shumway, R. R. Blandford, and B. W. Barker (1983), Two methods to improve location estimates - preliminary results, *Bulletin of the Seismological Society of America*, *73*, 281–295.

Choy, G. L., and J. L. Boatwright (1995), Global patterns of readiated seismic energy and apparent stress, *J. Geophys. Res.*, *100*(B9), 18,205–18,228.

Dziewonski, A. M., and F. Gilbert (1976), The effect of small, aspherical perturbations on travel times and a re-examination of the correction for ellipticity, *Geophysical Journal of the Royal Astronomical Society*, *44*, 7–17.

Dziewonski, A. M., T.-A. Chou, and J. H. Woodhouse (1981), Determination of earthquake source parameters from waveform data for studies of global and regional seismicity, *J. Geophys. Res.*, *86*, 2825–2852.

Engdahl, E. R., and R. H. Gunst (1966), Use of a high speed computer for the preliminary determination of earthquake hypocentres, *Bulletin of the Seismological Society of America*, *56*, 325–336.

Engdahl, E. R., and A. Villaseñor (2002), Global seismicity: 1900-1999, *International Handbook of Earthquake Engineering and Seismology, International Geophysics series*, *81A*, 665–690.

Engdahl, E. R., R. van der Hilst, and R. Buland (1998), Global teleseismic earthquake relocation with improved travel times and procedures for depth determination, *Bulletin of the Seismological Society of America*, *88*, 722–743.

Flinn, E. A., and E. R. Engdahl (1965), Proposed basis for geographical and seismic regionalization, *Reviews of Geophysics*, *3*(1), 123–149.

Flinn, E. A., E. R. Engdahl, and A. R. Hill (1974), Seismic and geographical regionalization, *Bulletin of the Seismological Society of America*, *64*, 771–993.

Gutenberg, B. (1945a), Amplitudes of P, PP and S and magnitude of shallow earthquakes, *Bulletin of the Seismological Society of America*, *35*, 57–69.

Gutenberg, B. (1945b), Magnitude determination of deep-focus earthquakes, *Bulletin of the Seismological Society of America*, *35*, 117–130.

Gutenberg, B. (1945c), Amplitudes of surface waves and magnitudes of shallow earthquakes, *Bulletin of the Seismological Society of America*, *35*, 3–12.

Gutenberg, B., and C. F. Richter (1956), Magnitude and Energy of earthquakes, *Ann. Geof.*, *9*, 1–5.

Hutton, L. K., and D. M. Boore (1987), The ML scale in southern California, *Bulletin of the Seismological Society of America*, *77*, 2074–2094.

IASPEI (2005), Summary of magnitude working group recommendations on standard procedures for determining earthquake magnitudes from digital data, `http://www.iaspei.org/commissions/CSOI.html#wgmm,http://www.iaspei.org/commissions/CSOI/summary_of_WG_recommendations_2005.pdf`.

IASPEI (2013), Summary of magnitude working group recommendations on standard procedures for determining earthquake magnitudes from digital data, `http://www.iaspei.org/commissions/CSOI/Summary_of_WG_recommendations_20130327.pdf`.

IDC (1999), IDC processing of seismic, hydroacoustic and infrasonic data, *IDC Documentation*.

Jeffreys, H., and K. E. Bullen (1940), *Seismological Tables*, British Association for the Advancement of Science.

Kanamori, H. (1977), The energy release in great earthquakes, *J. Geophys. Res.*, *82*, 2981–2987.

Kennett, B. L. N. (2006), Non-linear methods for event location in a global context, *Physics of the Earth and Planetary Interiors*, *158*, 45–64.

Kennett, B. L. N., E. R. Engdahl, and R. Buland (1995), Constraints on seismic velocities in the Earth from traveltimes, *Geophysical Journal International*, *122*, 108–124.

Kennett, B. L. N., E. R. Engdahl, and R. Buland (1996), Ellipticity corrections for seismic phases, *Geophysical Journal International*, *127*, 40–48.

Lee, W. H. K., R. Bennet, and K. Meagher (1972), A method of estimating magnitude of local earthquakes from signal duration, *U.S. Geol. Surv.*, Open-File Rep.

Murphy, J. R., and B. W. Barker (2006), Improved focal-depth determination through automated identication of the seismic depth phases pP and sP, *Bulletin of the Seismological Society of America*, *96*, 1213–1229.

NMSOP-2 (2012), *New Manual of Seismological Observatory Practice (NMSOP-2)*, IASPEI, GFZ, German Research Centre for Geosciences, Potsdam, doi:10.2312/GFZ.NMSOP-2, urn:nbn:de:kobv:b103-NMSOP-2, `http://nmsop.gfz-potsdam.de`.

Nuttli, O. W. (1973), Seismic wave attenuation and magnitude relations for eastern North America, *J. Geophys. Res.*, *78*, 876–885.

Richter, C. F. (1935), An instrumental earthquake magnitude scale, *Bulletin of the Seismological Society of America*, *25*, 1–32.

Ringdal, F. (1976), Maximum-likelihood estimation of seismic magnitude, *Bulletin of the Seismological Society of America*, *66*(3), 789–802.

Sambridge, M. (1999), Geophysical inversion with a neighbourhood algorithm, *Geophysical Journal International*, *138*, 479–494.

Sambridge, M., and B. L. N. Kennett (2001), Seismic event location: non-linear inversion using a neighbourhood algorithm, *Pure and Applied Geophysics*, *158*, 241–257.

Storchak, D. A., J. Schweitzer, and P. Bormann (2003), The IASPEI standard seismic phases list, *Seismological Research Letters*, *74*(6), 761–772.

Storchak, D. A., J. Schweitzer, and P. Bormann (2011), Seismic phase names: IASPEI standard, in *Encyclopedia of Solid Earth Geophysics*, edited by H. Gupta, pp. 1162–1173, Springer.

Tsuboi, C. (1954), Determination of the Gutenberg-Richter's magnitude of earthquakes occurring in and near Japan, *Zisin (J. Seism. Soc. Japan), Ser. II*(7), 185–193.

Tsuboi, S., K. Abe, K. Takano, and Y. Yamanaka (1995), Rapid determination of Mw from broadband P waveforms, *Bulletin of the Seismological Society of America*, *85*(2), 606–613.

Uhrhammer, R. A., and E. R. Collins (1990), Synthesis of Wood-Anderson Seismograms from Broadband Digital Records, *Bulletin of the Seismological Society of America*, *80*(3), 702–716.

Vaněk, J., A. Zapotek, V. Karnik, N. V. Kondorskaya, Y. V. Riznichenko, E. F. Savarensky, S. L. Solov'yov, and N. V. Shebalin (1962), Standardization of magnitude scales, *Izvestiya Akad. SSSR., Ser. Geofiz.*(2), 153–158, pages 108–111 in the English translation.

Villaseñor, A., and E. R. Engdahl (2005), A digital hypocenter catalog for the International Seismological Summary, *Seismological Research Letters*, *76*, 554–559.

Villaseñor, A., and E. R. Engdahl (2007), Systematic relocation of early instrumental seismicity: Earthquakes in the International Seismological Summary for 1960–1963, *Bulletin of the Seismological Society of America*, *97*, 1820–1832.

Wessel, P., and W. H. F. Smith (1998), New, improved version of the Generic Mapping Tools released, *EOS Trans. AGU*, *79*, 579, `http://gmt.soest.hawaii.edu/`.

Woessner, J., and S. Wiemer (2005), Assessing the quality of earthquake catalogues: estimating the magnitude of completeness and its uncertainty, *Bulletin of the Seismological Society of America*, *95*(2), doi:10/1785/012040,007.

Young, J. B., B. W. Presgrave, H. Aichele, D. A. Wiens, and E. A. Flinn (1996), The Flinn-Engdahl regionalisation scheme: the 1995 revision, *Physics of the Earth and Planetary Interiors*, *96*, 223–297.

REF TEK

Unshakable.

Complete Integrated Aftershock System Provides Quick and Easy Solution for Rapid Aftershock Deployment

Introduction

Rapid Aftershock Mobilization plays an essential role in the understanding of both focal mechanism and rupture propagation caused by strong earthquakes. A quick assessment of the data provides a unique opportunity to study the dynamics of the entire earthquake process in-situ. Aftershock study also provides practical information for local authorities regarding the post earthquake activity, which is very important in order to conduct the necessary actions for public safety in the area affected by the strong earthquake.

Due to a relatively short aftershock activity period (several weeks to several months), it is critical to provide rapid deployment of emergency personnel to the affected area in order to minimize the time required to estimate the extent and amplitude of strong shaking from aftershock events.

A dense array of seismic stations consisting of high resolution seismic recorders with short period seismometers and accelerometers is required in order to reduce the time needed to detect an event and provide high resolution maps of ground accelerations across the affected earthquake region. Therefore, the rapid aftershock mobilization of seismic equipment should comply with the following critical requirements:

- Light weight and small in size
- Integrated design with minimal or no external peripheral equipment
- Very low power consumption
- Minimal or no field programming
- Easy and quick data download in the field
- Low maintenance

What Does the 160-03 Offer?

The REF TEK High Resolution Aftershock System, Model 160-03, is a self-contained, fully integrated Aftershock System providing the customer with simple and quick deployment during aftershock emergency mobilization. The 160-03, six channel recorder, contains three major components integrated in one case:

160-03 at a Glance

- The 160-03 High Resolution Aftershock System provides an ideal solution and opportunity for both scientists and emergency response authorities to study rapid aftershock deployment.

- The 160-03 provides the following advanced features:
  - Self-contained System;
  - 7 Days Power Autonomy;
  - Integrated Sensors;
  - Compact and Light Weight;
  - State-of-the-Art ADC;
  - No user setup in the field;
  - No external peripherals;
  - Ultra-Low Power.

1) 24-bit resolution low power ADC with CPU and lid interconnect boards;
2) Power source; and
3) Three component 2 Hz (or 1Hz) sensors (two horizontals and one vertical) and a triaxial +/-4g MEMS accelerometer.

The self-contained rechargeable battery pack provides power autonomy for up to 7 days during continuous data acquisition at 200 sps on three weak motion and three triggered strong motion recording channels. For longer power autonomy, the 160-03 Aftershock System battery pack can be charged from an external source (solar power system). To download recorded data the customer simply connects a laptop to the 160-03 and the data is then automatically uploaded.

The 160-03 configuration is fixed based on a configuration file stored in the system, so no external command/control interface is required for parameter setup in the field. For visual control of the system performance in the field, the 160-03 has a built-in LED display which indicates the systems recording status, as well as a hot swappable USB drive and battery status. As an added customer convenience, four 160-03 systems can be housed in a small, lightweight, watertight rolling case that will keep the recorders safe during transport. The ease of having an all-in-one aftershock system also provides the customer flexibility in sending the equipment to the affected region via a more cost effective way as the equipment/carrying case can easily be checked on both domestic and international commercial flights.

160-03 Specifications

Model:	160-03
Mechanical	
Size:	6” (15.2 cm) high x 8.63” (21.9 cm) diameter
Weight:	7 lbs (3.2 kg)
Watertight Integrity:	IP67
Environmental	
Operating Temperature:	-30° C to +60° C
Storage Temperature:	-40° C to +70° C
Power	
Average Power:	<400 mW
A/D Converter	
Type:	Delta-Sigma Modulation, 24-bit output resolution
Dynamic Range:	>138 dB@100 sps
Channels:	6
Input impedance:	Matched to sensors
Sample Rates:	200 sps default; 100, 250,500 sps optional
Seismometer	
Type:	Moving coil / mass
Natural Frequency:	2 Hz or 1 Hz (customer specific)
Accelerometer	
Type:	± 4g
Frequency Response:	DC - 45 Hz
Damping:	0.7 to critical
Data Storage:	USB Flash
User Interface	
Type:	LED array consisting of 16 LED
Information:	Display indicating recording status, USB drive status, battery voltage, etc.
Power Control:	Magnetic switch to turn on both power and acquisition

Contact Us

www.reftek.com 214-440-1265 sales@reftek.com

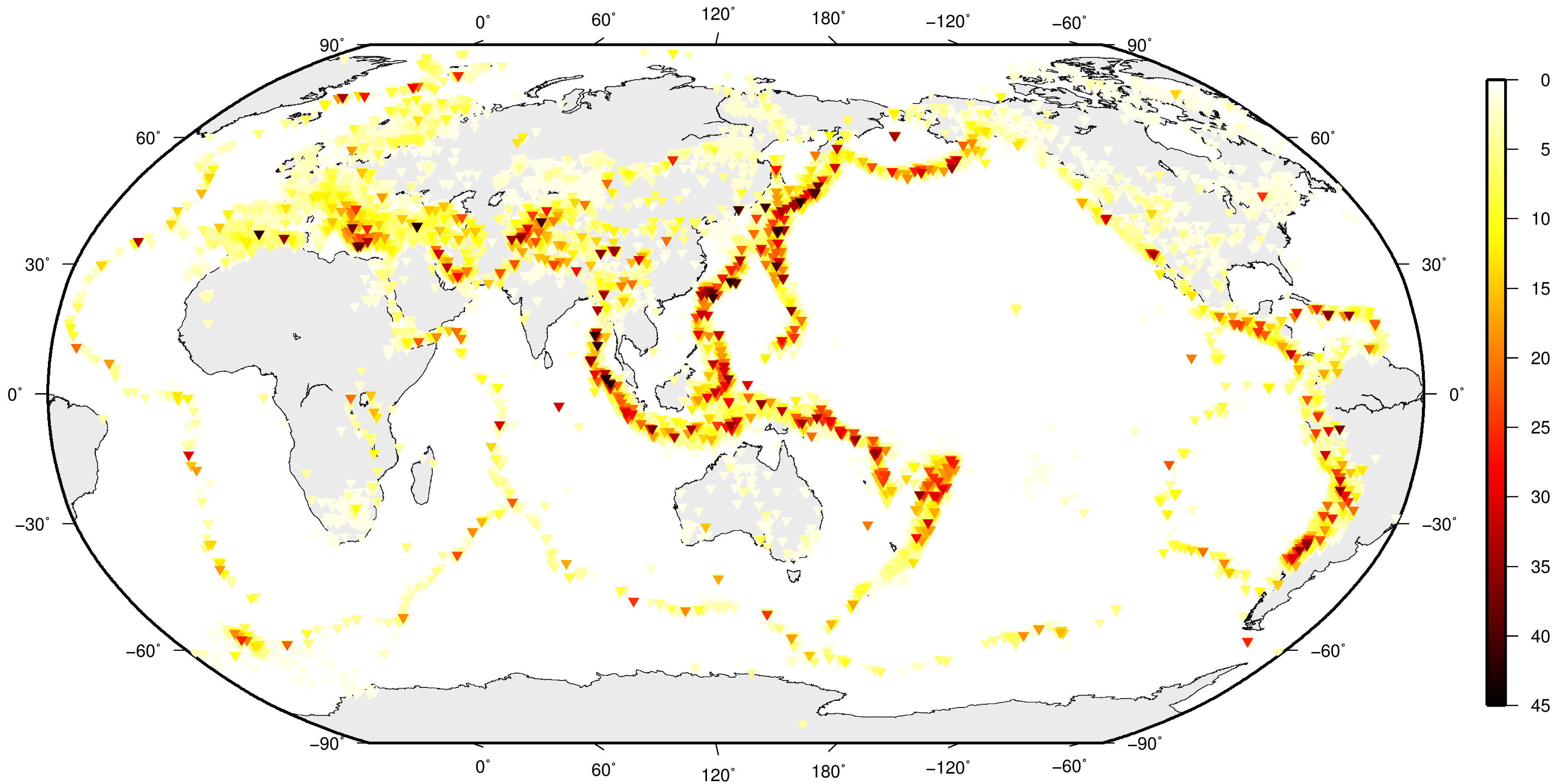

Map of events for 2010-01 to 2010-06 showing the numbers of data reporters for each event, see Chapter 9.